Analytical Investigation of Electromagnetic Fields in Mine Environments

Iterim Summary Report on Contract No. H0155008

Principal Investigator: James R. Wait
Environmental Research Laboratories
NOAA, U.S. Department of Commerce
Boulder, CO 80302

Co-Investigator: David A. Hill
Institute of Telecommunication Sciences
Office of Telecommunications
U.S. Department of Commerce
Boulder, CO 80302

Prepared for H. Kenneth Sacks
Technical Project Officer
Pittsburgh Mining & Safety Research Center
U.S. Bureau of Mines
4800 Forbes Avenue
Pittsburgh, PA 15213

15 November 1976

PREFACE

An attempt is made here to collect together various reports and publications that are based on research supported all or in part by Contract No. H0155008 for the past two years. The subject matter deals primarily with the excitation, transmission, and reception of electromagnetic waves in mine environments.

This contract from the U.S. Bureau of Mines with the Office of Telecommunications supports the efforts of James R. Wait (Principal Investigator and Consultant to OT), David A. Hill (Co-Investigator), and various associates within the Boulder scientific community. The contributions of Samir F. Mahmoud were supported, in part, by the contract while he was a Visiting Fellow with the Cooperative Institute for Research in Environmental Sciences at the University of Colorado. Administrative assistance in CIRES has been provided by Mrs. Lana R. Hope.

Much of the work carried out under the contract has been submitted in the form of Preliminary Reports to the Technical Project Officer at irregular but frequent intervals. Copies of this material have also been sent to other individuals and organizations including the following:

Mr. Arnold J. Farstad (Westinghouse Electric Corp., 8401 Baseline Rd., Boulder, CO 80303)
Mr. Robert L. Lagace (Research & Development Div., Arthur D. Little, Inc., Acorn Park, Cambridge, MA 02140)
Dr. A.G. Emslie (Research & Development Div., Arthur D. Little, Inc., Acorn Park, Cambridge, MA 02140)
Mr. John N. Murphy (Pittsburgh Mining & Safety Research Center, U.S. Bureau of Mines, Pittsburgh, PA 15213)
Dr. Howard E. Parkinson (Pittsburgh Mining & Safety Research Center, U.S. Bureau of Mines, Pittsburgh, PA 15213)

After suitable revision and with the aid of in-house projects within CIRES and the Department of Commerce, publication versions of the Preliminary Reports were prepared. Reprints of these articles, when available, are included in this summary report. In other cases, the Preliminary Reports themselves are included with any appropriate revision that has been considered desirable.

The principal objective in this project is to analyze the transmission characteristics of electromagnetic waves in tunnels and similar structures in mine environments. The approach is to postulate certain mathematical models that, while idealized, do allow for the various complications that may arise in an operational environment. The philosophy is to treat these complications first on a selective basis. Then, as appropriate, the combined influence of the various factors is considered.

The first two chapters or issuances are introductory reviews of the tunnel waveguide problem. They are based on presentations given at international conferences in Europe in 1974 and, hopefully, they serve as an introduction to the subject. The following group of chapters deal with the tunnel geometry of rectangular cross-section while the subsequent group of chapters deal with circular cross-section. In each case, the analysis becomes progressively more involved as additional complications are treated.

In most cases, the modes that propagate in the tunnel structures, have vastly different properties. An understanding of the excitation and propagation characteristics of these modes is vital if an optimum communication system is ever to be achieved.

Related guided wave problems included in this summary are the coal seam treated as a parallel slab waveguide and the mine hoist considered as a coaxial or cylindrical waveguide.

In carrying out this work, we have benefited greatly by contact with the following individuals: Quin Davis, Paul Delogne, Louis Deryck, R.H. Lagace, R. Liegeois, David Martin, J.N. Murphy, H. Parkinson, H.K. Sacks, and R.H. Spencer.

15 November 1976

James R. Wait

TABLE OF CONTENTS

TABLE OF CONTENTS - CONT'D

3
CHAPTER 1

Radio Science, Volume 10, Number 7, pages 753-759, July 1975

Theory of EM wave propagation through tunnels

James R. Wait

Cooperative Institute for Research in Environmental Sciences, University of Colorado, Boulder, Colorado 80302

(Received March 13, 1975.)

A rather ingenious communication technique is being developed for use in Belgian coal mines. The idea is to use a two-wire transmission line or equivalent loosely braided coaxial cable that can be suspended from the upper wall. A transmitter placed in the vicinity of the line excites a strongly unbalanced mode that normally would propagate like a coaxial or TEM mode with relatively high attenuation. The key step in the Belgian system, and the closely related French system, is to convert this unbalanced mode to a balanced mode that is much less attenuated because the return current flows mostly in the second wire rather than through the surrounding rock. The physical basis of this system has many similarities with the leaky feeder device described by Martin and used in British coal mines. We summarize the analysis of the propagation characteristics for an idealized mine tunnel of circular cross section. The extension to a rectangular tunnel is also considered. Some comparison is made with relevant experimental data. Actually, we deal only with the twin open wire pair that is the basic ingredient of the so-called INIEX/Deryck system. However, as suggested above, the leaky braided cable system and the slotted cylindrical shielded cables have common features. The important point is that propagation modes which depend on current flow in the tunnel walls will suffer excessive attenuation while modes which utilize the second conductor as a return current path will have less attenuation.

INTRODUCTION

It is probable that Marconi was aware of the limitations of electromagnetic wave transmission through rock media. In all cases reported in the literature, Marconi chose signal paths that favored propagation of energy through the atmosphere. However, in some cases he observed the adverse influence of intervening hills and ridges.

For this centennial dedication to Marconi, we would like to select a subject that finds its motivation in a need to communicate from point to point in the Earth. While direct transmission is certainly possible over limited ranges, a much more attractive possibility is to utilize tunnels or other waveguiding channels in the Earth's crust.

Our immediate interest is to consider applications to coal mines where nature has provided us with extensive quasihomogeneous conductive regions. With a little help from man, such regions are often interspersed with tunnels whose cross sections vary from circular to rectangular form. Also, in such tunnels, we often find longitudinal conductors such as pipes and tracks that may or may not be grounded to the surrounding medium. In some cases, enterprising engineers have strung transmission lines of various forms that act as active or passive conveyors of electromagnetic energy [*Deryck*, 1970, 1972, 1973; *Delogne*, 1973; *Delogne et al.*, 1973; *Martin*, 1970; *Fontaine et al.*, 1973; *Goddard*, 1973].

We should mention that there is a closely related class of problems in antenna theory. For example, if we locate a radiating system in highly conductive media such as the Earth, it should come as no surprise that the structure needs to be insulated over at least part of its length. This topic, which is the subject of a special journal issue [*Wait*, 1974], is not discussed here.

The plan of this paper is to consider the guided mode theory of transmission in an air-filled cylindrical tunnel in a conductive medium. Also, we allow for the possibility that the tunnel contains an axial conductor or system of conductors of a specified form. We outline the analysis of the permissible modes that may propagate along this structure. Our derivations will be quite brief but the interested reader can find further details in the quoted references.

CIRCULAR TUNNEL MODEL

Specifically, we consider an air-filled tunnel of circular cross section with radius a bounded by

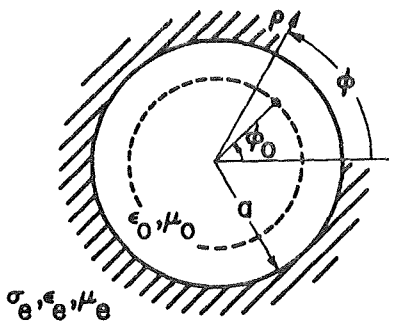

Fig. 1. Geometry for single wire conductor in a circular air-filled tunnel in homogeneous Earth.

a lossy dielectric medium. Within this uniform tunnel we locate a single relatively thin metal conductor of radius c_s whose conductivity is σ_s. The situation is illustrated in Figure 1 where we have chosen a cylindrical coordinate system (ρ,ϕ,z) to be coaxial with the guide. For the interior region $\rho < a$ the permittivity and permeability are ϵ_0 and μ_0 respectively. For the exterior region, the permittivity, conductivity and permeability are ϵ_e, σ_e, and μ_e respectively. The thin axial conductor is located at $\rho = \rho_0$ and $\phi = \phi_0$; its corresponding electric properties are ϵ_s, σ_s, and μ_s. Here we restrict attention to the case $0 < \rho_0 < a$. Later, we consider the effect of a second wire conductor that is parallel to the first.

We now consider the complex propagation constant of the dominant modes of the structure. Thus, we assume that the field of an individual mode varies with z according to $\exp(-\Gamma z)$ for an implied time factor $\exp(i\omega t)$ where the values of Γ are to be determined. As indicated elsewhere [*Wait and Hill*, 1974*a*], the fields can be determined by two scalar functions U and V that are, respectively, the z components of (axially directly) electric and magnetic Hertz vectors.

The current on the axial conductor can be designated $I\exp(-\Gamma z)$. The primary field within the tunnel from this travelling wave of current may be derived from the electric-type Hertz function U^p. It is well known that

$$U^p = (i\mu_0\omega/2\pi\gamma_0^2)\, I\exp(-\Gamma z) K_0\,[(\gamma_0^2 - \Gamma^2)^{1/2}\rho_d] \tag{1}$$

where $\gamma_0^2 = -\epsilon_0\mu_0\omega^2$, $\rho_d = [\rho^2 + \rho_0^2 - 2\rho\rho_0 \cdot \cos(\phi - \phi_0)]^{1/2}$, and K_0 is the modified Bessel function of the second kind. Now the total Hertz function within the guide can be written $U = U^p + U^s$, where U^s is the secondary part. The latter, for the region $\rho < a$, can be constructed by superimposing solutions of the type $I_m(\nu\rho) \cdot \exp(-im\phi)\exp(-\Gamma z)$ where I_m is a modified Bessel function of the first type, $\nu = (\gamma_0^2 - \Gamma^2)^{1/2}$ and m is any integer.

The above considerations, and the addition theorem for K_0 in (1), leads us to the representation [*Wait and Hill*, 1974*a*]

$$U = \sum_{m=-\infty}^{+\infty} U_m \exp[-im(\phi - \phi_0)] \tag{2}$$

where

$$U_m = (i\mu_0\omega/2\pi\gamma_0^2)\, I e^{-\Gamma z} I_m(\nu\rho_0)\{K_m(\nu\rho) - R_m[K_m(\nu a)/I_m(\nu a)]\, I_m(\nu\rho)\} \tag{3}$$

for the region $\rho_0 < \rho < a$ where R_m is yet to be determined. Similar considerations lead us to the corresponding representation for the magnetic type Hertz function for the region $\rho < a$. Thus,

$$V = \sum_{m=-\infty}^{+\infty} V_m \exp[-im(\phi - \phi_0)] \tag{4}$$

where

$$V_m = (i\mu_0\omega/2\pi\gamma_0^2)\, I e^{-\Gamma z} \Delta_m I_m(\nu\rho_0)\, I_m(\nu\rho) \tag{5}$$

For the external region $\rho > a$ the Hertz functions are both made up from solutions of the form

$$K_m(u\rho)\exp(-\Gamma z)\exp(-im\phi)$$

where

$$u = (\gamma_e^2 - \Gamma^2)^{1/2} \text{ and } \gamma_e^2 = i\mu_e\omega(\sigma_e + i\epsilon_e\omega)$$

The boundary conditions at the wall $\rho = a$ are that the tangential fields are continuous. Using these we may obtain expressions [*Wait and Hill*, 1974*b*] for the coefficients R_m and Δ_m in terms of modified Bessel functions of arguments va and ua. Then we can express the axial electric field E_z anywhere within the guide in terms of the still unknown current $I\exp(-\Gamma z)$ on the wire.

Now the boundary condition at the wire is

$$E_z = I Z_s \exp(-\Gamma z) \tag{6}$$

at $\rho_d = c_s$ for all values of z where Z_s is the series impedance of the wire. Because of the assumed

thinness of the wire, we can apply this condition at any point of the wire circumference. Thus, we choose the matching point at $\rho = \rho_0 + c_s$ and $\phi = \phi_0$. Thus (6) leads to the mode equation

$$(-i\mu_0\omega\nu^2/2\pi\gamma_0^2)\left\{K_0(\nu c) - \sum_{m=-\infty}^{+\infty} R_m[K_m(\nu a) \div I_m(\nu a)]\, I_m(\nu\rho_0)\, I_m[\nu(\rho_0 + c_s)]\right\} = Z_s \tag{7}$$

where the explicit result for the series impedance is

$$Z_s = (\eta_s/2\pi c_s)\, I_0(\gamma_s c_s)/I_1(\gamma_s c_s) \tag{8}$$

where $\gamma_s^2 = i\mu_s\omega(\sigma_s + i\epsilon_s\omega)$ and $\eta_s = i\mu_s\omega/\gamma_s$.

We now consider the extension [*Hill and Wait*, 1974*a*] of the solution to the case where two axial conductors of radii c_0 and c_1 are present. The situation is illustrated in Figure 2. Now I_0, the current on the conductor at (ρ_0,ϕ_0,z), is arbitrary, while I_1, the current on the conductor at (ρ_1,ϕ_1,z), is unknown. By superimposing solutions of the earlier single-wire source, we can construct an appropriate solution for E_z.

$$E_z = I_0 Z_{s0} e^{-\Gamma z} \quad \text{at} \quad \rho = \rho_0 + c_0, \phi = \phi_0 \tag{9}$$

$$E_z = I_1 Z_{s1} e^{-\Gamma z} \quad \text{at} \quad \rho = \rho_1 + c_1, \phi = \phi_1 \tag{10}$$

where Z_{s0} and Z_{s1} are the appropriate series impedances. The unknowns are I_1 (or I_1/I_0) and Γ. We can easily eliminate I_1 to yield a mode equation.

The method can be generalized to an arbitrary number of N thin axial conductors located within the guide. An impedance condition, as indicated above, can be assumed for each wire. This yields

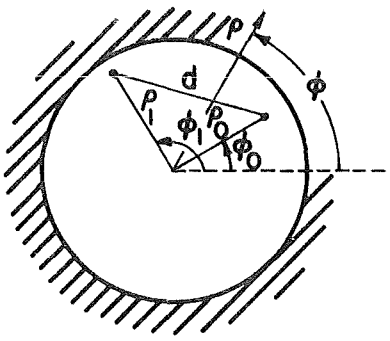

Fig. 2. Geometry for two arbitrarily located axial wires within tunnel.

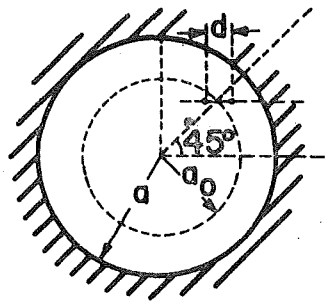

Fig. 3. Geometry for two axial wires located in a horizontal plane in the upper quadrant of the tunnel cross section. The mean distance to the tunnel wall is $a - a_0$.

a system of N linear equations for the N unknown wire currents. The system has a solution only if the following determinant is zero:

$$\begin{vmatrix} (A_{11} - Z_1) & A_{12} & \cdots & A_1 \\ A_{21} & (A_{22} - Z_2) & \cdots & A_{2N} \\ \vdots & \vdots & & \vdots \\ A_{N1} & A_{N2} & \cdots & \end{vmatrix} = 0 \tag{11}$$

where A_{ij} is the z component of the electric field (primary plus secondary) produced at the match point on wire i by a unit current on wire j and Z_j is the series impedance of wire j. In what follows, we will just consider the case of two axial conductors, i.e., $N = 2$.

The modes that have transmission-line character as the frequency is lowered are of particular interest here. As we shall see, there are two classes of these: in one case the current ratio I_1/I_0 is approximately $+1$ and in the other case the ratio is approximately -1. For obvious reasons, these are designated the monofilar and bifilar modes, respectively. Actually, in the unlikely case that $\rho_0 = \rho_1$, we have exactly $I_1 = \pm I_0$. Using an adaptation of Newton's method, solutions of the desired type have been obtained for the specific configuration shown in Figure 3. This is considered a reasonable idealization of the situation encountered in practice where the transmission line is suspended from the tunnel wall but offset from the centerline. An example is shown in Figure 4 where the following parameters are assumed: $a = 2$ m, $\epsilon_e = 10\epsilon_0$, $\sigma_e = 10^{-2}$ mhos m^{-1}, $\sigma_s = 10^6$ mhos m^{-1}, $c_s = 10^{-3}$ m = 1 mm, and $d =$ 0.02 m = 2 cm. Various values of the ratio a_0/a

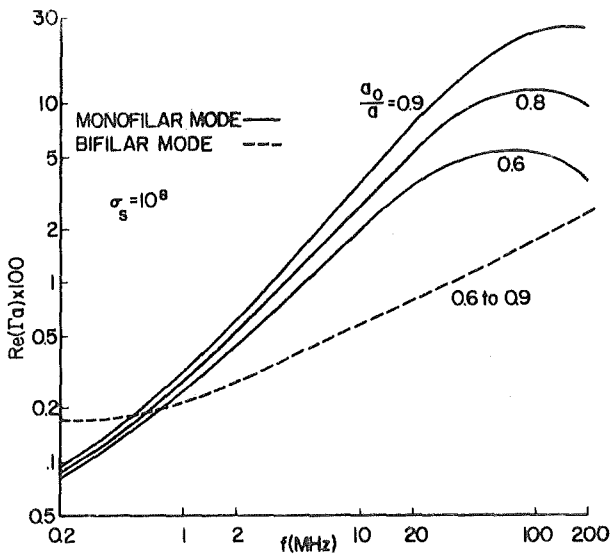

Fig. 4. The normalized attenuation rate as a function of frequency for the monofilar and bifilar modes for a wire conductivity $\sigma_s = 10^6$ mhos m^{-1}.

are shown for the monofilar mode but only the value 0.8 for the bifilar mode. In the latter case, the corresponding values for 0.9 and 0.6 are indistinguishable. Here the real part of (Γa), which is proportional to the attenuation rate, is plotted as

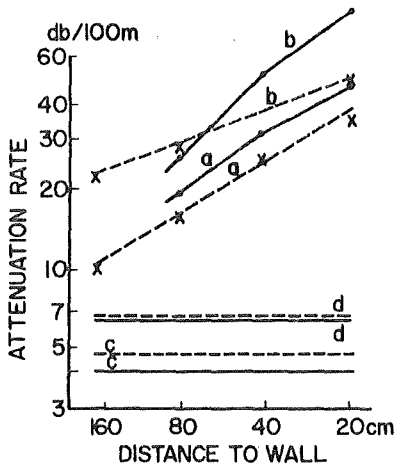

Fig. 5. Comparison of calculated (solid curves) and Deryck's observed (broken curves) data of attenuation rate as a function of the distance of the transmission line from the tunnel wall. Curves *a* and *b* are for the monofilar mode for 27 and 68 MHz, respectively, while curves *c* and *d* are for the bifilar mode for 27 and 68 MHz.

a function of frequency from 0.2 to 200 MHz. The increase of the monofilar mode attenuation as the wire conductor approaches the wall is apparent. Actually, the attenuation rates are quite dependent on the assumed wire conductivity but the dependence on the other parameters, such as c_s and d, is not so severe.

For the geometry of the tunnel guide considered in the preceding example, we can expect higher-order waveguide modes to appear when the frequency exceeds the cutoff value for the empty tube. This occurs at approximately 50 MHz in this case. For higher frequencies, we can expect the situation to be quite complicated. However, it appears we can always identify the monofilar and bifilar modes as the ones that are significantly influenced by the location and the series impedance of the wire conductor. Actually, we have calculated also these "waveguide modes" for various cylindrical geometries but the results are not given here. Suffice it to say that such modes have a very weak dependence on the conductivity of the axial wire conductors within the tunnel.

We can make a specific comparison of our calculated results of the attenuation rates with some experimental data published by *Deryck* [1973] for monofilar and bifilar mode propagation in a tunnel in Lanaye, Belgium. The actual tunnel has a total height of the order of 4 to 5 m and the width is of the order of 3 to 4 m. The comparison is indicated in Figure 5, where the abscissa is the distance of the transmission line from the tunnel wall and the ordinate is the attenuation rate in db per m. The calculated results use the same parameters as in Figure 4. As both the experimental and the theoretical curves show, there is a strong dependence on the proximity of the tunnel wall for the monofilar mode at both 27 and 68 MHz. On the other hand, there is virtually no dependence on the location of the transmission line for the case of the bifilar mode. This, of course, is an attractive feature for long distance communication. As *Deryck* [1972] indicates, conversion from the easily excited monofilar mode to the bifilar mode permits efficient point-to-point communication, even when the transmitting and/or receiving antennas are not closely coupled to the transmission line.

RECTANGULAR TUNNEL MODEL

A rigorous modal equation for the monofilar mode of a single wire in a rectangular tunnel has been

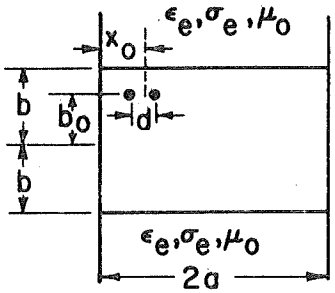

Fig. 6. The open wire T.L. (transmission line) inside a waveguide model of a rectangular tunnel.

recently obtained by *Mahmoud and Wait* [1974*a*] under some simplifying assumptions concerning the two side walls of the tunnel. Also, extensive numerical results on the properties of this mode have been reported [*Mahmoud and Wait*, 1974*a*; *Mahmoud*, 1974*a*]. We consider the configuration of the T.L. (transmission line) as shown in Figure 6. The two side walls of the tunnel are assumed to behave as either perfect electric or perfect magnetic conductors, while the other two walls are taken as generally lossy dielectric media. We adopt the nonrestrictive assumption that $d \gg c_s$ where c_s is the radius of any of the wires. As before, Γ is the complex propagation constant of the mode. So, apart from this common term, the currents in the two wires are given by I_1 and I_2. The boundary condition at the surface of each wire requires that the longitudinal electric field be equal to the current multiplied by the series impedance Z_w per unit length of the wire. Following *Mahmoud* [1974*b*], these conditions can be put in the convenient forms:

$$Z_{s1}(\Gamma)\, I_1 + Z_m(\Gamma)\, I_2 = Z_{w1}\, I_1 \tag{12}$$

$$Z_m(\Gamma)\, I_1 + Z_{s2}(\Gamma)\, I_2 = Z_{w2}\, I_2 \tag{13}$$

where $Z_{s1}(\Gamma)$ is defined as the longitudinal electric field at the surface of the first wire due to a unit current in that wire and a similar definition applied to $Z_{s2}(\Gamma)$. Here $Z_m(\Gamma)$ is the longitudinal electric field at the surface of one wire due to a unit current in the other wire.

By the elimination of I_1 and I_2 in (12) and (13), we obtain the modal equation for the unknown Γ as

$$[Z_{s1}(\Gamma) - Z_{w1}][Z_{s2}(\Gamma) - Z_{w2}] - Z_m^2 = 0 \tag{14}$$

This equation is greatly simplified when the two wires are identical since then $Z_{w1} = Z_{w2} = Z_w$. Furthermore, we can put $Z_{s1}(\Gamma) \simeq Z_{s2}(\Gamma) = Z_s \cdot (\Gamma)$, which is a very good approximation since d is much less than the guide width. Under the above conditions, the modal equation, (14), reduces to two simple equations given by

$$Z_s(\Gamma) + Z_m(\Gamma) - Z_w = 0 \tag{15}$$

and

$$Z_s(\Gamma) - Z_m(\Gamma) - Z_w = 0 \tag{16}$$

where the first equation implies that $I_1 = I_2$ and the second implies that $I_1 = -I_2$. These are the two equations that correspond to the monofilar and the bifilar modes respectively and their solutions give the propagation constants of these modes.

Equations 15 and 16 were solved numerically by *Mahmoud* [1974*b*] for several configurations in the frequency range 200 kHz to 200 MHz. The resulting values of the attenuation $\alpha_{\text{monofilar}}$ and α_{bifilar} are plotted in Figures 7 and 8 for the case of interest here. The following physical constants are assumed in Figure 7: $2a = 4$ m, $2b = 3$ m, $x_0 = a/2$, $d = a/100$, $c_s = 1$ mm. Here σ_s (the conductivity of

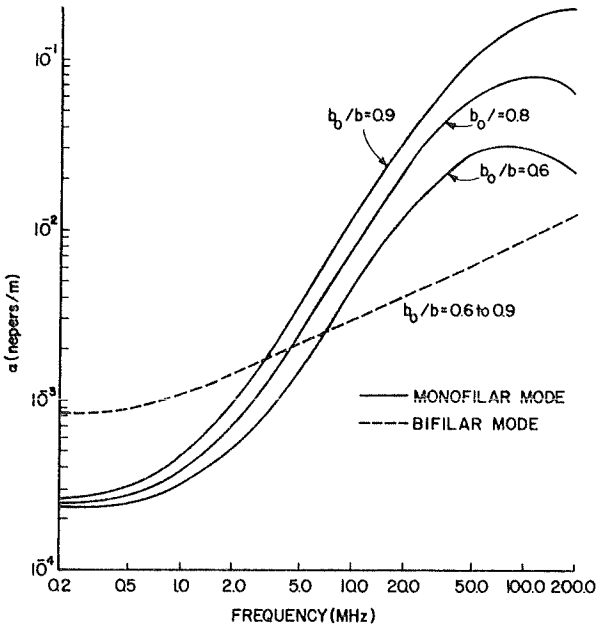

Fig. 7. Attenuation constant of the monofilar and the bifilar modes versus frequency for various values of b_0/b. Wire radii $c_s = 1$ mm.

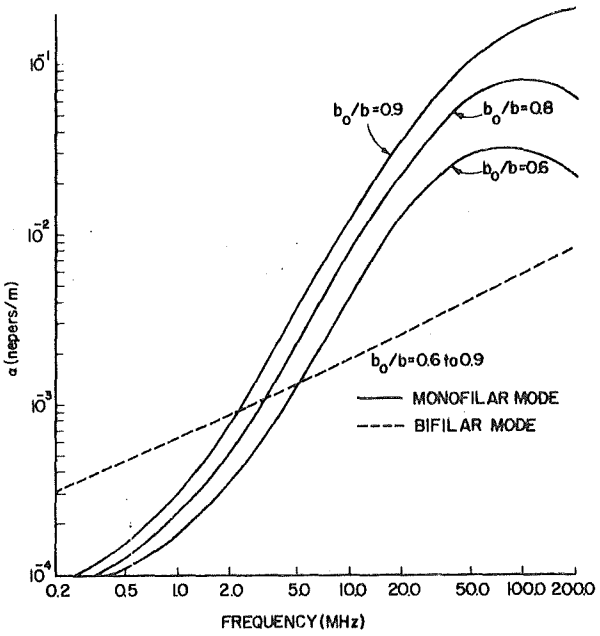

Fig. 8. Attenuation constant of the monofilar and the bifilar modes of configuration A versus frequency for various values of b_0/b. Wire radii $c_s = 2$ mm.

the wires) $= 10^6$ mho m^{-1}, $\epsilon_c = 10\,\epsilon_0$, and $\sigma_c = 10^{-2}$ mho m^{-1}.

In contrast with the monofilar mode, the attenuation of the bifilar mode is almost insensitive to variations of the parameter b_0/b in the frequency range considered and hence α_{bifilar} is shown for only one value of this parameter. To show the effect of varying the intrinsic parameters of the T.L., the wire radii are increased to 2 mm in Figure 8. By comparing with Figure 7 it is seen that α_{bifilar} is appreciably reduced at all frequencies, while $\alpha_{\text{monofilar}}$ is hardly affected for frequencies above about 12.5 MHz and considerably reduced at lower frequencies. Apparently, as the frequency is reduced below about 100 MHz, the guide walls behave more as good electrical conductors, hence reducing the attenuation of the monofilar mode. Thus, at low frequencies (of the order of few MHz and less), the attenuation of both modes becomes solely dependent on the intrinsic parameters σ_s and c_s. Furthermore, the ohmic losses of the T.L. are normally higher for the bifilar mode than those for the monofilar mode and hence the higher attenuation of the former mode at the low frequency end.

It is evident that the results presented here for the rectangular tunnel are very close to those for the circular tunnel. In fact, there is a complete consistency between the mode characteristics in the two guide geometries. This provides some confidence in the adequacy of the model used here for the rectangular tunnel.

Actually, the results shown in Figures 7 and 8 are obtained for a waveguide model with side walls that are perfect electric conductors. An alternative model is one in which these walls are perfect magnetic conductors. We computed values of attenuation rates for this model and it was found that the monofilar modes show much higher attenuation rates for frequencies below 25 MHz, while near 200 MHz the attenuation rates are only slightly different from those obtained for the first model. We believe, however, that the model with perfect electric side walls is a better approximation to the actual tunnel in the frequency range considered here, since the tunnel walls do tend to behave as good electrical conductors as the frequency is lowered.

FINAL REMARKS

In this paper, we have only considered the freely propagating modes of the axial structures. An important aspect in any communication design is how well these modes are excited. *Hill and Wait* [1974*a*,*b*] have considered the excitation mechanisms for both single and twin conductors in a circular tunnel model. Also, *Mahmoud* [1974*a*] had earlier treated the excitation by a dipole transmitter for the rectangular tunnel model. Other complicating factors that have been discussed are the effect of curvature of the tunnel axis [*Mahmoud and Wait*, 1974*b*] and the degrading influence of wall roughness [*Mahmoud and Wait*, 1974*c*]. An alternative method for allowing for finite wall conductivity using a geometrical optical approach is also given in the latter reference. In this method, all four walls of the rectangular waveguide may be lossy.

Acknowledgments. I am very grateful to D. A. Hill and S. F. Mahmoud for their contributions to this paper.

REFERENCES

Delogne, P. (1973), Les communications par radio en milieu souterrain, *Acta Tech. Belg. (Brussels)*, *9*(2), 18-26.

Delogne, P., L. Deryck, and R. Liegeois (1973), Guided propagation of radio waves, in *Proceedings of Thru-the-Earth Electromagnetics Workshop, Colorado School of Mines, Golden, Colorado, 15-17 August 1973*, pp. 49-53, National Technical Information Service, Springfield, VA 22151, acc. no. PB 231 154.

Deryck, L. (1970), Etude de modes de propagation d'ondes electromagnetiques, susceptibles d'exister sur une ligne bifilaire en milieu souterrain, *Ann. Mines Belg.*, *7*(8), 939-949.

Deryck, L. (1972), Radiocommunication in tunnels, *Electron. Lett.*, *8*(3), 71-72.

Deryck, L. (1973), Etude de la propagation des ondes electromagnetiques guidees dans les galerie souterraines, These de doctorat, Université de Liege, Belgium.

Fontaine, J., B. Demoulin, P. Degauque, and R. Gabillard (1973), Feasibility of radio communication in mine galleries by means of a coaxial cable having a high coupling impedance, in *Proceedings of Thru-the-Earth Electromagnetics Workshop, Colorado School of Mines, Golden, Colorado, 15-17 August 1973*, pp. 130-139, National Technical Information Service, Springfield VA 22151, acc. no. PB 231 154.

Goddard, A. E. (1973), Radio propagation measurements in coal mines at UHF and VLF, in *Proceedings of Thru-the-Earth Electromagnetics Workshop, Colorado School of Mines, Golden, Colorado, 15-17 August 1973*, pp. 54-61, National Technical Information Service, Springfield, VA 22151, acc. no. PB 231 154.

Hill, D. A., and J. R. Wait (1974*a*), Excitation of monofilar and bifilar modes on a transmission line in a circular tunnel, *J. Appl. Phys.*, *45*(8), 3402-3406.

Hill, D. A., and J. R. Wait (1974*b*), Gap excitation of an axial conductor in a circular tunnel, *J. Appl. Phys.*, *45*(11), 4774-4777.

Mahmoud, S. F. (1974*a*), Characteristics of EM guided waves for communication in coal mine tunnels, *IEEE Trans. Commun.*, *COM-22*(10), 1547-1554.

Mahmoud, S. F. (1974*b*), On the attenuation of monofilar and bifilar modes in mine tunnels, *IEEE Trans. Microwave Theory Tech.*, *MTT-22*(9), 845-847.

Mahmoud, S. F., and J. R. Wait (1974*a*), Theory of wave propagation along a thin wire inside a rectangular waveguide, *Radio Sci.*, *9*(3), 417-420.

Mahmoud, S. F., and J. R. Wait (1974*b*), Guided electromagnetic waves in a curved rectangular mine tunnel, *Radio Sci.*, *9*(5), 567-572.

Mahmoud, S. F., and J. R. Wait (1974*c*), Geometrical optical approach for electromagnetic wave propagation in rectangular mine tunnels, *Radio Sci.*, *9*(12), 1147-1158.

Martin, D. J. R. (1970), Radiocommunication in mines and tunnels, *Electron. Lett.*, *6*(18), 563-564.

Wait, J. R. (Ed.) (1974), Special Issue on ELF Communications, *IEEE Trans. Commun.*, *COM-22*(4), 353-588.

Wait, J. R., and D. A. Hill (1974*a*), Guided electromagnetic waves along an axial conductor in a circular tunnel, *IEEE Trans. Antennas Propagat.*, *AP-22*(4), 627-630.

Wait, J. R., and D. A. Hill (1974*b*), Coaxial and bifilar modes on a transmission line in a circular tunnel, *Appl. Phys.*, *4*(1), 1-6.

UDC 538.3:621.315.212.1:622.489

Theory of transmission of electromagnetic waves along multi-conductor lines in the proximity of walls of mine tunnels

JAMES R. WAIT, B.A.Sc., M.A.Sc., Ph.D.*

Based on a paper presented at the Symposium on Leaky Feeder Radio Communication Systems held at the University of Surrey on 9th and 10th April 1974.

SUMMARY

Using a boundary value analysis, the transmission of the propagation modes in the tunnel are considered. As expected, there is a conventional TEM-like mode that has relatively high loss due to the finite conductivity of the tunnel walls. In addition, however, we find that other modes exist when there are two or more axial conductors present in the tunnel. These have relatively low attenuation but such modes are difficult to excite. The optimum system requires the exploitation of both classes of modes. The object of this paper is to provide the analytical framework that can be used for the quantitative design of such systems.

* *Environmental Research Laboratories, National Oceanic and Atmospheric Administration, US Department of Commerce, Boulder, Colorado 80302.*

A rather ingenious communication technique is being developed for use in Belgian coal mines.[1-3] The idea is to use a two-wire transmission line or equivalent loosely braided coaxial cable that can be suspended from the upper wall. A transmitter placed in the vicinity of the line excites a strongly unbalanced mode that normally would propagate like a coaxial or TEM mode with relatively high attenuation. The key step in the Belgian system, and the closely related French system,[3] is to convert this unbalanced mode to a balanced mode that is much less attenuated because the return current flows mostly in the second wire rather than through the surrounding rock. The physical basis of this system has many similarities to the leaky feeder device described by Martin[4] and used in British coal mines.

Here we carry out an analysis of the propagation characteristics for an idealized mine tunnel of circular cross section. The extension to a rectangular tunnel is also mentioned. The theory is developed only for a uniform structure so that mode conversion is not accounted for, but in all other respects the problem is quite general. Some comparison is made with relevant experimental data. Actually, we deal only with a twin open wire pair that is the basic ingredient of the so-called INIEX/Deryck system. However, as suggested above, the leaky braided cable system and the slotted cylindrical shielded cables have common features. The important point is that propagation modes, that depend on current flow in the tunnel walls, will suffer excessive attenuation while modes that utilize the second conductor at a return current path will have less attenuation. While such features have been recognized by current workers, we have undertaken an analytical study that permits a quantitative understanding of the loss mechanisms.

Specifically, we consider an air-filled tunnel of circular cross-section with radius a bounded by a lossy dielectric medium. Within this uniform tunnel we locate a single relatively thin metal conductor of radius c_s whose conductivity is σ_s. The situation is illustrated in Fig. 1(a) where we have chosen a cylindrical coordinate system (ρ, ϕ, z) to be coaxial with the guide. For the interior region $\rho < a$ the permittivity and permeability ε_0 and μ_0 respectively. For the exterior region, the permittivity, conductivity and permeability are ε_e, σ_e and μ_e respectively. The thin axial conductor is located at $\rho = \rho_0$ and $\phi = \phi_0$; its corresponding electric properties are ε_s, σ_s and μ_s. Here we restrict attention to the case $0 < \rho_0 < a$. Later, we consider the effect of a second wire conductor that is parallel to the first.

We now consider the complex propagation constant of the dominant modes of the structure. Thus, we assume that the fields of an individual mode varies with z according to $\exp(-\Gamma z)$ for an implied time factor $\exp(j\omega t)$ where the values of Γ are to be determined. As indicated elsewhere,[5] the fields can be determined by two scalar functions U and V that are, respectively, the z components of (axially directly) electric and magnetic Hertz vectors.

The current on the axial conductor can be designated $I\exp(-\Gamma z)$. The primary field within the tunnel from

this travelling wave of current may be derived from the electric-type Hertz function U^P. It is well known that

$$U^P = \frac{j\mu_0\omega}{2\pi\gamma_0^2} I \exp(-\Gamma z) K_0[(\gamma_0^2-\Gamma^2)^{\frac{1}{2}}\rho_d] \quad (1)$$

where

$$\gamma_0^2 = -\varepsilon_0\mu_0\omega^2, \quad \rho_d = [\rho^2+\rho_0^2-2\rho\rho_0\cos(\phi-\phi_0)]^{\frac{1}{2}},$$

and K_0 is the modified Bessel function of the second kind. Now the total Hertz function within the guide can be written, $U = U^P + U^S$, where U^S is the secondary part. The latter, for the region $\rho < a$, can be constructed by superimposing solutions of the type

$$I_m(v\rho)\exp(-jm\phi)\exp(-\Gamma z)$$

where I_m is a modified Bessel function of the first type, $v = (\gamma^2-\Gamma^2)^{\frac{1}{2}}$ and m is any integer.

The above considerations and the addition theorem for K_0 in (1) leads us to the representation

$$U = \sum_{m=-\infty}^{+\infty} U_m e^{-jm(\phi-\phi_0)} \quad (2a)$$

where

$$U_m = \frac{j\mu_0\omega}{2\pi\gamma_0^2} I e^{-\Gamma z} I_m(v\rho_0) \times \times \left[K_m(v\rho) - R_m \frac{K_m(va)}{I_m(va)} I_m(v\rho)\right] \quad (2b)$$

for the region $\rho_0 < \rho < a$ where R_m is yet to be determined. Similar considerations lead us to the corresponding representation for the magnetic type Hertz function for the region $\rho < a$. Thus,

$$V = \sum_{m=-\infty}^{+\infty} V_m e^{-jm(\phi-\phi_0)} \quad (3a)$$

where

$$V_m = \frac{j\mu_0\omega}{2\pi\gamma_0^2} I e^{-\Gamma z}\Delta_m I_m(v\rho_0) I_m(v\rho). \quad (3b)$$

For the external region $\rho > a$ the Hertz functions are both made up from solutions of the form

$$K_m(u\rho)\exp(-\Gamma z)\exp(-jm\phi)$$

where $u = (\gamma_e^2-\Gamma^2)^{\frac{1}{2}}$ and $\gamma_e^2 = j\mu_e\omega(\sigma_e - j\varepsilon_e\omega)$.

The boundary conditions at the wall $\rho = a$ are that the tangential fields are continuous. Using these we obtain the following explicit results[5] for the coefficient R_m in (2b)

$$R_m = \frac{[(\gamma_0/v)K'_m(va)/K_m(va)] + Y_m\eta_0 + \delta_m\eta_0}{[(\gamma_0/v)I'_m(va)/I_m(va)] + Y_m\eta_0 + \delta_m\eta_0} \quad (4)$$

where

$$\delta_m\eta_0 = \frac{(jm\Gamma/a)^2[v^{-2}-u^{-2}]^2}{[(\gamma_0/v)I'_m(va)/I_m(va)] + (Z_m/\eta_0)} \quad (5)$$

and $\eta_0 = j\mu_0\omega/\gamma_0 \simeq 120\pi$ ohms, where

$$Z_m = -(j\mu_e\omega/u)K'_m(ua)/K_m(ua),$$

and

$$Y_m = (j\gamma_e^2/u\mu_e\omega)K'_m(ua)/K_m(ua).$$

We can express the axial electric field E_z anywhere within the guide in terms of the still unknown current

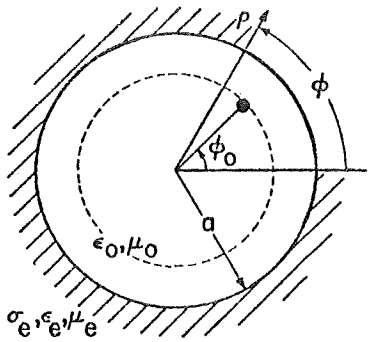

(a) Geometry for single wire conductor in circular air-filled tunnel in homogenous earth.

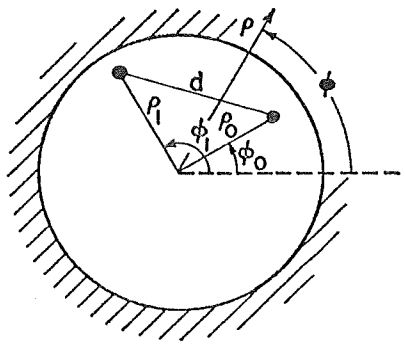

(b) Geometry for two arbitrarily located axial wires within tunnel.

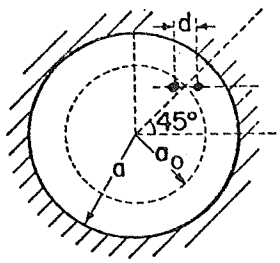

(c) Geometry for two axial wires located in a horizontal plane in the upper quadrant of the tunnel cross section. The mean distance to the tunnel wall is $a - a_0$.

Fig. 1.

$I\exp(-\Gamma z)$ on the wire. On combining (1), (2b) and the relation $E_z = -v^2U$, it follows that

$$E_z = -\frac{j\mu_0\omega I v^2}{2\pi\gamma_0^2} e^{-\Gamma z}\left[K_0(v\rho_d) - \sum_{m=-\infty}^{+\infty} R_m \frac{K_m(va)}{I_m(va)} \times \times I_m(v\rho_0)(I_m(v\rho)\, e^{-jm(\phi-\phi_0)}\right]. \quad (6)$$

Now the boundary condition at the wire is

$$E_z = IZ_s\exp(-\Gamma z) \quad (7)$$

at $\rho_d = c_s$ for all values of z where Z_s is the series impedance of the wire. Because of the assumed thinness of the wire, we can apply this condition at any point of the wire circumference. Thus, we choose the matching point at $\rho = \rho_0 + c_s$ and $\phi = \phi_0$. Thus (7) leads to the mode equation

$$\frac{-j\mu_0\omega v^2}{2\pi\gamma_0^2}\left[K_0(vc)-\sum_{m=-\infty}^{+\infty}R_m\frac{K_m(va)}{I_m(va)}\times\right.$$
$$\left.\times I_m(v\rho_0)I_m[v(\rho_0+c_s)]\right]=Z_s \qquad (8)$$

where the explicit result for the series impedance is

$$Z_s=\frac{\eta_s}{2\pi c_s}\frac{I_0(\gamma_s c_s)}{I_1(\gamma_s c_s)} \qquad (9)$$

where $\gamma^2=j\mu_s\omega(\sigma_s+j\varepsilon_s\omega)$ and $\eta_s=j\mu_s\omega/\gamma_s$.

We now consider the extension of the solution to the case where two axial conductors of radii c_0 and c_1 are present. The situation is illustrated in Fig. 1(b). Now I_0, the current on the conductor at (ρ_0, ϕ_0, z), is arbitrary, while I_1, the current on the conductor at (ρ_1, ϕ_1, z), is unknown. By superimposing solutions of the form (6) we can write

$$E_z=\frac{-j\mu\omega v^2}{2\pi\gamma^2}e^{-\Gamma z}\left\{I_0\left[K_0(v\rho_d)-\sum_{m=-\infty}^{\infty}R_m\frac{K_m(va)}{I_m(va)}\times\right.\right.$$
$$\times I_m(v\rho_0)I_m(v\rho)\,e^{-jm(\phi-\phi_0)}\Big]+I_1\left[K_0(v\rho_d')-\right.$$
$$-\sum_{m=-\infty}^{\infty}R_m\frac{K_m(va)}{I_m(va)}I_m(v\rho_1)I_m(v\rho)\times$$
$$\left.\left.\times e^{-jm(\phi-\phi_1)}\right]\right\} \qquad (10)$$

where

$$\rho_d=[\rho^2+\rho_0^2-2\rho\rho_0\cos(\phi-\phi_0)]^{\frac{1}{2}}$$

and

$$\rho_d'=[\rho^2+\rho_1^2-2\rho\rho_1\cos(\phi-\phi_1)]^{\frac{1}{2}}.$$

The two relevant boundary conditions are now:

$$E_z=I_0Z_{s0}e^{-\Gamma z}\quad\text{at}\quad\rho=\rho_0+c_0,\quad\phi=\phi_0. \qquad (11)$$

$$E_z=I_1Z_{s1}e^{-\Gamma z}\quad\text{at}\quad\rho=\rho_1+c_1,\quad\phi=\phi_1. \qquad (12)$$

where Z_{s0} and Z_{s1} are the appropriate series impedances. The unknowns are I_1 (or I_1/I_0) and Γ. We can easily eliminate I_1 to yield a mode equation.

The method can be generalized to an arbitrary number of N thin axial conductors located within the guide. An impedance condition as indicated above can be assumed for each wire. This yields a system of N linear equations for the N unknown wire currents. The system has a solution only if the following determinant is zero:

$$\begin{vmatrix}(A_{11}-Z_1) & A_{12} & \cdots & A_1\\ A_{21} & (A_{22}-Z_2) & \cdots & A_{2N}\\ \vdots & \vdots & & \vdots\\ A_{N1} & A_{N2} & \cdots & A_{NN}\end{vmatrix}=0 \qquad (13)$$

where A_{ij} is the z component of the electric field (primary plus secondary) produced at the match point on wire i by a unit current on wire j and Z_j is the series impedance of wire j. In what follows, we will just consider the case of two axial conductors, i.e. $N=2$.

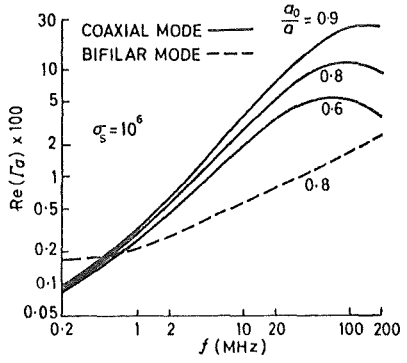

Fig. 2. The normalized attenuation rate as a function of frequency for the coaxial (or monofilar) and bifilar modes for a wire conductivity $\sigma_s=10^6$ S/m.

For the high-frequency modes of interest in air-filled tunnels, we expect Γ to be of the order of $\gamma_0=jk$ where $k=\omega/c$ is the free space wave number. Also, the bounding medium will have a conductivity and/or permittivity sufficiently high that $|\gamma_e a|\gg 1$. Thus, we find that $Z_m\simeq(j\mu_e\omega)/(\gamma^2+k^2)^{\frac{1}{2}}$ and $Y_m\simeq\gamma^2/[j\mu_e\omega(\gamma^2+k^2)^{\frac{1}{2}}]$. Also, in most cases at high frequencies, the conductivity of the metal wire will be sufficiently high that both $|\gamma_s c_s|\gg 1$ and $\sigma_s\gg\varepsilon_s\omega$. Then we can write

$$Z_s\simeq(\mu_s\omega/2\sigma_s)^{\frac{1}{2}}(1+j)/(\pi c_s).$$

In the actual calculations, these approximations are only made when they are valid.

The modes that have a transmission-line character as the frequency is lowered are of particular interest here. As we shall see, there are two classes of these: in one case the current ratio I_1/I_0 is approximately $+1$ and in the other case the ratio is approximately -1. For obvious reasons, these are designated the coaxial and bifilar modes, respectively. Actually, in the unlikely case that $\rho_0=\rho_1$, we have exactly $I_1=\pm I_0$. Using an adaptation of Newton's method, solutions of the desired type have been obtained for the specific configuration shown in Fig. 1(c). This is considered a reasonable idealization of the situation encountered in practice where the transmission line is suspended from the tunnel wall but offset from the centreline. An example is shown in Fig. 2 where the following parameters are assumed: $a=2$m, $\varepsilon_e=10\varepsilon_0$, $\sigma_e=10^{-2}$ S/m, $\sigma_s=10^6$ S/m, $c_s=10^{-3}$ m $=1$ mm, and $d=0{\cdot}02$ m $=2$ cm. Various values of the ratio a_0/a are shown for the coaxial or monofilar mode but only the value 0·8 for the bifilar mode. In the latter case, the corresponding values for 0·9 and 0·6 are indistinguishable. Here the real part of (Γa), which is proportional to the attenuation rate, is plotted as a function of frequency from 0·2 to 200 MHz. The increase of the coaxial mode attenuation as the wire conductor approaches the wall is apparent. Actually, the attenuation rates are quite dependent on the assumed wire conductivity but the dependence on the other parameters, such as c_s and d, is not so severe.

For the geometry of the tunnel guide considered in the preceding example, we can expect higher-order waveguide modes to appear when the frequency exceeds the cut-off value for the empty tube. This occurs approximately at 50 MHz in this case. For higher frequencies,

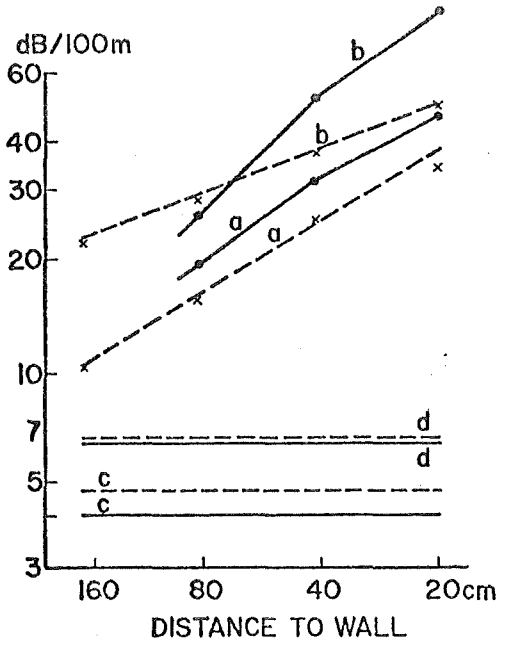

Fig. 3. Comparison of calculated (solid curves) and Deryck's observed (broken curves) data of attenuation rate as a function of the distance of the transmission line from the tunnel wall. Curves a and b are for the coaxial mode for 27 and 68 MHz, respectively, while curves c and d are for the bifilar mode for 27 and 68 MHz.

we can expect the situation to be quite complicated. However, it appears we can always identify the coaxial and bifilar modes as the ones that are significantly influenced by the location and the series impedance of the wire conductor. Actually, we have calculated also these 'waveguide modes' for various cylindrical geometries but the results are not given here. Suffice it to say that such modes have a very weak dependence on the conductivity of the axial wire conductors within the tunnel.

We can make a specific comparison of our calculated results of the attenuation rates with some experimental data published by Deryck[1] for coaxial and bifilar mode propagation in a tunnel in Lanaye, Belgium. The actual tunnel has a total height of the order of 4 to 5 m and the width is of the order of 3 to 4 m. The comparison is indicated in Fig. 3, where the abscissa is the distance of the transmission line from the tunnel wall and the ordinate is the attenuation rate in decibels per metre. The calculated results use the same parameters as in Fig. 2. As both the experimental and the theoretical curves show, there is a strong dependence on the proximity of the tunnel wall for the coaxial mode at both 27 and 68 MHz. On the other hand, there is virtually no dependence on the location of the transmission line for the case of the bifilar mode. This, of course, is an attractive feature for long distance communication. As Deryck[1] indicates, conversion from the easily excited coaxial mode to the bifilar mode permits efficient point-to-point communication, even when the transmitting and/or receiving antennas are not closely coupled to the transmission line.

In our analysis, we have adopted an idealized circular cross-section for the tunnel. Thus, strictly speaking, the calculated data are not valid for actual tunnels or haulageways in operational mines. However, it is interesting to note that the present results for the coaxial and bifilar modes are very similar to corresponding calculations carried out by Mahmoud[6] for rectangular tunnels. Unfortunately, an exact modal analysis[7] for the rectangular-shaped tunnel is only possible when the side walls are either perfectly electric or perfect magnetic conductors. Nevertheless, as we have illustrated in detail elsewhere,[8] the principal characteristics of the coaxial and bifilar modes are very similar in the two geometries. This suggests that the derived characteristics are qualitatively valid for non-circular tunnels provided the cross-sectional area is approximately the same.

Acknowledgments

I am very grateful to Dr. David A. Hill for his contributions to this paper. Also, I thank Dr. Samir F. Mahmoud for many useful discussions.

The views and conclusions contained in this document are those of the author and do not necessarily represent the official policy of the U.S. Bureau of Mines. The research was sponsored by USBM Contract HO122061, monitored by Dr. James A. Powell.

References

1. Deryck, L., 'Radio communication in tunnels', *Electronics Letters*, **8**, No. 3, pp. 71–2, 10th February 1972; 'Echanges d'energie entre modes de propagation sur ligne bifilaire', *Bull. Tech. 'Mines et Carriers'*, No. 134, December 1971 (Institut National des Industries Extractives, Belgium).
2. Delogne, P., Deryck, L. and Liégeois, R., 'Guided propagation of radio waves', Proceedings of Thru-the-Earth Electromagnetics Workshop, pp. 49–53, Colorado School of Mines, Golden, Colo., 15th–17th August 1973, edited by R. G. Geyer, Final Report USBM Grant No. G133023. (Available from National Technical Information Service, Springfield, Va 22151, U.S.A.).
3. Fontaine, J., Demoulin, B., Degauque, P. and Gabillard, R., 'Feasibility of radio communication in mine galleries by means of a coaxial cable having a high coupling impedance', Proceedings of Thru-the-Earth Electromagnetics Workshop, pp. 130–9, 1973.
4. Martin, D. J. R., 'Radio communication in mines and tunnels', *Electronics Letters*, **6**, pp. 563–4, 26th October 1970.
5. Wait, J. R. and Hill, D. A., 'Guided electromagnetic waves along an axial conductor in a circular tunnel', *IEEE Trans. on Antennas and Propagation*, **AP-22**, No. 4, pp. 627–30, July 1974.
6. Mahmoud, S. F., 'Characteristics of e.m. guided waves for communication in coal mine tunnels', *IEEE Trans. on Communications*, **COM-22**, No. 10, pp. 1547–54, October 1974.
7. Mahmoud, S. F. and Wait, J. R., 'Theory of wave propagation along a thin wire inside a rectangular waveguide', *Radio Science*, **9**, No. 4, pp. 417–20, March 1974.
8. Wait, J. R., Hill, D. A. and Mahmoud, S. F., 'Studies of electromagnetic waves on monofilar and bifilar structures in circular and rectangular mine tunnels', International Conference 'Radio: Roads, Tunnels and Mines', Liège, Belgium, 1st–5th April 1974.

Manuscript received by the Institution on 5th August 1974. (Paper No. 1640/Com. 110).

Radio Science, Volume 9, Number 3, pages 417–420, March 1974

Theory of wave propagation along a thin wire inside a rectangular waveguide

Samir F. Mahmoud and James R. Wait

Cooperative Institute for Research in Environmental Sciences, University of Colorado, Boulder, Colorado 80302

(Received December 12, 1973.)

A modal equation for the propagation constants along a thin wire located inside a rectangular waveguide is derived. The regions external to the two horizontal broad walls are homogeneous lossy dielectrics. To facilitate the analysis, the two narrow vertical walls are assumed to be either perfect electric or perfect magnetic reflectors. Special cases that have been treated earlier [*Wait*, 1972] are recovered.

INTRODUCTION

The problem of wave propagation along an infinitely long straight wire located in a stratified medium has recently received attention [*Wait*, 1972] due to its importance in several applications. A related problem, which arises in dealing with radio propagation in coal mines (A. E. Goddard, personal communication, 1972; A. G. Emslie, R. L. Lagace, and P. F. Strong, personal communication, 1973) is that of wave propagation along an infinite wire located inside a rectangular waveguide with imperfectly reflecting boundaries. Here, we investigate a simplified version of this problem where one parallel pair of the guide boundaries is considered to be a perfect reflector. The other two boundaries are plane interfaces that separate the inside medium (air) from the outside media, which are lossy dielectrics in general.

We deduce a modal equation for the propagation constants along the wire which is in a suitable form to yield numerical results. These will be reported subsequently (by S. F. M.). The derivation is basically similar to that introduced by *Wait* [1972] and the obtained modal equation reduces to that in the above reference when the appropriate boundaries recede to ∞.

FORMULATION

The geometry of the problem is illustrated in Figure 1. The boundaries along the whole planes $x = 0$ and $x = 2a$ are assumed to be either perfect electric or perfect magnetic walls (i.e., infinite conductivity or infinite permeability, respectively). The semi-infinite media above the plane $y = 2b$ and below the plane $y = 0$ have electrical constants ϵ_1, μ_0 and ϵ_2, μ_0 respectively. Here the permittivities ϵ_1 and ϵ_2 may be generally complex to account for ohmic losses. The interior of the guide is filled with air with constants ϵ_0, μ_0 taken to be the same as free space. As before [*Wait*, 1972], we assume that the wire carries a current of the form $I \exp(i\omega t - \Gamma z)$ where ω is the angular frequency and Γ is the propagation constant that is to be determined. The factor $\exp(i\omega t - \Gamma z)$, common to all fields, is dropped for convenience in what follows.

SOLUTION

The total electromagnetic fields in each medium can be obtained from any two appropriate scalar potentials. In the present problem, it is most convenient to choose these potentials to be axial and transverse electric potentials Π_z and Π_y rather than two axial electric and magnetic potentials as used before [*Wait*, 1972]. This choice results in a considerable simplication of the algebra because the incident Π_y on any of the interfaces $y = 0$ and $y = 2b$ does not couple with a reflected Π_z (although the reverse is not true). However, now both potentials are coupled by the axial conductor.

Now assuming that the boundaries $x = 0$ and $x = 2a$ are perfect electric walls, appropriate forms for Π_z, and Π_y, in region 1, $2b \geq y \geq y_0$ are

$$\Pi_{z1} = \sum_m A_m \sin(m\pi x/2a)\{\exp[u_m(2b - y)] + R_{m1} \exp[-u_m(2b - y)]\} \quad (1)$$

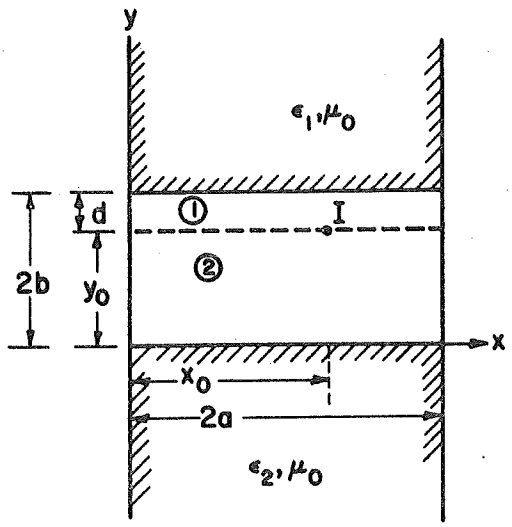

Fig. 1. Geometry for an infinite wire inside a rectangular waveguide.

$$\Pi_{y1} = \sum_m A_m R_{m1}^* \sin(m\pi x/2a) \cdot \exp[-u_m(2b - y)] + A_m^* \sin(m\pi x/2a) \cdot \{\exp[u_m(2b - y)] + S_{m1} \cdot \exp[-u_m(2b - y)]\} \quad (2)$$

Similarly for the region $y \geq 2b$, we write

$$\Pi_{z1} = \sum_m A_m T_{m1} \sin(m\pi x/2a) \cdot \exp[u_{m1}(2b - y)] \quad (3)$$

$$\Pi_{y1} = \sum_m (A_m T_{m1}^* + A_m^* \tau_{m1}) \cdot \sin(m\pi x/2a) \exp[u_{m1}(2b - y)] \quad (4)$$

where

$$u_m = [-k_0^2 - \Gamma^2 + (m\pi/2a)^2]^{1/2}$$

$$u_{m1} = [-k_1^2 - \Gamma^2 + (m\pi/2a)^2]^{1/2}$$

while $k_0^2 = \omega^2\mu_0\epsilon_0$, $k_1^2 = \omega^2\mu_0\epsilon_1$, and the integer m takes all values from 0 to ∞. The unknown reflection and transmission factors R_{m1}, R_{m1}^*, T_{m1}, T_{m1}^* and S_{m1}, and τ_{m1} are to be determined from the boundary conditions at the interface $y = 2b$. It is important to note that we can separately match those terms in equations 1 through 4 which involve the first four factors and those which involve the last two. The field components are related to the scalar potentials Π_z and Π_y by well-known formulas [*Wait*, 1959]. Thus we find that the resulting reflection coefficients are given by

$$R_{m1} = (u_m - u_{m1})/(u_m + u_{m1}) \quad (5)$$

$$R_{m1}^* = 2\Gamma[(u_m + u_{m1})^{-1} - k_0^2/(k_1^2 u_m + k_0^2 u_{m1})] \quad (6)$$

$$S_{m1} = (\epsilon_1 u_m - \epsilon_0 u_{m1})/(\epsilon_1 u_m + \epsilon_0 u_{m1}) \quad (7)$$

In a similar manner we obtain the potentials Π_z and Π_y in region 2, $y_0 \geq y \geq 0$, as:

$$\Pi_{z2} = \sum_m B_m \sin(m\pi x/2a) \cdot [\exp(u_m y) + R_{m2} \exp(-u_m y)] \quad (8)$$

$$\Pi_{y2} = \sum_m -B_m R_{m2}^* \sin(m\pi x/2a) \cdot \exp(-u_m y) + B_m^* \sin(m\pi x/2a) \cdot [\exp(u_m y) + S_{m2} \exp(-u_m y)] \quad (9)$$

where the reflection coefficients R_{m2}, R_{m2}^*, and S_{m2} are given by (5), (6), and (7) with a change of the subscript 1 to 2.

To proceed, we note that the coefficients A_m, A_m^*, B_m, and B_m^* are as yet unknowns to be determined from the boundary conditions at $y = y_0$. The source which has the form $I\,\delta(x - x_0)\,\delta(y - y_0)$ can be expanded in a Fourier series of the form

$$I\delta(x - x_0)\,\delta(y - y_0) = \delta(y - y_0) \sum I_m \sin(m\pi x/2a) \quad (10)$$

where

$$I_m = (I/a) \sin(m\pi x_0/2a) \quad (11)$$

The tangential fields at $y = y_0$ are continuous for each value of m, except for H_x which has a discontinuity equal to I_m. This reduces to the continuity of Π_z, Π_y, and $\partial\Pi_y/\partial y$, and the discontinuity of $\partial\Pi_z/\partial y$ such that

$$[\partial\Pi_{z2}/\partial y]_{y=y_0-} - [\partial\Pi_{z1}/\partial y]_{y=y_0+} = \sum_m I_m/i\omega\epsilon_0 \sin(m\pi x/2a)$$

Using (1) and (8) in the above equation and in the equation of the continuity of Π_z, and solving for the coefficients A_m and B_m we obtain:

$$A_m = (I_m/i\omega\epsilon_0 u_m) f_{m2}(y_0)/\Delta_m \quad (12)$$

$$B_m = (I_m/i\omega\epsilon_0 u_m) f_{m1}(d)/\Delta_m \quad (13)$$

where

$$f_{m1(2)}(y) = (1/2)[\exp(u_m y) + R_{m1(2)} \exp(-u_m y)] \quad (14)$$

$$\Delta_m = \exp(2u_m b)[1 - R_{m1}R_{m2} \exp(-4u_m b)] \quad (15)$$

The remaining two boundary conditions at $y = y_0$ give A_m^* and B_m^* as

$$A_m^* = [A_m R_{m1}^* S_{m2} \cdot \exp(-2u_m b) - B_m R_{m2}^*]/\Delta_m^* \quad (16)$$

$$B_m^* = [A_m R_{m1}^* - B_m R_{m2}^* S_{m1} \cdot \exp(-2u_m b)]/\Delta_m^* \quad (17)$$

where

$$\Delta_m^* = \exp(2u_m b)[1 - S_{m1}S_{m2} \exp(-4u_m b)] \quad (18)$$

In passing, we note that the natural modes of the empty guide are given by solutions of $\Delta_m = 0$ and $\Delta_m^* = 0$, corresponding to horizontally and vertically polarized modes respectively [*Wait*, 1970].

Now that all the terms in (1) and (2) are determined, we can obtain the axial electric field E_{z1} in region 1 as:

$$E_{z1} = -(i\omega\mu_0 I/\pi)B(\Gamma) \quad (19)$$

where

$$B(\Gamma) = (1 + \Gamma^2/k_0^2) \sum_m P_m(x; x_0) f_{m2}(y_0) \cdot f_{m1}(2b - y)/u_m \Delta_m - (\Gamma/k_0^2) \sum_m P_m(x; x_0) \cdot [R_{m1}^* f_{m2}(y_0) g_{m2}(y) + R_{m2}^* \cdot f_{m1}(d) g_{m1}(2b - y)]/\Delta_m \Delta_m^* \quad (20)$$

The only undefined terms in the above are

$$P_m(x; x_0) = (2\pi/a) \sin(m\pi x/2a) \sin(m\pi x_0/2a) \quad (21)$$

and

$$g_{m1(2)}(y) = (1/2)[\exp(u_m y) - S_{m1(2)} \exp(-u_m y)] \quad (22)$$

In the case when the planes $x = 0$ and $x = 2a$ correspond to perfect magnetic walls, equations 19 through 22 apply except that $P_m(x; x_0)$ is now redefined as

$$P_m(x; x_0) = (2\pi/a)\epsilon_m \cos(m\pi x/2a) \cos(m\pi x_0/2a)$$

where $\epsilon_m = 1$ for $m > 0$ and $1/2$ for $m = 0$.

Subject to the thin-wire assumption, we now obtain the desired modal equation for Γ by equating E_{z1} at $x = x_0$ and $y = y_0 + \rho$ by $Z_w I$ where ρ is the radius of the wire and Z_w is the series impedance of the wire. This is given in terms of the modified Bessel functions by *Wait* [1954],

$$Z_w = \eta_w I_0(\gamma_w \rho)/[2\pi\rho I_1(\gamma_w \rho)]$$

where

$$\eta_w = [i\mu_w\omega/(\sigma_w + i\epsilon_w\omega)]^{1/2}$$

$$\gamma_w = [i\mu_w\omega(\sigma_w + i\epsilon_w\omega)]^{1/2}$$

and ϵ_w, σ_w, and μ_w are the electrical parameters of the wire. Our modal equation is thus given by

$$D(\Gamma) + Z_w/(i\omega\mu_0/\pi) = 0 \quad (23)$$

where

$$D(\Gamma) = (1 + \Gamma^2/k_0^2) \sum P_m(x_0; x_0) f_{m2}(y_0) \cdot f_{m1}(d - \rho)/u_m \Delta_m - (\Gamma/k_0^2) \sum P_m(x_0; x_0) \cdot [R_{m1}^* f_{m2}(y_0) g_{m2}(y_0 + \rho) + R_{m2}^* \cdot f_{m1}(d) g_{m1}(d - \rho)]/\Delta_m \Delta_m^* \quad (24)$$

SPECIAL CASES

We now recover some of the important special cases of the modal equation, (23). First, when the wire lies on the upper boundary $y = 2b$, i.e., $y_0 = 2b - \rho$, and if $Z_w = 0$, a valid solution for Γ can be obtained from the behavior of the mth term in the summation of (23) as $m \to \infty$. Under this condition, the following approximations can be made:

$$u_m \to m\pi/2a$$

$$R_{m1}^* \to \Gamma[(\epsilon_1 - \epsilon_0)/(\epsilon_1 + \epsilon_0)]/u_m$$

$$f_{m1}(y), g_{m1}(y) \to \exp(u_m y)$$

$$\Delta_m, \Delta_m^* \to \exp(2u_m b)$$

Then the modal equation, (23), reduces to

$$(1 + \Gamma^2/k_0^2) - \Gamma^2/k_0^2(\epsilon_1 - \epsilon_0)/(\epsilon_1 + \epsilon_0) = 0$$

whose solution is $\Gamma^2 = -(k_0^2 + k_1^2)/2$.

This agrees with the result obtained earlier [*Coleman*, 1950; *Wait*, 1972] for the case of a thin wire on the interface between two semi-infinite homogeneous media.

Another important case is the case when the boundaries $x = 0$ and $x = 2a$ recede to $\mp\infty$ and the structure reduces to the parallel plate guide. In this case, the summation over m changes into an integration from $-\infty$ to $+\infty$ over the parameter λ which replaces $m\pi/2a$ everywhere. The trigonometric functions of x change into $\exp(-i\lambda x)$ and the

function $P_m(x; x_0)$ becomes simply $\exp(-i\lambda x)$ (for $x_0 = 0$).

Furthermore, if we allow the upper boundary $y = 2b$ to recede to $+\infty$ $(2b \to \infty)$, we will have the case of a wire above a plane interface between two half spaces which has been treated earlier [*Wait*, 1972]. Upon using the following substitutions in (24):

$$2b \to \infty;\ R_1, R_1^*, S_1 \to 0; \quad \text{and} \quad \Delta, \Delta^* \to \exp(2ub)$$

we obtain $D(\Gamma)$ in the form

$$\begin{aligned} D(\Gamma) = (1/4)(1 + \Gamma^2/k_0^2) \int_{-\infty}^{\infty} \{ &\exp(-u\rho) \\ &+ R_2 \exp[-u(2y_0 + \rho)]\} u^{-1}\, d\lambda \\ &- (1/2)(\Gamma^2/k_0^2) \int_{-\infty}^{\infty} [1/(u + u_2) \\ &- k_0^2/(k_2^2 u + k_0^2 u_2)] \\ &\cdot \exp[-u(2y_0 + \rho)]\, d\lambda \end{aligned} \tag{25}$$

where the quantities u, u_2, R_2 are understood to be functions of λ. Equation 25 can be put in a slightly different form if we recognize that (see equation 5)

$$R_2 = -1 + 2u/(u + u_2)$$

Hence

$$\begin{aligned} D(\Gamma) = (1/2)(1 + \Gamma^2/k_0^2)\{ &K_0[i(k_0^2 + \Gamma^2)^{1/2}\rho] \\ &- K_0[i(k_0^2 + \Gamma^2)^{1/2}(2y_0 + \rho)]\} \\ &+ \int_0^{\infty} [1/(u + u_2) + \Gamma^2/(k_2^2 u + k_0^2 u_2)] \\ &\cdot \exp[-u(2y_0 + \rho)]\, d\lambda \end{aligned} \tag{26}$$

Equation 26 is the same as the corresponding one in [*Wait*, 1972] except for a different choice of the matching point on the wire perimeter.

CONCLUSIONS

The modal equation for the propagation constants along a thin wire located inside a rectangular waveguide is derived in a fashion similar to that used earlier [*Wait*, 1972]. The merits of the derived equation is that it is in a suitable form for a numerical treatment. Some of the important special cases are recovered and are seen to agree with previous work.

REFERENCES

Coleman, B. L. (1950), Propagation of electromagnetic disturbances along a thin wire in a horizontally stratified medium, *Phil. Mag., Ser. 7, 41*, 276–288.

Wait, J. R. (1954), Reflection at arbitrary incidence from a parallel wire grid, *Appl. Sci. Res., B4*(6), 393–400.

Wait, J. R. (1959), *Electromagnetic Radiation from Cylindrical Structures*, p. 10, Pergamon, New York.

Wait, J. R. (1970), *Electromagnetic Waves in Stratified Media*, chap. 6, pp. 132–195, Pergamon, New York.

Wait, J. R. (1972), Theory of wave propagation along a thin wire parallel to an interface, *Radio Sci.*, 7(6), 675–679.

Reprinted by permission from
IEEE TRANSACTIONS ON COMMUNICATIONS
Vol. COM-22, No. 10, October 1974

Characteristics of Electromagnetic Guided Waves for Communication in Coal Mine Tunnels

SAMIR F. MAHMOUD, MEMBER, IEEE

Abstract—**We obtain numerical results of the attenuation and phase constants of the lowest order modes in a rectangular tunnel with an axial wire for various values of physical parameters that are important in intramine communications and remote control. Besides the perturbed free modes of the empty guide, a TEM-like mode, which is highly influenced by the wire impedance and location, is identified. Also the excitation mechanisms of the modes are considered from the standpoint of point-to-point communication within a mine tunnel.**

INTRODUCTION

THE IMPORTANCE of telecommunication in the operation of underground mine-tunnels is well recognized. For many years telephone lines have provided for such communication between the surface and the haulageways. However, recent measurements in mine tunnels [1] have shown that UHF radio signals can be effectively propagated through the tunnel and hence can provide a reliable alternative means of communication as well as remote control [2]. This means is considered more suited to modern mines where instantaneous communication to and among mobile men in the underground haulageways is increasingly in demand.

Normally, the haulageways are close to rectangular in cross section with dimensions of the order of few meters in width and height. Radio frequencies above about 500 MHz propagate through the tunnel via successive reflections from the tunnel walls. Due to the large dimensions of the cross section relative to the wavelength, the waves fall at almost grazing angles on the walls and hence suffer low loss. At lower frequencies (than 500 MHz) the

Paper approved by the Associate Editor for Communication Systems Disciplines of the IEEE Communications Society for publication without oral presentation. Manuscript received February 25, 1974; revised June 3, 1974.
The author is with Cairo University, Cairo, Egypt. He is on leave at the Cooperative Institute for Research in Environmental Sciences, University of Colorado, Boulder, Colo. 80302.

losses in the walls obviously increase while at higher frequencies than about 2 GHz, the excess loss due to the wall roughness becomes increasingly important as has been observed by Emslie *et al.* [3]. Thus the working range of radio frequencies for free propagation is considered to lie roughly between 500 MHz–2 GHz. However, haulageways usually contain longitudinal metallic pipes which can effectively alter the properties of the guided radio waves. The most important effect of these is the appearance of a coaxiallike mode which extends the lower end of the operating range of frequency, since this mode has a zero cutoff frequency.

Besides the possibility of free radio propagation in the tunnel, electromagnetic (EM) waves can also be guided along specially designed transmission lines (TL) working at frequencies well below the UHF band. Various types of TL's include the single-wire cable, the ribbon feeder [4], and coaxial lines that are designed to provide part of the fields outside the line (such as the braided coaxial line [5], the coaxial cable with annular slots [6], etc.). Basically, there are two distinct modes of wave propagation along a two-wire TL, the monofilar, and the bifilar modes. The monofilar, or the single-wire mode, is guided mainly between the TL and the inner walls of the tunnel while the bifilar, or the balanced mode, is characterized by antiphased current in the two wires of the TL and hence a less accessible signal in the tunnel. Obviously, the attenuation of the bifilar mode is considerably lower than that of the monofilar mode, since the latter suffers higher loss by the tunnel walls. In any given situation, it is very desirable to have means to control the amount of excitation of each of these modes in order to obtain the proper compromise between the signal accessibility in the tunnel and the total attenuation of the guided signal inside the cable. Some of these techniques are described by Deryck [7].

It is quite clear that a theoretical investigation of the various modes of propagation inside an actual tunnel is very complicated unless many simplifying assumptions are adopted. Emslie *et al.* [3] have derived an approximate formula for the attenuation constant of the lowest order modes of free preparation at UHF inside a rectangular tunnel. An estimate of the effect of roughness of the tunnel walls is also given by these authors. In a recent paper by Mahmoud and Wait [8], the authors have obtained a modal equation for the propagating modes for the case of a single wire inside a rectangular tunnel. To make possible a rigorous satisfaction of all the boundary conditions, the narrow walls of the guide were idealized as perfect electric or perfect magnetic walls. The resulting waveguide model is, nevertheless, believed to reveal the important characteristics of the propagating modes, as will be shown by the numerical results presented here.

NUMERICAL RESULTS

The geometry of the problem treated by Mahmoud and Wait [8] is shown in Fig. 1. The rectangular tunnel

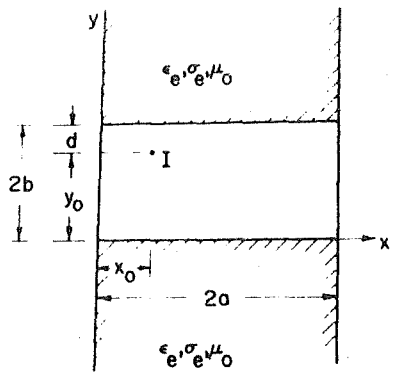

Fig. 1. A waveguide model of the tunnel.

is assumed to have horizontal and vertical dimensions equal to $2a$ and $2b$, respectively. The side walls are idealized as either perfect electric or perfect magnetic walls while the upper and lower walls are assumed to be lossy nonmagnetic homogeneous media of permittivity ϵ_e and conductivity σ_e. The interior of the tunnel is filled with air with constants ϵ_0,μ_0. The wire radius is ρ, the conductivity is σ_w and it is located at the point (x_0,y_0) inside the tunnel.

The modal equation developed in the previous paper is solved here for the propagation constant $\Gamma \equiv \alpha + i\beta$, where α and β are the attenuation and the phase constants, respectively. In Figs. 2–5, the following values are assumed: frequency = 1 GHz, $2a$ = 4.2667 m ($\simeq$ 14 ft), $2b = a$ = 2.1333 m ($\simeq$ 7 ft), ρ = 1 cm, $x_0 = a/2$, $\epsilon_e = 10\epsilon_0$, $\sigma_e = 10^{-2}$ mho/m, $\sigma_w = 10^5$ mho/m, and y_0 varies between b and $2b - \rho$. In Figs. 2–11, the solid curves refer to the case of perfect magnetic side walls, while the broken curves refer to the case of perfect electric side walls.

In Figs. 2–5, three types of modes are identified. The coaxial mode (labeled as CM) is a TEM-like mode which resembles the dominant mode in a coaxial circular guide. The other two types of modes are perturbed free modes of the empty guide and are labeled as $E_h(m,n)$ and $E_v(m,n)$ according to their dominant polarization (horizontal or vertical polarization, respectively). The integers m and n describe the mode order for the horizontal- and vertical-field variations in the usual sense. The following observations are derived from Figs. 2–5.

1) The phase velocity of the CM increases as the wire approaches the tunnel wall (Fig. 2).

2) The attenuation of the CM increases sharply as the wire approaches the tunnel wall (Fig. 3). This agrees with measurement in Belgium mine tunnels [2].

3) The $E_v(1,1)$ mode is significantly more affected by the wire than the $E_h(1,1)$ mode. The first may be related to the familiar vertically polarized ground wave with the forward wave tilt, hence the high interaction with the axial wire.

Figs. 6–9 show the effect of varying the wire conductivity σ_w. It is seen that both the phase constant and the attenuation of the CM are highly dependent on that parameter (Figs. 6 and 7). The CM becomes virtually cut off as the wire conductivity is decreased. On the

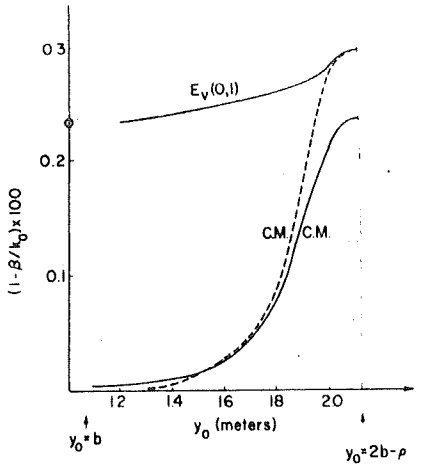

Fig. 2. Phase constant versus y_0 for the following parameters: $f = 1$ GHz, $a = 2b = 2.133$ m, $x_0 = a/2$, $\epsilon_e/\epsilon_0 = 10$, $\sigma_e = 10^{-2}$ mho/m, and $\sigma_w = 10^{+6}$ mho/m. ⊙ Unperturbed $E_v(0,1)$ mode. Solid curves and broken curves represent the cases of perfect magnetic and electric side walls, respectively.

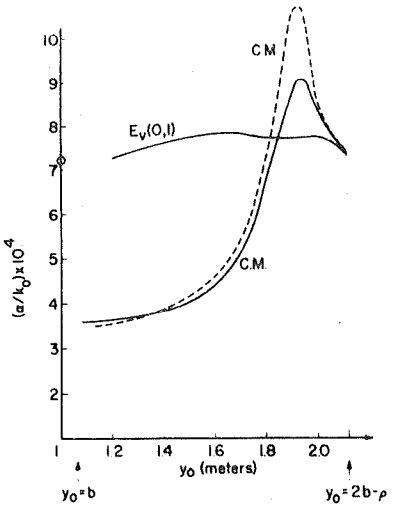

Fig. 3. Attenuation constant versus y_0. Same parameters as in Fig. 2.

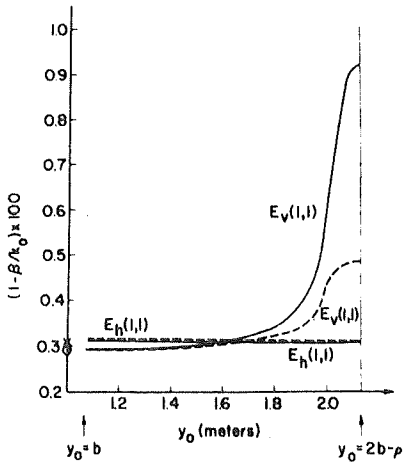

Fig. 4. Phase constant versus y_0. Same parameters as in Fig. 2. × unperturbed $E_h(1,1)$ mode. ⊙ unperturbed $E_v(1,1)$ mode.

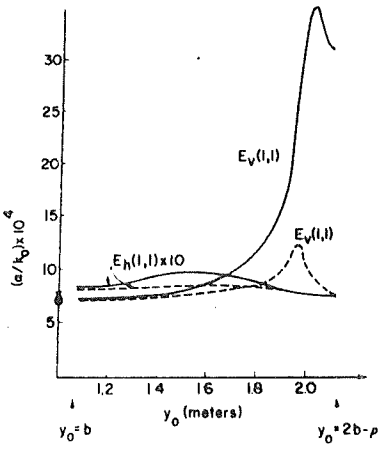

Fig. 5. Attenuation constant versus y_0. Same parameters as in Fig. 4.

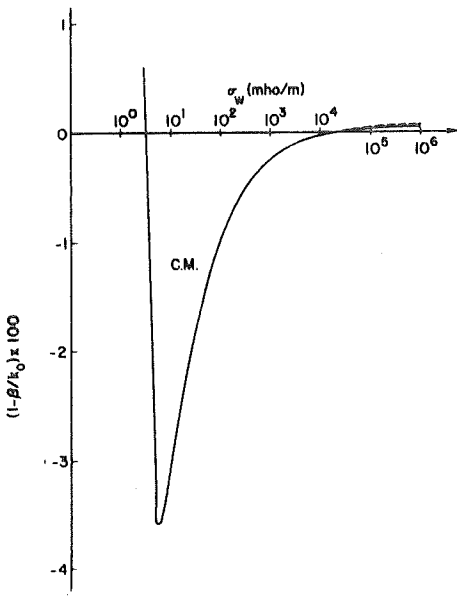

Fig. 6. Phase constant of the CM versus wire conductivity. $y_0 = 1.6$ m, and the other parameters are as in Fig. 2.

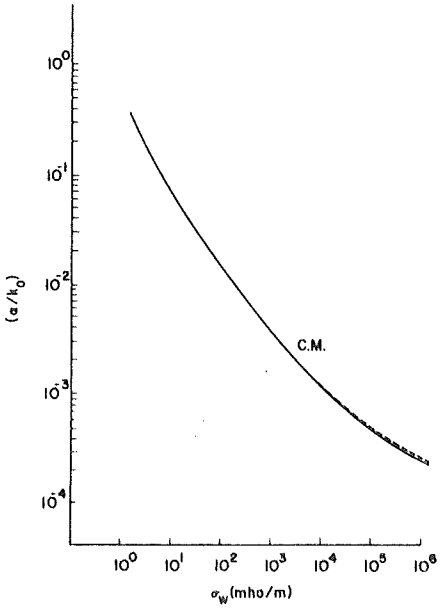

Fig. 7. Attenuation constant of the CM versus wire conductivity. Same parameters as in Fig. 6.

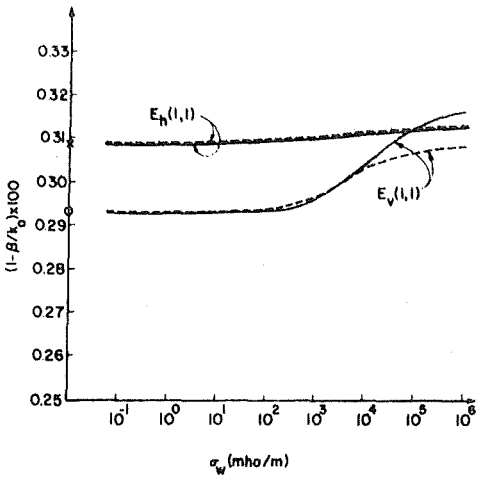

Fig. 8. Phase constant of the $E_h(1,1)$ and $E_v(1,1)$ modes versus wire conductivity. Same parameters as in Fig. 6.

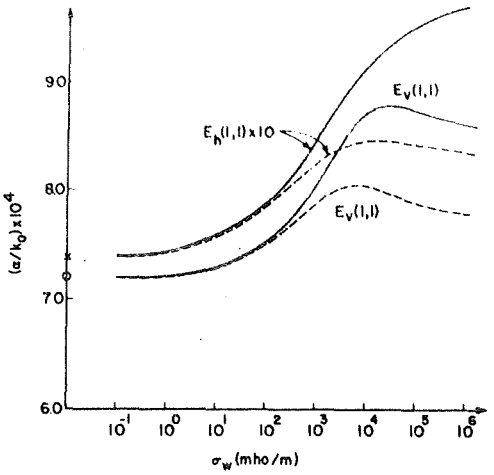

Fig. 9. Attenuation constant of the $E_h(1,1)$ and $E_v(1,1)$ modes versus wire conductivity. Same parameters as in Fig. 6.

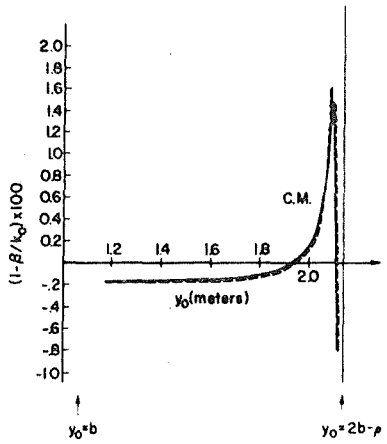

Fig. 10. Phase constant of the CM versus y_0. Same parameters as in Fig. 2, except ρ = 1 mm.

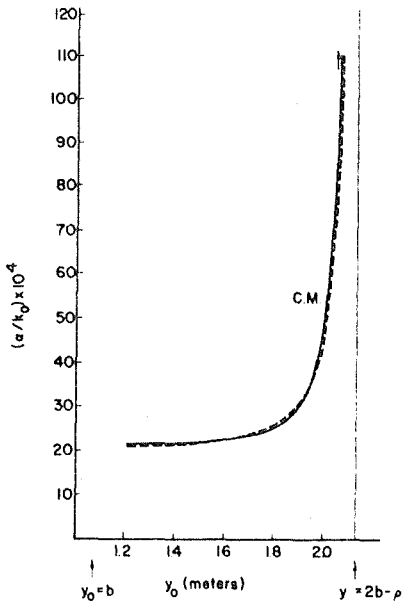

Fig. 11. Attenuation constant of the CM versus y_0. Same parameters as in Fig. 10.

other hand, (Figs. 8 and 9), the $E_v(1,1)$ and $E_h(1,1)$ modes show slight dependence on σ_w and tend to their unperturbed form as the latter becomes small.

The effect of reducing the wire radius to 1 mm is shown in Figs. 10 and 11. By comparing these with Figs. 2 and 3 (where ρ = 1 cm), it is clear that the increase in the phase velocity and the attenuation, as the wire approaches the guide wall, is more pronounced for the smaller wire case. The small differences observed between the electric and magnetic side-wall cases when ρ = 1 mm, suggest that the fields of the CM are concentrated near the wire.

Figs. 12 and 13 show that the attenuation of the CM increases as the frequency is reduced below 1 GHz, attains a peak which is accompanied by a reduction in the phase velocity, and then decreases monotonically as the frequency is further reduced. This effect can be easily explained since below 1 GHz the wall losses increase due to more penetrating fields. For considerably lower frequencies (~30 MHz or less) the walls behave more or less like good electrical conductors, and hence the attenuation is decreased. On the other hand, the free modes of the guide have monotonically increased attenuation (due to a cutoff phenomenon) with reduced frequency, and hence the coaxial mode becomes the dominant mode at low frequencies (i.e., 50 MHz or less for the present guide).

It is very constructive to compare the present results on the rectangular guide to those on the circular guide geometry treated by Wait and Hill [9]. We find a complete consistency between the mode characteristics in both guide geometries. This provides some support for the adequacy of the model used in this paper for the rectangular tunnel.

It is possible to estimate the effect of a finite loss in the side walls on the propagation constants of the modes by assuming that these walls behave as constant admit-

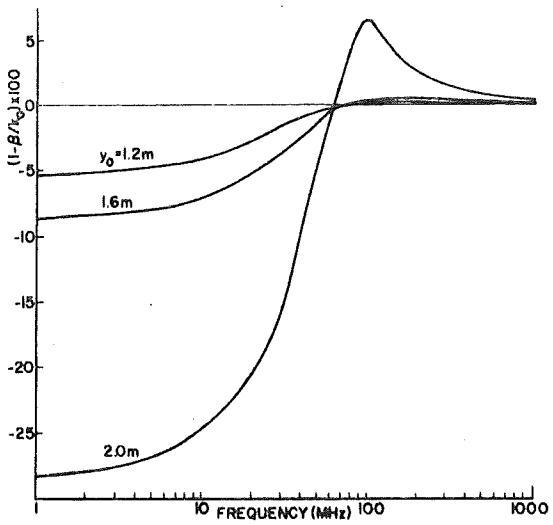

Fig. 12. Phase constant of the CM mode versus frequency for various values of y_0. Other parameters are as in Fig. 2. The side walls are assumed perfect electric conductors.

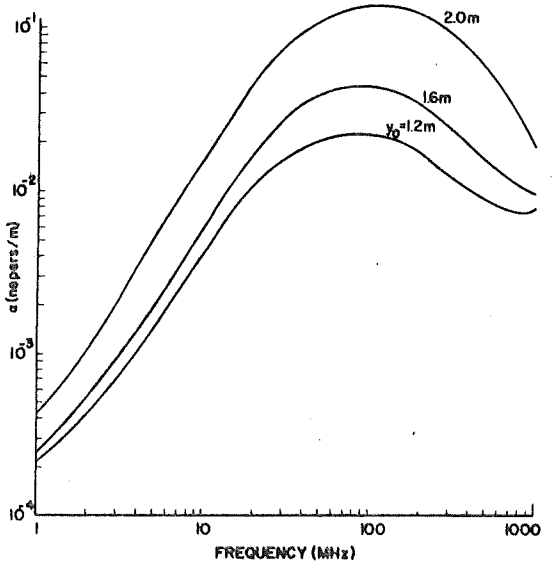

Fig. 13. Attenuation constant of the CM mode versus frequency. Same parameters as in Fig. 12.

tance or impedance boundaries and by using the simple perturbation technique. Unfortunately, however, this approach is found to have a very limited applicability in the present context since it applies only when the fields at the side walls are very small. Some of the results on the relative increase of the attenuation of the CM that are based on the perturbation technique are shown in Fig. 14. The side walls were assumed to have a constant impedance $Z = i\omega\mu_0/[\omega^2\mu_0(\epsilon_s - \epsilon_0) - i\omega\mu_0\sigma_s]^{1/2}$, which was obtained from a consideration of the Fresnel-reflection coefficient from the dielectric walls.

EXCITATION OF MODES

In the following we discuss the modal excitation by a dipole located inside the waveguide of Fig. 1. The purpose is to calculate the excited power in each of the lower order modes due to an assumed current distribution in the dipole.

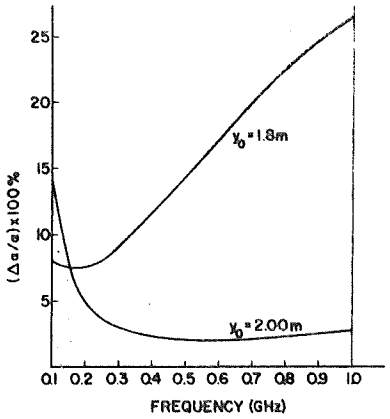

Fig. 14. Percentage increase in attenuation constant of the CM due to finite loss in the side walls versus frequency. Other parameters are as in Fig. 2.

First, assume that the source is a small dipole of moment $\bar{P}$, located at the point (x_a,y_a) in the $z = 0$ plane and lies totally, in an arbitrary direction, in this plane. The current density of the source can thus be written as

$$\bar{J}_a(x,y,z) = \bar{P}\delta(x - x_a)\delta(y - y_a)\delta(z). \quad (1)$$

Let the axial electric field due to the source be denoted by $E_{za}(x,y,z)$, which is, as yet, unknown. In order to determine this field, we shall use the known fields of an axial current at the point (x_0,y_0), which have been obtained by Mahmoud and Wait [8], and the reciprocity theorem. So assume a unit axial current at x_0,y_0 such that the current density is given by

$$J_z(x,y,z) = \exp(-i\beta z)\delta(x - x_0)\delta(y - y_0) \quad (2)$$

where $-\infty \leq \beta \leq \infty$ and let the total electric field produced by this current be

$$\bar{e}(x,y,\beta) = \{\bar{e}_t(x,y,\beta) + \bar{z}e_z(x,y,\beta)\} \exp(-i\beta z) \quad (3)$$

where $\bar{e}_t$ denotes the transverse components of the electric field and e_z the axial component. Explicit expressions for $\bar{e}_t$ and e_z are given in Appendix I.

Now we apply the reciprocity theorem to the two current densities given by (1) and (2) and their fields. Hence we get

$$\int_{x,y,z} \bar{J}_a(x,y,z)\cdot\bar{e}_t(x,y,\beta) \exp(-i\beta z)\, dxdydz$$

$$= \int_{x,y,z} J_z(x,y,z)E_{za}(x,y,z)\, dxdydz. \quad (4)$$

Upon substituting from (1) and (2), (4) is reduced to

$$\bar{P}\cdot\bar{e}_t(x_a,y_a,\beta) = \int_{-\infty}^{\infty} E_{za}(x_0,y_0,z) \exp(-i\beta z)\, dz$$

$$\triangleq E_{za}'(x_0,y_0,\beta) \quad (5)$$

where $E_{za}'(x_0,y_0,\beta)$ is recognized as the Fourier transform of $E_{za}(x_0,y_0,z)$, which in turn represents the average axial electric field at the surface of the wire due to the dipole current. Now we are in a position to obtain the induced

current in the axial wire $I_s(z)$. First, we expand this in a Fourier series, thus

$$I_s(z) = \frac{1}{2\pi}\int_{-\infty}^{\infty} I_s'(\beta)\exp(i\beta z)\,d\beta. \quad (6)$$

The boundary condition on the wire surface requires that

$$E_{sa}'(x_0,y_0,\beta) + I_s'(\beta)e_s(x_0,y_0+\rho,\beta) = Z_w I_s'(\beta), \quad -\infty \le \beta \le \infty. \quad (7)$$

Using (5) in (7) and solving for $I_s'(\beta)$, we obtain

$$I_s'(\beta) = \frac{-\bar{P}\cdot\bar{e}_t(x_a,y_a,\beta)}{e_s(x_0,y_0+\rho,\beta) - Z_w}. \quad (8)$$

Introducing the quantities $\bar{F}(x_a,y_a,\beta)$ and $D(\beta)$, defined by

$$\bar{F}(x_a,y_a,\beta) = (-i\omega\mu_0/\pi)\bar{e}_t(x_a,y_a,\beta) \quad (9)$$

and

$$D(\beta) = (-i\omega\mu_0/\pi)e_s(x_0,y_0,\beta) \quad (10)$$

we can write (8) in the alternative form

$$I_s'(\beta) = -\frac{\bar{P}\cdot\bar{F}(x_a,y_a,\beta)}{D(\beta) + Z_w/(i\omega\mu_0/\pi)}. \quad (11)$$

We notice that the zeros of the denominator on the right-hand side (RHS) of (11) determine the characteristic values of the propagation constants β_p of the waveguide modes [8]. So upon substituting from (11) into (6) and changing the integration into a summation of modes, we obtain

$$I_s(z) \simeq -i\,\mathrm{sgn}(z)\sum_p \frac{\bar{P}\cdot\bar{F}(x_a,y_a,\beta_p)}{(dD(\beta)/d\beta)_{\beta=\beta_p}}\exp(-i\beta_p z) \quad (12)$$

where $Im(\beta_p) < 0$ and Z_w is considered constant for the important range of β_p. Equation (12) applies for sufficiently high values of $|z|$ so that the neglect of the branch-cut contribution is justified. The total induced axial current in mode p due to an arbitrary line current $I_a(l_a)$ in the x–y plane is then given by

$$I_{sp} = -i\int_{l_a} I_a(l_a)\bar{F}(x_a,y_a,\beta_p)\cdot d\bar{l}_a/[dD(\beta)/d(\beta)]_{\beta=\beta_p} \cdot\exp(-i\beta_p|z|) \quad (13)$$

where the integration is taken over the line current l_a. The complex power carried by the pth mode (in the positive or negative z directions) is given by

$$P_p = |I_{sp}|^2 N_p^2 \quad (14)$$

where

$$N_p^2 = \int_{\text{cross section}} \bar{e}_t(x,y,\beta_p)\times\bar{h}_t^c(x,y,\beta_p)\cdot\bar{z}\,dxdy \quad (15)$$

with $\bar{h}_t^c(x,y,\beta_p)$ being the complex conjugate of the transverse magnetic field which is produced by the unit axial current given by (2). A more explicit expression for N_p^2 is given in Appendix II.

Now, it is convenient to define an excitation factor Λ_p for the pth mode as the ratio between the complex power P_p given by (14) and the maximum power excited by a $\lambda/2$ antenna, with a unit maximum current, in the dominant mode of an empty waveguide. The latter is similar to the original guide except that all the walls are perfect electric conductors. In such a guide, the dominant mode is the familiar TE_{10} mode and the maximum power excited in that mode by the assumed antenna is equal to $Z_0\lambda^2/([1-(\lambda/4a)^2]^{1/2}8\pi^2ab)$. Thus, combining (13) and (14), we can write Λ_p as

$$\Lambda_p = \frac{8\pi^2ab[1-(\lambda/4a)^2]^{1/2}}{\lambda^2 Z_0}\left|\int_{l_a} I_a(l_a)\bar{F}(x_a,y_a,\beta_p)\cdot d\bar{l}_a\right|^2 \cdot\frac{N_p^2}{|dD(\beta)/d\beta|_{\beta=\beta_p}^2}. \quad (16)$$

Some computed values of Λ_p for the CM, $E_h(1,1)$ and the $E_v(1,1)$ modes under various excitation conditions are given in Table I. The antenna locations are chosen according to the modal electric-field distributions, so as to maximize the power delivered by the antenna. The antenna current is assumed to have a sinusoidal variation and a maximum amplitude of unity (at the feeding point). At 1000 MHz, the horizontally polarized mode has the highest excitation coefficient when a $\lambda/2$ horizontal dipole is used. Furthermore, since this mode is the least attenuated mode, it will dominate over all other modes. For a $\lambda/2$ vertical dipole excitation, the CM and the $E_v(1,1)$ mode have comparable excitation coefficients which are considerably higher than that of $E_h(1,1)$ mode. For this type of excitation, the field polarization in the guide is mixed: the vertical and horizontal components of the electric field are of comparable magnitudes.

At 100 MHz and lower frequencies, the CM becomes the dominant mode in the guide. While the perturbed free modes are excited by the dipoles, they will be significant only in the near region of the source.

CONCLUSIONS

The modal equation derived earlier [8] for the geometry of Fig. 1 is solved numerically for the propagation constants of the lowest order modes. The results should have a direct use for intramine communication and remote control. A new TEM-like mode which depends heavily on the wire location and impedance is identified. This mode becomes the dominant mode of the guide at frequencies below the cutoff frequencies of the free modes, while at frequencies as high as 1 GHz it can have an attenuation constant which is lower than the vertically polarized mode.

The dipole excitation of the modes is considered and it is seen that the CM can be efficiently excited by (or received in) simple dipole antennas that lie in the transverse plane of the tunnel.

TABLE I
EXCITATION COEFFICIENT A_p
COMPUTED BY (16) FOR CM, $E_y(1,1)$ AND $E_y(1,2)$ MODES†

Frequency	Antenna Length & Orientation	Antenna Location (x_a, y_a)	CM	$E_y(1,1)$	$E_y(1,2)$
1000 MHz	$\frac{\lambda}{2}$ horizontal	(0.2a, b)	$6.21 \times 10^{-3}\ \angle -0.47°$	$2.5\ \angle +.004°$	$2.01 \times 10^{-2}\ \angle -.03°$
	$\frac{\lambda}{2}$ vertical	(0.6a, b)	$1.90\ \angle -0.47°$	$1.52 \times 10^{-2}\ \angle +.004°$	$1.68\ \angle -.05°$
			[0.149 dB/m]*	[0.0137 dB/m]	[0.191 dB/m]
100 MHz	$\frac{\lambda}{2}$ horizontal	(.25a, 1.25b	$1.14 \times 10^{-3}\ \angle -3.1°$	$2.92 \times 10^{-1}\ \angle 4.4°$	$4.72 \times 10^{-2}\ \angle -9.8°$
	$\frac{\lambda}{2}$ vertical	(a, 1.25b)	$1.97 \times 10^{-1}\ \angle -3.1°$	$2.22 \times 10^{-5}\ \angle 4.4°$	$3.55 \times 10^{-2}\ \angle -9.8°$
			[1.126 dB/m]	[1.822 dB/m]	[3.790 dB/m]

† The wire coordinates x_0, y_0 are $(0.5a, 1.875b)$ in all cases. The other guide parameters are as those in Fig. 2.
* The numbers in square brackets are attenuation constants of the modes.

APPENDIX I

THE MODAL FIELDS

The fields of the pth mode can be obtained from two scalar electric potentials π_x and π_y as [10]

$$e_x = -i\beta_p \frac{\partial}{\partial x}\pi_z + \frac{\partial^2}{\partial x \partial y}\pi_y$$

$$e_y = -i\beta_p \frac{\partial}{\partial y}\pi_z + \left(k_0^2 + \frac{\partial^2}{\partial y^2}\right)\pi_y$$

$$e_z = (k_0^2 - \beta_p^2)\pi_z - i\beta_p \frac{\partial}{\partial y}\pi_y$$

$$h_x = i\omega\epsilon_0(\partial\pi_z/\partial y + i\beta_p\pi_y)$$

$$h_y = -i\omega\epsilon_0\partial\pi_z/\partial x$$

$$h_z = i\omega\epsilon_0\partial\pi_y/\partial x \qquad (I.1)$$

where the factor $\exp(-i\beta_p z + i\omega t)$ is assumed to be common to all fields.

From [8], the potentials π_z and π_y in the interior region of the guide, produced by the axial current of (2), can be written as

$$\pi_z(x,y,\beta_p) = (-i\omega\mu_0/\pi k_0^2)\sum_{m=0}^{\infty} P_m(x,x_0) \cdot \begin{Bmatrix} f_m(d)f_m(y) \\ f_m(y_0)f_m(2b-y) \end{Bmatrix} \Big/ u_m\Delta_m, \quad y \lesseqgtr y_0 \qquad (I.2)$$

$$\pi_y(x,y,\beta_p) = (-i\omega\mu_0/\pi k_0^2)\sum_{m=0}^{\infty} P_m(x,x_0)R_m^*\{f_m(y_0)G_m(y) - f_m(d)G_m(2b-y)\}/u_m\Delta_m\Delta_m^* \qquad (I.3)$$

where

$$\begin{Bmatrix} f_m(y) \\ G_m(y) \end{Bmatrix} = \frac{1}{2}\left[\exp(+u_m y) + \begin{Bmatrix} R_m \\ S_m \end{Bmatrix}\exp(-u_m y)\right]$$

$$\begin{Bmatrix} \Delta_m \\ \Delta_m^* \end{Bmatrix} = \exp(2u_m b) - \begin{Bmatrix} R_m^2 \\ S_m^2 \end{Bmatrix}\exp(-2u_m b)$$

$$R_m = (u_m - u_{m1})/(u_m + u_{m1})$$

$$S_m = (k_e^2 u_m - k_0^2 u_{m1})/(k_e^2 u_m + k_0^2 u_{m1})$$

$$R_m^* = 2i\beta_p\{1/(u_m + u_{m1}) - k_0^2/(k_e^2 u_m + k_0^2 u_{m1})\}$$

$$u_m = ((m\pi/2a)^2 + \beta_p^2 - k_0^2)^{1/2}$$

$$u_{m1} = ((m\pi/2a)^2 + \beta_p^2 - k_e^2)^{1/2}$$

$$P_m(x,x_0) = \frac{2\pi}{a}\epsilon_m \begin{matrix}\sin \\ \cos\end{matrix}\left(\frac{m\pi x_0}{2a}\right) \begin{matrix}\sin \\ \cos\end{matrix}\left(\frac{m\pi x}{2a}\right)$$

for perfect electric or perfect magnetic side wall, respectively. $k_e^2 = \omega^2\mu_0(\epsilon_e - i\sigma_e/\omega)$, and $\epsilon_m = 1$ 2 for $m = 0$ and unity otherwise.

APPENDIX II

COMPLEX POWER OF A MODE

The complex power carried inside the guide by a given mode is defined as

$$N_p^2 = \int_{y=0}^{2b}\int_{x=0}^{2a}(e_x h_y^c - e_y h_x^c)\,dx\,dy \qquad (II.1)$$

where the superscript c denotes the complex conjugate operation. Using (I.1), the above can be expressed in terms of the potentials π_z and π_y as

$$N_p^2 = \int_{y=0}^{2b}\int_{x=0}^{2a}\left\{\frac{\partial}{\partial x}(-i\beta_p\pi_z + \pi_y)\left(i\omega\epsilon_0\frac{\partial}{\partial x}\pi_z^c\right) + i\omega\epsilon_0(\pi_z^{c\prime} + i\beta_p\pi_y^c)(-i\beta_p\pi_z' + k_0^2\pi_y + \pi_y'')\right\}dx\,dy \qquad (II.2)$$

where the prime indicates a differentiation with respect to y.

Before substituting (I.2) and (I.3) in (II.2), it is convenient to rewrite the first two equations in the following form

$$\pi_z(x,y,\beta_p) = (-i\omega\mu_0/\pi k_0^2) \sum_{m=0}^{\infty} P_m(x,x_0)\pi_{zm}(y) \quad \text{(II.3)}$$

$$\pi_y(x,y,\beta_p) = (-i\omega\mu_0/\pi k_0^2) \sum_{m=0}^{\infty} P_m(x,x_0)\pi_{ym}(y) \quad \text{(II.4)}$$

with $\pi_{zm}(y)$ and $\pi_{ym}(y)$ defined to make (II.3) and (II.4) identical to (I.2) and (I.3), respectively. k_0 is the free-space wavenumber.

Now we substitute from (II.3) and (II.4) in (II.2) and use the orthogonality of the sin or cos functions of x to obtain

$$N_p^2 = (2i\omega\mu_0/\pi k_0^2 a) \sum_{m=0}^{\infty} P_m(x_0,x_0) \cdot \int_{y=0}^{2b} \left\{ \left(\frac{m\pi}{2a}\right)^2 \pi_{zm}^c(-i\beta_p\pi_{zm} + \pi_{ym}') + (-i\beta_p\pi_{zm}' + (k_0^2 + u_m^2)\pi_{ym})(\pi_{ym}^{c\prime} - i\beta_p\pi_{ym}^c) \right\} dy. \quad \text{(II.5)}$$

Since π_{zm},π_{ym} and their derivatives satisfy the wave equation $\phi'' = u_m^2\phi$, the y integrations in (II.5) can be readily performed with due care to the discontinuity in π_{zm}' by $-1/2$ at $y = y_0$. The summation over m can be performed numerically.

ACKNOWLEDGMENT

The author wishes to thank Dr. J. R. Wait for many helpful discussions and for his encouragement.

REFERENCES

[1] A. E. Goddard, "Radio propagation measurements in coal mines at UHF and VHF," in *Proc. Through-the-Earth Electromagnetic Workshop* (Colorado School of Mines, Golden, Colo.), Aug. 21–24, 1973 (available from NTIS).
[2] P. Delogne, "Les communications par radio en milieu souterrain," *Acta Tech. (Belgium)*, vol. 9, pp. 17–26, 1973.
[3] A. G. Emslie, R. L. Lagace, and P. F. Strong, "Theory of propagation of UHF radio waves in coal mine tunnels," in *Proc. Golden Workshop* (Colorado School of Mines, Golden, Colo.), Aug. 21–24, 1973 (available from NTIS).
[4] D. J. R. Martin, "Radio communication in mines and tunnels," *Electron. Lett.*, vol. 6, pp. 563–564, 1970.
[5] ——, "Transferred surface currents in braided coaxial cables," *Electron. Lett.*, vol. 8, Aug. 3, 1972.
[6] R. De Keyser, P. Delogne, J. Janssens, and R. Liegeois, "Radio communication and control in mines and tunnels," *Electron. Lett.*, vol. 6, Oct. 26, 1970.
[7] L. Deryck, "Radio communication in tunnels," *Electron. Lett.*, vol. 8, Feb. 3, 1972.
[8] S. F. Mahmoud and J. R. Wait, "Theory of wave propagation along a thin wire inside a rectangular waveguide," *Radio Sci.*, vol. 9, pp. 417–420, Mar. 1974.
[9] J. R. Wait and D. A. Hill, "Guided electromagnetic waves along an axial conductor in a circular tunnel," *IEEE Trans. Antennas Propagat.* (Succinct Papers), vol. AP-22, pp. 627–630, July 1974.
[10] J. R. Wait, *Electromagnetic Radiation from Cylindrical Structures*. London, England: Pergamon, 1959, p. 10.

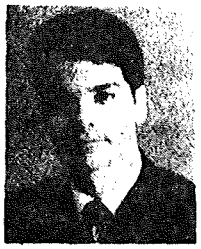

Samir F. Mahmoud (S'69–M'73) received the B.Sc. degree in electrical engineering from Cairo University, Cairo, Egypt, in 1964, and the M.Sc. and Ph.D. degrees from the Electrical Engineering Department, Queen's University, Kingston, Ont., Canada, in 1970 and 1973, respectively. His Ph.D. topic dealt with the electromagnetic aspects of obstacle detection schemes for guided ground-transportation systems.

He was appointed as a Teaching and Research Assistant at Cairo University, and for the academic year 1973–1974 he joined the Cooperative Institute for Research in Environmental Sciences at the University of Colorado, Boulder, as a Visiting Fellow. His current research topic is guided electromagnetic waves in mine tunnels.

Reprinted by permission from IEEE TRANSACTIONS ON MICROWAVE THEORY AND TECHNIQUES
Vol. MTT-22, No. 9, September 1974, pp. 845-847

On the Attenuation of Monofilar and Bifilar Modes in Mine Tunnels

SAMIR F. MAHMOUD

***Abstract*—The modal equations for both the monofilar and bifilar modes of a two open wire transmission line located in a waveguide model of a rectangular mine tunnel are derived by extending an earlier general analysis. Attenuation curves of both modes in the frequency range 200 kHz–200 MHz are presented for two distinct configurations of the transmission line that may be used in practice. It is demonstrated that the proximity of the lossy tunnel wall tends to increase greatly the attenuation rate for the monofilar modes but has relatively little effect on the bifilar modes.**

INTRODUCTION

Radio communication in mine tunnels can be provided by the free propagation of UHF waves in the tunnel which acts as a natural waveguide at this band of frequencies [1]. It is also possible to use much lower frequencies if a longitudinal conductor is stretched along the tunnel. Such a conductor will support a TEM-like mode, usually referred to as the monofilar mode, which is characterized by a zero cutoff frequency [2]. However, the fields of such a mode are accessible in the whole cross section of the tunnel at the expense of a high-power absorption by the tunnel walls. In order to reduce such loss, a two (or more) wire transmission line (TL) system should be used, whereby a new mode that has antiphased currents in the two wires is created. This mode, which is usually referred to as the bifilar mode, has fields that are concentrated in the near vicinity of the TL and hence suffers relatively low loss.

Attenuation measurements in some Belgium mine tunnels at 27 and 68 MHz affirm the lower attenuation of the bifilar mode relative to that of the monofilar mode [3]. The obviously important requirement of achieving controlled conversion between these two modes has been extensively studied by Delogne [2] and Deryck [4].

A rigorous modal equation for the monofilar mode of a single wire in a rectangular tunnel has recently been obtained by Mahmoud and Wait [5] under some simplifying assumptions concerning the two side walls of the tunnel. Also, extensive numerical results on the properties of this mode have been reported by the author [6]. In the present letter, we extend the analysis in [5] to derive the modal equations of the monofilar and bifilar modes of a two open wire TL inside the rectangular tunnel. Some specific results of the attenuation constants of these modes in a wide range of frequencies are presented.

THE MODAL EQUATIONS

We consider two configurations A and B of the TL as shown in Fig. 1. As in [5], the two side walls of the tunnel are assumed to behave as either perfect electric or perfect magnetic conductors, while the other two walls are taken as generally lossy dielectric media. In both configurations, A and B, we shall adopt the nonrestrictive assumption that $d \gg \rho$ where ρ is the radius of any of the wires. For a particular mode of propagation, all the fields in the guide and the currents in the two wires behave as $\exp(i\omega t - \Gamma z)$ where ω is the angular frequency and Γ is the complex propagation constant of the mode. So, apart from this common term, let the currents in the two wires be given by I_1 and I_2. The boundary condition at the surface of each wire requires that the longitudinal electric field be equal to the current multiplied by the series impedance Z_w per unit length of the wire. These conditions can be put in the convenient forms:

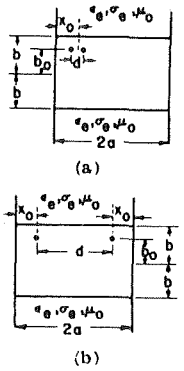

Fig. 1. Two configurations A and B of open wire TL inside a waveguide model of a rectangular tunnel.

$$Z_{s1}(\Gamma) I_1 + Z_m(\Gamma) I_2 = Z_{w1} I_1 \tag{1}$$

$$Z_m(\Gamma) I_1 + Z_{s2}(\Gamma) I_2 = Z_{w2} I_2 \tag{2}$$

where $Z_{s1}(\Gamma)$ is defined as the longitudinal electric field at the surface of the first wire due to a unit current in that wire and a similar definition applies to $Z_{s2}(\Gamma)$. $Z_m(\Gamma)$ is the longitudinal electric field at the surface of one wire due to a unit current in the other wire. These quantities are directly obtainable from (19) and (20) in [5] after the appropriate substitutions for the coordinates of the source and the observation point; e.g., $Z_{s1}(\Gamma)$ and $Z_m(\Gamma)$ for configuration A in Fig. 1 are given by

$$\begin{aligned} Z_{s1}(\Gamma) &= (-i\omega\mu_0/\pi) B(\Gamma) \,\Big|_{\substack{x_0 \to x_0 - d/2 \\ y_0 \to b + b_0 \\ x \to x_0 - d/2 \\ y \to b + b_0 + \rho}} \\ Z_m(\Gamma) &= (-i\omega\mu_0/\pi) B(\Gamma) \,\Big|_{\substack{x_0 \to x_0 - d/2 \\ y_0 \to b + b_0 \\ x \to x_0 + d/2 \\ y \to b + b_0 + \rho}} \end{aligned} \tag{3}$$

where $B(\Gamma)$ is given in [5].

By the elimination of I_1 and I_2 in (1) and (2), we obtain the modal equation for the unknown Γ as

$$(Z_{s1}(\Gamma) - Z_{w1})(Z_{s2}(\Gamma) - Z_{w2}) - Z_m^2 = 0. \tag{4}$$

This equation is greatly simplified when the two wires are identical since then, $Z_{w1} = Z_{w2} = Z_w$. Furthermore, we can put $Z_{s1}(\Gamma) \simeq Z_{s2}(\Gamma) = Z_s(\Gamma)$, which is an exact equation for configuration B in Fig. 1 (due to symmetry) and a very good approximation for configuration A since d is much less than the guide width. Under the preceding conditions, equation (4) reduces to two simple equations given by

$$Z_s(\Gamma) + Z_m(\Gamma) - Z_w = 0 \tag{5}$$

and

$$Z_s(\Gamma) - Z_m(\Gamma) - Z_w = 0 \tag{6}$$

where the first equation implies that $I_1 = I_2$ and the second implies that $I_1 = -I_2$. These are the two equations that correspond to the monofilar and the bifilar modes, respectively, and their solutions give the propagation constants of these modes.

Manuscript received February 28, 1974; revised May 6, 1974.
The author is with the Cooperative Institute for Research in Environmental Sciences, the University of Colorado, Boulder, Colo. 80302.

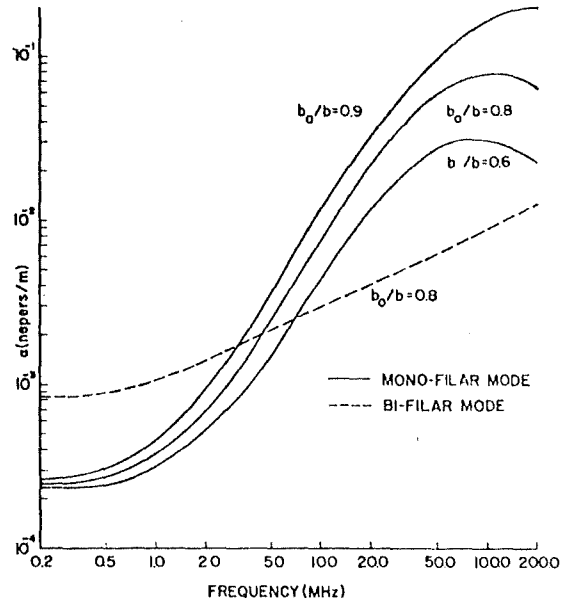

Fig. 2. Attenuation constant of the monofilar and the bifilar modes of configuration A versus frequency for various values of b_0/b. Wire radii ρ = 1 mm.

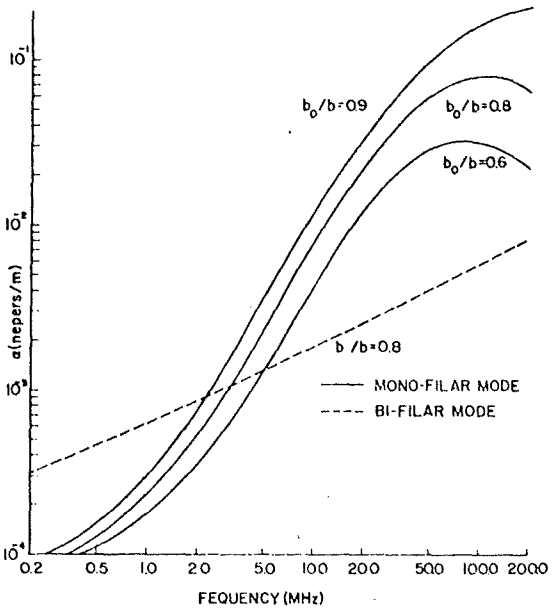

Fig. 3. Attenuation constant of the monofilar and the bifilar modes of configuration A versus frequency for various values of b_0/b. Wire radii ρ = 2 mm.

NUMERICAL RESULTS

Equations (5) and (6) are solved numerically for the two configurations A and B in the frequency range 200 kHz–200 MHz. The resulting values of the attenuation $\alpha_{\text{monofilar}}$ and α_{bifolar} are plotted in Figs. 2–4. The following physical constants are assumed in Fig. 2: $2a$ = 4 m, $2b$ = 3 m, $x_0 = a/2$, $d = a/100$, ρ = 1 mm, σ_w (the conductivity of the wires) = 10^6 mho/m, $\epsilon_r = 10\epsilon_0$, and $\sigma_r = 10^{-2}$ mho/m.

In contrast with the monofilar mode, the attenuation of the bifilar mode is almost insensitive to variations of the parameter b_0/b in all the frequency ranges considered and hence α_{bifilar} is shown for only one value of this parameter. To show the effect of varying the intrinsic parameters of the TL, the wire radii are increased to 2 mm in Fig. 3. By comparing with Fig. 2, it is seen that α_{bifilar} is appreciably reduced at all frequencies, while $\alpha_{\text{monofilar}}$ is hardly affected for frequencies above about 12.5 MHz and considerably reduced at lower frequencies. It is interesting to note the higher values of attenuation displayed by the bifilar mode over the monofilar mode for frequencies below a certain value in both Figs. 2 and 3.

The preceding observations can be explained as follows: as the frequency is reduced below about 100 MHz, the guide walls behave more as good electrical conductors, hence reducing the attenuation of the monofilar mode. Thus, at low frequencies (of the order of a few megahertz and less), the attenuation of both modes becomes solely dependent on the TL intrinsic parameters σ_w and ρ. Furthermore, the ohmic losses of the TL are normally higher for the bifilar mode than those for the monofilar mode and hence the higher attenuation of the former mode.

The attenuation curves for configuration B are shown in Fig. 4

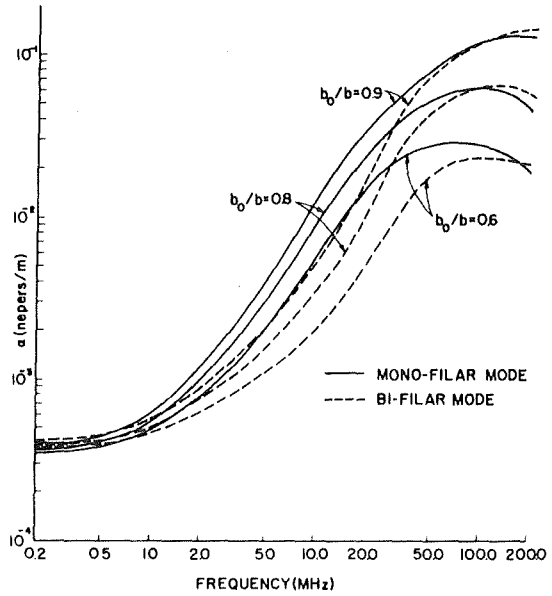

Fig. 4. Attenuation constant of the monofilar and the bifilar modes of configuration B versus frequency for various values of b_0/b. Wire radii = 1 mm.

for the same physical constants of Fig. 2. In this case, the bifilar mode shows strong dependence on the parameter b_0/b, supposedly because its fields are spread over the guide cross section and are significantly affected by the tunnel walls. As a further consequence of that, α_{bifilar} is much more frequency dependent than it is for configuration A.

It is relevant to mention here that similar results to those presented here are obtained for a circular guide with lossy dielectric walls by Wait and Hill (private communication). We find a complete consistency between the mode characteristics in both guide geometries. This provides some confidence in the adequacy of the model used here for the rectangular tunnel.

A final remark on the preceding model is now due. All the results of Figs. 2–4 are obtained for a waveguide model with side walls that are perfect electric conductors. An alternative model is one in which these walls are perfect magnetic conductors [6]. We computed values of attenuation rates for this model and it was found that the monofilar modes (and the bifilar mode of configuration B) show much higher attenuation rates for frequencies below 25 MHz, while near 200 MHz the attenuation rates are only slightly different from those obtained for the first model. We believe, however, that the model with perfect electric side walls is a better approximation to the actual tunnel in the frequency range considered here, since the tunnel walls do tend to behave as good electrical conductors as the frequency is lowered.

ACKNOWLEDGMENT

The author wishes to thank Dr. J. R. Wait for his constant encouragement and advice.

REFERENCES

[1] A. E. Goddard, "Radio propagation measurements in coal mines at UHF and VLF," in *Proc. Through-the Earth Electromagnetic Workshop* (Colorado School of Mines, Golden, Colo., Aug. 2–24, 1973) (Available from NTIS).
[2] P. Delogne, "Les communications par radio en milieu souterrain," *Acta Tech. Belg.* (Brussels), vol. 9, pp. 18–26, 1973.
[3] L. Deryck, "Étude de modes de propagation d'ondes electromagnetiques, susceptibles d'exister sur une ligne bifilaire en milieu souterrain," *Ann. Mines Belg.*, pp. 939–949, Aug. 1970.
[4] ——, "Radio communication in tunnels," *Electron. Lett.*, vol. 7, Dec. 29, 1971.
[5] S. F. Mahmoud and J. R. Wait, "Theory of wave propagation along a thin wire inside a rectangular waveguide," *Radio Sci.*, vol. 9, pp. 417–420, 1974.
[6] S. F. Mahmoud, "Characteristics of EM guided waves for communication in coal mine tunnels," *IEEE Trans. Commun.*, to be published Oct. 1974.

Radio Science, Volume 9, Number 5, pages 567–572, May 1974

Guided electromagnetic waves in a curved rectangular mine tunnel

Samir F. Mahmoud and James R. Wait

Cooperative Institute for Research in Environmental Sciences[1], *University of Colorado, Boulder, Colorado 80302*

(Received March 11, 1974.)

The transmission of VHF electromagnetic waves in a curved mine tunnel is analyzed using an idealized model in a cylindrical geometry. The tunnel cross section is assumed to be rectangular and the broad curved walls are imperfectly reflecting. The computations of the modal characteristics are facilitated by using a modified Airy function approximation of the rigorous cylindrical wave functions. The results indicated that the curvature of such tunnels will seriously increase the attenuation of the dominant low-order modes that are used for communications.

INTRODUCTION

The problem of guided wave propagation in waveguides with imperfectly reflecting boundaries arises in several applications, such as propagation in mine tunnels and in screened surface waveguides. It is observed that curvatures in these waveguides have a pronounced effect on the wave propagation losses [e.g., *Emslie et al.*, 1973]. In this paper we describe a quantitative investigation of this effect for the dominant modes of the guide.

We adopt a model of a rectangular waveguide with curved walls that are assumed to present a constant impedance or admittance to the tangential fields. The situation is illustrated in Figure 1. The other two straight walls are considered to behave as perfect electric or perfect magnetic conductors. In spite of the simplicity of such a model, it is believed to be capable of revealing the important characteristics of the dominant guided waves in a curved guide.

A great deal of work on curved rectangular waveguides has been carried out in the past. Attention, however, has been restricted to perfectly conducting walls. In this connection we mention the contributions of *Rice* [1948], *Waldron* [1957], *Cochran and Pecina* [1966], and *Wu* [1973].

FORMULATION

The geometry of the problem is illustrated in Figure 1. The fields are assumed to satisfy impedance boundary conditions on the walls $\rho = a - b$ and $\rho = a + b$ for $0 \leq z \leq 2h$, while the planes $z = 0$ and $z = h$ for $a - b \leq \rho \leq a + b$ are either electric or magnetic walls. Quite generally, the field components in the waveguide can be obtained from two z-directed electric and magnetic potentials Π and Π^* [*Wait*, 1959] for a time factor $\exp(i\omega t)$, as:

$$E_z = (-\gamma^2 + \partial^2/\partial z^2)\Pi$$

$$E_\rho = (\partial^2/\partial\rho\,\partial z)\Pi - (i\omega\mu/\rho)\,\partial\Pi^*/\partial\phi$$

$$E_\phi = (\partial^2/\partial\phi\,\partial z)(\Pi/\rho) + i\omega\mu\,\partial\Pi^*/\partial\rho \qquad (1)$$

$$H_z = (-\gamma^2 + \partial^2/\partial z^2)\Pi^*$$

$$H_\rho = (-i\gamma^2/\omega\mu\rho)\,\partial\Pi/\partial\phi + \partial^2\Pi^*/\partial\rho\,\partial z$$

$$H_\phi = (i\gamma^2/\omega\mu)\,\partial\Pi/\partial\rho + (1/\rho)\,\partial^2\Pi^*/\partial\phi\,\partial z \qquad (2)$$

General expressions of Π and Π^* are given as a double summation over all the possible modes, thus

$$\begin{pmatrix}\Pi\\ \Pi^*\end{pmatrix} = \sum_{m=0}^{\infty}\sum_{\nu=\nu_1,\nu_2} \left[\begin{pmatrix}a_{m,\nu}\\ c_{m,\nu}\end{pmatrix} J_\nu(u_m\rho) + \begin{pmatrix}b_{m,\nu}\\ d_{m,\nu}\end{pmatrix} H_\nu^{(2)}(u_m\rho)\right]\begin{pmatrix}\cos\lambda_m z\\ \sin\lambda_m z\end{pmatrix} \exp(-i\nu\phi) \qquad (3)$$

where the Bessel and Hankel functions, J_ν and $H_\nu^{(2)}$ respectively, are the conveniently chosen independent solutions; $\lambda_m = m\pi/2h$, m being any integer including zero, and $u_m = -\gamma^2 - \lambda_m^2$; $\gamma^2 = -\omega^2\mu\epsilon = -k_0^2$ and $\nu = \nu_1, \nu_2, \cdots$ are the characteristic propagation constants to be determined from the boundary conditions.

In (3), it is assumed that the straight walls are perfect electric walls. In the case of perfect magnetic walls, we merely exchange the sine and cosine terms.

[1] CIRES is a cooperative venture between the University of Colorado and the National Oceanic and Atmospheric Administration.

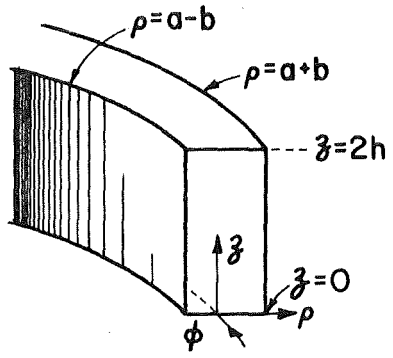

Fig. 1. Geometry of the problem. (Note that the medium within the tunnel is a homogeneous lossless medium with permittivity ϵ and permeability μ. Later we set these equal to their free-space values ϵ_0 and μ_0.)

THE CHARACTERISTIC MODES

The boundary conditions at the surfaces $\rho = a \pm b$ require that

$$E_z = \mp Z H_\phi \tag{4}$$

$$H_z = \pm Y E_\phi \tag{5}$$

with the higher sign applying to $\rho = a + b$ and the lower sign to $\rho = a - b$. The impedance Z and the admittance Y are assumed to represent the surface immittances presented by the outside media and should be chosen accordingly. Now we substitute in (4), from (1), (2), and (3), to obtain four homogeneous equations in the four coefficients, $a_{m,\nu}$, $b_{m,\nu}$, $c_{m,\nu}$, and $d_{m,\nu}$. For a nontrivial solution, it is required that the determinant of coefficients should vanish; thus we have:

$$\begin{vmatrix} (u^2 J_+ + Z_1 u J_+') & (u^2 H_+^{(2)} + Z_1 u H_+'^{(2)}) & J_+ Z i\nu\lambda/(a+b) & H_+^{(2)} Z i\nu\lambda/(a+b) \\ (u^2 J_- - Z_1 u J_-') & (u^2 H_-^{(2)} - Z_1 u H_-'^{(2)}) & -J_- Z i\nu\lambda/(a-b) & -H_-^{(2)} Z i\nu\lambda/(a-b) \\ -J_+ Y i\nu\lambda/(a+b) & -H_+^{(2)} Y i\nu\lambda/(a+b) & (u^2 J_+ - Y_1 u J_+') & (u^2 H_+^{(2)} - Y_1 u H_+'^{(2)}) \\ J_- Y i\nu\lambda/(a-b) & H_-^{(2)} Y i\nu\lambda/(a-b) & (u^2 J_- + Y_1 u J_-') & (u^2 H_-^{(2)} + Y_1 u H_-'^{(2)}) \end{vmatrix} = 0 \tag{6}$$

where the following abbreviations are used: $\lambda = \lambda_m$, $u = u_m$, $Z_1 = Zi\gamma^2/\omega\mu$, $Y_1 = Yi\omega\mu$, $J_\pm = J_\nu[u_m(a \pm b)]$,

$$J_\pm' = \left.\frac{\partial J_\nu(x)}{\partial x}\right|_{x = u_m(a \pm b)}$$

with similar definitions for $H_\pm^{(2)}$ and $H_\pm'^{(2)}$.

Now, for most cases of interest, the mean radius of curvature a is much greater than the free-space wavelength. Hence, both the order and the arguments of the Bessel functions in (6) are large, i.e., $|\nu|$, $|u_m(a \pm b)| \gg 1$ and for the important lower-order modes, the difference $|\nu - u_m(a \pm b)|$ is small. These conditions allow us to use the Airy function approximations for the Bessel functions [*Wait*, 1964, 1967], so

$$J_\nu(X) \simeq \pi^{-1/2}(2/X)^{1/3} v(t) \tag{7}$$

$$H_\nu^{(2)}(X) \simeq i\pi^{-1/2}(2/X)^{1/3} w_1(t) \tag{8}$$

where

$$v(t) = \pi^{1/2} Ai(t)$$

$$w_1(t) = \pi^{1/2}[Bi(t) - i\,Ai(t)]$$

and the functions $Ai(t)$ and $Bi(t)$ are those tabulated by *Miller* [1946]. The argument t is given by

$$(-t)^{1/2} = (X/2)^{1/3}(1 - \nu^2/X^2)^{1/2} \tag{9}$$

or

$$(t)^{1/2} = (X/2)^{1/3}(\nu^2/X^2 - 1)^{1/2} \tag{10}$$

The above form of t results in a better approximation of the Bessel functions as compared to the more familiar form used by *Wait* [1964]. For a complete discussion on the range of validity of the approximations in (7) and (8), the reader is referred to *Wait* [1967]. The logarithmic derivatives can also be approximated by:

$$J_\nu'(X)/J_\nu(X) \simeq -(2/X)^{1/3} v'(t)/v(t) \tag{11}$$

$$H_\nu'^{(2)}(X)/H_\nu(X) \simeq -(2/X)^{1/3} w_1'(t)/w_1(t) \tag{12}$$

Now using (7) through (12), the modal equation, (6), can be recast into the form:

$$\begin{vmatrix} [u^2 v(t_+) + q_1 u k_0 v'(t_+)] & [u^2 w(t_+) + q_1 u k_0 w'(t_+)] & (\omega\mu\nu\lambda q_1/x_+) v(t_+) & (\omega\mu\nu\lambda q_1/x_+) w(t_+) \\ [u^2 v(t_-) - q_1 u k_0 v'(t_-)] & [u^2 w(t_-) - q_1 u k_0 w'(t_-)] & -(\omega\mu\nu\lambda q_1/x_-) v(t_-) & -(\omega\mu\nu\lambda q_1/x_-) w(t_-) \\ -(k_0^2 q_2 \nu\lambda/x_+\omega\mu) v(t_+) & -(k_0^2 q_2 \nu\lambda/x_+\omega\mu) w(t_+) & [u^2 v(t_+) + q_2 u k_0 v'(t_+)] & [u^2 w(t_+) + q_2 u k_0 w'(t_+)] \\ (k_0^2 q_2 \nu\lambda/x_-\omega\mu) v(t_-) & (k_0^2 q_2 \nu\lambda/x_-\omega\mu) w(t_-) & [u^2 v(t_-) - q_2 u k_0 v'(t_-)] & [u^2 w(t_-) - q_2 u k_0 w'(t_-)] \end{vmatrix} \tag{13}$$

where $w(t) = w_1(t)$ and t_+ and t_- are given by (9) or (10) with X replaced by $u_m(a \pm b)$ respectively. The normalized quantities q_1, q_2, x_+, x_- are given by

$$q_1 = (iZ/\eta_0)(2/u_m a)^{1/3}$$

$$q_2 = (iY\eta_0)(2/u_m a)^{1/3}$$

$$x_\pm = k_0(a \pm b)(2/u_m a)^{1/3}$$

where $\eta_0 = (\mu/\epsilon)^{1/2}$ is the plane wave impedance. In what follows, $\mu = \mu_0$ and $\epsilon = \epsilon_0$, so $\eta_0 \simeq 120\pi$.

It is important to notice that when $m = 0(\lambda = 0)$, equation 13 reduces to two uncoupled modal equations for the $LSE_{0,n}$ modes (Longitudinal Section Electric: $E_z = 0$) and the $LSM_{0,n}$ modes (Longitudinal Section Magnetic: $H_z = 0$), corresponding to a waveguide with perfect magnetic or perfect electric narrow walls respectively. In this case $u^2 = u_0^2 = k_0^2$ and the modal equations of these modes are given by:

$$\{[w_1(t_+) + q_{1,2}w_1'(t_+)]/[v(t_+) + q_{1,2}v'(t_+)]\} \cdot \{[v(t_-) - q_{1,2}v'(t_-)]/[w_1(t_-) - q_{1,2}w_1'(t_-)]\} = 1 = e^{2in\pi}$$

$$n = 0, 1, \cdots \qquad (14)$$

where q_1 is used for the $LSM_{0,n}$ modes and q_2 for the $LSE_{0,n}$ modes. The above equation can also be written in terms of the functions $w_1(t)$ and $w_2(t)$ by use of the relation [*Wait*, 1970],

$$v(t) = i[w_1(t) - w_2(t)]$$

Equation 14 then takes the form

$$\{[w_1(t_+) + q_{1,2}w_1'(t_+)]/[w_2(t_+) + q_{1,2}w_2'(t_+)]\} \cdot \{[w_2(t_-) - q_{1,2}w_2'(t_-)]/[w_1(t_-) - q_{1,2}w_1'(t_-)]\} = 1 = e^{2in\pi} \qquad (15)$$

which is similar to the modal equation obtained earlier [*Wait*, 1964] for TM modes in a cylindrical model of the earth-ionosphere waveguide.

Equation 14 is particularly suitable for numerical solution of the slow modes for which Re $(t) > 0$ since then $w_1(t)$ is exponentially growing and $v(t)$ is exponentially decaying. These slow modes are analogous to the whispering gallery modes treated earlier [*Wait*, 1967]. On the other hand, (15) is more suitable for fast modes (Re $(t) < 0$).

NUMERICAL RESULTS

For the purpose of numerical investigation of the modal equations, (13) through (15), values of Z and Y are chosen to represent an external lossy dielectric medium with a dielectric constant ϵ_e (assumed $\gg \epsilon_0$) and conductivity σ_e. This can correspond to a mine tunnel waveguide. From a consideration of the Fresnel reflection coefficients of TE and TM plane waves on the walls, we obtain Z and Y approximately as:

$$Z/\eta_0 = k_0/(k_e^2 - k_0^2)^{1/2} \qquad (16)$$

$$Y\eta_0 = k_e^2/k_0(k_e^2 - k_0^2)^{1/2} \qquad (17)$$

where $k_e^2 = \omega^2\mu_e(\epsilon_e - i\sigma_e/\omega)$.

The quantities $(1 - \beta/k_0)$ and α/k_0 are plotted versus the curvature parameter b/a in Figures 2 through 5 for two values of the guide half-electrical length $k_0 b$. Here α and β are given by

$$\alpha + i\beta = iv/a$$

The quantity $\tan \delta_e = \sigma_e/\omega\epsilon_e$ in Figures 2 and 3 is fixed at 0.018 and in Figures 4 and 5 at 0.045. ϵ_e/ϵ_0 is taken equal to 10. In fact, one set of physical parameters that correspond to the above figures is as follows: $b = 3.5$ ft ($\simeq 1.067$ m), $\epsilon_e = 10\epsilon_0$, $\sigma_e = 10^{-2}$ mho m^{-1}, and the frequency $f = 1000$ MHz (in Figures 2, 3) and 400 MHz (in Figures 4, 5), but

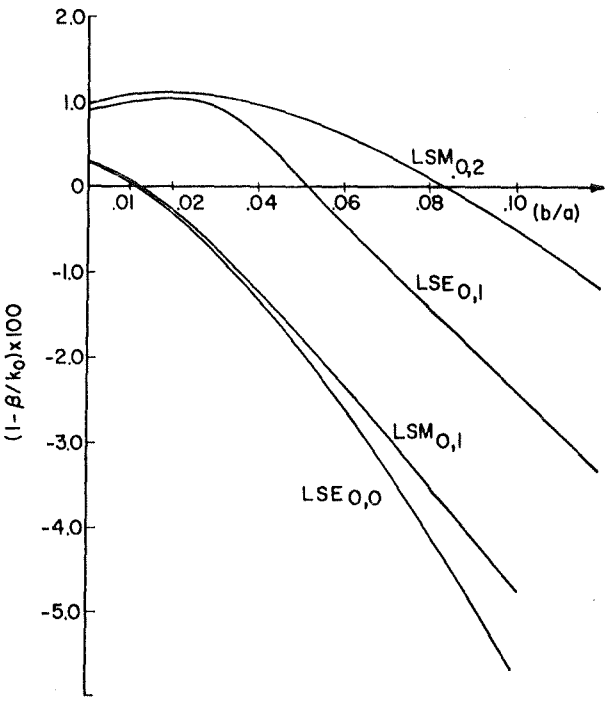

Fig. 2. Phase constants vs. b/a for $k_0 b = 22.4$, $\epsilon_e/\epsilon_0 = 10$, and $\tan \delta_e = 0.018$.

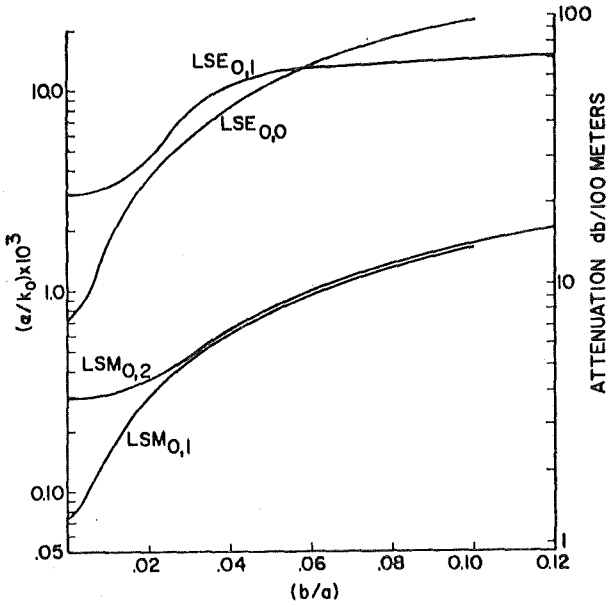

Fig. 3. Normalized attenuation rate vs. b/a for $k_0b = 22.40$, $\epsilon_e/\epsilon_0 = 10$ and $\tan \delta_e = 0.018$. The scale on the right-hand side gives the attenuation in db/100 m at 1000 MHz when $2b = 2.133$ m ($\simeq 7$ ft), and $\sigma_e = 10^{-2}$mho m^{-1}.

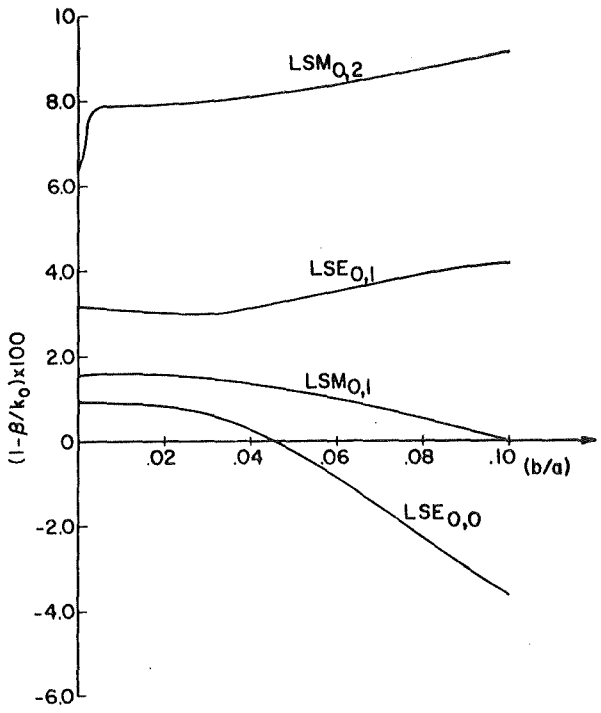

Fig. 4. Phase constants vs. b/a for $k_0b = 8.96$, $\epsilon_e/\epsilon_0 = 10$ and $\tan \delta_e = 0.045$.

with the dimensionless parameters used, the results are equally applicable to other sets of parameters. In the above figures, $m = 0$ and hence the modes are pure $LSE_{0,n}$ or $LSM_{0,n}$ according to type of walls at $z = 0, 2h$. In order to be consistent with the work of others [e.g., *Cochran and Pecina*, 1966], we choose the integer n to start from 0 for the LSE modes and from 1 for the LSM modes. The effect of curvature on the lowest-order mode ($LSE_{0,0}$ or $LSM_{0,1}$) is to lower its phase velocity and increase its attenuation. This mode tends to have its fields concentrated near the $\rho = a + b$ surface and hence behaves as the whispering gallery modes discussed by *Wait* [1967]. The curvature effects on the next higher order mode ($LSE_{0,1}$ or $LSM_{0,2}$) may be quite different; in particular, the attenuation of the $LSE_{0,1}$ mode may decrease with greater curvatures as a result of more grazing incidence of the rays on the guide wall at $\rho = a - b$, and hence this mode may become less attenuated than the lowest-order $LSE_{0,0}$ mode (Figures 3 and 5).

Normalized attenuation rates are plotted against the parameter k_0b for $LSE_{0,0}$ and $LSM_{0,1}$ modes in Figure 6. Here the product $\tan \delta_e \cdot k_0b$, rather than $\tan \delta_e$, is kept constant. This corresponds to a situation where the external medium of the guide has a constant conductivity σ_e while the frequency is varying. The ratio a/b takes the discrete values: ∞ (for a straight guide), 50, and 10. The typical decrease of attenuation with frequency observed in a straight waveguide is no longer a general characteristic in a curved waveguide. Similar effects are observed for the

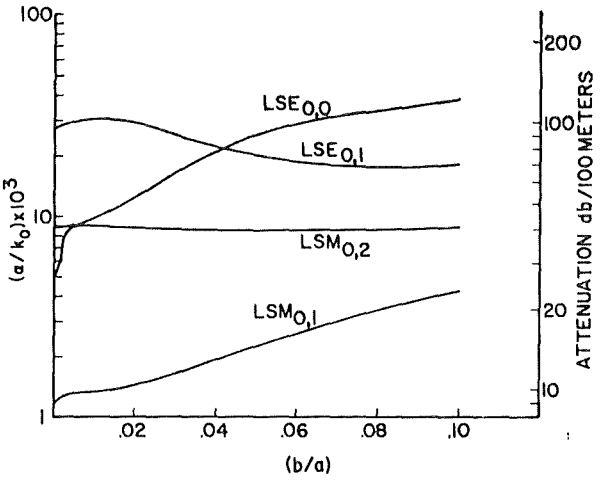

Fig. 5. Normalized attenuation rates vs. b/a for $k_0b = 8.96$, $\epsilon_e/\epsilon_0 = 10$ and $\tan \delta_e = 0.045$. The scale on the right-hand side gives the attenuation in db/100 m at 400 MHz when $2b = 2.133$ m ($\simeq 7$ ft) and $\sigma_e = 10^{-2}$mho m^{-1}.

next higher-order modes ($LSE_{0,1}$ and $LSM_{0,2}$) as illustrated in Figure 7. Of particular interest is the minimum of attenuation versus k_0b (or frequency) exhibited by the $LSE_{0,1}$ mode. The same phenomenon is observed with VLF modes in the earth-ionosphere guide [*Wait*, 1970, chap. 7] and is now considered to be a well-understood phenomenon.

When $m > 0$ (i.e., $\lambda > 0$), the modes are no longer pure LSE or LSM modes. However, we may continue to use the same nomenclature with the understanding that, e.g., $LSE_{m,n}$ is a hybrid mode that reduces to a longitudinal section electric mode when m becomes zero.

The attenuation of the modes $LSE_{1,0}$ and $LSM_{1,1}$ is plotted versus k_0b in Figure 8. It is seen that the attenuation rates show very little change from the corresponding case in Figure 6 where $m = 0$. This means that the coupling between the LSE and LSM modes is not appreciable in the range of electrical guide widths shown in these figures. It is worth mentioning that a reduction of tan δ_e to one tenth of its value in Figures 6 through 8 does not affect the attenuation rates by any significant amount. This is probably due to the fact that tan δ_e in these figures is already small (it has a maximum of 0.09) and hence the excess attenuation is due to more radiation rather than ohmic losses.

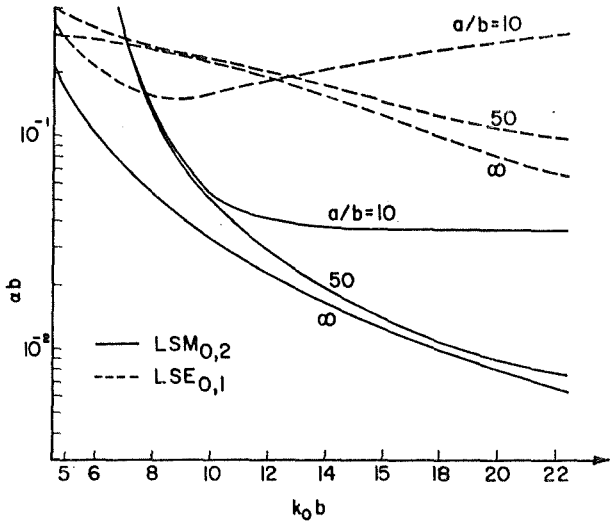

Fig. 7. Normalized attenuation rates vs. k_0b_1 for the same parameters as in Figure 6.

CONCLUDING REMARKS

In this paper, we have analyzed the propagating modes in a curved rectangular guide with imperfect but smooth walls. We found that the lowest-order mode has a whispering gallery character and as a result, the attenuation rate is increased significantly by the curvature. Actually, the attenuation of the $LSE_{0,1}$ mode may be decreased by the curvature and

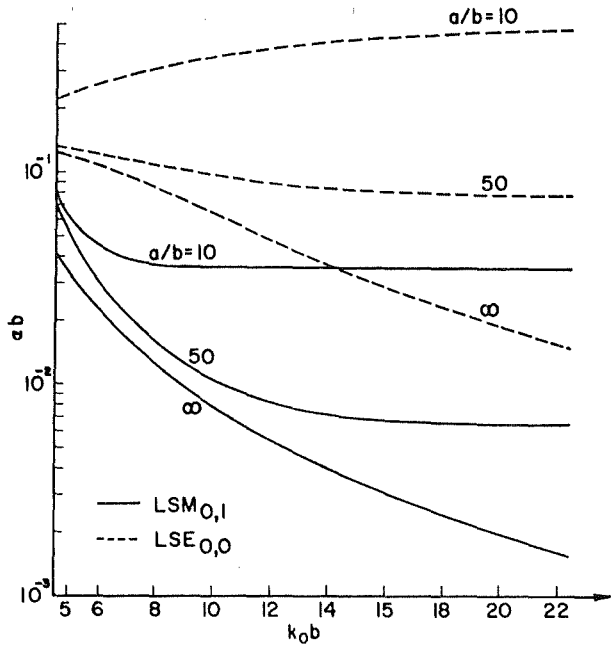

Fig. 6. Normalized attenuation rates vs. k_0b. $\epsilon_c/\epsilon_0 = 10$ and the product tan $\delta_e \cdot k_0b$ is kept constant and equal to 4.032.

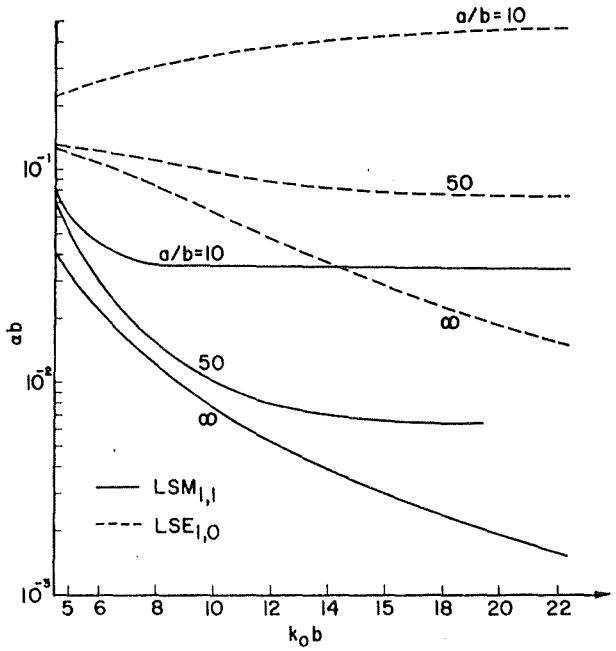

Fig. 8. Normalized attenuation rates vs. k_0b for the same parameters as in Figure 6.

hence this mode can become less attenuated than the lower $LSE_{0,0}$ mode.

REFERENCES

Cochran, J. A., and R. G. Pecina (1966), Mode propagation in continuously curved waveguides, *Radio Sci.*, *1*(6), 679–708.

Emslie, A. G., R. L. Lagace, and P. F. Strong (1973), Theory of propagation of UHF radio waves in coal mine tunnels, *Thru-the-Eaeth Electromagnetics Workshop*, eidted by R. G. Geyer, *Fin. Rep. USBM contract/grant G133023*, pp. 38–48, Department of the Interior, Bureau of Mines, Washington, DC.

Miller, J. C. P. (1946), *The Airy Integral*, Cambridge University Press, London.

Rice, S. O. (1948), Reflections from circular bends in rectangular wave guides—Matrix theory, *Bell Syst. Tech. J.*, *27*(2), 305–349.

Wait, J. R. (1959), *Electromagnetic Radiation from Cylindrical Structures*, p. 10, Pergamon, New York.

Wait, J. R. (1964), Two-dimensional treatment of mode theory of the propagation of VLF radio waves, *J. Res. Nat. Bur. Stand., Sect. D. 68D*(1), 81–93.

Wait, J. R. (1967), Electromagnetic whispering gallery modes in a dielectric rod, *Radio Sci.*, *2*(9), 1005–1017.

Wait, J. R. (1970), *Electromagnetic Waves in Stratified Media*, 2nd ed., pp. 76 and 112, Pergamon, New York.

Waldron, R. A. (1957), Theory of the helical waveguide of rectangular cross-section, *J. Brit. Inst. Radio Eng.*, *17*(10), 577–592.

Wu. C. P. (1973), Waveguide modes in curved waveguides, in *Computer Techniques for Electromagnetics*, edited by R. Mittra, pp. 279–281, Pergamon, New York.

Radio Science, Volume 9, Number 12, pages 1147–1158, December 1974

Geometrical optical approach for electromagnetic wave propagation in rectangular mine tunnels

Samir F. Mahmoud[1] *and James R. Wait*[2]

Cooperative Institute for Research in Environmental Sciences, University of Colorado, Boulder, Colorado 80302

(Received August 30, 1974.)

Electromagnetic wave propagation inside an empty rectangular mine tunnel with imperfect walls is considered. The modal expansion of the fields is complicated by the coupling of the basic modes by the imperfect walls. To avoid this difficulty, and in view of the large guide dimensions relative to the free space wavelength, a geometrical ray approach is proposed. To provide a theoretical foundation for the method, we first consider an idealized waveguide model with two perfectly reflecting side walls. The modal field expansion for this prototype model is fully analyzed to provide a satisfactory comparison between the modal and the geometrical ray sums. The proposed general ray method is then applied to the rectangular waveguide when all four walls are imperfectly conducting. Finally, the influence of wall roughness is considered by a relatively simple method.

INTRODUCTION

Recently, much attention has been paid to the possibility of radio communication in a mine tunnel environment [e.g., *Goddard*, 1973; *Emslie et al.*, 1973]. An interesting and rather fundamental problem arises in relation to electromagnetic wave propagation in a rectangular waveguide (representing the tunnel) which is assumed perfect in shape but whose four walls are generally characterized by a lossy dielectric medium. A close investigation of this problem shows that, although the Helmholtz wave equation is separable in Cartesian coordinates, the boundary conditions on the walls of the guide necessitate the coupling of the basic modal functions. As indicated by *Wait* [1967], this raises a fundamental difficulty in obtaining the modal eigenvalues and eigenfunctions for such a waveguide or any other whose cross section is different from the circular shape.

In this paper, a geometrical ray approach is proposed to obtain the fields at any point in the waveguide as a summation of rays from the source and all possible images, avoiding the elaborate task of determining the modal propagation constants. This approach is applicable when the waveguide dimensions are somewhat greater than a free-space wavelength, a condition that is usually satisfied in mine tunnel applications.

PROTOTYPE MODEL AND MODAL FORMULATION

An important idealized model of the above rectangular waveguide is one with perfectly reflecting side walls while the top and bottom walls are still lossy dielectric media. For this waveguide, the free modal propagation constants and modal fields are straightforward to obtain [*Mahmoud and Wait*, 1974] and hence it provides a means of checking the modal versus the geometrical ray sums for the field. For this reason, we present a detailed field analysis for the above guide in the next section. This is followed by a formulation of the geometrical ray sum for the general waveguide with four imperfect walls. The effect of roughness of the guide walls is also considered by using an approximate technique. Finally, some numerical results are presented for specific situations of practical interest.

The geometry of the problem is shown in Figure 1. The source is assumed to be an infinitesimally short horizontal dipole of moment $P \exp(i\omega t)$ and located at the point $(x_0, y_0, 0)$ in the Cartesian frame. The resulting current density in the guide can be expressed, apart from the time factor $\exp(i\omega t)$, as

[1] Present address: Electrical Engineering Department, Cairo University, Egypt.

[2] Consultant to the Institute for Telecommunication Sciences, Office of Telecommunications.

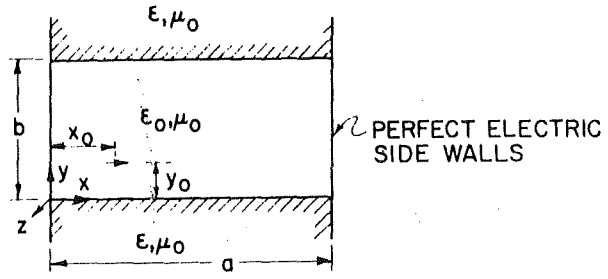

Fig. 1. A horizontal dipole inside a rectangular waveguide with perfect side walls.

$$\mathbf{J}(x, y, z) = P\,\delta(x - x_0)\,\delta(y - y_0)\,\delta(z)\mathbf{x} \qquad (1)$$

where $\mathbf{x}$ is a unit vector in the x direction. Applying the z Fourier transform operator, we transform $\mathbf{J}(x, y, z)$ into $\mathbf{J}(x, y; \beta)$ given by

$$\mathbf{J}(x, y; \beta) = \int_{-\infty}^{\infty} \exp(i\beta z)\,\mathbf{J}(x, y, z)\,dz = P\,\delta(x - x_0)\,\delta(y - y_0)\mathbf{x} \qquad (2)$$

All the fields in the waveguide are transformed in a similar fashion and, as a result, the derivative $\partial/\partial z$ is now equivalent to the multiplication factor $(-i\beta)$. Generally, the fields can be obtained from two appropriate scalar potentials. The most convenient two potentials, for the present waveguide, are electric and magnetic potentials directed normally to the two imperfect walls (i.e., in the y direction). Let these be denoted by Π_y and Π_y^* respectively. This choice simplifies the analysis to follow since Π_y and Π_y^* are not coupled at the interfaces $y = 0$ and $y = b$ (although they are coupled by the source). It should be noted here, however, that for the general waveguide with four imperfect walls, any two chosen potentials will always be coupled at two or more of the walls.

The lossless waveguide region $0 < x < a$, $0 < y < b$ has electrical characteristics ϵ_0, μ_0 that can be assumed to be the same as free space. The lossy regions for $0 < x < a$ and, $y < 0$ and $y > b$ have corresponding parameters ϵ, μ_0 where $\epsilon = \epsilon_1 - i\sigma_1/\omega$ in terms of the real permittivity ϵ_1 and real conductivity σ_1.

Suitable expansions for Π_y and Π_y^* (assuming perfect electric side walls) are given below. For $b \geq y \geq y_0$,

$$\Pi_y = \sum_m A_m \sin(m\pi x/a)\{\exp[u_m(b - y)] + S_m \exp[-u_m(b - y)]\} \qquad (3)$$

$$\Pi_y^* = \sum_m A_m^* \cos(m\pi x/a)\{\exp[u_m(b - y)] + R_m \exp[-u_m(b - y)]\} \qquad (4)$$

while for $y \geq b$,

$$\Pi_{y1} = \sum_m T_m \sin(m\pi x/a) \exp[u_{m1}(b - y)] \qquad (5)$$

$$\Pi_{y1}^* = \sum_m T_m^* \cos(m\pi x/a) \exp[u_{m1}(b - y)] \qquad (6)$$

where the above potentials are functions of β which appears in u_m and u_{m1} as

$$u_m = [-k_0^2 + (m\pi/a)^2 + \beta^2]^{1/2}$$

$$u_{m1} = [-k_1^2 + (m\pi/a)^2 + \beta^2]^{1/2}$$

$$k_0^2 = \omega^2\mu_0\epsilon_0, \quad k_1^2 = \omega^2\mu_0\epsilon$$

and the summation over m is from 0 to $+\infty$. The tangential field components at the interface $y = b$ are given in terms of Π_y and Π_y^* as follows [*Wait*, 1959].

$$e_x = \partial^2\Pi_y/\partial x\,\partial y + \omega\mu_0\beta\Pi_y^*$$

$$e_z = -i\beta\,\partial\Pi_y/\partial y - i\omega\mu_0\,\partial\Pi_y^*/\partial x$$

$$h_x = -\omega\epsilon_0\beta\Pi_y + \partial^2\Pi_y^*/\partial x\,\partial y$$

$$h_z = i\omega\epsilon_0\,\partial\Pi_y/\partial x - i\beta\,\partial\Pi_y^*/\partial y$$

for $b \geq y \geq y_0$, while for $y \geq b$, ϵ_0 is replaced by ϵ. The continuity of these field components at $y = b$ reduces to the continuity of Π_y, Π_y^*, and their y derivatives. This results in S_m and R_m given by

$$S_m = (\epsilon u_m - \epsilon_0 u_{m1})/(\epsilon u_m + \epsilon_0 u_{m1}) \qquad (7)$$

$$R_m = (u_m - u_{m1})/(u_m + u_{m1}) \qquad (8)$$

While A_m and A_m^* are still arbitrary and unrelated. This means that the two potentials are uncoupled by the interface as stated above. We recognize S_m and R_m as the Fresnel reflection coefficients for vertically and horizontally polarized waves respectively [*Wait*, 1970]. The present choice of y-directed Hertz vectors is a simplification over the forms used previously by *Mahmoud and Wait* [1974].

In a similar fashion, the potentials Π_y and Π_y^* for $0 \leq y \leq y_0$ are obtained as

$$\Pi_y = \sum_m B_m \sin(m\pi x/a)[\exp(u_m y) + S_m \exp(-u_m y)] \qquad (9)$$

$$\Pi_y^* = \sum_m B_m^* \cos(m\pi x/a)[\exp(u_m y) + R_m \exp(-u_m y)] \qquad (10)$$

The four coefficients A_m, A_m^*, B_m, and B_m^* are to be determined from the continuity of e_x, e_z, and h_x at $y = y_0$ plane and the discontinuity of h_z by the source. This reduces to the continuity of Π_y^* and $\partial\Pi_y/\partial y$ at $y = y_0$ and the discontinuity of both Π_y and $\partial\Pi_y^*/\partial y$ such that

$$h_x|_{y_0+} - h_x|_{y_0-} = -\omega\epsilon_0\beta(\Pi_y|_{y_0+} - \Pi_y|_{y_0-}).$$
$$+ (\partial/\partial x)[(\partial\Pi_y^*/\partial y)_{y_0+} - (\partial\Pi_y^*/\partial y)_{y_0-}] = 0 \quad (11)$$
$$h_z|_{y_0+} - h_z|_{y_0-} = i\omega\epsilon_0(\partial/\partial x)(\Pi_y|_{y_0+} - \Pi_y|_{y_0-})$$
$$- i\beta[(\partial\Pi_y^*/\partial y)_{y_0+} - (\partial\Pi_y^*/\partial y)_{y_0-}] = P\,\delta(x - x_0)$$
$$= (2P/a)\sum_m \delta_m \cos(m\pi x_0/a)\cos(m\pi x/a) \quad (12)$$

where $\delta_m = 1$ for $m \neq 0$ and $= \frac{1}{2}$ for $m = 0$. The last equality is obtained by expanding the delta function in a cosinusoidal series in the interval $(0, a)$.

Substituting from (3), (4), (9), and (10) in (11) and (12), we obtain

$$A_m g_m(b - y_0) - B_m g_m(y_0) = X_m \quad (13)$$
$$A_m^* f_m'(b - y_0) + B_m^* f_m'(y_0) = Y_m \quad (14)$$

where

$$X_m = (P/i\omega\epsilon_0 a)\,\delta_m \cos(m\pi x_0/a)(m\pi/a)/(k_0^2 + u_m^2)$$
$$Y_m = (P/ia)\beta/[u_m(k_0^2 + u_m^2)]$$

and the functions $f_m(y)$, $g_m(y)$, $f_m'(y)$, and $g_m'(y)$ are defined by

$$\left.\begin{matrix} f_m(y) \\ g_m(y) \end{matrix}\right\} = (1/2)\exp(u_m y) + (1/2)\left\{\begin{matrix} R_m \\ S_m \end{matrix}\right\}\exp(-u_m y) \quad (15)$$

$$\left.\begin{matrix} f_m'(y) \\ g_m'(y) \end{matrix}\right\} = (1/2)\exp(u_m y) - (1/2)\left\{\begin{matrix} R_m \\ S_m \end{matrix}\right\}\exp(-u_m y) \quad (16)$$

The equations for the continuity of Π_y^* and $\partial\Pi_y/\partial y$ at $y = y_0$ give

$$-A_m g_m'(b - y_0) = B_m g_m'(y_0) \quad (17)$$
$$A_m^* f_m(b - y_0) = B_m^* f_m(y_0) \quad (18)$$

Now, solving equations (13), (14), (17), and (18), we obtain

$$A_m = 2g_m'(y_0)X_m/\Delta_m$$
$$B_m = -2g_m'(b - y_0)X_m/\Delta_m$$
$$A_m^* = 2f_m(y_0)Y_m/\Delta_m^*$$
$$\text{and} \quad B_m^* = 2f_m(b - y_0)Y_m/\Delta_m^*$$

where

$$\left.\begin{matrix} \Delta_m \\ \Delta_m^* \end{matrix}\right\} = \exp(u_m b) - \left\{\begin{matrix} S_m^2 \\ R_m^2 \end{matrix}\right\}\exp(-u_m b) \quad (19)$$

Hence we obtain Π_y and Π_y^* in (3), (4), (9), and (10) in the form

$$\Pi_y = (4P/i\omega\epsilon_0 a)\sum_m \frac{(m\pi/a)}{k_0^2 + u_m^2}\,\delta_m \cos(m\pi x_0/a)$$
$$\cdot \sin(m\pi x_0/a)\left\{\begin{matrix} g_m'(y_0)g_m(b - y) \\ -g_m'(b - y_0)g_m(y) \end{matrix}\right\}\Big/\Delta_m \quad (20)$$

$$\Pi_y^* = (4P/ia)\beta\sum_m \frac{1}{k_0^2 + u_m^2}\,\delta_m \cos(m\pi x_0/a)$$
$$\cdot \cos(m\pi x/a)\left\{\begin{matrix} f_m(y_0)f_m(b - y) \\ f_m(b - y_0)f_m(y) \end{matrix}\right\}\Big/ u_m\Delta_m^*$$
$$\text{for} \quad \begin{cases} b \geq y \geq y_0 \\ y_0 \geq y \geq 0 \end{cases} \quad (21)$$

Finally, we take the inverse transform of (20) and (21) to obtain Π_y and Π_y^* as functions of x, y, z:

$$\Pi_y(x, y, z) = (1/2\pi)\cdot\int_{-\infty}^{\infty} \exp(-i\beta z)(\text{RHS of 20})\,d\beta \quad (22)$$

$$\Pi_y^*(x, y, z) = (1/2\pi)\cdot\int_{-\infty}^{\infty} \exp(-i\beta z)(\text{RHS of 21})\,d\beta \quad (23)$$

where RHS refers to the right-hand side.

The integration over β in (22) and (23) can be changed into a summation of residues in the complex β plane in a routine manner to obtain

$$\Pi_y(x, y, z) \simeq [-4\,\text{sgn}(z)P/\omega\epsilon_0 a]$$
$$\cdot \sum_{n=1,2,\cdots}\sum_m [\exp(-i\beta_{mn}|z|)F_m'(x, x_0)(m\pi/a)/(k_0^2 + u_n^2)]g_n'(y_0)g_n(y)u_n/\beta_{mn}(\partial\Delta/\partial u)_{u_n} \quad (24)$$

$$\Pi_y^*(x, y, z) \simeq (-4P/a)\sum_{n=1,2,\cdots}$$
$$\cdot \sum_m [\exp(-i\beta_{mn}^*|z|)F_m(x, x_0)/(k_0^2 + u_n^2)]$$
$$\cdot f_n(y_0)f_n(y)/(\partial\Delta^*/\partial u)_{u_n} \quad (25)$$

where $f_n(y) = f_m(y)|_{\beta=\beta_n}$ etc. and where u_n and u_n^*, $n = 1, 2, \cdots$ are the roots of the equations $\Delta(u) = 0$ and $\Delta^*(u) = 0$ respectively. Also note that

$$\beta_{mn} = [k_0^2 - (m\pi/a)^2 + u_n^2]^{1/2}$$

and

$$\beta_{mn}^* = [k_0^2 - (m\pi/a)^2 + u_n^{*2}]^{1/2}$$

The functions $F_m(x, x_0)$ and $F_m'(x, x_0)$ are given by

$$\{F_m(x, x_0), F_m'(x, x_0)\} = \delta_m \cos(m\pi x_0/a) \cdot \{\cos(m\pi x/a), \sin(m\pi x/a)\}$$

Actually, the representations given by (24) and (25) are not exact since we have neglected the continuous spectrum associated with the branch line integrations around the branch point at $\beta = [k_1^2 - (m\pi/a)^2]^{1/2}$. The corresponding lateral waves are heavily damped when the external media are finitely conducting, e.g., $\epsilon_1\omega/\sigma_1 < 10$.

RAY SUM FOR PROTOTYPE MODEL

To cast equations (22) and (23) into a summation of rays, the terms $1/\Delta_m$ and $1/\Delta_m^*$ are first expanded in the manner

$$\left.\begin{matrix}1/\Delta_m \\ 1/\Delta_m^*\end{matrix}\right\} = \exp(-u_m b) \sum_n \left\{\begin{matrix}S_m^{2n} \\ R_m^{2n}\end{matrix}\right\} \exp(-2nu_m b)$$

Upon substituting back into (22) and (23), we encounter the following type of integral

$$I_{mj} = (1/2\pi) \int_{-\infty}^{\infty} \exp(-i\beta z) \cdot \exp[-u_m(y - y_j)] q(\beta)\, d\beta$$

This can be evaluated by the method of stationary phase to obtain:

$$I_{mj} \simeq \exp(i\pi/4)\lambda_m \cos\phi_j q(\lambda_m \sin\phi_j) \cdot \exp(-i\lambda_m r_j)/(2\pi\lambda_m r_j)^{1/2}$$

valid for $\lambda_m r_j \gg 1$. In the above q is a slowly varying function of β. In addition,

$$\lambda_m = (\beta^2 - u_m^2)^{1/2} = [k_0^2 - (m\pi/a)^2]^{1/2}$$
$$\phi_j = \tan^{-1} z/|y - y_j|$$
$$r_j = (z^2 + |y - y_j|^2)^{1/2}$$

The symbol j runs over all the images in the $y = 0$ and $y = b$ walls in any arbitrary order that we need not specify here. The location of these images are $y_j = 2lb \pm y_0$; $l = -\infty$ to ∞. We finally obtain Π_y and Π_y^* as the following summation of images

$$\Pi_y(x, y, z) = (P/i\omega\epsilon_0 a) \sum_m (m\pi/a) F_m'(x, x_0) \cdot \sum_j [(S)^{n_j}/(k_0^2 - \lambda_m^2 \cos^2\phi_j)] \cdot [\exp(-i\lambda_m r_j + i\pi/4)](2\pi\lambda_m r_j)^{-1/2} \quad (26)$$

$$\Pi_y^*(x, y, z) = (P/ia) \sum_m F_m(x, x_0) \cdot \sum_j [(R)^{n_j}/(k_0^2 - \lambda_m^2 \cos^2\phi_j)] \cdot [\exp(-i\lambda_m r_j + i\pi/4)](2\pi\lambda_m r_j)^{-1/2} \quad (27)$$

where n_j is the number of reflections on the $y = 0$ and $y = b$ walls involved in forming the jth images. It is easy to verify that for images at $y_j = 2lb + y_0$, $n_j = 2|l|$ and for images located at $y_j = 2lb - y_0$, $n_j = |l| + |l-1|$. We note that S and R are functions of u_m (see equations 7 and 8) for which we substitute $(i\lambda_m \cos\phi_j)$.

The fields excited by a vertical dipole can be obtained by following a similar analysis as above. In this case, however, the fields may be obtained from only one scalar potential Π_y (i.e., $\Pi_y^* = 0$). Alternatively, we can use the reciprocity theorem to derive these fields from those excited by the horizontal dipole. Here we shall only state the results. Thus, as a modal expansion, Π_y^v excited by an infinitesimally short vertical dipole of moment P located at $(x_0, y_0, 0)$, is given by

$$\Pi_y^v(x, y, z) = (-4P/\omega\epsilon_0 a) \sum_{n=1,2,\cdots} \cdot \sum_m \exp(-i\beta_{mn} z) F_m^v(x, x_0) \cdot g_n(y_0) g_n(y)/\beta_{mn}(\partial\Delta/\partial u)_{u_n} \quad (28)$$

where $F_m^v(x, x_0) = \sin(m\pi x_0/a) \sin(m\pi x/a)$. Then, the corresponding ray sum is

$$\Pi_y^v(x, y, z) = (P/i\omega\epsilon_0 a) \sum_m F_m^v(x, x_0) \sum_j (S)^{n_j} \cdot \exp(-i\lambda_m r_j + i\pi/4)/(2\pi\lambda_m r_j)^{1/2} \quad (29)$$

where the symbols occurring above have the same meaning as in (26). It should be noticed that the summation over m in (26), (27), and (29) can also be transformed into a ray sum from images in the side walls; however, this is not exploited here.

COMPARISON OF MODES AND RAYS FOR PROTOTYPE MODEL

A comparison between mode and ray summations of the electric field is shown in Figures 2 and 3. In Figure 2, the source is a $\lambda/2$ horizontal dipole and in Figure 3, it is a $\lambda/2$ vertical dipole. The following physical constants are assumed: $a = 2b = 4.26$ m ($\simeq$ 14 ft), $x_0 = a/4$, $y_0 = 0.2b$, $y = 0.3b$. The frequency is 1 GHz and the effective wall impedances

Z_h, for horizontal polarization, and Z_v, for vertical polarization, are given by

$$Z_h = \eta_0/(\epsilon/\epsilon_0 - 1)^{1/2}$$

$$Z_v = \eta_0(\epsilon/\epsilon_0 - 1)^{1/2}/(\epsilon/\epsilon_0)$$

where ϵ is the complex dielectric constant of the walls, $\epsilon = \epsilon_1 - i\sigma_1/\omega\epsilon_0$, with $\epsilon_1 = 10\ \epsilon_0$ and $\sigma_1 = 10^{-2}$ mho m^{-1}. The electric fields E_x and E_y in the figures are obtained from the potentials Π_y, Π_y^*, and Π_y^v by

$$E_x|_{\text{horiz. dipole}} = \partial\Pi_y^2/\partial y\ \partial x + i\omega\mu_0\ \partial\Pi_y^*/\partial z$$

$$E_y|_{\text{vert. dipole}} = (k_0^2 + \partial^2/\partial y^2)\Pi_y^v$$

The comparison in Figures 2 and 3 shows a very close agreement between the mode and ray sums up to a distance of 2000 m for the horizontal dipole case and about 500 m for the vertical dipole case. The disagreement for distances greater than 500 m in the latter case is possibly due to the high total attenuation of the field and hence the severe cancellation of the terms of the ray series.

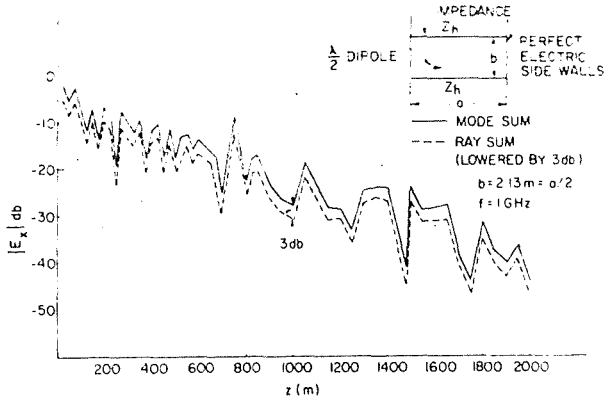

Fig. 2. Horizontal electric field versus distance z from the source. Modal and geometrical ray sums.

LIMIT TO THE PARALLEL PLATE GUIDE

The above results can be specialized to the parallel plate waveguide by allowing the two side walls to recede to $-\infty$ and $+\infty$ in the negative and positive x directions. In this case, the $\delta(x-x_0)$ term in (2) is expanded as

$$(1/2\pi)\int_{-\infty}^{+\infty} \exp\,[-i\kappa(x - x_0)]\,d\kappa$$

and hence all the preceding summations over m are replaced by a similar integral. Hence, as an example, equation 23 for Π_y^* now becomes

$$\Pi_y^*(x, y, z) = (1/2\pi)\int_{-\infty}^{\infty} \exp\,(-i\beta z)\beta\ d\beta(P_i/i\pi)$$

$$\cdot\int_{-\infty}^{\infty} \exp\,(-i\kappa x)\,d\kappa\begin{Bmatrix} f(y_0)f(b-y) \\ f(b-y_0)f(y)\end{Bmatrix} \Big/ [u\Delta^*(k_0^2 + u^2)]$$

$$\text{for } \begin{cases} b \geq y \geq y_0 \\ y_0 \geq y \geq 0 \end{cases} \qquad (30)$$

where $u^2 = -k_0^2 + \beta^2 + \kappa^2$, and x_0 is taken to be zero. To reduce the above expression into a modal sum, the second integral is transformed in the κ plane into a residue sum to give

$$\Pi_y^*(x, y, z) = (-P/\pi)\int_{-\infty}^{\infty} \exp\,(-i\beta z)\beta\ d\beta$$

$$\cdot\sum_{n=1,2,\cdots} \exp\,(-i\lambda_n\kappa)f_n(y_0)f_n(y)$$

$$\div [\lambda_n(k_0^2 + u_n^2)(\partial\Delta^*/\partial u)_{u_n}] \qquad (31)$$

where u_n, $n = 1, 2, \ldots$, are the roots of the equation $\Delta^*(u) = 0$ and $\lambda_n^2 = k_0^2 + u_n^2 - \beta^2$. As before, we have neglected the continuous spectrum associated with the branch-line integration.

Now making use of the integral representation for the Hankel function

$$H_0^{(2)}[k(z^2 + x^2)^{1/2}] = (1/\pi)\int_{-\infty}^{\infty} \exp\,(-i\beta z)\,d\beta$$

$$\cdot \exp\,[-i(k^2 - \beta^2)^{1/2}x]/(k^2 - \beta^2)^{1/2}$$

equation 31 reduces finally to

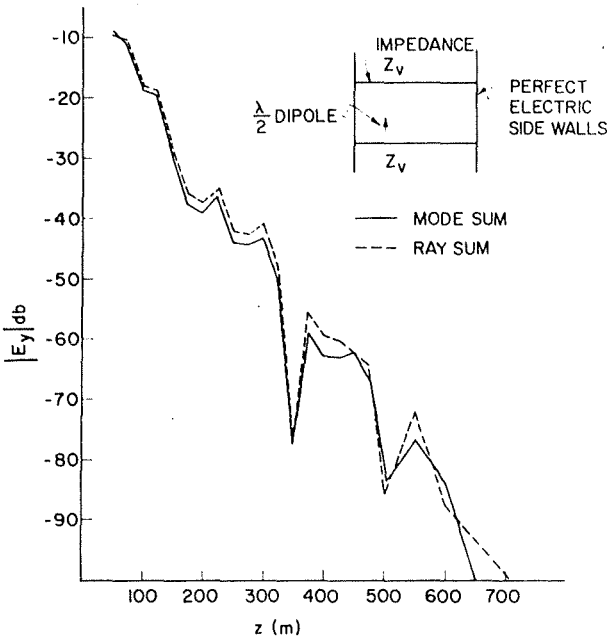

Fig. 3. Vertical electric field versus distance z from the source. Modal and geometrical ray sums.

$$\Pi_y^*(x, y, z) = -iP \sum_{n=1,2,\cdots} (\partial/\partial z) \cdot H_0^{(2)}[(k_0^2 + u_n^2)^{1/2}(z^2 + x^2)^{1/2}] \cdot f_n(y_0) f_n(y)/[(k_0^2 + u_n^2)(\partial\Delta^*/\partial u)_{u_n}] \quad (32)$$

To obtain a ray sum equivalent to (32), we expand the term $1/\Delta^*$ in (30) as before and perform the κ integration to get

$$(k_0^2 + \partial^2/\partial y^2)\Pi_y^*(x, y, z) = -(P/2) \cdot \int_{-\infty}^{\infty} \exp(-i\beta z)\beta\, d\beta \sum_i (R)^{n_i} H_0^{(2)}[(k_0^2 - \beta^2)^{1/2}\rho] = -(P/4\pi k_0) \sum_i (R)^{n_i}(\partial/\partial z)[\exp(-ik_0 r_i)/r_i] \quad (33)$$

where $\rho = [x^2 + (y-y_j)^2]^{1/2}$, $r_j = (\rho^2 + z^2)^{1/2}$, and j and n_j are defined as in equation 27. Similar expressions to (32) and (33) can also be derived for Π_y' and Π_y''.

SUMMATION OF RAYS FROM ONE-DIMENSIONAL ARRAY OF SOURCES

In what follows, an analytical expression for the geometrical ray sum from a source and its images in a parallel plate guide is obtained. The situation is illustrated in Figure 4 where the source at $y = y_0$, $z = 0$ produces images at $y_j = 2nb \pm y_0$, $z = 0$. The total field at an observation point (y, z) can be expressed as

$$S = S^+ + S^- \quad (34)$$

where S^+ is the contribution of the source and images as $y_j = 2nb + y_0$ while S^- is the contribution of images at $y_j = 2nb - y_0$, $n = -\infty$ to ∞. It is easy to verify that the number of reflections involved in producing an image at $y_j = 2nb + y_0$ is $2|n|$ and at $y_j = 2nb - y_0$ is $|n| + |n-1|$. Hence, apart from a possible directive pattern of the source, S^+ and S^- are given by

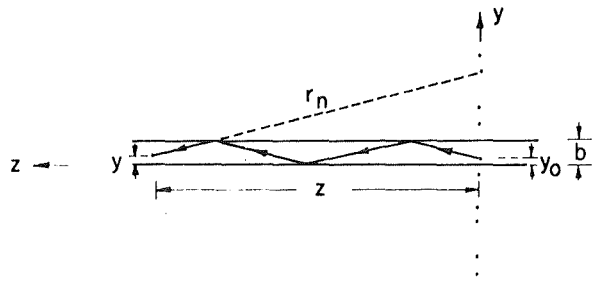

Fig. 4. The images in a parallel plate waveguide.

$$S^+ = \sum_{n=-\infty}^{\infty} (R)^{2|n|}[\exp(-ik_0 r_n^+)/r_n^+] \quad (35)$$

$$S^- = \sum_{n=-\infty}^{\infty} (R)^{|n|+|n-1|}[\exp(-ik_0 r_n^-)/r_n^-] \quad (36)$$

where $r_n^{\pm} = [z^2 + (2nb \pm y_0 - y)^2]^{1/2}$ and R is the reflection coefficient from the guide walls given by

$$R = -(C_y - \Delta)/(C_y + \Delta)$$

with $C_y = |2nb \pm y_0 - y|/r^{\pm}$, and Δ is a quantity related to the effective surface impedance. (This Δ should not be confused with that used in the previous section.) In particular, when $|\epsilon| \gg \epsilon_0$,

$$\Delta = (\epsilon/\epsilon_0 - 1 + C_y^2)^{1/2} \simeq (\epsilon/\epsilon_0 - 1)^{1/2}$$

for horizontally polarized waves or

$$\Delta = (\epsilon/\epsilon_0 - 1 + C_y^2)^{1/2}/(\epsilon/\epsilon_0) \simeq (\epsilon/\epsilon_0 - 1)^{1/2}/(\epsilon/\epsilon_0)$$

for vertically polarized waves, ϵ being the complex permittivity of the guide walls.

Since the images become weaker as they move away from the guide plates, we can assume that for the images of significant contribution to the field $z \gg |2nb \pm y_0 - y|$, which is valid as long as z is not in the very near field zone. Under this assumption we can use the following approximations:

$$r^{\pm} \simeq z + |2nb \pm y_0 - y|^2/2z \quad (37)$$

$$R \simeq -\exp(-2C_y/\Delta) \simeq -\exp(-2|2nb \pm y_0 - y|/z\Delta) \quad (38)$$

Substituting back in (35), S^- becomes

$$S^+ = [\exp(-ik_0 z)/z]\left\{\sum_{n=1}^{\infty} \exp[-ik_0(2nb + y_0 - y)^2/2z - 4(2nb + y_0 - y)n/z\Delta] + \sum_{n=1}^{\infty} \exp[-ik_0(2nb - y_0 + y)^2/2z - 4(2nb - y_0 + y)n/z\Delta] + \exp[-ik_0(y_0 - y)^2/2z]\right\}$$

$$= [\exp(-ik_0 z)/z]\left[\sum_{n=1}^{\infty} \exp(-\alpha n^2 - \beta n - \gamma) + \sum_{n=1}^{\infty} \exp(-\alpha n^2 + \beta n - \gamma) + \exp(-\gamma)\right]$$

$$= [\exp(-ik_0 z)/z][\exp(-\gamma)] \cdot \left[1 + 2\sum_{n=1}^{\infty} \cosh \beta n \exp(-\alpha n^2)\right]$$

where

$$\alpha = 2ik_0b^2/z + 8b/z\Delta$$

$$\beta = 2ik_0(y_0 - y)b/z + 4(y_0 - y)/z\Delta$$

$$\gamma = ik_0(y_0 - y)^2/2z$$

The above expression can be written in terms of the Jacobi theta function of the third kind [*Gradshteyn and Ryzhik*, 1965] defined by

$$\theta_3(q, u) \triangleq 1 + \sum_{n=1}^{\infty} q^{-n^2} \cos 2un$$

$$\equiv \prod_{n=1}^{\infty} (1 + 2q^{2n-1} \cos 2u + q^{2(2n-1)})(1 - q^{2n}) \quad (39)$$

Hence

$$S^+ = [\exp(-ik_0z)/z] \exp(-\gamma)\theta_3(e^{-\alpha}, i\beta/2) \quad (40)$$

Similarly we obtain

$$S^- = -[\exp(-ik_0z)/z] \exp(-\gamma^-)\theta_3(e^{-\alpha}, i\beta^-/2) \quad (41)$$

where

$$\beta^- = 2ik_0b(y_0 + y)/z + 4(y_0 + y)/z\Delta - 4b/z\Delta$$

and

$$\gamma^- = ik_0(y_0 + y)^2/2z + 2(y_0 + y)/z\Delta$$

The validity of the above expressions depends mainly on the approximation (38) for the reflection coefficient R. For horizontally polarized waves, the numerical results in Figure 5 show a close agreement between direct summation of the ray series and expressions (34), (40), and (41). For vertically polarized waves, however, we have found poor agreement. This is a consequence of the invalidity of (38) which fails to approximate R due to the existence of a Brewster angle. The computation of the θ_3 function is very much facilitated by using the product expression in (39) since part of this product, between $n = N$ (a sufficiently large number) and ∞, can be obtained in a simple form.

GENERAL RECTANGULAR GUIDE

Here we consider the general case of a rectangular guide with four imperfect walls that are characterized by a complex dielectric constant ϵ. The fields are obtainable from any two suitable scalar potentials which are generally coupled at the guide walls. The two scalar potentials chosen here are the electric Hertz potentials Π_x and Π_y.

In developing a ray series for the fields inside the waveguide, we need first to obtain the reflection coefficients of the potentials Π_x and Π_y at any particular air-dielectric interface in the waveguide. Assume an incident plane wave Π_x^{inc} at the $y = b$ interface to be

$$\Pi_x^{inc} = A \exp[-ik_xx - ik_y(y - b) - ik_zz]$$

Let the reflected Π_x^{refl} and the transmitted Π_x^{trans} be

$$\Pi_x^{refl} = AR \exp[-ik_xx + ik_y(y - b) - ik_zz]$$

$$\Pi_x^{trans} = AT \exp[-ik_xx - ik_{y1}(y - b) - ik_zz]$$

Beside the above waves, we find that a y-directed potential Π_y is needed in both media to satisfy the boundary conditions at the interface. Let Π_y^{refl} and Π_y^{trans} be given by

$$\Pi_y^{refl} = AR^* \exp[-ik_xx + ik_y(y - b) - ik_zz]$$

and

$$\Pi_y^{trans} = AT^* \exp[-ik_xx - ik_{y1}(y - b) - ik_zz]$$

where

$$k_x^2 + k_y^2 + k_z^2 = k_0^2$$

and

$$k_x^2 + k_{y1}^2 + k_z^2 = \epsilon k_0^2/\epsilon_0$$

By satisfying the boundary conditions at the interface, we readily find the Fresnel reflection coefficients R and R^* to be

$$R(k_y) = (k_y - k_{y1})/(k_y + k_{y1}) \quad (42)$$

and

$$R^*(k_x, k_y) = 2k_x[1/(k_y + k_{y1}) - \epsilon_0/(\epsilon k_y + \epsilon_0 k_{y1})] \quad (43)$$

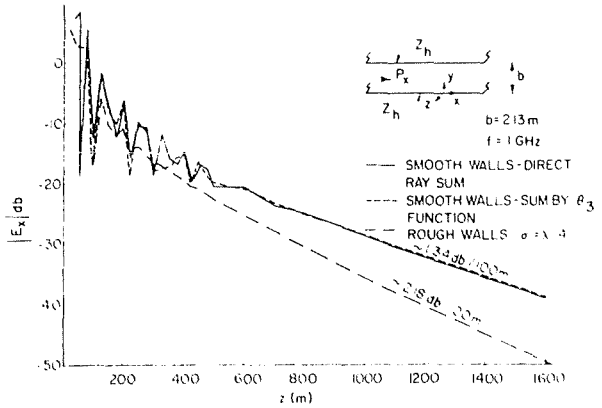

Fig. 5. Horizontal electric field versus distance z from the source inside a parallel plate waveguide. Smooth and rough walls.

In the case of an incident Π_y plane wave on the $y = b$ interface, the Fresnel reflection coefficient is given by

$$S(k_y) = (\epsilon k_y - \epsilon_0 k_{y1})/(\epsilon k_y + \epsilon_0 k_{y1}) \qquad (44)$$

while no Π_x is needed.

Although the above reflection coefficients are strictly valid only for incident plane waves on infinite plane interfaces, they are practically as valid for incident spherical waves when these are several wavelengths from the source and when the interface is only of finite extent. In other words, the waves emanating from the source are assumed to be sharply defined rays far enough from the source, and hence their reflections are affected only by the local conditions of the interface. This is actually the basis of developing the ray series to follow for the fields in the waveguide whose cross-sectional dimensions are sufficiently greater than a free-space wavelength.

Now we define a 2 × 2 reflection coefficient matrix [Γ] for each interface as follows:

$$\begin{bmatrix} \Pi_x^{\text{refl}} \\ \Pi_y^{\text{refl}} \end{bmatrix} = [\Gamma] \begin{bmatrix} \Pi_x^{\text{inc}} \\ \Pi_y^{\text{inc}} \end{bmatrix}$$

This will be given by

$$[\Gamma] = \begin{bmatrix} R(k_y) & 0 \\ \pm R^*(k_x, k_y) & S(k_y) \end{bmatrix} \qquad (45)$$

for the interfaces at $y = b$ and $y = 0$ where the plus sign applies to the first interface and the minus sign to the second. Similarly

$$[\Gamma] = \begin{bmatrix} S(k_x) & \pm R^*(k_y, k_x) \\ 0 & R(k_x) \end{bmatrix} \qquad (46)$$

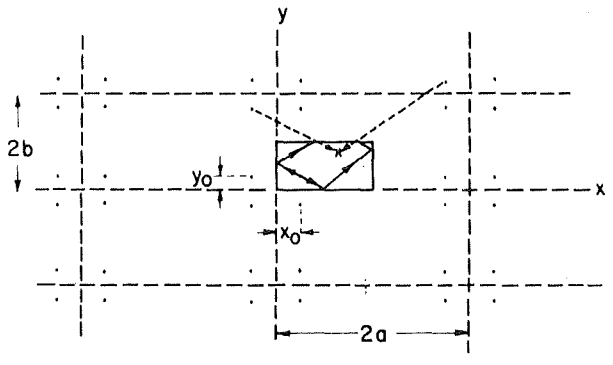

Fig. 6. The set of images in a rectangular waveguide.

for the interfaces at $x = a$ and $x = 0$ respectively. In the above, R, R^*, and S are defined by (42-44). The total field in the guide due to a given source is thus equal to the sum of ray contributions from all images added to that of the source. This situation is illustrated in Figure 6. Hence we have

$$\begin{bmatrix} \Pi_x'(x, y, z) \\ \Pi_y'(x, y, z) \end{bmatrix} = (1/4\pi i\omega\epsilon_0) \sum_l \cdot \sum_j [\exp(-ik_0 r_{lj})/r_{lj}][M_{lj}] \begin{bmatrix} P_x \\ P_y \end{bmatrix} \qquad (47)$$

where P_x and P_y are the x- and y-directed dipole moments of the source which is assumed to be an infinitesimally short dipole located at $(x_0, y_0, 0)$. The integers l and j run over all the images (and the source) in any arbitrary order that we need not specify here.

$$r_{lj} = [z^2 + (x - x_l)^2 + (y - y_j)^2]^{1/2}$$

(x_l, y_j) are the coordinates of the l-j image, where

$$x_l = 2ma \pm x_0, \qquad m = -\infty \text{ to } \infty$$

$$y_j = 2nb \pm y_s, \qquad n = -\infty \text{ to } \infty$$

and $[M_{lj}]$ is the product of all the reflection coefficient matrices involved in producting the l-j image with due care to the exact order of multiplication and the dependence of the reflection coefficients on the directional cosines of the ray. The horizontal and vertical electric field components are obtained from (47) and the following relations [*Wait*, 1959]:

$$E_x(x, y, z) = (k_0^2 + \partial^2/\partial x^2)\Pi_x' + \partial^2\Pi_y'/\partial y\,\partial x$$

$$E_y(x, y, z) = \partial^2\Pi_x'/\partial x\,\partial y + (k_0^2 + \partial^2/\partial y^2)\Pi_y'$$

Equation 47 is actually an exact equation, provided that the geometrical ray approximation is valid, since it takes account of the coupling between the Π_x and Π_y potentials through the term R^*. From equation 43 we see that for grazing rays ($k_x/k_0 \ll 1$, $k_y \ll k_{y1}$, and $\epsilon\, k_y \ll \epsilon_0 k_{y1}$), $R^* \simeq 2k_x k_y$, i.e., R^* becomes of a second-order magnitude relative to R and S (42 and 44), which then approaches unity. Since these grazing rays contribute most to the field, we may conclude that the coupling term R^* is of little importance. However, this statement is only true if we are interested in the fields of major polarization e.g., Π_x (or E_x) due to a horizontal dipole moment P_x in which case, however, Π_y is appreciably affected

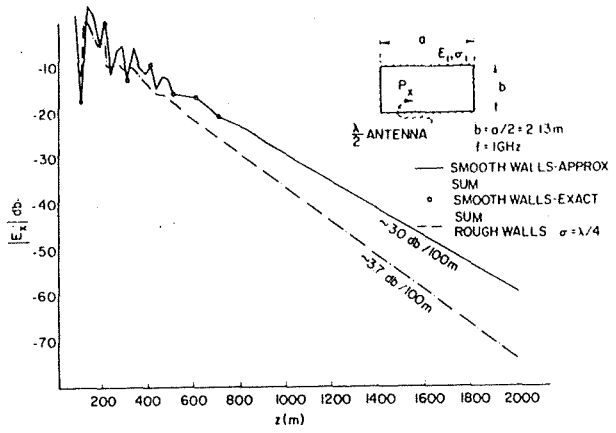

Fig. 7. Horizontal electric field versus distance z from the source inside a rectangular waveguide. Smooth and rough walls, 1 GHz.

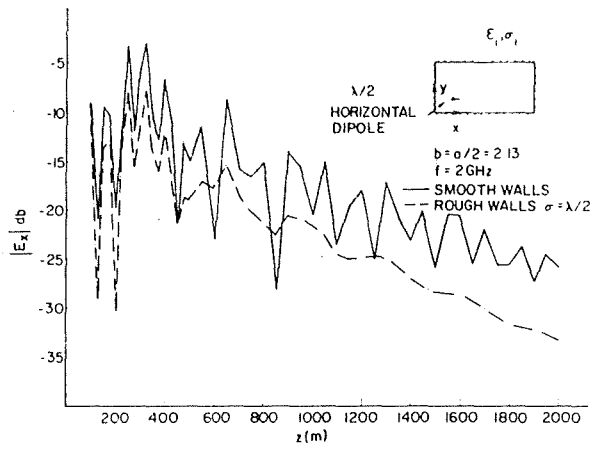

Fig. 9. Horizontal electric field versus distance z from the source inside a rectangular waveguide. Smooth and rough walls, 2 GHz.

by the coupling term. Hence, if we neglect R^* in (47) we can obtain the approximate formulas

$$\Pi_x'(x, y, z) \simeq (1/4\pi i\omega\epsilon_0) \sum_l \cdot \sum_i \exp(-ik_0 r_{li}) S^{n_i} R^{n_j} P_x \qquad (48)$$

and

$$\Pi_y'(x, y, z) \simeq (1/4\pi i\omega\epsilon_0) \sum_l \cdot \sum_i \exp(-ik_0 r_{li}) R^{n_i} S^{n_j} P_y \qquad (49)$$

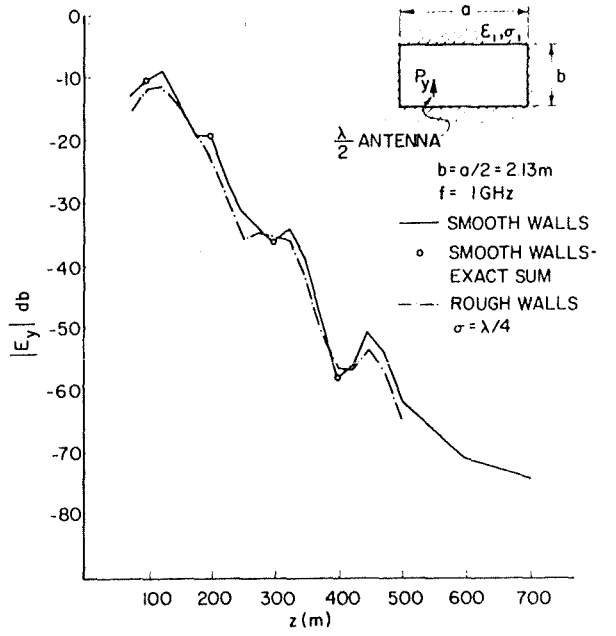

Fig. 8. Vertical electric field versus distance z from the source inside a rectangular waveguide. Smooth and rough walls, 1 GHz.

where n_l and n_j are the numbers of reflection on the vertical and horizontal walls, respectively, involved in forming the l-j image.

Some specific numerical results for the horizontal and vertical excitations at 1 and 2 GHz are shown in Figures 7 through 10. The solid curves are computed from the approximate equations (48, 49) and the small circles in Figures 7 and 8 represent points computed on the basis of the more exact expression (47). It is seen that the agreement between the exact and approximate expressions is very good.

CONSIDERATION OF WALL ROUGHNESS

So far the wall roughness has been neglected. This, however, may be important at the range of

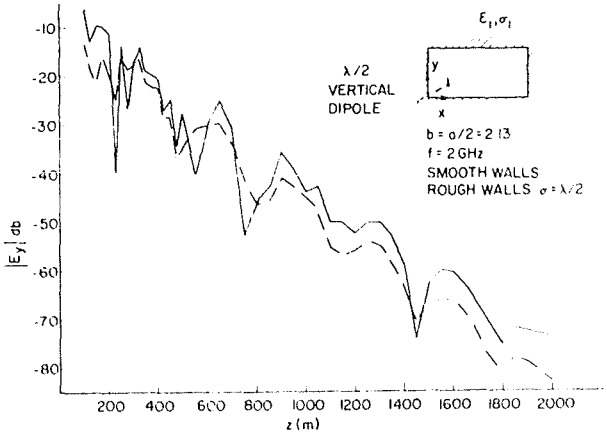

Fig. 10. Vertical electric field versus distance z from the source inside a rectangular waveguide. Smooth and rough walls, 2 GHz.

frequencies considered. For example, at 2 GHz the standard deviation of the mine tunnel walls may be of the order of $\lambda_0/2$. The simplest way to account for the roughness is to modify the Fresnel reflection coefficient in the specular direction while neglecting the nonspecular scattering. Using results obtained theoretically by *Beckmann and Spizzichino* [1963] and experimentally by *Beard* [1961], the specular Fresnel reflection coefficient R from a rough surface is given by

$$R = R_0 \exp(-\phi^2/2) \tag{50}$$

where R_0 is the Fresnel reflection coefficient from an average smooth surface, and $\phi = 4\pi\sigma \sin\psi/\lambda_0$. Here the rough surface is assumed to have a gaussian distribution with a standard deviation equal to σ, while ψ is the grazing angle of ray incidence. This expression is valid for values of $\sigma \sin\psi/\lambda_0 < 0.1$ [*Beard*, 1961], i.e., $\phi < 1.256$. Actually, for all cases of interest in the present investigation, this condition is well satisfied.

The simplicity of formula (50) makes it easy to incorporate the roughness effect in the geometrical ray series for the parallel plate waveguide (see Figures 5 and 11) as well as for the general rectangular waveguide (see Figures 7 through 10). We notice in these figures that the percentage increase of the attenuation due to roughness is greater when the horizontal polarization is dominant than when the vertical polarization is dominant. Also, this increase is greater for the higher frequencies (compare Figures 7 and 8 for 1 GHz with Figures 9 and 10 for 2 GHz).

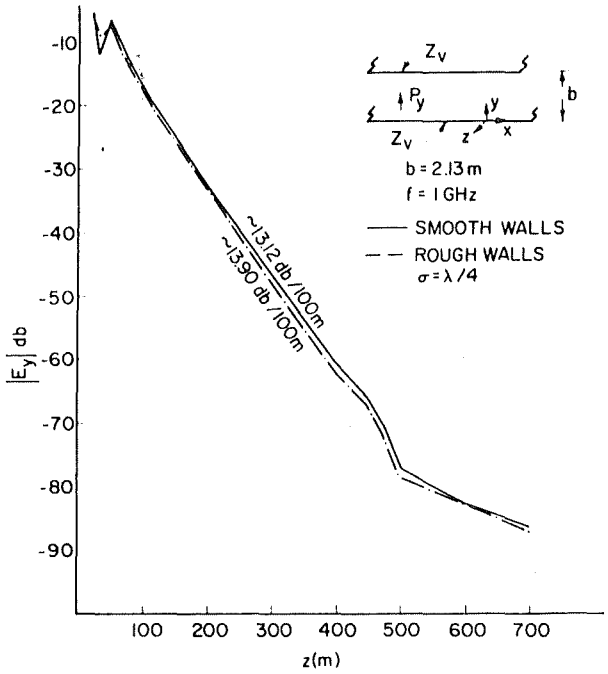

Fig. 11. Vertical electric field versus distance z from the source inside a parallel plate waveguide. Smooth and rough walls.

Equation 50 can also be incorporated in the modal equation for the parallel plate waveguide to study the effect of roughness on the first few dominant modes. This study should also help understand the same effect in the general rectangular waveguide. The modal equation for the parallel plate waveguide of width b is given by *Wait* [1970] as

$$R^2(k_y) \exp(-i2k_y b) = \exp(-i2n\pi) \tag{51}$$

For a rough surface guide, we substitute for $R(k_y)$ from (50), hence

$$R(k_y) = -[(k_y - k_0\Delta)/(k_y + k_0\Delta)] \exp(-2k_y^2\sigma^2)$$

where ϕ is replaced by $2k_y\sigma$, k_y is the wave number in the y direction (see Figure 4) and Δ is given by $\Delta = \Delta_h \simeq (\epsilon/\epsilon_0 - 1)^{1/2}$ for horizontally polarized waves and $\Delta = \Delta_v \simeq (\epsilon/\epsilon_0 - 1)^{1/2}/(\epsilon/\epsilon_0)$ for vertically polarized waves. Under the condition $n\pi/k_0 b\Delta \ll 1$, which is usually valid for lower-order modes, we can rewrite $R(k_y)$ in the approximate form

$$R(k_y) \simeq -\exp(-2k_y/k_0\Delta - 2k_y^2\sigma^2)$$

Hence (51) reduces to the quadratic equation

$$k_y^2\sigma^2 + k_y(1/k_0\Delta + ib) - in\pi = 0$$

whose solution can be put in the form

$$k_y \simeq k_{y0} + \delta k_{y0}$$

where

$$k_{y0} = n\pi/(b - i2/k_0\Delta)$$

and

$$\delta k_{y0} = i2(n\pi/b)^2\sigma^2(1 + i\sigma/k_0 b\Delta)/b$$

The corresponding longitudinal attenuation constant α is obtained from the relation

$$\alpha = R_e[(k_0^2 - k_y^2)^{1/2}] \simeq \alpha_0 + \delta\alpha$$

where

$$\alpha_0 \simeq 2(n\pi/b)^2/k_0^2\Delta b \tag{52}$$

$$\delta\alpha \simeq 2(n\pi/b)^3\sigma^2/k_0 b \tag{53}$$

and hence

$$\delta\alpha/\alpha_0 \simeq (n\pi/b)k_0\sigma^2\Delta \qquad (54)$$

In the above, k_{y0} and α_0 apply to the case of smooth walls ($\sigma = 0$) and δk_y and $\delta\alpha$ are the changes in these quantities due to roughness.

According to (54) we can see that $(\delta\alpha/\alpha_0)$ is a monotonically increasing function of frequency. However, the overall attenuation $\alpha + \delta\alpha$ decreases with frequency due to more grazing incidence of rays on the guide walls. Since Δ_v is smaller than Δ_h by a factor approximately equal to ϵ/ϵ_0, we also find from (54) that $\delta\alpha/\alpha_0$, for horizontal polarization, is greater than that for vertical polarization.

Numerical solutions of the modal equation (51) are presented in Figures 12 and 13 for horizontal and vertical polarizations. The parameter ϕ' on these figures is defined as $2n\pi\sigma/b$ and it is approximately equal to ϕ in (50) since $\sin\psi \simeq n\pi/k_0 b$. These results are seen to agree with the remarks stated above. We should admit, however, that this rough surface modification of the mode equation is certainly not rigorous. For one thing, it ignores the possible reconversion of the incoherent energy

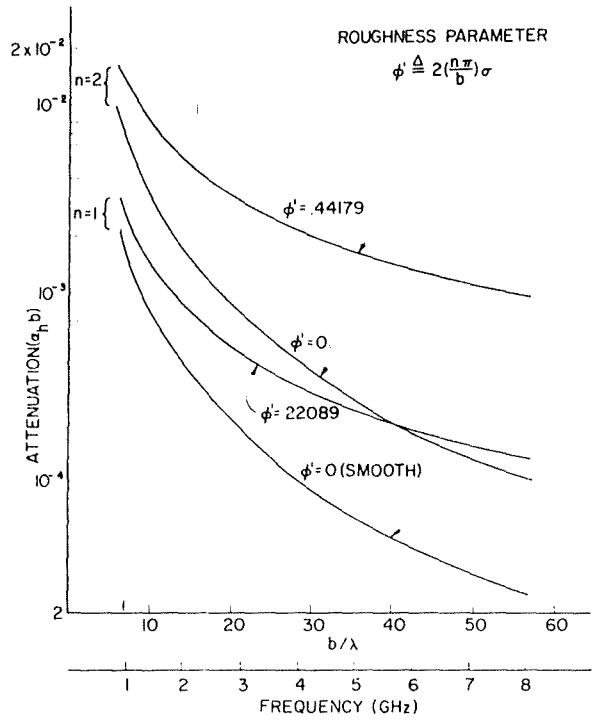

Fig. 12. Effect of roughness on the attenuation of horizontally polarized modes in a parallel plate waveguide. The lower horizontal scale corresponds to $b = 2.13$ m.

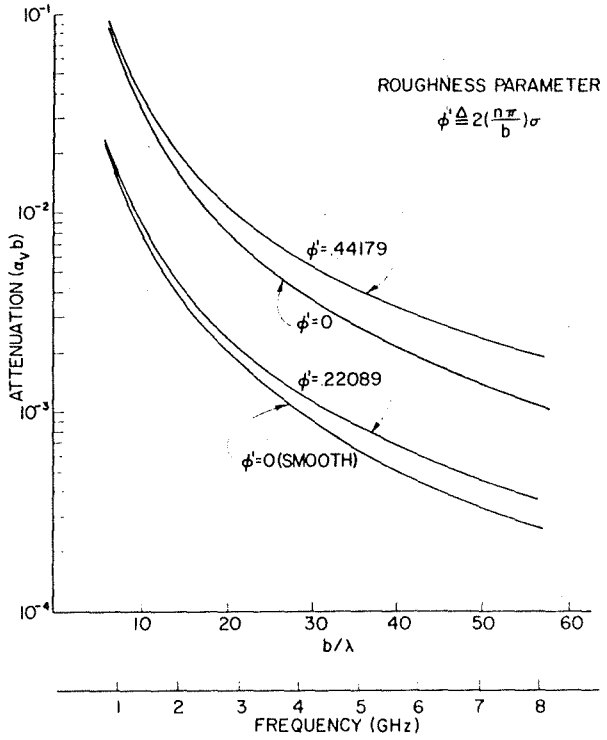

Fig. 13. Effect of roughness on the attenuation of vertically polarized modes in a parallel plate waveguide. The lower horizontal scale corresponds to $b = 2.13$ m.

back into the coherent portion following the multiple bounces in the guiding structure. We feel confident, however, that the present approach should give a reasonable estimate on the expected modification of the attenuation rate to roughness. If anything, it will lead to a more pessimistic picture than if we fully accounted for the reconverted energy from the incoherent waves.

CONCLUSIONS

Electromagnetic field excitation in a rectangular waveguide with imperfect walls, which may represent a mine tunnel, has been considered. Modal and geometrical ray sums have been obtained for the prototype model (i.e., when the two narrow side walls are assumed to be perfect reflectors). When all walls are imperfect, the modal propagation constants are not easy to obtain since the simple modes are intrinsically coupled. For this case, a geometrical ray summation has been derived, taking into account the coupling between the horizontally and vertically polarized rays. It is found, however, that this coupling can be neglected if only the field components of major polarization are of interest. Finally, the

effect of small roughness in the guide walls has been incorporated in the geometrical ray summation as well as in the modal equation for the case of a parallel plate waveguide. It has been demonstrated that the percentage increase in modal attenuation due to a typical wall roughness for mine tunnels increases with frequency although the overall attenuation is always a decreasing function of frequency due to a more grazing incidence of rays on the guide walls.

REFERENCES

Beard, C. I. (1961), Coherent and incoherent scattering of microwaves from the ocean, *IRE Trans. Antennas Propagat.*, *9*(9), 470–483.

Beckmann, P., and A. Spizzichino (1963), *The Scattering of Electromagnetic Waves from Rough Surfaces*, p. 124, Pergamon, New York.

Emslie, A. G., R. L. Lagace, and P. F. Strong (1973), Theory of propagation of UHF radio waves in coal mine tunnels, *Proceedings of Golden Workshop, School of Mines, Golden, Colorado, August 21–24*, pp. 38–48, Acc. No. PB 231 154, National Technical Information Service, Alexandria, Va.

Goddard, A. E. (1973), Radio propagation measurements in coal mines at UHF and VHF, *Proceedings of Thru-the-Earth Electromagnetic Workshop, Colorado School of Mines, Golden, Colorado, August 21–24*, pp. 54–61, Acc. No. PB 231 154, National Technical Information Service, Alexandria, Va.

Gradshteyn, L. S., and L. I. Ryzhik (1965), *Tables of Integrals, Series, and Products*, 4th ed., p. 923, Academic, New York.

Mahmoud, S. F., and J. R. Wait (1974), Theory of wave propagation along a thin wire inside a rectangular waveguide, *Radio Sci.*, *9*(3), 417–420.

Wait, J. R. (1959), *Electromagnetic Radiation from Cylindrical Structures*, p. 10, Pergamon, New York.

Wait, J. R. (1967), A fundamental difficulty in the analysis of cylindrical waveguides with impedance walls, *Electron. Lett.*, *3*(2), 87–88.

Wait, J. R. (1970), *Electromagnetic Waves in Stratified Media*, 2nd ed., chap. 6, p. 130, Pergamon, New York.

82 IEEE TRANSACTIONS ON COMMUNICATIONS, VOL. COM-24, NO. 1, JANUARY 1976

Calculated Channel Characteristics of a Braided Coaxial Cable in a Mine Tunnel

SAMIR F. MAHMOUD, MEMBER, IEEE, AND JAMES R. WAIT, FELLOW, IEEE

Abstract—**The braided coaxial cable is studied as a communication scheme in a mine tunnel. A simplified rectangular waveguide model is adopted for the tunnel, and the shield of the cable is assumed to behave as a single inductive transfer impedance. Specific results on the attenuation of the monofilar and bifilar (or coaxial) modes of propagation, taking into account the possible existence of a thin lossy film on the cable, are presented. In order to estimate the maximum possible range of communication, we consider the coupling factors of these modes to transmitting and receiving dipoles inside the tunnel, and we present results on these factors for various cable parameters and over a wide range of frequencies.**

INTRODUCTION

SEVERAL communication schemes in mine tunnels have recently been discussed. These include the two-wire open transmission line [1], the slotted coaxial cable [2], and the braided coaxial line [3], [4], all of which provide what is usually termed "continuous access guided communication." For any of these lines, one can identify two principal modes of propagation: the monofilar mode which provides a low coupling loss to the receiving or a transmitting antenna inside the tunnel, but which has a relatively high rate of attenuation; and the bifilar (or coaxial) mode which has the opposite properties. The design problem of a communication scheme in a given tunnel environment involves the best utilization of the properties of these two modes in order to achieve the longest range of communication.

In this paper, we consider the braided coaxial cable as a scheme of communication in mine tunnels. Thus, theoretical design data on the attenuation rates and coupling losses of the monofilar and bifilar modes are presented for various cable parameters and mine environments. Previous related work in the literature includes that due to Fontaine *et al.* [3], who considered the imperfect shield of the braided cable to provide a continuous coupling between two transmission lines, the first consisting of the outer shield of the cable and the earth, and the second being the cable itself with an assumed perfect shield. However, in their work, no detailed analysis of the tunnel walls and tunnel environment is attempted. Wait and Hill [4] have considered such effects on the attenuation of the modes in a circular tunnel.

Paper approved by the Associate Editor for Wire Communication of the IEEE Communications Society for publication after presentation at the U.S. National Meeting of URSI (International Union of Radio Science), Boulder, CO, October 1975. Manuscript received May 5, 1975; revised August 4, 1975.

S. F. Mahmoud was with the Cooperative Institute for Research in Enviromental Sciences, University of Colorado, Boulder, CO 80302. He is now with the Department of Electrical Engineering, Cairo University, Giza, Egypt.

J. R. Wait is with the Cooperative Institute for Research in Enviromental Sciences, University of Colorado, Boulder, CO 80302.

MODELING OF THE TUNNEL AND CABLE

The mine tunnel is modeled as a rectangular waveguide whose broad walls are a lossy dielectric medium with permittivity ϵ_e and conductivity σ_e. However, the narrow side walls are considered to behave as perfect electric conductors in order that a rigorous analytical treatment of the modes of propagation becomes possible. This tunnel model has been previously used, and has provided results for the case of a single wire inside the tunnel [5] that are in good agreement with measurements in an actual tunnel [1] and with theoretical results for a circular tunnel [6].

The outer shield of the braided coaxial cable is modeled as a transfer impedance $Z_T(\Omega/\text{m})$ which is taken equal to $j\omega L$, L being an inductance per unit length. A dielectric jacket of permittivity ϵ_c and an outer radius c surrounds the braid and is assumed to be covered by a thin outer lossy layer of mine dust or conducting fluid with a transfer impedance Z_L which is purely resistive. The filling dielectric of the cable has a permittivity ϵ, an outer radius b, and an inner radius a, and the inner conductor has a conductivity σ_w, with a resulting series impedance $z_w(\Omega/\text{m})$. As indicated in Fig. 1, the cable is located with its axis at distances $(s - s_0)$ and $(l - l_0)$ from the top and the side walls, respectively. The outer radius c of the jacket is sufficiently small compared to distances from all the walls, so that an azimuthally symmetrical current distribution inside the cable can be assumed for the important modes of the tunnel. In the following, we derive an equation for the modal propagation constants inside the rectangular tunnel containing the braided cable by extending a previous derivation [7].

MODAL PROPAGATION CONSTANTS

The fields for a given mode are assumed to have the dependence $\exp(i\omega t - \Gamma z)$ where ω is the applied angular frequency, Γ is the modal propagation constant for which solutions are being sought, and z is a distance along the axis of the tunnel. Looking from outside the cable, this appears to the tunnel as a line source with a longitudinal current $I_c = 2\pi c H_\phi$ where H_ϕ is the azimuthal magnetic field on the outside surface of the jacket ($\rho = c$). This current produces fields everywhere inside the tunnel, and the average longitudinal electric field E_z at $\rho = c + 0$, i.e., just outside the jacket, has been derived in an earlier paper [7] and is given by

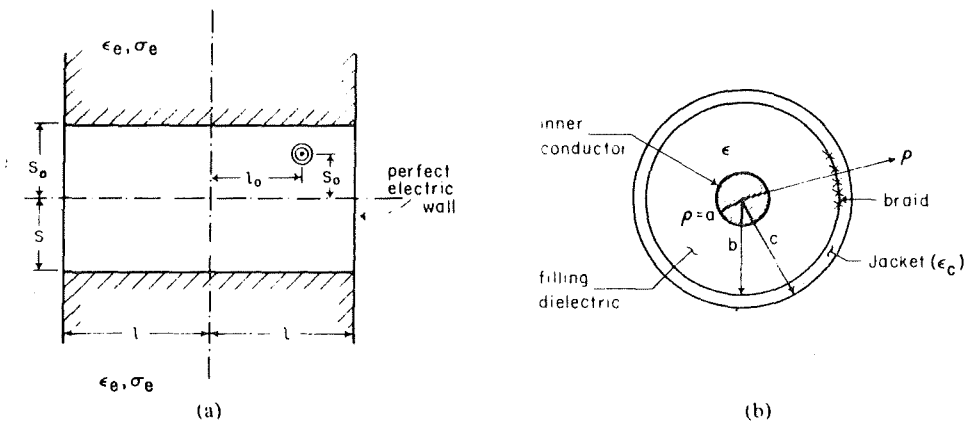

Fig. 1. (a) Rectangular waveguide model showing the location of the cable. (b) Internal structure of the braided coaxial cable.

$$E_z\,|_{\rho=c+0} = (i\omega\mu_0/\pi)D(\Gamma)\cdot I_c \tag{1}$$

where $D(\Gamma)$ is a function of the propagation constant Γ among other parameters pertaining to the tunnel dimensions, wall electrical constants, and the location and radius of the cable. $D(\Gamma)$ is given explicitly by a rather lengthy expression in the above reference, and hence will not be reproduced here.

In order to satisfy the boundary conditions requiring the continuity of E_z at the jacket outer surface, it is necessary to obtain this field at $\rho = c - 0$ from a consideration of the currents and fields inside the cable. Generally, this task involves expressing the fields in different regions in terms of appropriate Bessel functions and applying the boundary conditions at the respective interfaces. Considerable simplification results, however, if a quasi-static solution is used [4]. Such a solution requires that the condition βb, $\beta c \ll 1$ be satisfied where β is any transverse wavenumber in one of the dielectric regions inside the cable. This condition is usually met for the important modes of propagation except, perhaps, at UHF.

Wait and Hill [4] show that the effective series impedance per unit length $Z(\Gamma)$, defined as $E_z(\rho = c - 0)/I_c$, is given by

$$Z(\Gamma) = Z_L(Z_c + Z_b)/(Z_L + Z_c + Z_b) \tag{2}$$

where

$$Z_b = Z_T(Z' + Z_{\bar{w}})/(Z_T + Z' + Z_{\bar{w}}) \tag{3}$$

where

$$Z'(\Gamma) = -(\omega^2\mu\epsilon + \Gamma^2)\ln(b/a)/2\pi i\omega\epsilon \tag{4}$$

and

$$Z_c(\Gamma) = -(\omega^2\mu\epsilon_c + \Gamma^2)\ln(c/b)/2\pi i\omega\epsilon_c. \tag{5}$$

This is just the input impedance looking to the right at point (c) of the circuit shown in Fig. 2. Here the series impedances $Z'(\Gamma)$ and $Z_c(\Gamma)$ account for the filling dielectric and the jacket. The currents I_a, I_b, and I_c are interpreted as $\oint H_\phi dl$ where H_ϕ is the azimuthal magnetic field integrated over the circumferences at $\rho = a$, b, and c, respectively.

Fig. 2. Transverse equivalent circuit of the braided coaxial cable [4]. Solid and broken arrows represent the current flow lines for the monofilar and bifilar modes, respectively.

Now the modal equation is obtained by equating (1) by $I_cZ(\Gamma)$, and thus

$$(-i\omega\mu_0/\pi)\cdot D(\Gamma) = Z(\Gamma). \tag{6}$$

In relation to the equivalent circuit of Fig. 2, $(-i\omega\mu_0/\pi)\cdot D(\Gamma)$ is equal to minus the external impedance $Z_{ext}(\Gamma)$ looking into the tunnel from the jacket outer surface. Solutions of the modal equation (6) result in the monofilar mode, the bifilar mode, and the perturbed normal modes of the empty tunnel. The latter, however, have the property of being cut off at frequencies lower than about 50 MHz for typical tunnel dimensions, and hence will not be important for transmission in this range of frequency.

NUMERICAL SOLUTION OF THE MODAL EQUATION

The modal equation (6) has been solved for Γ of the monofilar and bifilar modes using the Newton-Raphson method. Previous results on Γ of the monofilar mode in a tunnel containing a single wire [5] have been used as initial roots in the above iterative method. For the bifilar mode, very good starting values of Γ are readily obtained from the equivalent circuit of Fig. 2 if we assume that both Z_L and Z_{ext} are much greater than Z_T, hence, by neglecting their effect, the modal equation takes the approximate form

$$Z_w + Z'(\Gamma) + Z_T \simeq 0. \tag{7}$$

Using (4) in (7), we obtain the approximate result

$$\Gamma_{bif}^2 = -\omega^2\mu\epsilon + [2\pi i\omega\epsilon(Z_w + Z_T)/\ln(b/a)]. \tag{8}$$

Some numerical computations on the attenuation rates of the monofilar and bifilar modes are shown in Figs. 3 and 4. Here $Z_L = 1/\sigma d$ with σd varying from 10^{-3} to 10^{-1} ℧ and $Z_T = i\omega L$ with $L = 40$ and 4 nH/m in Figs. 3 and 4, respectively. The following observations are evident from Figs. 3 and 4.

1) The attenuation of the bifilar mode is markedly affected by the conductivity of the inner conductor of the cable as it varies from $\sigma_w = 10^6$ to 5.7×10^7 ℧/m (Fig. 3). This is due to a concentration of the fields of this mode inside the cable.

2) The effect of the outer lossy film is to increase the attenuation of both modes, this increase being higher at higher frequencies and more pronounced for the bifilar mode.

3) The attenuation of the bifilar mode in Fig. 4 is seen to be much less sensitive to the conductivity of the outer lossy film. This is a result of reducing the braid transfer impedance Z_T relative to its value in Fig. 3. Such a reduction, however, causes a higher coupling loss to receiving or transmitting dipoles in the tunnel, as will be shown in the next section.

4) As has been observed in previous work [1], [5], [6], the attenuation of the monofilar mode increases as the cable approaches the tunnel wall (Fig. 3), while the bifilar mode remains almost unaffected.

It is quite interesting to notice a remarkable similarity between the above results and those obtained by Wait and Hill [4] for a circular tunnel model. The main difference occurs for the monofilar mode at the lower frequencies where the attenuation rate is very small in any case. Such differences can be attributed to the particular tunnel model being adopted. We may conclude, however, that the remarks 1)–4) stated above are, to a great extent, independent of the particular shape of the tunnel.

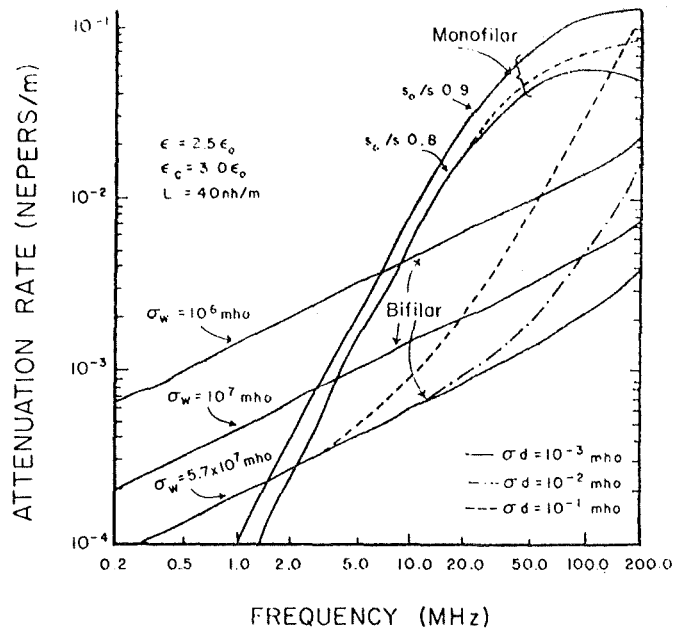

Fig. 3. Attenuation rates of the monofilar and bifilar modes versus frequency, $L = 40$ nH/m. In this figure and Fig. 4, $l = 2$ m, $s = 1.5$ m, $l/l_0 = 1/2$, $a = 1.5$ mm, $b = 10$ mm, and $c = 11.5$ mm, $\epsilon_c = 10\epsilon_0$ and $\sigma_c = 10^{-2}$ ℧/m.

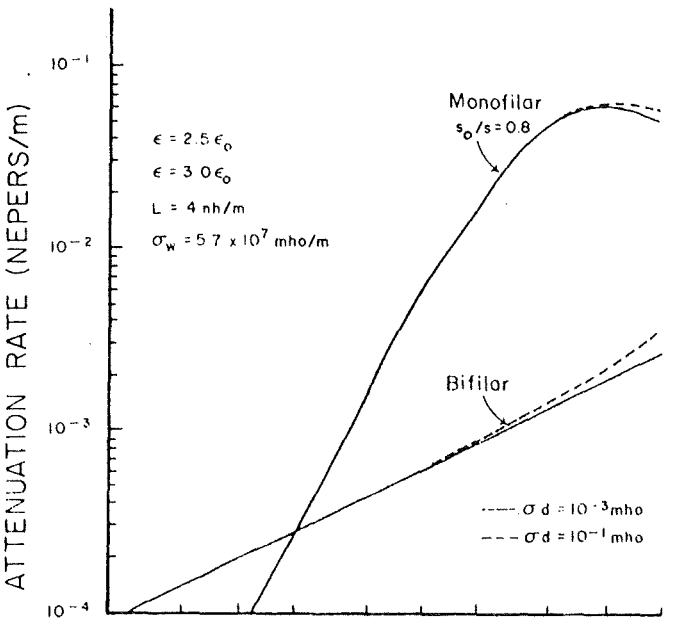

Fig. 4. Attenuation of the monofilar and bifilar modes versus frequency, $L = 4$ nH/m.

COUPLING LOSS AND COMMUNICATION RANGE

A transmitting dipole located inside the tunnel excites both the monofilar and bifilar modes among the normal modes of the empty tunnel. The latter, however, are of less importance due to their cutoff properties. Let $[\bar{e}_p, \bar{h}_p] \exp(-\Gamma_p z)$ for $p = 1, 2, \cdots$ represent the vector electric and magnetic field distributions of the pth mode, p being an integer that runs over all possible modes. Thus, a short dipole of moment $\bar{P} = I\bar{l}$, located at the point $(x_0, y_0, 0)$, will excite a summation of these modes given by

$$[\bar{E}, \bar{H}] = \sum_p \Lambda_p(x_0, y_0)[\bar{e}_p, \bar{h}_p] \exp(-\Gamma_p |z|). \tag{9}$$

Here, $\Lambda_p(x_0, y_0)$ is the excitation factor of the pth mode, and is a function of the dipole orientation and location in the tunnel cross section [8]. Thus,

$$\Lambda_p(x_0, y_0) = I\bar{l} \cdot \bar{e}_p(x_0, y_0) \Big/ \left[\int_S \bar{e}_p \times \bar{h}_p \cdot \bar{z}\, dS\right] \tag{10}$$

where the last integration is taken over the tunnel cross section.

Now, we assume that a similar dipole is used for reception and is located at (x_1, y_1, z_1); then, the received open-circuited voltage V is given by

$$V = \sum_p \bar{l} \cdot \bar{e}_p(x_1, y_1)\Lambda_p(x_0, y_0) \exp(-\Gamma_p z_1)$$

which, upon using (10), becomes

$$V = (1/I) \sum_p \Lambda_p(x_1, y_1)\Lambda_p(x_0, y_0)\left[\int_S \bar{e}_p \times \bar{h}_p \cdot \bar{z}\, dS\right] \cdot \exp(-\Gamma_p z_1). \tag{11}$$

Now, it is convenient to define another excitation factor, say, $\Lambda_p'(x,y)$, according to

$$\Lambda_p'(x,y) = \bar{l} \cdot \bar{e}_p(x,y) \Big/ \left[\eta \int_S \bar{e}_p \times \bar{h}_p \cdot \bar{z}\, dS \right]^{1/2} \tag{12}$$

where $\eta = \sqrt{\mu_0/\epsilon_0}$ is the free-space wave impedance which has been added only to render $\Lambda_p'(x,y)$ a dimensionless quantity. Hence, expression (11) can be recast in the form

$$(V/\eta I) = \sum_p \Lambda_p'(x_0,y_0)\Lambda_p'(x_1,y_1) \exp(-\Gamma_p z_1). \tag{13}$$

We thus find that the received voltage is made up of a summation of individual voltages induced by each propagating mode in the tunnel. It is clear that as z_1 increases, there comes a distance beyond which only one mode is responsible for the total received voltage. This mode is the least attenuated mode which, in our case, is the bifilar mode. The maximum possible range of communication is clearly a function of the properties of this mode alone, specifically, its excitation factors and attenuation rate. To express these ideas more thoroughly, we define a total loss L_p (in decibels) for the pth mode as follows:

$$L_p = -20 \log_{10} |\Lambda_p'(x_0,y_0)\Lambda_p'(x_1,y_1)| + \alpha_p z_1 \tag{14}$$

where $\alpha_p = 8.7$ Re (Γ_p). For a given transmitted power and minimum S/N ratio at the receiver, the total loss L_p of the bifilar mode cannot exceed a certain maximum $\hat{L}_p$, which in turn determines the maximum possible communication range. In the following, we shall find an estimate to the quantity L_p for the monofilar and bifilar modes.

As is apparent from (14), L_p is dependent on the locations of the transmitting and receiving dipoles and their orientations. However, in order to obtain meaningful results without the specification of any particular dipole location or orientation, and which can still reflect the effects of the line and tunnel parameters, we use the following argument. The fields of the monofilar and the bifilar modes outside the cable are linearly proportional to their respective modal currents on the outside surface of the cable, that is, $I_c = 2\pi c H_\varphi$ (at $\rho = c$). Furthermore, if we assume that the dipoles are always oriented to have maximum possible interaction with the modal fields, then a reasonable approximation to Λ_p' in (12) is

$$\Lambda_p' = \text{const}\, \eta^{1/2} \left| (I_c)_p f(\Gamma_p/k_0) \Big/ \left[\int_S \bar{e}_p \times \bar{h}_p \cdot \bar{z}\, dS \right]^{1/2} \right| \tag{15}$$

where k_0 is the free-space wavenumber and $f(\Gamma_p/k_0)$ is a function that represents the dependence of the modal fields on the modal propagation constant Γ_p and is, as yet, unknown. A look at the appropriate formulas [5, Appendix I] for the modal fields shows that the dependence on Γ_p is quite complicated. However, in the low-frequency limit, it is readily shown in Appendix I of this paper that the transverse fields are linearly proportional to Γ_p; hence, $f(\Gamma_p/k_0)$ in (15) is taken to be (Γ_p/k_0). This low-frequency approximation is believed to to be quite valid up to frequencies for which $2k_0 l \sim \pi$, and probably is still acceptable for higher frequencies. For typical tunnel dimensions, $2l = 4$ m; hence, the upper frequency limit is about 37.5 MHz.

Now the current I_c for the monofilar and bifilar modes is easily obtained from the circuit of Fig. 2 under the normalization $I_a = 1$. The flow of currents of the monofilar and bifilar modes are different, and are shown in Fig. 2 by solid and dashed arrows, respectively. It is straightforward to obtain $I_{c,\text{mono}}$ and $I_{c,\text{bif}}$ as

$$I_{c,\text{mono}} = [(Z_c(\Gamma_{\text{mono}}) + Z_L)(Z'(\Gamma_{\text{mono}}) + Z_T + Z_w) + Z_T(Z'(\Gamma_{\text{mono}}) + Z_w)]/Z_L Z_T \tag{16}$$

and

$$I_{c,\text{bif}} = Z_L Z_T / [(Z_c(Z_{\text{bif}}) + Z_T)(Z_{\text{ext}}(\Gamma_{\text{bif}}) + Z_L) + Z_{\text{ext}}(\Gamma_{\text{bif}})Z_L]. \tag{17}$$

In the special case when the outer lossy film is absent, i.e., $Z_L = \infty$, (16) and (17) take the simple forms

$$I_{c,\text{mono}} = [Z'(\Gamma_{\text{mono}}) + Z_T + Z_w]/Z_T \tag{18}$$

$$I_{c,\text{bif}} = Z_T/[Z_{\text{ext}}(\Gamma_{\text{bif}}) + Z_c(\Gamma_{\text{bif}}) + Z_T], \tag{19}$$

and as a check, if $Z_T = 0$, corresponding to a perfect shielding of the cable, the above two equations will imply that the bifilar mode has zero fields outside the cable, while the monofilar mode has zero fields inside the cable, as we would expect. Finally, the integration in (15) is obtained by a seminumerical method using expressions for the modal fields that were given before [5].

By combining (15) and (14), we arrive at

$$L_p = \text{const} - 20 \log_{10} \left| \eta(\Gamma_p/k_0)^2 I_{cp}{}^2 \Big/ \cdot \left[\int_S \bar{e}_p \times \bar{h}_p \cdot \bar{z}\, dS \right] \right| + \alpha_p z_1. \tag{20}$$

The coupling loss may be obtained from the above by putting $z_1 = 0$. Computed results of α_{mono}, α_{bif}, and the coupling loss for the monofilar and bifilar modes are tabulated for a range of frequencies in Tables I-III for the following three cases.

Case a: $L = 40$ nH/m, $\epsilon = 2.5\epsilon_0$.
Case b: $L = 4$ nH/m, $\epsilon = 2.5\epsilon_0$.
Case c: $L = 40$ nH/m, $\epsilon = 1.5\epsilon_0$.

The other cable parameters are held constant in all three cases. These are $1/\sigma d = 10^3\ \Omega$, $\sigma_w = 5.7 \times 10^7$ S/m, $\epsilon_c = 3\epsilon_0$, and the cable and tunnel dimensions are the same as in Fig. 3.

In case b, the cable has the least braid leakage, and in case c, the permittivity of the dielectric filling is chosen low to allow for a higher coupling between the fields of the bifilar mode and a transmitting or a receiving dipole. As would be expected, the coupling loss for the bifilar mode is highest in case b and lowest in case c. The quantity $R_{\min}$ in the last columns of Tables I-III is defined as the communication range at which both the monofilar and bifilar modes contribute equally to the received signal. Hence, at this range ($z_1 =$

TABLE I
COUPLING LOSS (CASE *a*)

Freq. (MHz)	α_{mono} (dB/km)	α_{bif} (dB/km)	Coupling Loss		R_{min} (km)
			Monofilar	Bifilar	
100	521.2	19.2	7.22	88.7	0.162
50	419.5	12.5	7.75	91.1	0.205
25	203.6	8.60	8.33	92.4	0.431
12.5	72.1	5.91	9.10	93.1	1.26
6.25	20.3	4.10	9.84	93.8	5.26

TABLE II
COUPLING LOSS (CASE *b*)

Freq. (MHz)	α_{mono} (dB/km)	α_{bif} (dB/km)	Coupling Loss		R_{min} (km)
			Monofilar	Bifilar	
100	534.5	16.8	7.55	139.4	0.255
50	428.6	11.9	7.99	140.2	0.316
25	206.2	8.42	8.52	141.5	0.671
12.5	73.1	5.95	9.24	141.3	1.96
6.25	20.4	4.24	10.04	140.6	8.25

TABLE III
COUPLING LOSS (CASE *c*)

Freq. (MHz)	α_{mono} (dB/km)	α_{bif} (dB/km)	Coupling Loss		R_{min} (km)
			Monofilar	Bifilar	
100	516.8	19.8	7.33	75.4	0.137
50	415.0	13.6	7.79	76.7	0.172
25	201.0	9.42	8.40	76.2	0.354
12.5	71.1	5.84	9.11	75.5	1.02
6.25	20.0	3.55	9.91	73.4	3.85

R_{min}), $L_{mono} = L_{bif}$, and at distances greater than R_{min}, the bifilar mode becomes the dominant propagating mode. In any well-designed communication scheme, the received signal-to-noise ratio S/N at R_{min} is well above the minimum allowable ratio; hence the maximum possible communication range R should be greater than R_{min}. As an example, assuming that the transmitter power and the received noise are such that the total signal loss L_{bif} is limited to, say, 150 dB for acceptable reception, then from Tables I-III we find that the maximum possible communication ranges at 25 MHz in the three tabulated cases are, respectively, $R = 6.69$, 1.08, and 7.82 km.

To study the dependence of R on the operating frequency, a detailed consideration of the maximum transmitter power and received noise as functions of the frequency should be investigated. This is outside the scope of this paper. The above results, however, show clearly the effects of the main cable parameters on the communication range, and should help in the design of a communication link in an actual tunnel.

CONCLUSIONS

A study of the important characteristics of the braided coaxial cable for communication in a mine tunnel has been presented. The analysis used accounts fully for the continuous exchange of energy between the tunnel and the cable. This is in contrast to the method of Fontaine *et al.* [3], who employed a perturbation-type coupled mode formalism. The results on the attenuation rates and coupling losses of the two principal modes of propagation obtained are believed to reveal the role of the various cable parameters in system design. We should stress, however, that in the present analysis, the braided cable and the tunnel are assumed to be completely uniform in the axial direction. Lateral variations of the cable parameters will cause additional coupling between the propagating bifilar and monofilar modes and the higher order cutoff modes. These mode conversion effects, whether intentional or accidental, play a role in the overall performance of the leaky cable systems in a mine tunnel environment. This aspect of the subject is receiving our attention.

APPENDIX I

In this Appendix, we prove that the transverse modal fields are linearly proportional to the modal progagation constant Γ in the low-frequency limit. The reader is referred to an earlier paper [5, Appendix I] for the basic equations and the symbols that will be used here.

The transverse modal fields [5] e_x and e_y are given by

$$e_x = -\Gamma\partial\Pi_z/\partial x + \partial^2\Pi_y/\partial x\partial y \tag{I-1}$$

$$e_y = -\Gamma\partial\Pi_z/\partial y + (k_0^2 + \partial^2/\partial y^2)\Pi_y \tag{I-2}$$

where Π_z and Π_y are two electric potentials that are not reproduced here. In the low-frequency limit, k_0, k_e, and Γ are neglected relative to $(\partial/\partial x)$ or $(\partial/\partial y)$; hence, the following substitutions are valid: $u_m \to u_{m1} \to m\pi/2l$, $R_m \to 0$, $S_m \to (\epsilon_1 - \epsilon_0)/(\epsilon_1 + \epsilon_0)$, $R_m^* \to \Gamma(\epsilon_1 - \epsilon_0)/((\epsilon_1 + \epsilon_0)u_m)$, $\Delta_m \to \Delta_m^* \to \exp(2u_m s)$. Using the above substitutions in the expressions of Π_z and Π_y, we find

$$\begin{aligned}
\partial\Pi_z/\partial x &\to (-i\omega\mu_0 I_c/\pi k_0^2)\sum_{m=0}^{\infty}(2\pi/l)\sin(m\pi x_0/l) \\
&\quad \cdot \cos(m\pi x/l)\exp(-u_m|y - y_0|) \\
&= (-i\omega\mu_0 I_c/k_0^2 l)\,\mathrm{Im}\left\{\sum_{m=0}^{\infty}\exp[-(m\pi/2l)\right. \\
&\quad \cdot (|y - y_0| - i(x + x_0)] - \exp[-(m\pi/2l) \\
&\quad \left. \cdot (|y - y_0| - i(x - x_0))]\right\} \\
&= (-i\eta/k_0 l)\,\mathrm{Im}\{[1 - \exp(-(\pi/2l) \\
&\quad \cdot (|y - y_0| - i(x + x_0))]^{-1} \\
&\quad - [1 - \exp(-(\pi/2l)(|y - y_0| - i(x - x_0))]^{-1}\}
\end{aligned}$$

where $x_0 = l + l_0$, $y_0 = s + s_0$, and Im stands for the imaginary part. Similar expressions are obtained for $\partial^2\Pi_y/\partial x\partial y$, $\partial\Pi_z/\partial y$, and $\partial^2\Pi_y/\partial y^2$. Substituting in (I-1) and (I-2), we arrive after simple algebra at

$$\begin{aligned}
e_x \to (i\eta I_c\Gamma/k_0 l)\,\mathrm{Im}\,[&X(|y - y_0|) \\
&- \epsilon' X(3s - s_0 - y) - \epsilon' X(y + y_0) \\
&- \epsilon'^2 X(3s - s_0 + y) - \epsilon'^2 X(4s + y_0 - y)]
\end{aligned} \tag{I-3}$$

and

$$e_y \to (i\eta I_c \Gamma / k_0 l)\ \mathrm{Re}\ [\pm X(|y - y_0|) - \epsilon' X(3s - a_0 - y) - \epsilon' X(y + y_0) - \epsilon'^2 X(3s - s_0 + y) - \epsilon'^2 X(4s + y_0 - y)], \quad \dot{y} \lesseqgtr y_0 \quad (I\text{-}4)$$

where Re stands for the real part and the function $X(y)$ is defined as

$$X(y) = [1 - \exp(-(\pi/2l)(y - i(x + x_0)))]^{-1} - [1 - \exp(-(\pi/2l)(y - i(x - x_0)))]^{-1}$$

and $\epsilon' = (\epsilon_1 - \epsilon_0)/(\epsilon_1 + \epsilon_0)$. Equations (I-3) and (I-4) show that the transverse fields are linearly proportional to Γ in the low-frequency limit.

ACKNOWLEDGMENT

We would like to thank Dr. D. A. Hill for his useful comments and L. Hope for her help in preparing the manuscript.

REFERENCES

[1] L. Deryck, "Exchanges d'energie entre modes de propagation sur ligne bifilaire," *Bull. Tech. "Mines et Carriers"* (Institut National des Industries Extractives, Belgium), no. 134, Dec. 1971.

[2] R. DeKeyser, P. Delogne, J. Janssens, and R. Liegeois, "Radio communication and control in mines and tunnels," *Electron. Lett.*, vol. 6, Oct. 26, 1970.

[3] J. Fontaine, B. Demoulin, P. Degauque, and R. Gabillard, "Feasibility of a radio communication in mine galleries by means of a coaxial cable having a high coupling impedance," in *Proc. Thru-the-Earth Electromagn. Workshop*, Colorado School of Mines, Golden, Aug. 1973. Available from Nat. Tech. Inform. Service, Alexandria, VA, Publ. 231 154.

[4] J. R. Wait and D. A. Hill, "Propagation along a braided coaxial cable in a circular tunnel," *IEEE Trans. Microwave Theory Tech.*, vol. MTT-23, pp. 401-406, May 1975.

[5] S. F. Mahmoud, "Characteristics of EM guided waves for communication in coal mine tunnels," *IEEE Trans. Commun.*, vol. COM-22, pp. 1547-1554, Oct. 1974.

[6] J. R. Wait and D. A. Hill, "Guided electromagnetic waves along an axial conductor in a circular tunnel," *IEEE Trans. Antennas Propagat.* (Succinct Papers), vol. AP-22, pp. 627–630, July 1974.

[7] S. F. Mahmoud and J. R. Wait, "Theory of wave propagation along a thin wire inside a rectangular waveguide," *Radio Sci.*, vol. 9, pp. 417–420, Mar. 1974.

[8] R. E. Collin, *Field Theory of Guided Waves*. New York: McGraw-Hill, 1960, p. 484.

Comments on "Calculated Channel Characteristics of a Braided Coaxial Cable in a Mine Tunnel"

PAUL P. DELOGNE

In the above paper[1] numerical evaluations of the coupling loss of a Hertz dipole to the monofilar and bifilar mode are presented in a normalized mode. The purpose of this correspondence is to draw the attention of potential users to the practical significance and limitations of these results.

In most works related to this subject, a bifilar coupling loss C_{bif} is defined as the ratio of the power radiated by a mobile dipole antenna to the part of that power converted into the bifilar mode or, equivalently, as the ratio of the power transported by the bifilar mode to the power available at the output of a mobile receiving dipole antenna. A monofilar coupling loss C_{mono} is defined in a similar way. It is clear that C_{bif} and C_{mono} are only useful concepts allowing range (i.e., signal-to-noise ratio) calculations if some conditions are met; this requires that the transmitter power and receiver noise are intrinsic characteristics of the equipment. They should thus be independent of the fact that the antenna is located in a tunnel, which requires that its input impedance and particularly the real part of it remains constant. This seems to be the case to some extent in the VHF and UHF bands. At lower frequencies, however, this is not at all true because the antenna is closer to an inductive or capacitive coupling device than to a radiating one. If, indeed, the antenna is small compared to the wavelength, the power radiated in free space and the one excited in the monofilar and bifilar modes can be quite different; hence, what should be called the coupling loss is not at all evident.

Mahmoud and Wait propose a normalized definition of two coupling losses L_{bif} and L_{mono}, but this calls for some comments. The first one is that according to their definition, L_{bif} and L_{mono} are relative to a mobile-to-mobile transmission and include twice the coupling effect of the antenna to the mode considered. A second comment is that L_{bif} and L_{mono} are only defined to some unknown constant K, which is the same for the two modes and which is independent on the frequency. As a result, as far as the classical coupling losses have meaning, one may write

$$C_{mono} = (L_{mono} + K)/2$$
$$C_{bif} = (L_{bif} + K)/2.$$

The authors have shown that L_{mono} and L_{bif} are to a large extent independent on the frequency, and this is consequently true for C_{mono} and C_{bif} too. Experience has confirmed this in the VHF and UHF range and has shown that C_{mono} is in the range 20–35 dB according to the positions of the cable and antenna in the tunnel cross section. So the contant K is in the range 32–62 dB and C_{bif} is very high (53–60 dB for case *a*, 78–86 dB for case *b*, and 46–53 dB for case *c*). Note also that the range called R_{min} by Mahmoud and Wait does not depend on K for mobile-to-mobile communication, and their numerical values are thus correct, but the range R_{min} would depend on K for fixed-to-mobile communications.

These values can be used for realistic range calculations in the VHF and UHF bands. However, it should be noted that the values of α_{bif} quoted by Mahmoud and Wait are optimistic because they do not take the influence of the braid loss into account; actual values are easily 50–100 percent higher. Moreover, it is expected that with transfer inductances as high as 40 nH/m, there will be a marked increase of α_{bif} when the cable comes close to the wall.

The author is with the Laboratoire de Telecommunications, Louvain-La-Neuve, Belgium.

[1] S. F. Mahmoud and F. R. Wait, *IEEE Trans. Commun.*, vol. COM-24, pp. 82–87, Jan. 1976.

At lower frequencies, conclusions are not straightforward. They require a detailed analysis of the coupling process for actual transmitting antennas; the noise generated in the loss resistance of the receiving antenna can be another important factor because the real part of the coupling impedance can be very small.

Reply by J. R. Wait[2]

JAMES R. WAIT

Prof. Delogne has made some very useful and pertinent comments on the subject of this paper.

An improved but, alas, a more complicated approach to the coupling losses is contained in a recent paper, "Calculated transmission loss for a leaky feeder communication system in a circular tunnel," by D. A. Hill and J. R. Wait, *Radio Sci.*, vol. 11, pp. 315–321, Apr. 1976.

[2] Paper approved by the Editor for Transmission Systems of the IEEE Communications Society for publication without oral presentation. Manuscript received April 30, 1976.

The author is with the Environmental Research Laboratories, National Oceanic and Atmospheric Administration, U.S. Department of Commerce, Boulder, CO 80302.

Reply by S. F. Mahmoud[3]

S. F. MAHMOUD

The comments of Prof. Delogne on our paper[1] seem very appropriate and instructive. I do agree with Prof. Delogne that at low frequencies, questions related to the receiver noise and perhaps the receiver matching become of primary importance.

The coupling loss in the aforementioned paper[1] is actually related only to the mutual impedance between the transmitting and receiving antennas but does not include the input resistances of these antennas. This drawback has been repaired in the paper "Calculated transmission loss for a leaky feeder communication systems in a circular tunnel" by Hill and Wait [1]. However, by limiting the antenna input resistance to a certain minimum value at the lower frequencies, the two definitions of the coupling loss in our paper[1] and [1] become identical (within a constant).

It is interesting to notice that both papers confirm the result that the coupling loss is a very slowly varying function of frequency for frequencies less than about 35 MHz. This is so in spite of the different approaches used in the two papers. Specifically, the coupling loss in Mahmoud and Wait's paper[1] is obtained without assigning any particular location or orientation of the antennas; hence, it can be considered as some kind of average coupling loss over various locations and orientations.

REFERENCES

[1] D. A. Hill and J. R. Wait, "Calculated transmission loss for a leaky feeder communication system in a circular tunnel," *Radio Sci. (Special Issue on Subsurface Telecommunications and Geophysical Probing)*, vol. 11, pp. 315–321, Apr. 1976.

[3] Paper approved by the Editor for Transmission Systems of the IEEE Communications Society for publication without oral presentation. Manuscript received May 28, 1976.

The author is with the Department of Electrical Engineering, Cairo University, Giza, Egypt.

Reprinted by permission from IEEE TRANSACTIONS ON ANTENNAS AND PROPAGATION
Vol. AP-22, No. 4, July 1974, pp. 627-630

Guided Electromagnetic Waves Along an Axial Conductor in a Circular Tunnel

JAMES R. WAIT AND DAVID A. HILL

Abstract—**A method to calculate the propagation characteristics of the guided modes in a circular tunnel bounded by lossy dielectric media is presented. The effect of an axial thin wire within the tunnel is also accounted for in the boundary value treatment of the problem. It is found that the attenuation of the transverse electromagnetic (TEM) or coax type mode is greatly increased when the conductor is moved toward the tunnel wall.**

INTRODUCTION

In many operational coal mines, it is desired to communicate along tunnel-like structures that may extend up to 7 or 8 km. While conventional telephone lines may be used, it has been found very convenient and effective to transmit VHF radio signals directly through the haulageway [1]. Normally, these tend to be rectangular in cross section and are located within coal seams. In United States mines, these tunnels are crisscrossed by approximately an equal number at right angles. Also, within most tunnels, there is a high voltage power cable that is suspended from the top wall. In addition, numerous metal roof bolts are located throughout the mine. It is evident that the transmission of electromagnetic waves in such a structure is very complicated. Nevertheless, in order to understand observations and to improve communication procedures, it seems worthwhile to analyze some idealized models of the situation.

Emslie *et al.* [2] have developed an approximate theory for the empty rectangular guide with lossy dielectric walls. Their ingenious development is an extension of an earlier analysis by Marcatili and Schmeltzer [3] for rectangular dielectric rods surrounded by free space. More recently, Mahmoud and Wait [4] and Mahmoud [5] have considered a rectangular waveguide bounded on the horizontal walls by a finite conductivity and permittivity, but the (narrower) side wall was idealized as having perfect magnetic or electric boundaries. This model permitted the rigorous satisfaction of the boundary conditions. Also, it was feasible to include the effect of axial conductors within the tunnel. The latter are obviously important if the frequency is sufficiently low that the modes for the empty guides are "cut off." Here we consider another idealized model that should provide new insight into the problem.

Specifically, we consider an air-filled tunnel of circular cross section with radius a bounded by a lossy dielectric medium. Within this uniform tunnel we located a relatively thin metal conductor of radius c, whose conductivity is σ. The situation is illustrated in Fig. 1 where we have chosen a cylindrical coordinate system (ρ,ϕ,z) to be coaxial with the guide. For the interior region $\rho < a$, the permittivity and permeability are ϵ_0 and μ_0, respectively. For the exterior region, the

Manuscript received December 12, 1973; revised February 19, 1974.
The authors are with the Institute for Telecommunication Sciences, Office of Telecommunications, United States Department of Commerce, Boulder, Colo. 80302.

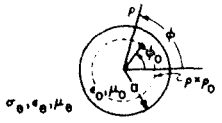

Fig. 1. Geometry of circular tunnel waveguide with axial conductor at distance ρ_0 from tunnel axis.

permittivity, conductivity, and permeability are ϵ_e, σ_e, and μ_e respectively. The thin axial conductor is located at $\rho = \rho_0$ and $\phi = \phi_0$; its corresponding electric properties are ϵ_s, σ_s, and μ_s. Here we restrict attention to the case $0 < \rho_0 < a$.

FORMULATION

Our objective now is to calculate the complex propagation constant of the dominant modes of the structure. Thus we assume that the field of an individual mode varies with z according to $\exp(-\Gamma z)$ for an implied time factor $\exp(i\omega t)$ where the values of Γ are to be determined. To obtain the solution, we exploit the fact that the fields can be completely determined by two scalar functions U and V that are, respectively, the z components of the (axially directly) electric and magnetic Hertz vectors.

The current on the axial conductor can be designated $I \exp(-\Gamma z)$. The primary field within the tunnel from this traveling wave of current may be derived from the electric-type Hertz function U^p. It is well known that [6]

$$U^p = \frac{i\mu_0\omega}{2\pi\gamma_0^2} I \exp(-\Gamma z) K_0[(\gamma_0^2 - \Gamma^2)^{1/2}\rho_d] \tag{1}$$

where $\gamma_0^2 = -\epsilon_0\mu_0\omega^2$, $\rho_d = [\rho^2 + \rho_0^2 - 2\rho\rho_0 \cos(\phi - \phi_0)]^{1/2}$, and K_0 is the modified Bessel function of the second kind. Now the total Hertz function within the guide can be written $U = U^p + U^s$ where U^s is the secondary part. The latter, for the region $\rho < a$, can be constructed by superimposing solutions of the type $I_m(v\rho) \exp(-im\phi) \exp(-\Gamma z)$ when I_m is a modified Bessel function of the first type, $v = (\gamma_0^2 - \Gamma^2)^{1/2}$, and m is any integer.

The above considerations and the addition theorem for K_0 in (1) lead us to the representation

$$U = \sum_{m=-\infty}^{+\infty} U_m \exp[-im(\phi - \phi_0)] \tag{2a}$$

or

$$U = \frac{i\mu_0\omega}{2\pi\gamma_0^2} I \exp(-\Gamma z) \sum_{m=-\infty}^{+\infty} I_m(v\rho_0)\left[K_m(v\rho) - R_m \frac{K_m(va)}{I_m(va)} I_m(v\rho)\right] \cdot \exp[-im(\phi - \phi_0)] \tag{2b}$$

for the region $\rho_0 < \rho < a$, where R_m is yet to be determined. Similar considerations lead us to the corresponding representation for the magnetic type Hertz function for the region $\rho < a$. Thus

$$V = \sum_{m=-\infty}^{+\infty} V_m \exp[-im(\phi - \phi_0)] \tag{3a}$$

or

$$V = \frac{i\mu_0\omega}{2\pi\gamma_0^2} I \exp(-\Gamma z) \sum_{m=-\infty}^{+\infty} \Delta_m I_m(v\rho_0) I_m(v\rho) \exp[-im(\phi - \phi_0)]. \tag{3b}$$

For the external region $\rho > a$ the Hertz functions are both made up from solutions of the form $K_m(u\rho) \exp(-\Gamma z) \exp(-im\phi)$ where $u = (\gamma_e^2 - \Gamma^2)^{1/2}$ and $\gamma_e^2 = i\mu_e\omega(\sigma_e + i\epsilon_e\omega)$.

For the region $\rho < a$, the tangential field components for the mth harmonic can be obtained from the mth harmonic of the Hertz functions as follows:

$$E_{\phi m} = \left(\frac{im\Gamma}{\rho}\right) U_m + i\mu_0\omega \frac{\partial V_m}{\partial \rho}$$

$$H_{\phi m} = \left(\frac{i\gamma_0^2}{\mu_0\omega}\right) \frac{\partial U_m}{\partial \rho} + \left(\frac{im\Gamma}{\rho}\right) V_m \tag{4}$$

$$E_{zm} = -v^2 U_m \text{ and } H_{zm} = -v^2 V_m$$

then, for example, the total axial field is

$$E_z = \sum_{m=-\infty}^{+\infty} E_{zm} \exp[-im(\phi - \phi_0)] \tag{5}$$

For the region $\rho > a$, the corresponding field quantities are obtained by replacing μ_0, γ_0^2, and v by μ_e, γ_e^2, and u, respectively.

WALL BOUNDARY CONDITIONS

The boundary conditions at the wall $\rho = a$ are that the tangential fields are continuous. For the present problem this is equivalent to applying the following conditions on the internal fields at $\rho = a$:

$$E_{\phi m} = \alpha_m E_{zm} + Z_m H_{zm} \tag{6}$$

$$H_{\phi m} = -Y_m E_{zm} + \alpha_m H_{zm} \tag{7}$$

where

$$\alpha_m = -\frac{im\Gamma}{(u^2 a)} \tag{8}$$

$$Z_m = -\left(\frac{i\mu_e\omega}{u}\right) \frac{K_m'(ua)}{K_m(ua)} \tag{9}$$

and

$$Y_m = \left(\frac{i\gamma_e^2}{u\mu_e\omega}\right) \frac{K_m'(ua)}{K_m(ua)}. \tag{10}$$

The wall impedance conditions in this form can be readily generalized to a concentrically layered external media and to certain anisotropic media. Here we will restrict attention to the homogeneous isotropic external region.

Using (2b), (3b), and (4), we readily obtain the following algebraic pair

$$\Delta_m[i\mu_0\omega v I_m' + Z_m v^2 I_m] + R_m\left[-\frac{im\Gamma}{a} K_m - \alpha_m v^2 K_m\right] = -\frac{im\Gamma}{a} K_m - \alpha_m v^2 K_m \tag{11}$$

and

$$\Delta_m\left[\frac{im\Gamma}{a} I_m + \alpha_m v^2 I_m\right] + R_m\left[-\frac{i\gamma_0^2 v}{\mu_0\omega} \frac{K_m I_m'}{I_m} + Y_m v^2 K_m\right] = -\frac{i\gamma_0^2 v}{\mu_0\omega} K_m' + Y_m v^2 K_m \tag{12}$$

where the arguments of the Bessel functions and their derivatives are va. Eliminating Δ_m from (11) and (12), we obtain the explicit result

$$R_m = \frac{[(\gamma_0/v) K_m'(va)/K_m(va)] + Y_m\eta_0 + \delta_m\eta_0}{[(\gamma_0/v) I_m'(va)/I_m(va)] + Y_m\eta_0 + \delta_m\eta_0} \tag{13}$$

where

$$\delta_m\eta_0 = \frac{(im\Gamma/a)^2[v^{-2} - u^{-2}]^2}{[(\gamma_0/v) I_m'(va)/I_m(va)] + (Z_m/\eta_0)} \tag{14}$$

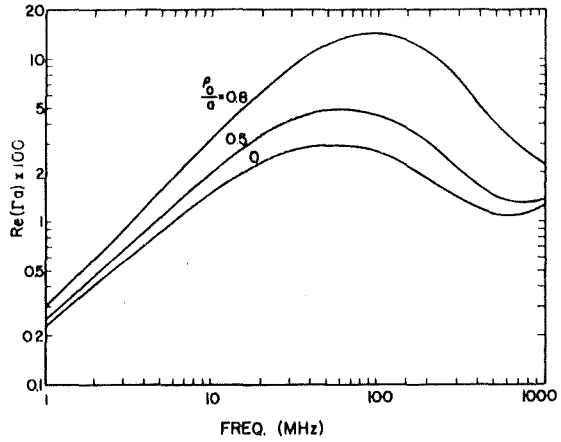

Fig. 2. Attenuation rate of COAX or TEM type mode as function of frequency for various locations of wire conductor. Multiply ordinate by 132.4 to convert to dB/100 ft.

and

$$\eta_0 = i\mu_0\omega/\gamma_0 \simeq 120\pi\ \Omega.$$

We now can express the axial electric field E_z anywhere within the guide in terms of the still unknown current $I \exp(-\Gamma z)$ on the wire. Using (1), (2b), and (4), this is given by

$$E_z = -\frac{i\mu_0\omega I v^2}{2\pi\gamma_0^2}\exp(-\Gamma z)\left[K_0(v\rho_d) - \sum_{m=-\infty}^{+\infty} R_m \frac{K_m(va)}{I_m(va)} I_m(v\rho_0) \cdot I_m(v\rho)\exp(-im(\phi-\phi_0))\right]. \quad (15)$$

WIRE BOUNDARY CONDITION

The boundary condition at the wire is

$$E_z = IZ_s \exp(-\Gamma z) \quad (16)$$

at $\rho_d = c_s$, for all values of z, where Z_s is the series impedance of the wire. Because of the assumed thinness of the wire, we can apply this condition at any point of the wire circumference. Thus we choose the matching point at $\rho = \rho_0 + c_s$ and $\phi = \phi_0$. Thus (16) leads to the mode equation

$$\frac{-i\mu_0\omega v^2}{2\pi\gamma_0^2}\left[K_0(vc) - \sum_{m=-\infty}^{+\infty} R_m \frac{K_m(va)}{I_m(va)} I_m(v\rho_0) I_m[v(\rho_0+c_s)]\right] = Z_s. \quad (17)$$

The explicit result for the series impedance [6] is

$$Z_s = \frac{\eta_s}{2\pi c_s}\frac{I_0(\gamma_s c_s)}{I_1(\gamma_s c_s)} \quad (18)$$

where $\gamma_s^2 = i\mu_s\omega(\sigma_s + i\epsilon_s\omega)$ and $\eta_s = i\mu_s\omega/\gamma_s$.

In principle, the problem as posed is solved when Γ is determined from (17). This mode equation is exact, subject only to the assumed thinness of the metal wire centered at (ρ_0,ϕ_0) inside the guide. In order to render the problem tractable, we will make a number of simplifying assumptions that are well justified on physical grounds.

SOME NUMERICAL RESULTS

For the high-frequency modes of interest we expect Γ to be on the order of $\gamma_0 = ik$, where $k = \omega/c$ is the free space wave number. Also, the bounding medium will have a conductivity and/or permittivity sufficiently high that $|\gamma_e a| \gg 1$. Involking these assumptions, we can approximate (9) and (10) as follows:

$$Y_m \simeq \frac{(i\mu_e\omega)}{(\gamma_e^2 + k^2)^{1/2}}$$

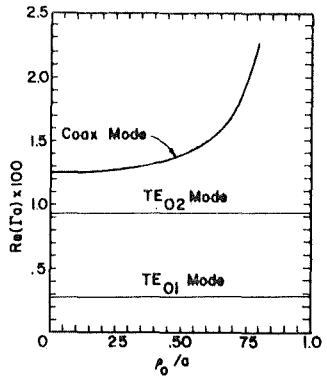

Fig. 3. Attenuation rate of COAX and TE modes for frequency of 1 MHz as function of wire conductor offset.

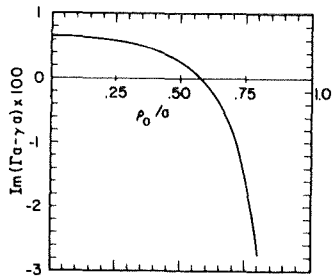

Fig. 4. Phase characteristic for COAX mode at 1 GHz.

and

$$Y_m \simeq \frac{\gamma_e^2}{[i\mu_e\omega(\gamma_e^2 + k^2)^{1/2}]}.$$

Also, in most cases at high frequencies, the conductivity of the metal wire will be sufficiently high that both $|\gamma_s c_s| \gg 1$ and $\sigma_s \gg \epsilon_s\omega$. Then from (18) we can obviously write

$$Z_s \simeq \left(\frac{\mu_s\omega}{2\sigma_s}\right)^{1/2}\frac{(1+i)}{(2\pi c_s)}.$$

With the simplifications indicated, some numerical solutions of (17) have been obtained. Of particular interest is the mode that has a transverse electromagnetic (TEM) character as the frequency is lowered. Using an adaptation of Newton's method, solutions of this type have been obtained. An example is shown in Fig. 2 where the following parameters are assumed: $a = 2m$, $\epsilon_e = 10\epsilon_0$, $\sigma_e = 10^{-2}$ mho/m, $\sigma_s = 10^5$ mho/m, $c_s = 10^{-2}$ m = 1 cm. Here the real part of (Γa) which is proportional to the attenuation rate, is plotted as a function of frequency from 1 to 1000 MHz. Three values of ρ_0/a, namely 0, 0.5, and 0.8 are indicated. *The ordinate in Fig. 2 is converted to dB per 100 ft in (obsolete) English units by multiplying by 132.4. Then the vertical scale extends from roughly 0.13 to 26 dB/100 ft.* The increase of the attenuation as the wire conductor approaches the wall is in accordance with the observations of Delogne *et al.* [7] in Belgian coal mines. Also Mahmoud [5] in his numerical studies of the rectangular guide has confirmed this effect.

For the geometry of the tunnel guide considered in the preceding example, we can expect higher order waveguide modes to appear when the frequency exceeds the cutoff value for the empty tube. This occurs approximately at 50 MHz in this case. For higher frequencies, we can expect the situation to be quite complicated. However, it appears we can always identify the TEM or COAX type mode as the one that is significantly influenced by the location and the series impedance of the wire conductor. In Figs. 3 and 4, we show the attenuation and phase characteristics for this COAX mode at a frequency of 1 GHz where the abscissa is the ratio ρ_0/a. The other parameters are the same as those shown in Fig. 2. We also show the attenuation rates for the TE_{01} and TE_{02} modes in Fig. 3 for the same

structures which are determined from the simplified mode equation $R_0^{-1} = 0$. In this case the wire conductor has no effect whatsoever on the modes of this type since the electric field has only a ϕ component. There is another class of modes here that can be described as perturbed TM and perturbed hybrid EH modes[1] that do interact with the wire conductor. A numerical study of these modes is presently underway. However, at least for the present geometry, they would appear to have attenuations greater than those shown in Fig. 3.

Another interesting point illustrated in Fig. 4 is that the phase velocity of the COAX mode is less than c when the wire conductor is at the center of the guide, but it becomes greater than c as the wire moves toward the wall. An analogous effect has been observed by Mahmoud [7] in his study of the rectangular guide.

[1] EH is standard nomenclature for modes that are neither E nor H type.

REFERENCES

[1] A. E. Goddard, "Radio propagation measurements in coal mines at UHF and VLF," in *Proc. Through-the-Earth Electromagnetics Workshop*, Colorado School of Mines, Golden, Colo., Aug. 15–17, 1973, available from Nat. Tech. Inform. Service, Alexandria, Va.

[2] A. G. Emslie, R. L. Lagace, and P. F. Strong, "Theory of the propagation of UHF radio waves in coal mine tunnels," in *Proc. Through-the-Earth Electromagnetics Workshop*, Colorado School of Mines, Golden, Colo., Aug. 15–17, 1973, available from Nat. Tech. Inform. Service, Alexandria, Va.

[3] E. A. J. Marcatili and R. A. Schmeltzer, "Hollow metallic and dielectric wave guides for long distance optical transmission and lasers," *Bell Syst. Tech. J.*, vol. 43, pp. 1783–1809, July 1964.

[4] S. F. Mahmoud and J. R. Wait, "Wave propagation along a thin wire inside a rectangular waveguide. Part I," *Radio Sci.*, vol. 9, Mar. 1974.

[5] S. F. Mahmoud, "Characteristics of EM guided waves for communication in coal mine tunnels, *IEEE Trans. Comm.*

[6] J. R. Wait, *Electromagnetic Radiation from Cylindrical Structures*. London: Pergamon, 1959 |

[7] P. Delogne, L. Deryck, and R. Liegois, "*Guided propagation of radio waves*," in *Proc. Through-the-Earth Electromagnetics Workshop*, Colorado School of Mines, Golden, Colo., Aug. 15–17, 1973, available from Nat. Tech. Inform. Service, Alexandria, Va.

Appl. Phys. 4, 307–312 (1974)

Applied Physics

Coaxial and Bifilar Modes on a Transmission Line in a Circular Tunnel

James R. Wait and David A. Hill

Institute for Telecommunication Sciences, Office of Telecommunications, U. S. Department of Commerce, Boulder, Colo. 80302, USA

Received 19 February 1974 / Accepted 15 May 1974

Abstract. We consider the axial propagation characteristics of a two-wire transmission line in a circular tunnel bounded by lossy dielectric media. The two modes of greatest interest correspond to conditions when the currents are either in-phase or anti-phase. The effect of the proximity of the tunnel wall is also accounted for in the boundary value treatment of the problem. The attenuation of the coaxial (unbalanced) mode is found to be greatly increased when the conductor is moved toward the tunnel wall but the bifilar (balanced) mode is much less affected.

In coal mines, it may be desired to communicate at distances up to 10 or 20 km along tunnels and haulageways [1, 2]. A rather ingenious communication technique is being developed for use in Belgian coal lines [3]. The idea is to use a two-wire transmission line or an equivalent loosely braided coaxial cable that can be suspended from the upper wall. A transmitter placed in the vicinity of the line excites a strongly unbalanced mode that normally would propagate like a coaxial or TEM mode with relatively high attenuation. The key step in the Belgian system, is to convert this unbalanced mode to a balanced mode that is much less attenuated because the return current flows mostly in the second wire rather than through the surrounding rock.

Here we carry out an analysis of the propagation characteristics for an idealized mine tunnel of circular cross section. The theory is developed only for a uniform structure so that mode conversion is not accounted for, but in all other respects, the problem is quite general. Some comparison is made with relevant experimental data.

Specifically, we consider an air-filled tunnel of circular cross-section with radius a bounded by a lossy dielectric medium. Within this uniform tunnel we locate a single relatively thin metal conductor of radius c_s whose conductivity is σ. The situation is illustrated in Fig. 1a where we have chosen a cylindrical coordinate system (ϱ, ϕ, z) to be coaxial with the guide. For the interior region $\varrho < a$ the permittivity and permeability are ε_0 and μ_0, respectively. For the exterior region, the permittivity, conductivity and permeability are ε_e, σ_e, and μ_e, respectively. The thin axial conductor is located at $\varrho = \varrho_0$ and $\phi = \phi_0$: its corresponding electric properties are ε_s, σ_s, and μ_s. Here we restrict attention to the case $0 < \varrho_0 < a$. Later, we investigate the effect of a second wire conductor that is parallel to the first.

Formulation

We now consider the complex propagation constant of the dominant modes of the structure. Thus, we assume that the fields of an individual mode varies with z according to $\exp(-\Gamma z)$ for an implied time factor $\exp(i\omega t)$, where the values of Γ are to be determined. The fields can be determined by two scalar functions U and V that are, respectively, the z components of (axially directly) electric and magnetic Hertz vectors.

The current on the axial conductor can be designated $I\exp(-\Gamma z)$. The primary field within the tunnel

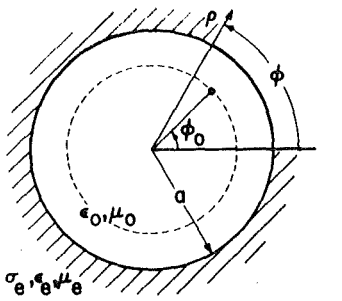

a

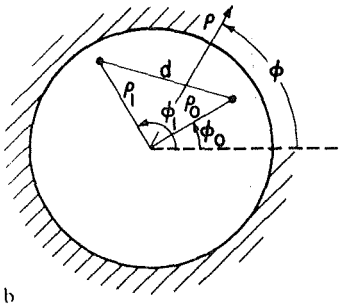

b

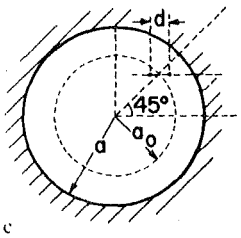

c

Fig. 1. (a) Geometry for single wire conductor in circular air-filled tunnel in homogeneous earth. (b) Geometry for two arbitrarily located axial wires within tunnel. (c) Geometry for two axial wires located in a horizontal plane in the upper quadrant of the tunnel cross-section. The mean distance to the tunnel wall is $a - a_0$

from this travelling wave of current may be derived from the electric-type Hertz function U^p. It is well known that [4]

$$U^p = \frac{i\mu_0\omega}{2\pi\gamma_0^2} I \exp(-\Gamma z)\, K_0[(\gamma_0^2 - \Gamma^2)^{\frac{1}{2}} \varrho_d]. \tag{1}$$

where $\gamma_0^2 = -\varepsilon_0\mu_0\omega^2$, $\varrho_d = [\varrho^2 + \varrho_0^2 - 2\varrho\varrho_0\cos(\phi - \phi_0)]^{\frac{1}{2}}$, and K_0 is the modified Bessel function of the second kind. The total Hertz function within the guide can be written, $U = U^p + U^s$, where U^s is the secondary part. The latter, for the region $\varrho < a$, can be constructed by superimposing solutions of the type $I_m(v\varrho)\exp(-im\phi)\exp(-\Gamma z)$ where I_m is a modified Bessel function of the first type, $v = (\gamma_0^2 - \Gamma^2)^{\frac{1}{2}}$, and m is any integer.

The above considerations and the addition theorem for K_0 in (1) leads us to the representation

$$U = \sum_{m=-\infty}^{+\infty} U_m e^{-im(\phi-\phi_0)}. \tag{2a}$$

where

$$U_m = \frac{i\mu_0\omega}{2\pi\gamma_0^2} I e^{-\Gamma z}\, I_m(v\varrho_0) \cdot \left[K_m(v\varrho) - R_m \frac{K_m(va)}{I_m(va)} I_m(v\varrho)\right] \tag{2b}$$

for the region $\varrho_0 < \varrho < a$, where R_m is yet to be determined. Similar considerations lead us to the corresponding representation for the magnetic-type Hertz function for the region $\varrho < a$. Thus.

$$V = \sum_{m=-\infty}^{+\infty} V_m e^{-im(\phi-\phi_0)}. \tag{3a}$$

where

$$V_m = \frac{i\mu_0\omega}{2\pi\gamma_0^2} I e^{-\Gamma z}\, \Delta_m I_m(v\varrho_0)\, I_m(v\varrho). \tag{3b}$$

For the external region $\varrho > a$ the Hertz functions are both made up from solutions of the form $K_m(u\varrho)\exp(-\Gamma z)\exp(-im\phi)$, where $u = (\gamma_e^2 - \Gamma^2)^{\frac{1}{2}}$ and $\gamma_e^2 = i\mu_e\omega(\sigma_e + i\varepsilon_e\omega)$.

For the region $\varrho < a$, the tangential field components for the m'th harmonic can be obtained from the m'th harmonic of the Hertz functions as follows

$$E_{\phi m} = (im\Gamma/\varrho)\, U_m + i\mu_0\omega\hat{c}\, V_m/\hat{c}\varrho \tag{4}$$

$$H_{\phi m} = (i\gamma_0^2/\mu_0\omega)\,\hat{c}\, U_m/\hat{c}\varrho + (im\Gamma/\varrho)\, V_m \tag{5}$$

$$E_{zm} = -v^2 U_m \quad \text{and} \quad H_{zm} = -v^2 V_m \tag{6}$$

then. for example. the total axial field is given by

$$E_z = \sum_{m=-\infty}^{+\infty} E_{zm} e^{-im(\phi-\phi_0)}. \tag{7}$$

For the region $\varrho > a$. the corresponding field quantities are obtained by replacing μ_0, γ_0^2 and v by μ_e, γ_e^2, and u, respectively.

Application of Boundary Conditions

The boundary conditions at the wall $\varrho = a$ are that the tangential fields are continuous. For the present problem this is equivalent to applying the following

conditions on the internal fields at $\varrho = a$

$$E_{\phi m} = \alpha_m E_{zm} + Z_m H_{zm} \tag{8}$$

$$H_{\phi m} = -Y_m E_{zm} + \alpha_m H_{zm}, \tag{9}$$

where

$$\alpha_m = -imI'/(u^2 a), \tag{10}$$

$$Z_m = -(i\mu_c\omega/u)\,\mathrm{K}'_m(ua)/\mathrm{K}_m(ua), \tag{11}$$

and

$$Y_m = (i\gamma_c^2/u\mu_c\omega)\,\mathrm{K}'_m(ua)/\mathrm{K}_m(ua). \tag{12}$$

As usual, the primes above denote differentiation of the Bessel function with respect to the indicated argument. The wall impedance conditions in this form can be readily generalized to a concentrically layered external media [4]. Here we will restrict attention to the homogeneous isotropic external region. We readily obtain the following explicit results for the coefficient R_m in (2b)

$$R_m = \frac{[(\gamma_0/v)\,\mathrm{K}'_m(va)/\mathrm{K}_m(va)] + Y_m\eta_0 + \delta_m\eta_0}{[(\gamma_0/v)\,\mathrm{I}'_m(va)/\mathrm{I}_m(va)] + Y_m\eta_0 + \delta_m\eta_0}, \tag{13}$$

where

$$\delta_m\eta_0 = \frac{(imI'/a)^2[v^{-2} - u^{-2}]^2}{[(\gamma_0/v)\,\mathrm{I}'_m(va)/\mathrm{I}_m(va)] + (Z_m/\eta_0)} \tag{14}$$

and $\eta_0 = i\mu_0\omega/\gamma_0 \simeq 120\pi\ \Omega$.

We now can express the axial electric field E_z anywhere within the guide in terms of the still unknown current $I\exp(-\Gamma z)$ on the wire. Using (1), (2b), and (6), this is given by

$$E_z = -\frac{i\mu_0\omega I v^2}{2\pi\gamma_0^2} e^{-\Gamma z}\left[\mathrm{K}_0(v\varrho_d) - \sum_{m=-\infty}^{+\infty} R_m \frac{\mathrm{K}_m(va)}{\mathrm{I}_m(va)}\,\mathrm{I}_m(v\varrho_0)\cdot \mathrm{I}_m(v\varrho)\,e^{-im(\phi-\phi_0)}\right]. \tag{15}$$

The boundary condition at the wire is

$$E_z = I Z_s \exp(-\Gamma z) \tag{16}$$

at $\varrho_d = c_s$ for all values of z, where Z_s is the series impedance of the wire. Because of the assumed thinness of the wire, we can apply this condition at any point of the wire circumference. Thus, we choose the matching point at $\varrho = \varrho_0 + c_s$ and $\phi = \phi_0$. Thus (16) leads to the mode equation

$$\frac{-i\mu_0\omega v^2}{2\pi\gamma_0^2}\left\{\mathrm{K}_0(vc) - \sum_{m=-\infty}^{+\infty} R_m \frac{\mathrm{K}_m(va)}{\mathrm{I}_m(va)}\cdot \mathrm{I}_m(v\varrho_0)\,\mathrm{I}_m[v(\varrho_0 + c_s)]\right\} = Z_s. \tag{17}$$

The explicit result for the series impedance [4] is

$$Z_s = \frac{\eta_s}{2\pi c_s}\frac{\mathrm{I}_0(\gamma_s c_s)}{\mathrm{I}_1(\gamma_s c_s)}, \tag{18}$$

where $\gamma_s^2 = i\mu_s\omega(\sigma_s + i\varepsilon_s\omega)$ and $\eta_s = i\mu_s\omega/\gamma_s$.

Extension to Two-Conductor System

We now consider the extension of the solution to the case where two axial conductors of radii c_0 and c_1 are present. The situation is illustrated in Fig. 1b. Now I_0, the current on the conductor at (ϱ_0, ϕ_0, z), is arbitrary, while I_1, the current on the conductor at (ϱ_1, ϕ_1, z), is unknown. By superimposing solutions of the form (15) we can write

$$E_z = \frac{-i\mu\omega v^2}{2\pi\gamma^2} e^{-\Gamma z}\left\{I_0\left[\mathrm{K}_0(v\varrho_d) - \sum_{m=-\infty}^{\infty} R_m \frac{\mathrm{K}_m(va)}{\mathrm{I}_m(va)}\,\mathrm{I}_m(v\varrho_0)\,\mathrm{I}_m(v\varrho)\,e^{-im(\phi-\phi_0)}\right] + I_1\left[\mathrm{K}_0(v\varrho'_d) - \sum_{m=-\infty}^{\infty} R_m \frac{\mathrm{K}_m(va)}{\mathrm{I}_m(va)}\cdot \mathrm{I}_m(v\varrho_1)\,\mathrm{I}_m(v\varrho)\,e^{-im(\phi-\phi_1)}\right]\right\}, \tag{19}$$

where $\varrho_d = [\varrho^2 + \varrho_0^2 - 2\varrho\varrho_0\cos(\phi - \phi_0)]^{\frac{1}{2}}$ and $\varrho'_d = [\varrho^2 + \varrho_1^2 - 2\varrho\varrho_1\cos(\phi - \phi_1)]^{\frac{1}{2}}$. The two relevant boundary conditions are

$$E_z = I_0 Z_{s0} e^{-\Gamma z} \quad \text{at} \quad \varrho = \varrho_0 + c_0,\ \phi = \phi_0, \tag{20a}$$

$$E_z = I_1 Z_{s1} e^{-\Gamma z} \quad \text{at} \quad \varrho = \varrho_1 + c_1,\ \phi = \phi_1, \tag{20b}$$

where Z_{s0} and Z_{s1} are the appropriate series impedances. The unknowns are I_1 (or I_1/I_0) and Γ. We can easily eliminate I_1 to yield a mode equation. This can be written as follows

$$\begin{vmatrix} A_0 & A_1 \\ B_0 & B_1 \end{vmatrix} = 0, \tag{21}$$

where the elements of the above determinant are

$$A_0 = \frac{\gamma_0}{V^2}\frac{2\pi Z_{s0}}{\eta_0} + K_0(v c_0) - \sum_m R_m \frac{K_m(va)}{I_m(va)} I_m[v(\varrho_0 + c_0)]\, I_m(v\varrho_0) \tag{22}$$

$$A_1 = K_0(v\varrho_d') - \sum_m R_m \frac{K_m(va)}{I_m(va)} \cdot I_m[v(\varrho_0 + c_0)]\, I_m(v\varrho_1)\, e^{-im(\phi_0 - \phi_1)} \tag{23}$$

$$B_0 = K_0(v\varrho_d) - \sum_m R_m \frac{K_m(va)}{I_m(va)} \cdot I_m[v(\varrho_1 + c_1)]\, I_m(v\varrho_0)\, e^{-im(\phi_1 - \phi_0)} \tag{24}$$

$$B_1 = \frac{\gamma_0}{v^2}\frac{2\pi Z_{s1}}{\eta_0} + K_0(v c_1) - \sum_m R_m \frac{K_m(va)}{I_m(va)} I_m[v(\varrho_1 + c_1)]\, I_m(v\varrho_1)\,. \tag{25}$$

In (23), ϱ_d' is evaluated at $\varrho = \varrho_0 + c_0$ and $\phi = \phi_0$, and in (24), ϱ_d is evaluated at $\varrho = \varrho_1 + c_1$ and $\phi = \phi_1$. In the case of identical wires we have: $Z_{s0} = Z_{s1} = Z_s$, $c_0 = c_1 = c_s$. In what follows this assumption will be adopted.

For the high-frequency modes of interest we expect Γ to be of the order of $\gamma_0 = ik$, where $k = \omega/c$ is the free space wave number. Also, the bounding medium will have a conductivity and/or permittivity sufficiently high that $|\gamma_e a| \gg 1$. Invoking these assumptions, we can approximate (9) and (10) as follows

$$Z_m \simeq (i\mu_e\omega)/(\gamma_e^2 + k^2)^{\frac{1}{2}} \tag{26}$$

and

$$Y_m \simeq \gamma_e^2/[i\mu_e\omega(\gamma_e^2 + k^2)^{\frac{1}{2}}]\,. \tag{27}$$

Also, in most cases at high frequencies, the conductivity of the metal wire will be sufficiently high that both $|\gamma_s c_s| \gg 1$ and $\sigma_s \gg \varepsilon_s\omega$. Then from (18) we can obviously write

$$Z_s \simeq (\mu_s\omega/2\sigma_s)^{\frac{1}{2}}(1 + i)/(2\pi c_s)\,. \tag{28}$$

With the simplifications indicated, some numerical solutions of (21) have been obtained. The actual computer program utilizes the approximations in (26) and (27) only when $|\gamma_e a|$ is sufficiently large and utilizes the approximation in (28) only when $|\gamma_s c_s|$ is sufficiently large in order to keep the frequency range completely general. Of particular interest are the modes that have a transmission-line character as the frequency is lowered. As we shall see, there are two

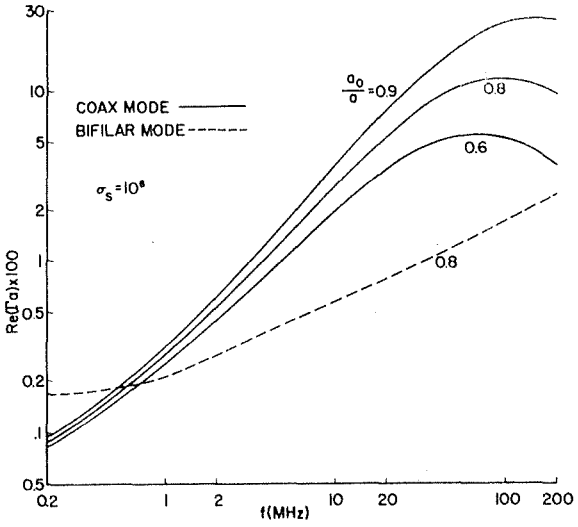

Fig. 2. The normalized attenuation rate as a function of frequency for the coaxial and bifilar modes for a wire conductivity $\sigma_s = 10^6$ mhos m

classes of these: in one case the current ratio I_1/I_0 is approximately $+1$ and in the other case the ratio is approximately -1. For obvious reasons, these are designated the coaxial and bifilar modes, respectively. Actually, in the unlikely case that $\varrho_0 = \varrho_1$, we have exactly $I_1 = \pm I_0$. Using an adaptation of Newton's method, solutions of the desired type have been obtained for the specific configuration shown in Fig. 1c. This is considered a reasonable idealization of the situation encountered in practice where the transmission line is suspended from the tunnel wall but offset from the centerline. An example is shown in Fig. 2 where the following parameters are assumed: $a = 2$ m, $\varepsilon_e = 10\varepsilon_0$, $\sigma_e = 10^{-2}$ mhos/m, $\sigma_s = 10^6$ mhos/m, $c_s = 10^{-3}$ m $= 1$ mm, and $d = 0.02$ m $= 2$ cm. Various values of the ratio a_0/a are shown for the coax mode but only the value 0.8 for the bifilar mode. Actually, in the latter case, the corresponding values for 0.9 and 0.6 are indistinguishable. The attenuation of the bifilar mode is also insensitive to the orientation of the two-wire line, and an approximate attenuation expression which neglects tunnel effects is given in the Appendix. Here the real part of Γa, which is proportional to the attenuation rate, is plotted as a function of frequency from 0.2 to 200 MHz. The increase of the coaxial mode attenuation as the wire conductor approaches the wall is apparent. Also Mahmoud [5], in his numerical studies of the rectangular guide, has confirmed this effect. Actually,

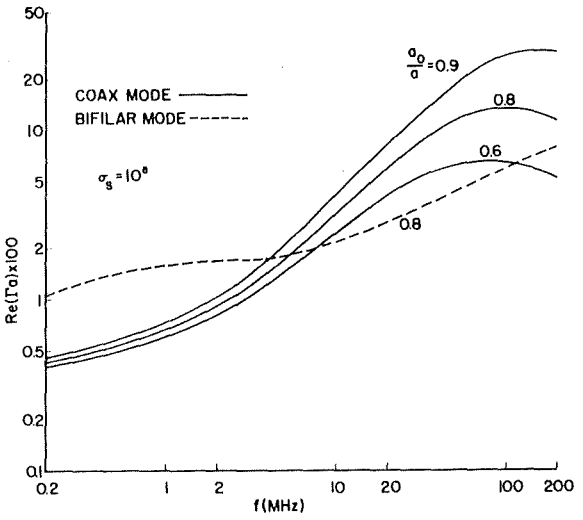

Fig. 3. The normalized attenuation rate as in Fig. 2 but for $\sigma_s = 10^5$ mhos/m.

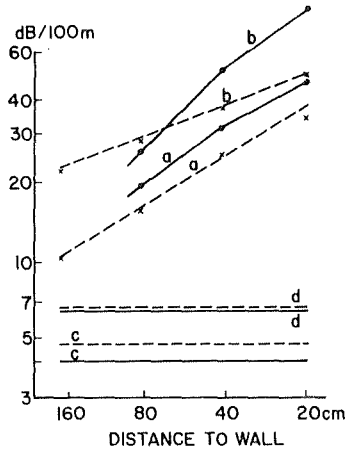

Fig. 4. Comparison of calculated (solid curves) and Deryck's observed (broken curves) data of attenuation rate as a function of the distance of the transmission line from the tunnel wall. Curves *a* and *b* are for the coaxial mode for 27 and 68 MHz, respectively, while curves *c* and *d* are for the bifilar mode for 27 and 68 MHz.

the attenuation rates are quite dependent on the assumed wire conductivity. As illustrated in Fig. 3, the losses are greatly increased when σ_s is assigned the value of 10^5 mhos/m corresponding to a steel cable, for example. Actually, the dependence on the other parameters, such as c_s and d, is not so severe.

For the geometry of the tunnel guide considered in the preceding example, we can expect higher-order waveguide modes to appear when the frequency exceeds the cut-off value for the empty tube. This occurs approximately at 50 MHz in this case. For higher frequencies, we can expect the situation to be quite complicated. However, it appears we can always identify the coax and bifilar modes as the ones that are significantly influenced by the location and the series impedance of the wire conductor. Modes that do not depend on the wires have been considered elsewhere by the authors and by Mahmoud [5].

Now we can make a specific comparison of our calculated results of the attenuation rates with some experimental data published by Deryck [6] for coaxial and bifilar mode propagation in a tunnel in Lanaye, Belgium. The actual tunnel has a total height of the order of 4–5 m and the width is of the order of 3–4 m. The comparison is indicated in Fig. 4, where the abscissa is the distance of the transmission line from the tunnel wall and the ordinate is the attenuation rate in dB per meter. The calculated results use the same parameters as in Fig. 2. As both the experimental and the theoretical curves show, there is a strong dependence on the proximity of the tunnel wall for the coaxial mode at both 27 and 68 MHz. On the other hand, there is virtually no dependence on the location of the transmission line for the case of the bifilar mode. This, of course, is an attractive feature for long distance communication. As Deryck [7] indicates, conversion from the easily excited coaxial mode to the bifilar mode permits efficient point-to-point communication, even when the transmitting and or receiving antennas are not closely coupled to the transmission line.

Concluding Remarks

In our analysis, we have adopted an idealized circular cross-section for the tunnel. Thus, strictly speaking, the calculated data are not valid for actual tunnels or haulageways in operational mines. However, it is interesting to note that the present results for the coaxial and bifilar modes are very similar to corresponding calculations carried out by Mahmoud for rectangular tunnels. Unfortunately, an exact modal analysis for the rectangular shaped tunnel is only possible when the side walls are either perfect electric or perfect magnetic conductors. Nevertheless, the principal characteristics of the coaxial and bifilar modes are very similar in the two geometries.

This suggests that the derived characteristics are qualitatively valid for non-circular tunnels provided the cross-sectional area is approximately the same.

Appendix

Since the tunnel has only a small effect on the bifilar mode, it is possible to derive an approximate expression for the propagation constant by considering only the primary fields of the two-wire line. The current ratio I_1/I_0 is approximately -1, and the mode equation reduces to

$$A_0 - A_1 = 0, \tag{29}$$

where

$$A_0 \simeq \frac{\gamma_0}{\Gamma^2}\,\frac{2\pi Z_s}{\eta_0} + K_0(\Gamma c_s)$$

and

$$A_1 \simeq K_0(\Gamma \varrho_d').$$

Since ϱ_d' is approximately equal to the wire spacing d and the modified Bessel functions can be replaced by the log term in the small argument expansion, (29) can be solved for Γ; i.e.

$$\Gamma = \gamma_0\left|1 + \frac{2\pi Z_s}{\gamma_0\eta_0 \ln(d/c)}\right|^{\frac{1}{2}}. \tag{30}$$

where Z_s is given by (18) or the simplified form in (28). The above expression for Γ was actually used as a starting value in the numerical determination of Γ by Newton's method. Unfortunately, no such convenient expression is available for the coaxial mode.

References

1. A. E. Goddard: Proceedings of Thru-the-Earth Electromagnetics Workshop, Colo. School of Mines, Golden, Colo., 15–17 August 1973, Available from National Technical Information Service, Alexandria, VA
2. A. G. Emslie, R. L. Lagace, P. F. Strong: Proceedings of Thru-the-Earth Electromagnetic Workshop, Colo. School of Mines, Golden, Colo., 15–17 August 1973, Available from National Technical Information Service, Alexandria, VA
3. P. Delogne, L. Deryck, R. Liegeois: Proceedings of Thru-the-Earth Electromagnetics Workshop, Colo. School of Mines, Golden, Colo., 15–17 August 1973, Available from National Technical Information Service, Alexandria, VA
4. J. R. Wait: *Electromagnetic Radiation from Cylindrical Structures* (Pergamon Press, Oxford 1959)
5. S. F. Mahmoud: Characteristics of EM guided waves for communication in coal mine tunnels, submitted to IEEE Trans. on Communication, February 1974
6. L. Deryck: Bulletin Technique "Minus et Carriers", No. 134, Dec. 1971 (Institut National des Industries Extractives, Belgium)
7. L. Deryck: Electronics Letters **8**, 3 (1972)

CHAPTER 12

Excitation of monofilar and bifilar modes on a transmission line in a circular tunnel

David A. Hill

Institute for Telecommunications Sciences, Office of Telecommunications, U. S. Department of Commerce, Boulder, Colorado 80302

James R. Wait

Cooperative Institute for Research in Environmental Sciences, University of Colorado, Boulder, Colorado 80302

(Received 27 March 1974; in final form 9 May 1974)

We consider the excitation of monofilar and bifilar modes on a transmission line in a circular tunnel by a short dipole antenna. As expected, the monofilar mode is excited more strongly by an antenna placed in the tunnel, but the bifilar mode has lower attenuation. The excessive losses in the monofilar or coaxial mode are attributed to the return current flow along the tunnel walls. In the bifilar or transmission-line mode the fields are more confined to the region of the wire conductors.

I. INTRODUCTION

In coal mines it is desirable to communicate for long distances along tunnels and haulageways. An ingenious communication technique which is being developed for use in Belgian coal mines[1,2] utilizes a two-wire transmission line that can be suspended from the upper wall. A transmitter placed in the tunnel excites mainly the monofilar mode which propagates like a coaxial or TEM mode. The key step in the Belgian system is to convert this mode to a bifilar mode which is less attenuated because the return current flows in the second wire rather than through the surrounding rock. This mode converter, in its simplest form,[1,2] is often just an inductance inserted in one line and a capacitor inserted in the other so that the monofilar mode is transformed into the bifilar mode. The monofilar mode could also be called the balanced or symmetrical mode, and the bifilar mode could be called the unbalanced or asymmetrical mode. In other cases, this conversion is achieved by random imperfections in the system such as nonuniformities in the tunnel cross section and/or changes in the wire spacing. Here we consider only the excitation of the modes on an idealized uniform structure.

The propagation constants of these modes have been examined by Mahmoud[3] for a rectangular tunnel and by Wait and Hill[4] for a circular tunnel. Here, we examine the excitation of these modes by an electric dipole in a circular tunnel containing a two-wire line. The same principles would apply to the excitation of the corresponding type modes on a single braided coaxial cable that is often used in mine communications.[5] However, we do not consider this situation explicitly here.

II. FORMULATION

The geometry, of the tunnel and the source dipole of moment **P** in the plane $z=0$, is shown in Fig. 1. Consequently, the source current density $\mathbf{J}_a$ can be written

$$\mathbf{J}_a(\rho, \phi, z) = \mathbf{P}\delta(\rho - \rho_a)\delta(\phi - \phi_a)\delta(z)/\rho, \tag{1}$$

where δ is the Dirac delta function. As indicated cylindrical coordinates (ρ, ϕ, z) are adopted so that the source is located at $(\rho_a, \phi_a, 0)$. This current source produces an axial electric field $E_{za}(\rho, \phi, z)$ that can be determined by an application of the method of reciprocity. The method was used by Mahmoud[6] for a rectangular tunnel containing a single axial conductor. The technique of exploiting the reciprocity theorem has been used extensively in the calculation of excitation efficiencies for VLF modes in the earth-ionosphere waveguide.[7,8]

We will also determine the wire currents $I_0(z)$ and $I_1(z)$ excited by the current source at $(\rho_a, \phi_a, 0)$. These wire currents are indicative of the strength of the excited monofilar and bifilar modes.

To facilitate our analysis, we write the axial current density for $z>0$ carried by the wires J_z in the form

$$J_z(\rho, \phi, z) = \exp(-i\beta z)\rho^{-1}[I_0\delta(\rho - \rho_0)\delta(\phi - \phi_0) + I_1\delta(\rho - \rho_1)\delta(\phi - \phi_1)], \tag{2}$$

for a time factor $\exp(i\omega t)$. Here $i\beta$ is the propagation constant of a given mode on the structure. The total field **e** of this current can be separated into transverse and axial components in the following manner:

$$\mathbf{e}(\rho, \phi, z) = \exp(-i\beta z)\{I_0[\mathbf{e}_{t0}(\rho, \phi, \beta) + \hat{z}e_{z0}(\rho, \phi, \beta)] + I_1[\mathbf{e}_{t1}(\rho, \phi, \beta) + \hat{z}e_{z1}(\rho, \phi, \beta)]\}. \tag{3}$$

Explicit field expressions can be derived from z components of electric and magnetic Hertz vectors[4] and will be given later.

We now apply the reciprocity theorem[9] to the current

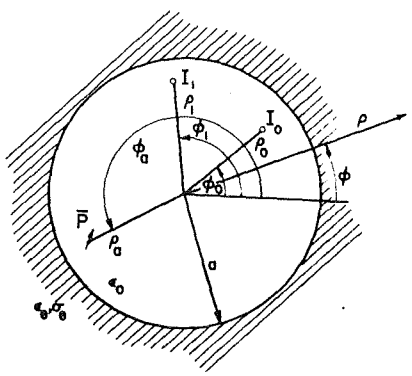

FIG. 1. Geometry for two wires and a source dipole in a circular air-filled tunnel in a homogeneous earth.

densities given by Eqs. (1) and (2) and their fields to yield the following:

$$\int_{-\infty}^{\infty}\int_{0}^{2\pi}\int_{0}^{\infty}\mathbf{J}_a(\rho,\phi,z)\cdot[I_0\,\mathbf{e}_{t0}(\rho,\phi,\beta) - I_1\mathbf{e}_{t1}(\rho,\phi,\beta)]\exp(-i\beta z)\rho\,d\rho\,d\phi\,dz = \int_{-\infty}^{\infty}\int_{0}^{2\pi}\int_{0}^{\infty}J_z(\rho,\phi,z)E_{za}(\rho,\phi,z)\rho\,d\rho\,d\phi\,dz. \quad (4)$$

The integrations in Eq. (4) can be carried out to obtain

$$I_0\mathbf{P}\cdot\mathbf{e}_{t0}(\rho_a,\phi_a,\beta)+I_1\mathbf{P}\cdot\mathbf{e}_{t1}(\rho_a,\phi_a,\beta) = I_0\int_{-\infty}^{\infty}E_{za}(\rho_0,\phi_0,z)\exp(-i\beta z)\,dz + I_1\int_{-\infty}^{\infty}E_{za}(\rho_1,\phi_1,z)\times\exp(-i\beta z)\,dz \triangleq I_0E'_{za}(\rho_0,\phi_0,\beta)+I_1E'_{za}(\rho_1,\phi_1,\beta), \quad (5)$$

where E'_{za} is the Fourier transform of E_{za}. Since I_0 and I_1 are arbitrary at this point, we can derive the following from Eq. (5):

$$E'_{za}(\rho_0,\phi_0,\beta)=\mathbf{P}\cdot\mathbf{e}_{t0}(\rho_a,\phi_a,\beta),\qquad E'_{za}(\rho_1,\phi_1,\beta)=\mathbf{P}\cdot\mathbf{e}_{t1}(\rho_a,\phi_a,\beta). \quad (6)$$

In order to obtain the induced wire currents, $I_0(z)$ and $I_1(z)$, we write them as Fourier transforms

$$I_0(z)=\frac{1}{2\pi}\int_{-\infty}^{\infty}I'_0(\beta)\exp(i\beta z)\,dz,\qquad I_1(z)=\frac{1}{2\pi}\int_{-\infty}^{\infty}I'_1(\beta)\exp(i\beta z)\,dz. \quad (7)$$

The boundary conditions at the wire match points require that

$$E'_{za}(\rho_0+c,\phi_0,\beta)+I'_0(\beta)e_{z0}(\rho_0+c,\phi_0,\beta)+I'_1(\beta)e_{z1}(\rho_0+c,\phi_0,\beta)=I'_0(\beta)Z_s,$$
$$E'_{za}(\rho_1+c,\phi_1,\beta)+I'_0(\beta)e_{z0}(\rho_1+c,\phi_1,\beta)+I'_1(\beta)e_{z1}(\rho_1+c,\phi_1,\beta)=I'_1(\beta)Z_s, \quad (8)$$

where

$$Z_s=\frac{\eta_s}{2\pi c}\frac{I_0(\gamma_s c)}{I_1(\gamma_s c)},\qquad \gamma_s^2\approx i\omega\mu\sigma_s,\qquad \eta_s=\frac{i\omega\mu}{\gamma_s},$$

σ_s is the wire conductivity, and c is the wire radius. The above expression for the wire series impedance per unit length[10,11] Z_s is actually an approximation which is valid for $|\gamma_s|^2 \gg |\beta|^2$. For sufficiently small values of c, Eq. (6) can be substituted into Eq. (8) to obtain

$$\begin{bmatrix}A_0(\beta) & A_1(\beta)\\ B_0(\beta) & B_1(\beta)\end{bmatrix}\begin{bmatrix}I'_0(\beta)\\ I'_1(\beta)\end{bmatrix}=\begin{bmatrix}-\mathbf{P}\cdot\mathbf{e}_{t0}(\rho_a,\phi_a,\beta)\\ -\mathbf{P}\cdot\mathbf{e}_{t1}(\rho_a,\phi_a,\beta)\end{bmatrix}, \quad (9)$$

where

$$A_0(\beta)=e_{z0}(\rho_0+c,\phi_0,\beta)-Z_s,\qquad A_1(\beta)=e_{z1}(\rho_0+c,\phi_0,\beta),$$
$$B_0(\beta)=e_{z0}(\rho_1+c,\phi_1,\beta),\qquad B_1(\beta)=e_{z1}(\rho_1+c,\phi_1,\beta)-Z_s.$$

Using Cramer's rule, $I'_0(\beta)$ can be written

$$I'_0(\beta)=[-B_1(\beta)\,\mathbf{P}\cdot\mathbf{e}_{t0}(\rho_a,\phi_a,\beta)+A_1(\beta)\,\mathbf{P}\cdot\mathbf{e}_{t1}(\rho_a,\phi_a,\beta)]\,[\Delta(\beta)]^{-1}, \quad (10)$$

where $\Delta(\beta)=A_0(\beta)B_1(\beta)-A_1(\beta)B_0(\beta)$.

A similar expression can be written for $I'_1(\beta)$. The zeros of $\Delta(\beta)$ are the characteristic values β_p of the waveguide modes that were examined previously.[4]

The wire current $I_0(z)$ is obtained by substituting Eq. (10) into Eq. (7) and converting the integral into the following residue series:

$$I_0(z)\approx i\sum_p[-B_1(\beta_p)\mathbf{P}\cdot\mathbf{e}_{t0}(\rho_a,\phi_a,\beta_p)+A_1(\beta_p)\mathbf{P}\cdot\mathbf{e}_{t1}(\rho_a,\phi_a,\beta_p)]\,[(d\Delta/d\beta)|_{\beta=\beta_p}]^{-1}\times\exp(-i\beta_p z), \quad (11)$$

where $I_m(\beta_p)<0$ and $|z|$ is sufficiently large that the heavily damped branch cut contribution can be ignored. At resonance, it is easy to see that

$$I'_1(\beta_p)/I'_0(\beta_p)=-B_0(\beta_p)/B_1(\beta_p). \quad (12)$$

Also, for sufficiently small c, $B_0(\beta)\approx A_1(\beta)$. Consequently, Eq. (11) can be rewritten in the following convenient form:

$$I_0(z)\approx-\operatorname{sgn}(z)i\sum_p\frac{B_1(\beta_p)}{(d\Delta/d\beta)|_{\beta=\beta_p}}\times\mathbf{P}\cdot\mathbf{e}_t(\rho_a,\phi_a,\beta_p)\exp(-i\beta_p|z|), \quad (13)$$

where

$$\mathbf{e}_t(\rho_a,\phi_a,\beta_p)=\mathbf{e}_{t0}(\rho_a,\phi_a,\beta_p)+\frac{I'_1(\beta_p)}{I'_0(\beta_p)}\mathbf{e}_{t1}(\rho_a,\phi_a,\beta_p).$$

Since $\mathbf{e}_t(\rho_a,\phi_a,\beta_p)$ can be considered the transverse modal field normalized to unity current in wire zero, Eq. (13) now contains the expected form of $\mathbf{P}$ dotted into the modal field. The denominator of Eq. (13) and the factor $B_1(\beta_p)$ have actually been computed in solutions of the mode equation $\Delta(\beta)=0$ by means of Newton's method for specific cases.[4] The behavior of $\mathbf{e}_t$ is considered in Sec. III.

III. TRANSVERSE FIELD VARIATIONS

The transverse electric field variation of a given mode is of interest in both the excitation problem as shown in Eq. (13) and the reception problem. For normalization purposes, let the current in wire zero be unity and the other current be $I'_1(\beta)$. For the monofilar mode, $I'_1(\beta_p)\approx 1$, and for the bifilar mode, $I'_1(\beta_p)\approx -1$. The exact values emerge from the solution of the mode equation.[4] All electric and magnetic field components can be derived from z components of electric and magnetic Hertz vectors, Π_z and Π_z^*. The transverse electric field required in Eq. (13) is

$$\mathbf{e}_t(\rho,\phi,\beta)=\hat{\rho}e_\rho(\rho,\phi,\beta)+\hat{\phi}e_\phi(\rho,\phi,\beta), \quad (14)$$

where

$$e_\rho=-\Gamma\frac{\partial\Pi_z}{\partial\rho}-\frac{i\omega\mu}{\rho}\frac{\partial\Pi_z^*}{\partial\phi}$$

and

$$e_\phi=-\frac{\Gamma}{\rho}\frac{\partial\Pi_z}{\partial\phi}+i\omega\mu\frac{\partial\Pi_z}{\partial\rho}.$$

Here we have let $\Gamma=i\beta$, and the z variation is $\exp(-\Gamma z)$. By substituting the known expressions[4] for Π_z and Π_z^* into Eq. (14) and carrying out the differentiations, the following expressions for e_ρ and e_ϕ are obtained in a form suitable for computation:

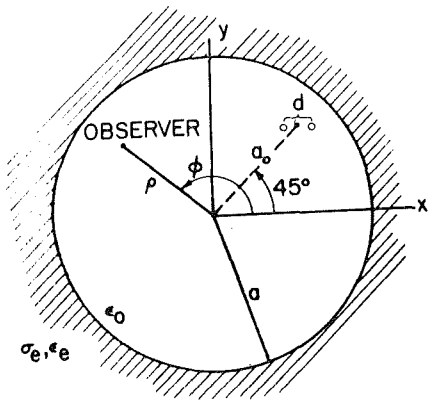

FIG. 2. Special geometry for a two-wire transmission line in a circular tunnel.

$$e_\rho = \frac{\eta_0}{2\pi}\left[\frac{\Gamma v}{\gamma}\left(\frac{\rho-\rho_0\cos(\phi-\phi_0)}{\rho_d}K_1(v\rho_d) - I_1'(\beta)\frac{\rho-\rho_1\cos(\phi-\phi_1)}{\rho_d'}K_1(v\rho_d')\right) + \sum_{m=0}^{\infty}\left(\frac{\Gamma v}{\gamma}\epsilon_m R_m\frac{K_m(va)}{I_m(va)}I_m'(v\rho) + \frac{2i}{\rho}m\eta_0\Delta_m I_m(v\rho)\right) \times[I_m(v\rho_0)\cos m(\phi-\phi_0) + I_1'(\beta)I_m(v\rho_1)\cos m(\phi-\phi_1)]\right], \quad (15)$$

$$e_\phi = \frac{\eta_0}{2\pi}\left[\frac{\Gamma}{\gamma}\left(\frac{v\rho_0\sin(\phi-\phi_0)}{\rho_d}K_1(v\rho_d) + I_1'(\beta)\frac{v\rho_1\sin(\phi-\phi_1)}{\rho_d'}K_1(v\rho_d')\right) - 2\sum_{m=1}^{\infty}\left(\frac{\Gamma}{\gamma\rho}mR_m\frac{K_m(va)}{I_m(va)}I_m(v\rho) + v i\eta_0\Delta_m I_m'(v\rho)\right) \times[I_m(v\rho_0)\sin m(\phi-\phi_0) + I_1'(\beta)I_m(v\rho_1)\sin m(\phi-\phi_1)]\right]$$

where $\rho < a$,

$$\rho_d = [\rho^2+\rho_0^2-2\rho\rho_0\cos(\phi-\phi_0)]^{1/2},$$
$$\rho_d' = [\rho^2+\rho_1^2-2\rho\rho_1\cos(\phi-\phi_1)]^{1/2},$$
$$v = (\gamma^2-\Gamma^2)^{1/2},$$
$$\epsilon_m = 1, \quad m = 0$$
$$= 2, \quad m \neq 0,$$

γ is the free-space propagation constant, a is the tunnel radius, η_0 is the characteristic impedance of free space, and I_m and K_m are modified Bessel functions of order m. The quantities R_m and Δ_m are determined from the tunnel boundary conditions and are given by[4]

$$R_m = \frac{\{(\gamma/v)K_m'(va)[K_m(va)]^{-1}\} + Y_m\eta_0 + \delta_m\eta_0}{\{(\gamma/v)I_m'(va)[I_m(va)]^{-1}\} + Y_m\eta_0 + \delta_m\eta_0},$$

$$\Delta_m = \left(\frac{K_m(va)}{I_m(va)}\frac{R_m-1}{\eta_0}\right)\frac{(im\Gamma/a)(v^{-2}-u^{-2})}{\{(\gamma/v)I_m'(va)[I_m(va)]^{-1}\} + Z_m/\eta_0}, \quad (16)$$

where

$$\delta_m\eta_0 = \frac{(im\Gamma/a)^2(v^{-2}-u^{-2})^2}{\{(\gamma/v)I_m'(va)[I_m(va)]^{-1}\} + Z_m/\eta_0},$$

$$Z_m = -(i\omega\mu/u)K_m'(ua)[K_m(ua)]^{-1},$$
$$Y_m = (i\gamma_e^2/u\mu\omega)K_m'(ua)[K_m(ua)]^{-1},$$
$$u = (\gamma_e^2-\Gamma^2)^{1/2},$$
$$\gamma_e^2 = i\omega\mu(\sigma_e + i\omega\epsilon_e),$$

ω is the angular frequency, and σ_e and ϵ_e are the conductivity and permittivity of the surrounding rock. In the numerical evaluation of Eqs. (15) and (16), the required modified Bessel functions are quickly computed by recurrence (backward for I_m and forward for K_m).

In order to treat a specific numerical example, consider the special geometry of Fig. 2. Let x and y be the horizontal and vertical coordinates where a horizontal two-wire transmission line of wire spacing d is centered at $\rho = a_0$ and $\phi = 45°$. The horizontal and vertical electric field components, e_x and e_y, at the observation point (ρ, ϕ) are given by

$$e_x = e_\rho\cos\phi - e_\phi\sin\phi,$$
$$e_y = e_\rho\sin\phi + e_\phi\cos\phi. \quad (17)$$

These rectangular components are the ones of interest when considering transmission or reception with horizontal or vertical dipoles. For convenience, we consider a case for which the propagation constants of the monofilar and bifilar modes have already been computed[4]: frequency = 20 MHz, $a = 2$ m, $\epsilon_e/\epsilon_0 = 10$, $\sigma_e = 10^{-2}$ mho/m, wire conductivity $\sigma_s = 10^6$ mho/m, wire radius $c = 10^{-3}$ m, $d = 0.02$ m, and $a_0/a = 0.8$. Solutions of this mode equation for this case yield for the monofilar mode:

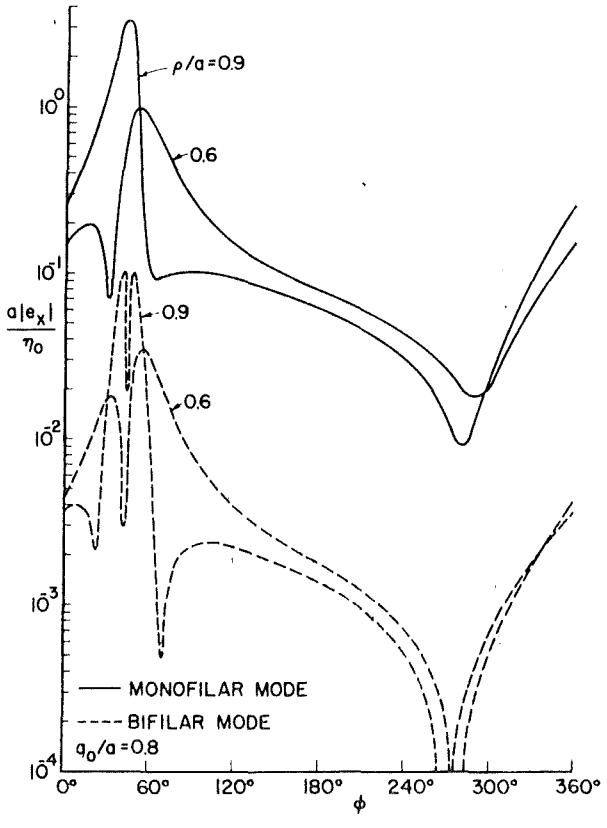

FIG. 3. Magnitude of the horizontal electrical field as a function of azimuth angle ϕ for both monofilar and bifilar modes.

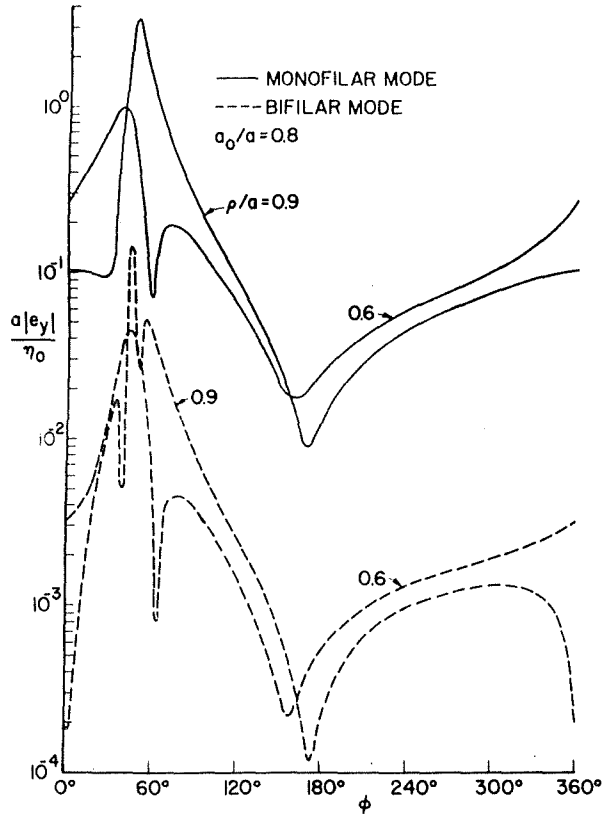

FIG. 4. Magnitude of the vertical electric field as a function of azimuth angle ϕ for both monofilar and bifilar modes.

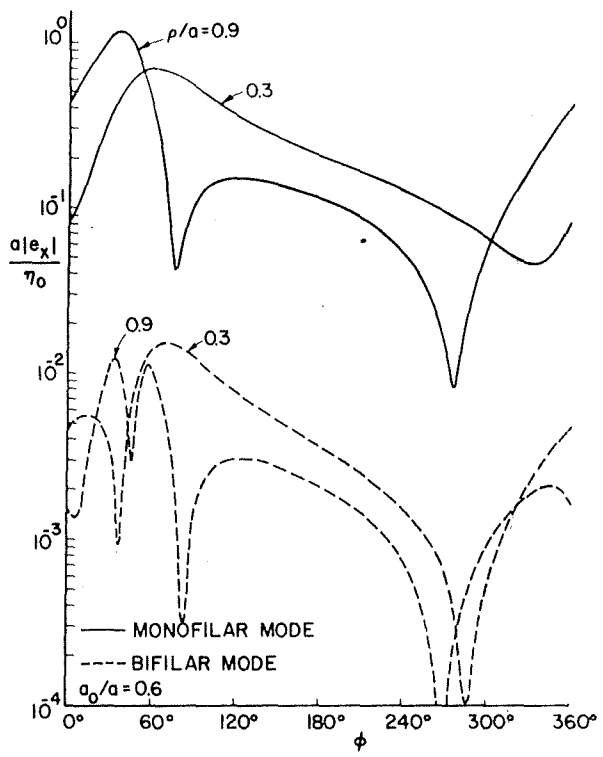

FIG. 5. Magnitude of the horizontal electric field as a function of azimuth angle ϕ for both monofilar and bifilar modes. The value of a_0/a has been decreased to 0.6.

$$\Gamma a = 5.478\times10^{-2} + i8.882\times10^{-1}, \qquad (18)$$

$$I_1/I_0 = 0.9189 \angle -0.898°;$$

for the bifilar mode:

$$\Gamma a = 7.809\times10^{-3} + i8.547\times10^{-1},$$

$$I_1/I_0 = -1.0127 \angle 0.264°.$$

Here we have designated the wire closest to the wall as wire zero. Note that the $R_e(\Gamma a)$, which proportional to the attenuation, is about seven times greater for the monofilar mode, and that the current ratios I_1/I_0 are close to ± 1 as expected. For the frequency and tunnel size considered here, only the monofilar and bifilar modes carry significant power since all other modes are "cut off".

Substitution of the numerical results of Eq. (18) into Eq. (15) yields the desired field quantities. In Fig. 3, the normalized horizontal field $a|e_x|/\eta_0$ is shown as a function of ϕ for $\rho/a = 0.6$ and 0.9 for both modes, and in Fig. 4 the normalized vertical field $a|e_y|/\eta_0$ is shown for the same cases. The field variations are rather complicated in the vicinity of the transmission line ($\phi = 45°$), but the important point is that field strength of the bifilar mode is generally down by a factor of about 100 from that of the monofilar mode throughout the tunnel.

In order to demonstrate that the above trends do not depend on the location of the transmission line, we consider a second example where the distance of the line from the wall is doubled, $a_0/a = 0.6$. All other parameters are the same as above. Solution of the mode

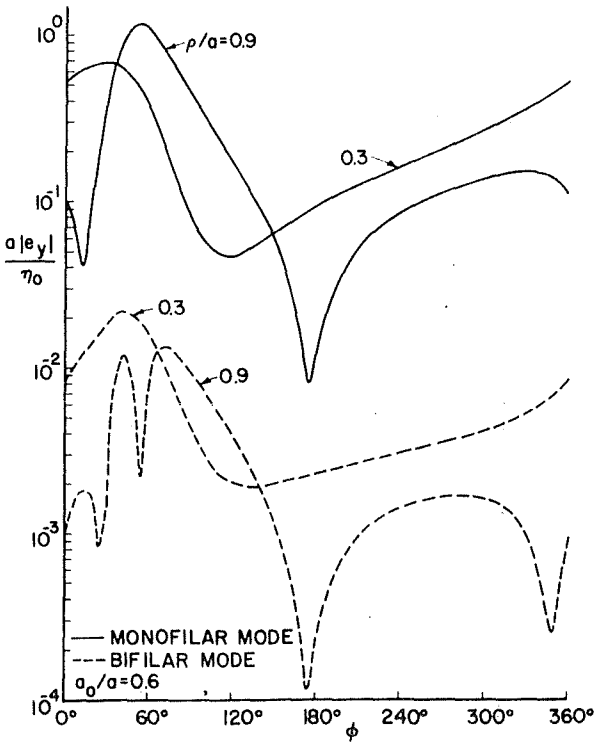

FIG. 6. Magnitude of the vertical electric field as a function of azimuth angle ϕ for both monofilar and bifilar modes. The value of a_0/a has been decreased to 0.6.

equation yields for the monofilar mode

$$\Gamma a = 3.505\times10^{-2} + i8.610\times10^{-1},$$
and
$$I_1/I_0 = 0.9324 \angle -0.810°. \quad (19)$$

For the bifilar mode, Γa and I_1/I_0 are virtually unchanged from the previous values. In Figs. 5 and 6, the normalized horizontal and vertical electric fields are shown for $\rho/a = 0.3$ and 0.9. Again, the field strength of the bifilar mode is generally down by a factor of about 100 from that of the monofilar mode throughout the tunnel.

V. CONCLUDING REMARKS

We have examined the excitation of monofilar and bifilar modes on a two-wire transmission line in a circular tunnel. Although the circular tunnel model is highly idealized, previous attenuation calculations[4] have agreed quite closely with those of Mahmoud[3] for a rectangular tunnel with perfectly conducting side walls and with experimental data of Deryck[1] taken in actual mine tunnels.

The transverse field variations shown in Figs. 3 and 4 illustrate the expected result that the monofilar mode is much easier to excite or receive than the bifilar mode. Below about 50 MHz, these are the only modes which are not cut off. However, at higher frequencies (e.g., greater than about 50 MHz), there are perturbed empty tunnel modes which will propagate.

[1]L. Deryck, *Bulletin Technique "Mines et Carriers", No.* 134 (Institut National des Industries Extractives, Belgium, 1971).
[2]P. Delogne, L. Deryck, and R. Liegeois, Proceedings of Thru-the-Earth Electromagnetics Workshop, edited by R.G. Geyer, pp. 49—53 (unpublished).
[3]S. F. Mahmoud (unpublished).
[4]J.R. Wait and D.A. Hill, Preliminary Report to U.S. Bureau of Mines, 1974 (unpublished).
[5]J. Fontaine, B. Demoulin, P. Degauque, and R. Gabillard, Proceedings of Thru-the-Earth Electromagnetics Workshop, edited by R.G. Geyer, pp. 130—139, (unpublished); Final Report on U.S. Bureau of Mines Contract No. G133023, 1973 (unpublished), available from N.T.I.S., Springfield, Va.
[6]S.F. Mahmoud (unpublished).
[7]J.R. Wait, *Electromagnetic Waves in Stratified Media*, 2nd. ed. (Pergamon, Oxford, England, 1970).
[8]J. Galejs, *Terrestrial Propagation of Long Electromagnetic Waves* (Pergamon, Oxford, England, 1972).
[9]G.D. Monteath, *Applications of the Electromagnetic Reciprocity Principle* (Pergamon, Oxford, England, 1973).
[10]S.A. Schelkunoff, *Electromagnetic Waves* (Van Nostrand, New York, 1943), 260—266.
[11]J.R. Wait, *Electromagnetic Radiation from Cylindrical Structure* (Pergamon, Oxford, England, 1959), pp. 142—148.

CHAPTER 13

Gap excitation of an axial conductor in a circular tunnel

David A. Hill and James R. Wait

Insitute for Telecommunication Sciences, Office of Telecommunications, U. S. Department of Commerce, Boulder, Colorado 80302

(Received 13 May 1974; in final form 25 July 1974)

We consider the excitation of modes on an axial conductor in a circular tunnel by a circumferential gap. Numerical results are presented for the power into the monofilar mode and the attenuation of the mode. The power delivered to the monofilar mode increases as the conductor approaches the tunnel wall, but the attenuation also increases. The results have application to systems which use coaxial cables for long-distance communication in mine tunnels.

I. INTRODUCTION

In order to communicate for long distances along mine tunnels and haulageways, it has been found advantageous to utilize a two-conductor transmission line which will support two types of dominant modes,[1] monofilar and bifilar. In the monofilar mode, the forward current is carried by the transmission line and the return current is carried by the tunnel walls. In the bifilar mode, the return current is carried by the second conductor. The monofilar mode has the advantage that it is readily excited (or received) by an antenna located in the tunnel, but also the disadvantage of higher attenuation due to loss in the surrounding rock. A key step in practical systems is the conversion from the monofilar or symmetrical mode to the bifilar or asymmetrical mode.

The actual transmission line can be either a two-wire line, as in the INIEX/Deryck[2] system, or a coaxial cable. The attenuation and excitation of the modes on a two-wire line have been studied both analytically[3,4] and experimentally.[2] When the transmission line is a coaxial cable, the bifilar mode propagates between the inner and outer conductors, and the monofilar mode propagates between the outer conductor and the tunnel walls. Mode conversion is accomplished either discretely by spaced slots as in the INIEX/Delogne system[1] or continuously through a loosely braided outer conductor.[5] Here we examine the excitation of a circular conductor by a circumferential voltage source. As far as the external fields are concerned the conductor itself appears to be solid metal.

In what follows, all field quantities vary harmonically with time according to the time factor $\exp(i\omega t)$, where ω is the angular frequency.

II. FORMULATION

A circular conductor of radius c_s is located within a circular tunnel as shown in Fig. 1. Since the conductor radius is assumed small compared to both a wavelength and the tunnel radius a, the primary fields[6] of the conductor current can be determined from the z component of a Hertz vector Π^p:

$$\Pi^p = \int_{-\infty}^{\infty} F(\lambda) K_0(v\rho_d) \exp(-i\lambda z)\, d\lambda \qquad (1)$$

$$= \int_{-\infty}^{\infty} F(\lambda) \sum_{m=-\infty}^{\infty} I_m(v\rho_0) K_m(v\rho) \exp[-im(\phi-\phi_0)] \times \exp(-i\lambda z)\, d\lambda \quad (\rho > \rho_0),$$

where $\rho_d = [\rho^2 + \rho_0^2 - 2\rho\rho_0 \cos(\phi-\phi_0)]^{1/2}$, $v = (\lambda^2 - k^2)^{1/2}$, k is the free-space wave number, I_m and K_m are modified Bessel functions of order m, and $F(\lambda)$ is unknown at this point. For $\rho < \rho_0$, ρ and ρ_0 are interchanged. The boundary conditions at the tunnel wall ($\rho = a$) are that the tangential fields (E_z, E_ϕ, H_z, H_ϕ) are continuous. Consequently, the total fields in the tunnel can be derived from the following z components of the electric and magnetic Hertz vectors,[4,7] Π and Π^m:

$$\Pi = \int_{-\infty}^{\infty} F(\lambda) \sum_m I_m(v\rho_0) \left(K_m(v\rho) - R_m(\lambda) \frac{K_m(va)}{I_m(va)} I_m(v\rho) \right) \times \exp[-im(\phi-\phi_0)] \exp(-i\lambda z)\, d\lambda, \qquad (2)$$

$$\Pi^m = \int_{-\infty}^{\infty} F(\lambda) \sum_m \Delta_m(\lambda) I_m(v\rho_0) I_m(v\rho) \exp[-im(\phi-\phi_0)] \times \exp(-i\lambda z)\, d\lambda,$$

where

$$R_m(\lambda) = \frac{(ik/v)K_m'(va)[K_m(va)]^{-1} + Y_m\eta_0 + \delta_m\eta_0}{(ik/v)I_m'(va)[I_m(va)]^{-1} + Y_m\eta_0 + \delta_m\eta_0},$$

$$\Delta_m(\lambda) = [1 - R_m(\lambda)] \frac{K_m(va)}{I_m(va)} \frac{(m\lambda/a)(v^{-2} - u^{-2})\eta_0^{-1}}{(ik/v)I_m'(va)[I_m(va)]^{-1} + Z_m/\eta_0}$$

$$\delta_m\eta_0 = \frac{(m\lambda/a)^2 (v^{-2} - u^{-2})^2}{(ik/v)I_m'(va)[I_m(va)]^{-1} + Z_m/\eta_0},$$

$$Z_m = -(i\omega\mu_0/u)K_m'(ua)[K_m(ua)]^{-1},$$

$$Y_m = (k_e^2/i\omega\mu_0 u)K_m'(ua)[K_m(ua)]^{-1},$$

$$u = (\lambda^2 - k_e^2)^{1/2}, \quad \text{and} \quad k_e^2 = -i\omega\mu_0(\sigma_e + i\omega\epsilon_e).$$

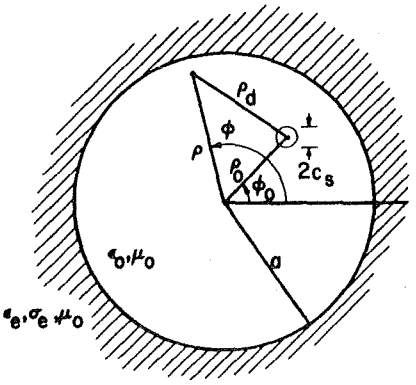

FIG. 1. Geometry for an axial conductor in a circular tunnel. The conductor is excited by a gap at $z = 0$.

The conductor is excited by a gap of width $2d$ centered at $z=0$. In the gap, the electric field E_z is approximately given by $V/2d$, where V is the gap voltage. In order to determine $F(\lambda)$ in Eq. (2), we assume that E_z and the conductor current $I(z)$ satisfy the following impedance relationship for all z:

$$E_z = (V/2d)\, p_d(z) + Z_s I(z) \quad \text{at } \rho_d = c_s, \tag{3}$$

where

$$p_d(z) = 1, \quad |z| < d$$
$$= 0, \quad |z| > d.$$

Z_s is the series impedance per unit length which is explicitly given by[6]

$$Z_s = \frac{\eta_s}{2\pi c_s} \frac{I_0(ik_s c_s)}{I_1(ik_s c_s)}, \tag{4}$$

where $k_s^2 = -i\omega\mu_0(\sigma_s + i\omega\epsilon_s)$, $\eta_s = \omega\mu_0/k_s$, and σ_s and ϵ_s are the conductivity and permittivity of the axial conductor. The following expression for E_z at the match point $(\phi=\phi_0, \rho=\rho_0+c_s)$ can be derived from Eq. (2):

$$E_z\Big|_{\substack{\rho=\rho_0+c_s \\ \phi=\phi_0}} = \left(k^2 + \frac{\partial^2}{\partial z^2}\right)\Pi\Big|_{\substack{\rho=\rho_0+c_s \\ \phi=\phi_0}}$$
$$= -\int_{-\infty}^{\infty} v^2 F(\lambda)\exp(-i\lambda z)\left(K_0(vc_s) - \sum_m R_m(\lambda) \frac{K_m(va)}{I_m(va)} I_m(v\rho_0)\, I_m[v(\rho_0+c_s)]\right) d\lambda. \tag{5}$$

The current $I(z)$ can be determined approximately by examining the azimuthal magnetic field $H_{\phi'}$ around the conductor. Thus

$$I(z) \simeq 2\pi c_s H_{\phi'} \simeq 2\pi c_s \frac{k^2}{i\omega\mu_0} \frac{\partial \Pi}{\partial \rho_d}\Big|_{\rho_d = c_s}$$
$$\simeq -2\pi c_s \frac{k^2}{i\omega\mu_0} \int_{-\infty}^{\infty} vF(\lambda) K_1(vc_s)\exp(-i\lambda z)\, d\lambda. \tag{6}$$

Since vc_s is small, Eq. (6) reduces to

$$I(z) \simeq \frac{-2\pi k^2}{i\omega\mu_0} \int_{-\infty}^{\infty} F(\lambda)\exp(-i\lambda z)\, d\lambda. \tag{7}$$

The following expansion for the source function in Eq. (3) is also useful:

$$\frac{V}{2d} p_d(z) = \frac{V}{2\pi} \int_{-\infty}^{\infty} \frac{\sin(\lambda d)}{\lambda d} \exp(-i\lambda z)\, d\lambda. \tag{8}$$

By substituting Eqs. (5), (7), and (8) into Eq. (3), we can solve for $F(\lambda)$:

$$F(\lambda) = \frac{-V}{2\pi D(\lambda)} \frac{\sin(\lambda d)}{\lambda d}, \tag{9}$$

where

$$D(\lambda) = v^2\left(K_0(vc_s) - \sum_m R_m(\lambda) \frac{K_m(va)}{I_m(va)} I_m(v\rho_0) I_m[v(\rho_0+c_s)]\right) + \frac{2\pi i k}{\eta_0} Z_s.$$

The zeros of $D(\lambda)$ are the characteristic values of the waveguide modes λ_s which have been examined previously.[7] There is also a branch point at $\lambda = k_e$, but the branch cut contribution corresponds to lateral waves in the lossy external medium and is heavily damped. Consequently, the branch cut contribution can be neglected for most applications (sufficiently large $|z|$). In evaluating the λ integrations in Eq. (2) by the residue theorem, it is necessary to close the contour in the lower half-plane for positive z and in the upper half-plane for negative z with the following results:

$$\Pi = iV \sum_s \frac{\sin(\lambda_s d)}{\lambda_s d} \frac{\exp(-i\lambda_s|z|)}{D'(\lambda_s)} \times \sum_m \exp[-im(\phi-\phi_0)] I_m(v_s\rho_0) \times \left(K_m(v_s\rho) - R_m(\lambda_s)\frac{K_m(v_s a)}{I_m(v_s a)} I_m(v_s\rho)\right), \tag{10}$$

$$\Pi^m = iV\,\mathrm{sgn}(z) \sum_s \frac{\sin(\lambda_s d)}{\lambda_s d} \frac{\exp(-i\lambda_s|z|)}{D'(\lambda_s)} \times \sum_m \exp[-im(\phi-\phi_0)]\, \Delta_m(\lambda_s) I_m(v_s\rho_0) I_m(v_s\rho),$$

where $v_s^2 = \lambda_s^2 - k^2$,

$$\mathrm{sgn}(z) = +1, \quad z > 0,$$
$$= -1, \quad z < 0,$$

and the branch cut contribution has been neglected. The actual field components are given by

$$E_z = \left(k^2 + \frac{\partial^2}{\partial z^2}\right)\Pi, \quad H_z = \left(k^2 + \frac{\partial^2}{\partial z^2}\right)\Pi^m,$$
$$E_\rho = \frac{\partial^2 \Pi}{\partial z\, \partial \rho} - \frac{i\omega\mu_0}{\rho} \frac{\partial \Pi^m}{\partial \phi},$$
$$H_\rho = \frac{i\omega\epsilon_0}{\rho} \frac{\partial \Pi}{\partial \phi} + \frac{\partial^2 \Pi^m}{\partial z\, \partial \rho}, \tag{11}$$
$$E_\phi = \frac{1}{\rho} \frac{\partial^2 \Pi}{\partial z\, \partial \phi} + i\omega\mu_0 \frac{\partial \Pi^m}{\partial \rho},$$
$$H_\phi = -i\omega\epsilon_0 \frac{\partial \Pi}{\partial \rho} + \frac{1}{\rho} \frac{\partial^2 \Pi^m}{\partial z\, \partial \phi}.$$

III. CALCULATION OF POWER

In order to judge the effectiveness of the modal excitation, it is useful to calculate the power which is supplied to the waveguide modes by the source gap. The total power supplied to the tunnel is most easily determined by integrating the Poynting vector over the entire axial conductor and tunnel wall surfaces. The ρ component of the Poynting vector $S_{\rho'}$ at the tunnel wall $(\rho=a)$ is given by

$$S_{\rho'} = (E_\phi H_z^* - E_z H_\phi^*)\big|_{\rho=a}, \tag{12}$$

where $*$ denotes complex conjugate and the usual factor of $\frac{1}{2}$ is omitted because rms values are assumed for the field quantities. The normal component of the Poynting vector $S_{\rho'}$ at the conductor surface is approximately given by

$$S_{\rho'} \simeq -(E_z H_\phi^*)\big|_{\rho'=c_s} = -(Z_s/2\pi c_s)\, I(z)\, I^*(z). \tag{13}$$

From Eqs. (7) and (9) and the residue theorem, $I(z)$ is

$$I(z) = \frac{2\pi k V}{\eta_0} \sum_s \frac{\sin(\lambda_s d)}{\lambda_s d} \frac{\exp(-i\lambda_s|z|)}{D'(\lambda_s)}. \tag{14}$$

The total power P is given by

$$P = P_t + P_w, \tag{15}$$

where

$$P_t = 2\int_0^\infty \int_0^{2\pi} \mathrm{Re}(S_\rho)\, a\, d\phi\, dz,$$

$$P_w = -4\pi c_s \int_d^\infty \mathrm{Re}(S_{\rho'})\, dz,$$

Re indicates the real part, and the evenness of S_ρ and $S_{\rho'}$ in z has been utilized. The azimuthal symmetry of $S_{\rho'}$ in ϕ' has also been used in P_w. To simplify the following numerical results, it is useful to set d equal to zero. The singularity in the susceptance due to a delta-gap source is well known in linear antenna theory,[8] but the delta gap presents no problem in the calculation of real power here.

When the actual field expressions are substituted into Eq. (15), the ϕ and z integrations are easily performed because only exponentials are involved. The resultant forms for P_t and P_w are

$$P_t = \frac{-4\pi V^2}{\eta_0}\,\mathrm{Re}\sum_s \sum_p \frac{1}{D'(\lambda_s)D'(\lambda_p)^* i(\lambda_s - \lambda_p^*)} \times \sum_m I_m(v_s\rho_0)\, I_m(v_p\rho_0)^* \Big\{ [v_p^2 \eta_0 \Delta_m(\lambda_p)\, I_m(v_p a)]^* \times \{m\lambda_s K_m(v_s a)[1 - R_m(\lambda_s)] + ika v_s \eta_0 \Delta_m(\lambda_s) I_m'(v_s a)\} + \Big[m\lambda_p \eta_0 \Delta_m(\lambda_p)\, I_m(v_p a) + ika v_p \Big(K_m'(v_p a) - R_m(\lambda_p) \times \frac{K_m(v_p a)}{I_m(v_p a)}\, I_m'(v_p a) \Big) \Big]^* \{ v_s^2 K_m(v_s a)[1 - R_m(\lambda_s)] \} \Big\} \tag{16}$$

and

$$P_w = \frac{2V^2}{\eta_0}(2\pi k)^2\,\mathrm{Re}\Big(\frac{Z_s}{\eta_0} \sum_s \sum_p \frac{1}{D'(\lambda_s)D'(\lambda_p)^* i(\lambda_s - \lambda_p^*)} \Big).$$

In a lossless waveguide, the modes are orthogonal and the cross terms in the summation ($s \neq p$) have no contribution. However, for the lossy waveguide case,[9] this is not necessarily true.

If only the total power P is desired, it can be derived in a simpler manner by integrating the Poynting vector over the source gap. For $d = 0$, this is equivalent to multiplying the real part of the current at $z = 0$ by V.

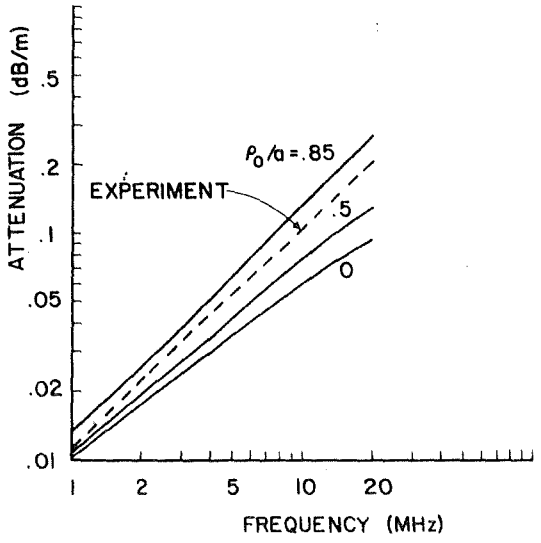

FIG. 2. Attenuation of the monofilar mode as a function of frequency for three conductor locations. The experimental curve corresponds to $\rho_0/a = 0.85$.

Consequently, from Eq. (14) the total power is given by

$$P = V\,\mathrm{Re}[I(0)] = \frac{V^2 2\pi k}{\eta_0} \sum_s^\infty \mathrm{Re}\Big(\frac{1}{D'(\lambda_s)} \Big). \tag{17}$$

Strictly speaking, Eq. (14) is not valid in the gap ($|z| < d$), but the same result for P in Eq. (17) can be obtained by rigorously integrating the Poynting vector over the gap and letting d approach zero.[10]

We now consider a numerical example which is applicable to the use of a coaxial cable in a mine tunnel. The following tunnel parameters are assumed: $a = 2m$, $\epsilon_e/\epsilon_0 = 10$, and $\sigma_e = 10^{-2}$ mho/m. The conductor parameters are $\sigma_s = 10^5$ mho/m and $c_s = 0.35$ cm, where c_s is a fairly standard value.[5] The frequency range of interest[1,5] is roughly 1—20 MHz. In this frequency range, the perturbed empty tunnel modes are essentially "cut off" and can be neglected. However, at frequencies above about 50 MHz they can be important and their attenuation has been studied.[11] The first step is the numerical solution for the characteristic value of the monofilar mode, λ_1, from the equation $D(\lambda) = 0$. Newton's method has been used to solve this equation with the advantage that the solution automatically yields $D'(\lambda_1)$ which is needed in Eq. (16). The attenuation α_1 is given by

$$\alpha_1 = 8.686\,\mathrm{Im}(-\lambda_1) \quad (dB/m), \tag{18}$$

where Im refers to the imaginary part. The attenuation as a function of frequency is plotted for three values of ρ_0/a in Fig. 2. Also plotted is an empirical curve for α_1 which is derived from coal mine measurements.[5] The tunnel shape was different, but the separation between the conductor and the wall was 0.3 m which corresponds to the $\rho_0/a = 0.85$ curve. Considering the uncertainties in the parameters, the agreement is quite good. The increase in attenuation with increasing frequency and decreasing wall conductor separation has been noted both experimentally[2] and theoretically.[7,12]

The preceding values of λ_1 and $D'(\lambda_1)$ can be used to calculate the power into the monofilar mode as given by Eq. (16) with only the $s = p = 1$ term included or by Eq. (17) with only the $s = 1$ term included. Higher-order modes should be negligible because they have large negative imaginary parts of λ_s. The normalized power is shown in Fig. 3 for the same parameters as used in Fig. 2. It is interesting that there is a slight local maximum at about 7 MHz which was determined by a different analysis to be the optimum frequency in the braided coaxial cable system.[5] The total power and the power into the conductor are shown as a function of ρ_0/a for 7 MHz in Fig. 4. As expected, the power lost in the conductor P_w is a small fraction of either the total power P or the power lost through the tunnel walls P_t. The attenuation is also shown and is seen to increase as ρ_0/a increases.

IV. CONCLUDING REMARKS

We have examined the gap excitation of modes on an axial conductor in a circular tunnel and given numerical results for the monofilar mode. For the range of frequencies and parameters of interest in mine communications, the power into the monofilar mode is increased as the conductor approaches the wall, but the attenuation also increases. Although the circular tunnel is

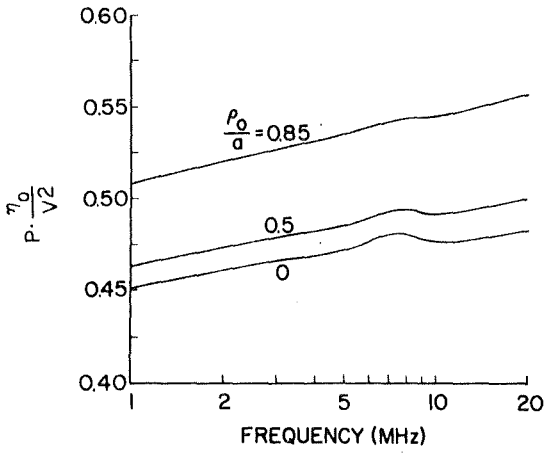

FIG. 3. Power supplied to the monofilar mode as a function of frequency for three conductor locations.

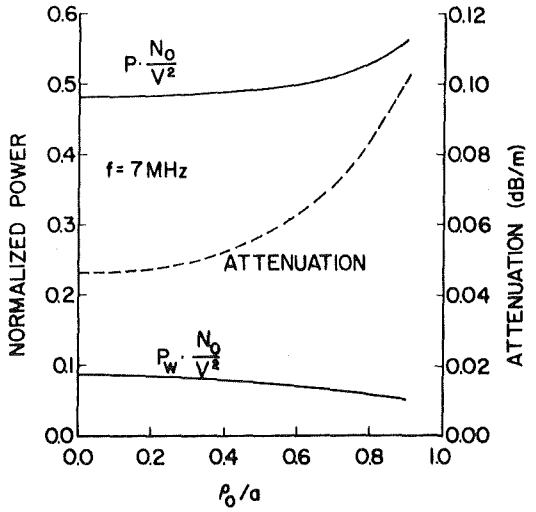

FIG. 4. Total power P supplied to the monofilar mode as a function of conductor position at 7 MHz. The power lost in the conductor P_w and the mode attenuation are also shown.

highly idealized, attenuation results[3,7] have shown good agreement with theory for a rectangular tunnel[12] and with experimental data taken in actual mine tunnels.[1]

The results here have application to coaxial cable systems for both discrete slot excitation and continuous excitation as through a leaky outer braid. However, a useful extension would be to solve a more complicated modal equation including directly the effects of the dielectric filler, the braid, and the jacket of the cable.

In this paper we have not considered the effect of the higher-order modes in the tunnel. A numerical evaluation of Eq. (17) for all integer values of s is needed to specify the *total* power supplied by the gap in the outer conductor of the coaxial cable. Also, for a complete systems design, we need to analyze the coupling of all the modes *inside* the coaxial conductor with all the modes in the tunnel region. These tasks are now occupying our serious attention.

ACKNOWLEDGMENT

The authors wish to thank Professor Paul Delogne for suggesting the simpler alternative method of calculating the power.

[1] P. Delogne, L. Deryck, and R. Liegeois, *Proceedings of Thru-the-Earth Electromagnetics Workshop*, edited by R.G. Geyer (N.T.I.S., Springfield, Va., 1973), pp. 49—53.
[2] L. Deryck, *Bulletin Technique "Mines et Carriers"*, *No.* 134 (Institut National des Industries Extractives, Belgium, 1971).
[3] J.R. Wait and D.A. Hill, J. Appl. Phys. (to be published).
[4] D.A. Hill and J.R. Wait, J. Appl. Phys. **45**, 3402 (1974).
[5] J. Fontaine, B. Demoulin, P. Degauque, and R. Gabillard, in Ref. 1, pp. 130—139.
[6] J.R. Wait, *Electromagnetic Radiation from Cylindrical Structures* (Pergamon, New York, 1959), pp. 142—148.
[7] J.R. Wait and D.A. Hill, IEEE Trans. Antennas Propag. 22, 627 (1974).
[8] T.T. Wu and R.W.P. King, J. Appl. Phys. 30, 74 (1959).
[9] J. Van Bladel, *Electromagnetic Fields* (McGraw-Hill, New York, 1964), pp. 304—306.
[10] Paul Delogne (private communication).
[11] D.A. Hill and J.R. Wait, IEEE AP-S International Symposium, Atlanta, 1974 (unpublished).
[12] S.F. Mahmoud (unpublished).

CHAPTER 14

Electromagnetic fields of a coaxial cable with an interrupted shield located in a circular tunnel

David A. Hill

Institute for Telecommunication Sciences, Office of Telecommunications, U.S. Department of Commerce, Boulder, Colorado 80302

James R. Wait*

Cooperative Institute for Research in Enviromental Sciences, University of Colorado/NOAA, Boulder, Colorado 80302

(Received 5 May 1975)

An expression for the gap admittance of a coaxial cable within a circular tunnel is derived using a quasistatic method. Coupling between the TEM mode within the cable and the monofilar mode within the tunnel is computed, and 25% of the cable power is typically transferred to the tunnel from a single cable gap. The results have application to the use of leaky coaxial cables for communication in mine tunnels.

PACS numbers: 84.40.N

I. INTRODUCTION

One method of communication along mine tunnels utilizes a two-conductor transmission line which will support two dominant modes designated as monofilar and bifilar.[1] If the transmission line is an ideal coaxial cable, the bifilar mode is simply the TEM mode within the cable. In the monofilar mode, the forward current is carried by the cable shield and the return current is carried by the tunnel walls. The monofilar mode is readily excited or recieved by an antenna in the tunnel, but suffers from higher attenuation due to loss in the surrounding rock.[2] The INIEX/Delogne system[3] utilizes a circumferential gap in the cable shield to achieve conversion between the two modes.

In order to gain a quantitative understanding of this mode conversion, we examine such a coaxial cable in an idealized circular tunnel. The fields external to the cable for this geometry have been analyzed previously.[4] Here we consider the complete problem of coupling from a TEM mode inside the cable to the modes in the tunnel, particularly the monofilar mode. This situation is illustrated in Fig. 1 and is described in more detail below.

The gap voltage and field distribution are not assumed, but are determined from a quasistatic method similar to that employed by Chang[5] and Hurd[6] in a free-space analysis. The final result of our analysis is an efficiency factor for the coupling between the TEM cable mode and the monofilar mode. This is an essential parameter in the design of such systems for communications.

II. GAP ADMITTANCE

We first derive an expression for the gap voltage when a TEM wave within the coaxial cable is incident upon the gap. The cable geometry is shown in Fig. 1 with respect to a cylindrical coordinate system (ρ, ϕ, z). The solid inner conductor of radius a and the shield of radius b and of negligible thickness are assumed to be perfect conductors. The insulation $(a < \rho < b)$ has permittivity ϵ. A circumferential gap in the shield is centered at $z = 0$. The circular tunnel of radius a' is also shown in Fig. 1 with respect to a tunnel-centered cylindrical coordinate system (ρ', ϕ', z). The tunnel region for $\rho' < a'$ and $\rho > b$ is characterized by zero conductivity and free-space permittivity ϵ_0, and the external region $\rho' > a'$ is characterized by conductivity σ_e and permittivity ϵ_e. Free-space permeability μ_0 is assumed everywhere. Finally, we note that the axis of the coaxial cable is located at ρ_0, ϕ_0.

We first consider the fields in the tunnel $(\rho' < a')$, but external to the cable $(\rho > b)$. If the cable radius is small compared with a wavelength and the tunnel radius,

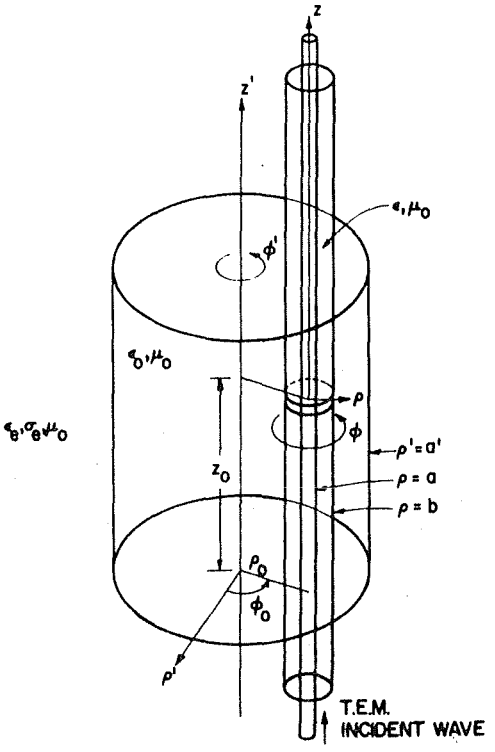

FIG. 1. Coaxial cable with an interrupted shield contained within a circular tunnel. A TEM incident wave is propagating in the positive z direction. (Note drawing is not to scale since b is much smaller than a'.) Gap is located at $z = 0$ or $z' = z_0$.

the primary fields can be derived from the following electric Hertz vector that has only a z component Π_p,

$$\Pi_p = \int_{-\infty}^{\infty} F(\lambda) K_0(v\rho) \exp(-i\lambda z)\, d\lambda, \tag{1}$$

where $v = (\lambda^2 - k_0^2)^{1/2}$, $k_0 = \omega(\mu_0\epsilon_0)^{1/2}$, K_0 is a modified Bessel function of zero order, and $F(\lambda)$ is unknown at this point. The time variation of all field quantities is $\exp(i\omega t)$, where ω is the angular frequency. The secondary fields are determined by applying the boundary conditions that the tangential electric and magnetic fields $(E_{z'}, E_{\phi'}, H_{z'}, H_{\phi'})$ are continuous at the tunnel wall ($\rho' = a'$). As indicated before,[4] the total fields in the tunnel region can be obtained from electric and magnetic Hertz vectors that have only z components Π_e and Π_m. These are given explicitly by

$$\Pi_e = \int_{-\infty}^{\infty} F(\lambda)\{K_0(v\rho) - \textstyle\sum_m R_m(\lambda)[K_m(va')/I_m(va')] \times I_m(v\rho_0) I_m(v\rho') \exp[-im(\phi' - \phi_0)]\} \exp(-i\lambda z)\, d\lambda, \tag{2}$$

$$\Pi_m = \int_{-\infty}^{\infty} F(\lambda) \textstyle\sum_m \Delta_m(\lambda) I_m(v\rho_0) I_m(v\rho') \times \exp[-im(\phi' - \phi_0)] \exp(-i\lambda z)\, d\lambda,$$

where

$$R_m = \frac{(ik_0/v)K_m'(va')/K_m(va') + Y_m\eta_0 + \delta_m\eta_0}{(ik_0/v)I_m'(va')/I_m(va') + Y_m\eta_0 + \delta_m\eta_0},$$

$$\delta_m\eta_0 = \frac{(m\lambda/a')^2(v^{-2} - u^{-2})^2}{[(ik_0/v)I_m'(va')/I_m(va')] + Z_m/\eta_0},$$

$$Z_m = \frac{-(i\omega\mu_0/u)K_m'(ua')}{K_m(ua')},$$

$$Y_m = \frac{(k_e^2/i\omega\mu_0 u)K_m'(ua')}{K_m(ua')},$$

$u = (\lambda^2 - k_e^2)^{1/2}$, $k_e^2 = -i\omega\mu_0(\sigma_e + i\omega\epsilon_e)$, $\eta_0 = (\mu_0/\epsilon_0)^{1/2}$, I_m and K_m are modified Bessel functions of order m, and the summations on m run over integers from $-\infty$ to ∞. The explicit expression for $\Delta_m(\lambda)$ has been given previously[4] but is not required here.

In order to derive the desired Green's function, we consider first a delta gap at $z = 0$. The axial electric field E_z at $\rho = b$ is thus given by

$$E_z\big|_{\rho=b} = V\delta(z) = (V/2\pi)\int_{-\infty}^{\infty} \exp(-i\lambda z)\, d\lambda, \tag{3}$$

where V is the delta gap voltage and the second expression is the integral representation of a delta function. We can also determine E_z by operating on Π_e and evaluating the expression at an equivalent point, $\phi' = \phi_0$ and $\rho' = \rho_0 + b$. Thus

$$E_z\Big|_{\substack{\rho'=\rho_0+b \\ \phi'=\phi_0}} = \left(k_0^2 + \frac{\partial^2}{\partial z^2}\right)\Pi_e\Big|_{\substack{\rho'=\rho_0+b \\ \phi'=\phi_0}} = -\int_{-\infty}^{\infty} F(\lambda) D(\lambda) \exp(-i\lambda z)\, d\lambda, \tag{4}$$

where

$$D(\lambda) = v^2\{K_0(vb) - \textstyle\sum_m R_m(\lambda)[K_m(va')/I_m(va')] \times I_m(v\rho_0) I_m[v(\rho_0 + b)]\}.$$

By equating (3) and (4), $F(\lambda)$ is found to be

$$F(\lambda) = -V/2\pi D(\lambda). \tag{5}$$

The azimuthal magnetic field in the unprimed space H_ϕ is given by

$$H_\phi = -i\omega\epsilon_0 \frac{\partial \Pi_e}{\partial \rho} + \frac{1}{\rho}\frac{\partial^2 \Pi_m}{\partial z\, \partial \phi}. \tag{6}$$

Now it is convenient to define an average magnetic field evaluated at $\rho = b$:

$$\bar{H}_\phi = (2\pi)^{-1}\int_0^{2\pi} H_\phi\big|_{\rho=b}\, d\phi. \tag{7}$$

Then $\bar{H}_\phi$ is approximately given by

$$\bar{H}_\phi \approx -i\omega\epsilon_0 \frac{\partial \Pi_e}{\partial \rho}\bigg|_{\rho=b} \approx i\omega\epsilon_0 \int_{-\infty}^{\infty} vF(\lambda) K_1(vb) \exp(-i\lambda z)\, d\lambda, \tag{8}$$

bearing in mind that b is small compared with the wavelength. By introducing Hankel functions of the second kind $H_0^{(2)}$ and $H_1^{(2)}$ and using (4) and (5), $\bar{H}_\phi$ in (8) can be rewritten

$$\bar{H}_\phi = \frac{i\omega\epsilon_0 V}{2\pi} \int_{-\infty}^{\infty} \frac{H_1^{(2)}(\beta b) \exp(-i\lambda z)}{\beta[H_0^{(2)}(\beta b) + \Lambda(\lambda)]}\, d\lambda, \tag{9}$$

where

$$\Lambda(\lambda) = \frac{2}{\pi i}\textstyle\sum_m R_m(\lambda)\dfrac{K_m(va')}{I_m(va')} I_m(v\rho_0) I_m[v(\rho_0 + b)],$$

$$\beta = -iv = (k_0^2 - \lambda^2)^{1/2}.$$

We now consider a finite gap of width δ centered at $z = 0$ with a voltage V and an electric field distribution $\hat{f}(z)$. The field distribution is normalized such that

$$\int_{-\delta/2}^{\delta/2} \hat{f}(z)\, dz = 1. \tag{10}$$

From (9), it is seen that the external field $\bar{H}_\phi$ can now be written as an integral of a Green's function over the gap

$$\bar{H}_\phi = (V/2\pi\delta)\int_{-\delta/2}^{\delta/2} \hat{f}(z') G_0(b, z, z')\, dz, \tag{11}$$

where

$$G_0(b, z, z') = i\omega\epsilon_0 \int_{-\infty}^{\infty} \frac{H_1^{(2)}(\beta b) \exp(-i\lambda|z - z'|)}{\beta[H_0^{(2)}(\beta b) + \Lambda(\lambda)]}\, d\lambda.$$

The internal magnetic field at the gap ($\rho = b^-$) can be written as the sum of an incident TEM mode and an integral over the gap:

$$\bar{H}_\phi = \frac{I_0}{2\pi b}\exp(-ikz) + \frac{V}{2\pi\delta}\int_{-\delta/2}^{\delta/2} \hat{f}(z') G(b, z, z')\, dz', \tag{12}$$

where $k = \omega(\mu_0\epsilon)^{1/2}$, $I_0 = 2\pi b h_0$, h_0 is the incident magnetic field at the center of the gap, and $G(b, z, z')$ has been given previously.[7] By equating (11) and (12), we obtain the following integral equation for $\hat{f}(z')$:

$$\frac{I_0}{2\pi b}\exp(-ikz) - \frac{V}{2\pi\delta}\int_{-\delta/2}^{\delta/2} \hat{f}(z')[G_0(b, z, z') - G(b, z, z')]\, dz' = 0. \tag{13}$$

This integral equation is of the same form as that obtained by Chang[5] and Hurd[6] and by Wait and Hill[7,8] for a coated cable. However, $G_0(b, z, z')$, as given by (11) is considerably more complicated because it includes the effect of the tunnel boundary.

In order to solve (13), we employ a quasistatic method which assumes that δ is small compared to a wavelength. Some of the details are omitted because the procedure is the same as that employed for the coated cable in free space.[8] As it turns out, $G_0(b, z, z')$ can be approximated

in the following manner:

$$G_0(b,z,z') = i\omega\epsilon_0\left[\int_{-\infty}^{\infty}\frac{1}{\beta}\left(\frac{H_1^{(2)}(\beta b)}{H_0^{(2)}(\beta b)+\Lambda(\lambda)}-i\right)\exp(-i\lambda|z-z'|)\,d\lambda + i\int_{-\infty}^{-\infty}\frac{1}{\beta}\exp(-i\lambda|z-z'|)\,d\lambda\right] \quad (14)$$

$$\approx i\omega\epsilon_0\left[\int_0^{\infty}\frac{2}{\beta}\left(\frac{H_1^{(2)}(\beta b)}{H_0^{(2)}(\beta b)+\Lambda(\lambda)}\right)d\lambda - 2K_0(ik_0|z-z'|)\right]$$

$$\approx 2i\omega\epsilon_0[N_0+\ln|z-z'|+\ln(\tfrac{1}{2}k_0)+C]$$

$$= 2i\omega\epsilon_0\ln[\kappa_0|z-z'|],$$

where $\kappa_0=\frac{1}{2}k_0\exp(C+N_0)$,

$$N_0=\int_0^{\infty}\frac{1}{\beta}\left(\frac{H_1^{(2)}(\beta b)}{H_0^{(2)}(\beta b)+\Lambda(\lambda)}-i\right)d\lambda+\frac{i\pi}{2},$$

and $C=0.5772\cdots$ is Euler's constant. Since the interior problem has already been solved, we merely restate the desired approximation[8] for $G(b,z,z')$,

$$G(b,z,z')\approx -2i\epsilon\omega\left(\ln\kappa|z-z'|+\frac{i\pi}{2kb\ln(b/a)}\right), \quad (15)$$

where

$$\kappa=[\pi/(b-a)]\exp N,$$

$$N=\sum_{s=1}^{\infty}\left(\frac{1}{s}+\frac{i\pi}{bs}\frac{[J_0(u_s a)]^2}{[J_0(u_s a)]^2-[J_0(u_s b)]^2}\right),$$

$$u_s=(k^2-\lambda_s^2)^{1/2},$$

J_0 is the zero-order Bessel function, and λ_s is the propagation constant of the s-order evanescent TM mode. Since the dependence of G_0 and G on z and z' has been reduced to $\ln|z-z'|$, (13) can be solved for $\hat{f}(z')$:

$$\hat{f}(z')=\frac{\delta/2}{\pi[(\delta/2)^2-(z')^2]^{1/2}}, \quad (16)$$

where it has been noted that $\hat{f}(z')$ has the correct edge behavior as $|z'|\to\frac{1}{2}\delta$.

By substituting (14)–(16) into (13), it is possible to relate V to I_0 in terms of a total gap admittance Y_t which is the sum of an external admittance Y_e, an internal admittance Y_i, and a small capacitance term $i\omega C_0$. Thus

$$V=-I_0Y_t^{-1}=-I_0(Y_e+Y_i+i\omega C_0)^{-1}, \quad (17)$$

where

$$i\omega C_0=\frac{2ik_0b}{\eta_0}\left(1+\frac{\epsilon}{\epsilon_0}\right)\ln(2), \quad (18)$$

$$Y_e=-\frac{2ik_0b}{\eta_0}\left[\ln\left(\frac{k_0\delta}{4}\right)+N_0+C\right], \quad (19)$$

$$Y_i=\frac{Y_0}{2}-i\frac{2kb}{\eta}\left[\ln\left(\frac{\pi\delta}{2(b-a)}\right)+N\right], \quad (20)$$

and where $Y_0=2\pi[\eta\ln(b/a)]^{-1}$ and $\eta=(\mu_0/\epsilon)^{1/2}$. Y_0 is the characteristic admittance of the TEM mode in the cable. The expression for V in (17) is used in Sec. III to derive a coupling factor between the cable and the tunnel.

III. POWER COUPLING FACTOR

At frequencies of most interest to mine communications (< 50 MHz), most of the power supplied by the cable gap to the tunnel goes into the monofilar mode. Also, the small amount of power which goes into the waveguide modes and the continuous spectrum is rapidly attenuated away from the gap because the waveguide modes are evanescent and the continuous spectrum corresponds to heavily damped lateral waves in the lossy rock walls. Consequently, we consider the useful tunnel power to be the power in the monofilar mode P_m. Thus we define a power coupling factor C_m as the ratio

$$C_m=P_m/P_{\mathrm{TEM}}, \quad (21)$$

where $P_{\mathrm{TEM}}=\frac{1}{2}|I_0|^2/Y_0$ is the power in the coaxial cable incident on the gap.

The propagation constant of the monofilar mode λ_0 has been computed for a wide range of parameters from the mode equation[2]

$$D(\lambda_0)=0, \quad (22)$$

where $D(\lambda)$ has been defined in (4). For small gaps, the power in the monofilar mode is given by[4]

$$P_m=\frac{\pi k_0}{\eta_0}|V^2|\,\mathrm{Re}\left(\frac{1}{D'(\lambda_0)}\right) = \frac{\pi k_0}{\eta_0}\frac{I_0^2}{|Y_t|^2}\,\mathrm{Re}\left(\frac{1}{D'(\lambda_0)}\right), \quad (23)$$

where (17) has been used in obtaining the second expression for P_m. By substituting (23) into (21),

$$C_m=2\pi k_0Y_0\,\mathrm{Re}[1/D'(\lambda_0)]/|Y_t|^2\eta_0. \quad (24)$$

If we had considered all power external to the cable as useful power, as assumed by Delogne,[3] the external coupling factor C_e would have been

$$C_e=Y_0\mathrm{Re}(Y_e)/|Y_t|^2. \quad (25)$$

In general, $C_m<C_e$, although for frequencies well below 50 MHz the difference is small, in some cases.

IV. NUMERICAL RESULTS

Before considering a specific numerical example, we must consider some computational aspects involved in evaluating N_0 as given by the integral in (14). In order for the integral to converge, $\Lambda(\lambda)$ must approach zero more rapidly than $H_0^{(2)}(\beta b)$ as $\lambda\to\infty$. By employing asymptotic expansions, the ratio for large λ is found to be

$$\Lambda(\lambda)/H_0^{(2)}(\beta b)\sim f(\lambda)\exp[-2\lambda(a'-\rho_0-b)], \quad (26)$$

where $f(\lambda)$ is algebraic in λ. Note that $(a'-\rho_0-b)$ is the distance from the edge of the cable to the tunnel wall. If λ_t is the actual upper limit used in the numerical integration, then (26) implies that $\lambda_t(a'-\rho_0-b)\gg 1$. If this condition is satisfied then the asymptotic behavior of the integrand is the same as in the free-space case. However, even then it is required that $\lambda_t b\gg 1$ for a small truncation error and that $\lambda_t\delta\ll 1$ in order to neglect the factor $\exp(-i\lambda|z-z'|)$ in (14). In order to be able to choose λ_t to satisfy these three conditions,

TABLE I. N_0 and external admittance Y_e.

Frequency (MHz)	Free space ($a'=\infty$) N_0	Y_e (mmhos)
5	$-54.7+i230.6$	$1.281+i0.359$
10	$-32.5+i128.6$	$1.428+i0.464$
20	$-19.29+i72.56$	$1.612+i0.620$
50	$-9.58+i34.89$	$1.939+i0.958$

In tunnel ($a'=2$ m, $\epsilon_e/\epsilon_0=10$, $\sigma_e=10^{-2}$ mhos/m)

Frequency	ρ_0 (m)	N_0	Y_e (mmhos)
5	0.0	$-16.0+i270.2$	$1.501+i0.144$
5	1.0	$-16.2+i279.2$	$1.551+i0.145$
5	1.7	$-16.9+i314.5$	$1.747+i0.149$
10	0.0	$-11.9+i137.0$	$1.523+i0.235$
10	1.0	$-11.5+i142.0$	$1.577+i0.231$
10	1.7	$-11.0+i160.2$	$1.780+i0.226$
20	0.0	$-10.78+i69.90$	$1.553+i0.430$
20	1.0	$-9.86+i72.72$	$1.616+i0.410$
20	1.7	$-8.68+i82.65$	$1.837+i0.384$
50	0.0	$-12.70+i31.73$	$1.763+i1.132$
50	1.0	$-10.11+i32.65$	$1.814+i0.988$
50	1.7	$-6.04+i36.68$	$2.038+i0.726$

the following two conditions must be satisfied:

$$\delta/b \ll 1 \quad \text{and} \quad \delta/(a'-\rho_0-b) \ll 1. \tag{27}$$

These are not serious restrictions, so long as large gaps are not considered.

We now consider a numerical example which is applicable to mine communications. The following tunnel parameters are assumed: $a'=2$ m, $\epsilon_e/\epsilon_0=10$, and $\sigma_e=10^{-2}$ mhos/m. The following cable parameters are typical[9]: $a=2.68$ mm, $b=1$ cm, and $\epsilon/\epsilon_0=2.5$. A gap width δ of 1 mm is assumed, but the results are not very sensitive to changes in δ. We consider various cable locations in the tunnel and a frequency range from 5 to 50 MHz.

Table I contains numerical values of N_0 given by (14) and Y_e given by (19). Note that $\mathrm{Re}(Y_e)$ increases both with frequency and with ρ_0. The values for $\rho_0=1.7$ m are probably most representative of operational conditions since the cable will generally be located near the wall. For comparison, free-space results were also computed from (14) by setting $\Lambda(\lambda)=0$ and are shown in Table I. Again $\mathrm{Re}(Y_e)$ increases with frequency.

Table II contains numerical values of N given by (15), $i\omega C_0$ given by (18), and Y_i given by (20). Note that Re $\mathrm{Re}(Y_i)$ is independent of frequency and $\mathrm{Im}(Y_i)$ increases with frequency. Since these quantities are properties of the cable only, they are independent of ρ_0.

Table III contains results for C_m given by (24) and the attenuation rate. The attenuation rate in dB/100 m is given by 868.8 $\mathrm{Im}(-\lambda_0)$ where λ_0 is given by (22). The numerical solution of (22) is accomplished by a modification of Newton's method.[2] Note that attenuation rate increases considerably with both frequency and ρ_0. However, C_m has a rather weak frequency dependence and increases only slightly with ρ_0. Consequently, it appears

TABLE II. N, $i\omega C_0$, and internal admittance (Y_i).

Frequency (MHz)	N	$i\omega C_0$ (mmhos)	Y_i (mmhos)
5	-0.0514	$i0.013$	$10.006+i0.022$
10	-0.0514	$i0.027$	$10.006+i0.044$
20	-0.0514	$i0.054$	$10.006+i0.088$
50	-0.0514	$i0.135$	$10.006+i0.221$

that lower frequencies are more advantageous because of the lower attenuation rate which would permit a greater distance between slots for a given signal level.

V. CONCLUDING REMARKS

We have obtained results for coupling between a TEM mode within a coaxial cable and the monofilar mode within the surrounding tunnel resulting from a circumferential gap in the cable shield. The actual INIEX/Delogne cable has a dielectric coating which we have neglected here for simplicity. This simplification is not important in the frequency range which we consider here (5—50 MHz), but could be important at higher frequencies where the dielectric coating can support a tightly bound surface or Goubau wave.[7,9] The INIEX/Delogne cable also utilizes lumped circuit elements at the cable gap in order to control the radiated power [proportional to $\mathrm{Re}(Y_e)$] and to minimize the reflection of the TEM mode within the cable. Our calculations show that about 25% of the cable power is released to the tunnel, whereas the lumped circuit elements of the INIEX/Delogne cable are adjusted to release only about 10% of the power to the tunnel.[3] It would be a useful theoretical extension to modify the gap voltage expression in (17) to allow for lumped circuit elements.

The numerical results in Table III indicate that the decrease in attenuation of the monofilar mode with frequency favors lower frequencies for coupling from the cable to the tunnel at a significant distance from the gap. However, the efficiency of the receiving antenna decreases as the frequency is decreased. Consequently, we can expect a minimum in coupling loss at some frequency. It would be a useful extension to include the antenna efficiency and cable attenuation to enable a com-

TABLE III. Coupling factor (C_m) and attentuation rate.

Frequency (MHz)	ρ_0 (m)	Coupling factor, C_m (%)	Attenuation rate (dB/100 m)
5	0.0	23.3	3.42
5	1.0	23.7	4.26
5	1.7	25.6	7.04
10	0.0	22.8	6.04
10	1.0	23.4	8.13
10	1.7	25.6	15.50
20	0.0	22.9	9.51
20	1.0	23.6	14.1
20	1.7	26.0	31.8
50	0.0	21.7	12.0
50	1.0	23.3	20.0
50	1.7	27.0	65.0

plete calculation of path loss between two antennas in the presence of a cable with arbitrary gap locations. These extensions are now occupying our attention.

ACKNOWLEDGMENTS

The authors would like to thank Ms. Lana Slusher for her help in preparing the manuscript. They also acknowledge the support of the U.S. Bureau of Mines.

[1]P. Delogne, L. Deryck, and R. Liegeois, in *Proceedings of Thru-the-Earth Electromagnetics Workshop*, edited by R.G. Geyer (N.T.I.S., Springfield, Va., 1973), pp. 49—53.
[2]J.R. Wait and D.A. Hill, IEEE Trans. Antennas Propag. AP-22, 627 (1974).
[3]P. Delogne, International Conference on Radio: Roads, Tunnels and Mines, Liege, Belgium, 1974, pp. 129—136 (unpublished).
[4]D.A. Hill and J.R. Wait, J. Appl. Phys. 45, 4774 (1974).
[5]D.C. Chang, IEEE Trans. Antennas Propag. AP-21, 792 (1973).
[6]R.A. Hurd, Can. J. Phys. 51, 946 (1973).
[7]J.R. Wait and D.A. Hill, IEEE Trans. Antennas Propag. AP-23, 470 (1975).
[8]J.R. Wait and D.A. Hill, IEEE Trans. Antennas Propag. (to be published).
[9]P. Delogne and R. Liegeois, Ann. Telecommun. 26, 85 (1971).

IEEE TRANSACTIONS ON MICROWAVE THEORY AND TECHNIQUES, VOL. MTT-23, NO. 5, MAY 1975

Propagation Along a Braided Coaxial Cable in a Circular Tunnel

JAMES R. WAIT, FELLOW, IEEE, AND DAVID A. HILL, MEMBER, IEEE

Abstract—**The modes of propagation along a coaxial structure contained within a circular tunnel are considered. The primary objective is to develop an approximate impedance boundary condition at the outer surface of the shielded cable that can be used in previously developed formalisms for axial conductors in tunnels. It is assumed that the metal braid can be characterized by a surface-transfer impedance. We also account for the possibility that a lossy film exists on the outer surface of the dielectric jacket of the cable.**

INTRODUCTION

THERE IS A NEED to understand how electromagnetic waves propagate in tunnels if improved communication systems in mines are to be developed in a logical fashion. One approach now being developed is to exploit the leaky-feeder principle [1]. In this method, which can be described as continuous-access communications, the signals are guided by transmission lines or shielded conductors. The principal idea is that energy can be coupled into and out of the transmission channel by antennas that only need be in the general vicinity of the two-wire line or cable.

In developing the theory of mode propagation along axial conducting structures in cylindrical tunnels, we need to apply an impedance boundary condition at the outer surface of the guiding structure. In the case of a bare metallic wire, the appropriate expression to use is the series impedance Z_i defined as follows: $Z_i = E_a/I$ where $I = \oint H_t\, ds$. Here, E_a is the average axial field at the surface of the conductor, while H_t is the azimuthal magnetic field. For a thin circular wire of radius a with electromagnetic constants σ_w, ϵ_w, and μ_w, we can use the following argument.

FORMULATION FOR IMPEDANCE OF AN INNER CONDUCTOR

A cylindrical coordinate system (ρ, ϕ, z) is adopted such that the surface of the wire is $\rho = a$. If the external fields are now locally uniform, we can neglect the azimuthal variation around the wire and consider only the axial current flow. For fields that vary as $\exp(-\Gamma z + i\omega t)$ where Γ is a propagation constant, the Hertz vector has only a z component Π_w. Thus, within the wire $\rho \leq a$, we can write

$$E_z = (k_w^2 + \partial^2/\partial z^2)\Pi_w = (k_w^2 + \Gamma^2)\Pi_w$$
$$H_\phi = -(\sigma_w + i\epsilon_w\omega)\,\partial\Pi_w/\partial\rho \qquad (1)$$

where

$$ik_w = [(i\mu_w\omega)(\sigma_w + i\epsilon_w\omega)]^{1/2}.$$

The appropriate form of the solution for Π_w is the modified Bessel function $I_0[i(k_w^2 + \Gamma^2)^{1/2}\rho]$ times a constant factor. Thus according to our basic definition

$$Z_i = E_z/(2\pi\rho H_\phi)\,|_{\rho=a} \qquad (2)$$

or

$$Z_i = \frac{i(k_w^2 + \Gamma^2)^{1/2}}{2\pi(\sigma_w + i\epsilon_w\omega)a}\,\frac{I_0[i(k_w^2 + \Gamma^2)^{1/2}a]}{I_1[i(k_w^2 + \Gamma^2)^{1/2}a]}. \qquad (3)$$

In the usual case where $|\Gamma^2| \ll |k_w^2|$ this simplifies to

$$Z_i \simeq \frac{(i\mu_w\omega)^{1/2}}{2\pi(\sigma_w + i\epsilon_w\omega)^{1/2}a}\,\frac{I_0(ik_wa)}{I_1(ik_wa)}. \qquad (4)$$

In the dc limit (i.e., $\omega \to 0$) we see that Z_i reduces to the expected form $(\pi a^2\sigma_w)^{-1}$.

In previous papers on this subject, we have used the boundary condition $E_z = IZ_i$ to apply to the surface of the thin wire even when the external region is complex. Two examples were axial conductors in a circular tunnel [2] and an axial conductor in a rectangular tunnel [3]. The justification for this type of boundary condition is that the external fields are locally uniform. Thus, on physical grounds, we expect the results to be valid when the wire radius is small compared with the distance to neighborhood surfaces and when the quantity $|\beta a| \ll 1$. Here β is the effective transverse wavenumber in the external region. There is some experimental support for this analytical approach to such problems [4].

EXTENSION TO BRAIDED SHIELD, DIELECTRIC LAYERS, AND OUTER LOSSY FILM

We now wish to extend this series-impedance concept to the case where the axial wire conductor is covered by a layer of perfect insulation of radius b with dielectric constant ϵ and free-space permeability μ_0. To allow for the presence of a metal braided shield, we assume that there is a thin uniform sheath of radius b with a designated transfer impedance Z_T in ohms/meter. Surrounding this, we have a coating whose dielectric constant is ϵ_c; it is also assumed lossless and a has a free-space permeability. Finally, to allow for a layer of mine dust or conducting

Manuscript received July 31, 1974; revised November 22, 1974.
The authors are with the Institute for Telecommunication Sciences, Office of Telecommunications, U.S. Department of Commerce, Boulder, Colo. 80302.

fluid, we assume there is a thin outer layer of conductive material with a transfer impedance Z_L. This situation is illustrated in Fig. 1 where the cross section of this braided coaxial cable with lossy outer sheath is depicted.

The situation is admittedly simplified, particularly with regard to the thin uniform sheath representation of the braided shield. In fact, the nonuniformities of the braid and random perforations of the shield will play an important role in the performance of an actual system. However, for present purposes we will consider just a uniform or smoothed-out version of the braid. We can rely on other work [5] to give us an estimate on the expected value of the transfer impedance Z_T. In a similar fashion, we justify the use of the transfer impedance Z_L for the external lossy film. The appropriate value here can be estimated from the approximate formula $Z_L \simeq (2\pi c\sigma d)^{-1}\ \Omega/\mathrm{m}$, where σd is the conductivity–thickness product of the lossy film. Such an easily recognizable expression is justified when d is small compared with the electric skin depth $(2/\sigma\mu\omega)^{1/2}$ of the film material, and also d should be small compared with the radius c.

The brief derivation given below for the effective series impedance follows the classical approach for cylindrical structures [6], [7].

The axial electric field and the azimuthal magnetic field for the three regions thus have the following form for fields that vary as $\exp(i\omega t - \Gamma z)$:

$$\left.\begin{aligned} E_z &= (k^2 + \Gamma^2)\Pi = \beta^2\Pi \\ H_\phi &= -i\epsilon\omega\partial\Pi/\partial\rho \end{aligned}\right\} \quad \text{for} \quad a < \rho < b \tag{5}$$

$$\left.\begin{aligned} E_z &= (k_c^2 + \Gamma^2)\Pi_c = \beta_c^2\Pi_c \\ H_\phi &= -i\epsilon_c\omega\partial\Pi_c/\partial\rho \end{aligned}\right\} \quad \text{for} \quad b < \rho < c \tag{6}$$

and

$$\left.\begin{aligned} E_z &= (k_0^2 + \Gamma^2)\Pi_0 = \beta_0^2\Pi_0 \\ H_\phi &= -i\epsilon_0\omega\partial\Pi_0/\partial\rho \end{aligned}\right\} \quad \text{for} \quad \rho > c \tag{7}$$

where Π, Π_c, and Π_0 are the Hertz potentials for the three respective regions. Also β, β_c, and β_0 are the corresponding transverse wavenumbers and they are defined as indicated above. Now in any of the three regions, the Hertz potentials can be written as linear combinations of the Bessel functions J_0 and Y_0 with arguments $\beta\rho$, $\beta_c\rho$, and $\beta_0\rho$, respectively. Then, for example, for the first region we deduce readily that

$$\left.\begin{aligned} E_z &= \beta^2[PJ_0(\beta\rho) + QY_0(\beta\rho)] \\ H_\phi &= i\epsilon\omega\beta[PJ_1(\beta\rho) + QY_1(\beta\rho)] \end{aligned}\right\} \quad \text{for} \quad a < \rho < b \tag{8}$$

and

$$\left.\begin{aligned} E_{cz} &= \beta_c^2[MJ_0(\beta_c\rho) + NY_0(\beta_c\rho)] \\ H_{c\phi} &= i\epsilon_c\omega\beta_c[MJ_1(\beta_c\rho) + NY_1(\beta_c\rho)] \end{aligned}\right\} \quad \text{for} \quad b < \rho < c. \tag{9}$$

Here P, Q, M, and N are constants yet to be determined. We have similar expressions in the external region, but here we utilize the fact that the "scattered" field is an outgoing wave and thus the solution for Π_0 is characterized by a linear combination of J_0 and $H_0^{(2)}$ where the latter is the Hankel function of the second kind. Thus we can write

$$\left.\begin{aligned} E_{0z} &= A[J_0(\beta_0\rho) + R_0H_0^{(2)}(\beta_0\rho)] \\ H_{0\phi} &= Ai\epsilon_0\omega\beta_0^{-1}[J_1(\beta_0\rho) + R_0H_1^{(2)}(\beta_0\rho)] \end{aligned}\right\} \quad \text{for} \quad \rho > c. \tag{10}$$

Here A can be regarded as the strength of the axial electric field of the "primary" wave at $\rho = 0$ that would exist if the structure were not present. The coefficient R_0 then determines the relative strength of the scattered field. Obviously, if the parameter $|\beta_0 c|$ is not sufficiently small, we would need to include Bessel functions of order m and the factor $\exp(im\phi)$ in the solutions for all the Hertz potentials.

The boundary conditions for the problem can now be stated succintly as follows:

$$E_z = 2\pi aZ_iH_\phi \quad \text{at} \quad \rho = a \tag{i}$$

$$E_z = E_{cz} \quad \text{at} \quad \rho = b \tag{ii}$$

$$H_\phi - H_{c\phi} = -(2\pi bZ_T)^{-1}E_z \quad \text{at} \quad \rho = b \tag{iii}$$

$$E_{cz} = E_{0z} \quad \text{at} \quad \rho = c \tag{iv}$$

$$H_{c\phi} - H_{0\phi} = -(2\pi cZ_L)^{-1}E_z \quad \text{at} \quad \rho = c. \tag{v}$$

Here (i) is the impedance boundary condition that we impose at the surface of the inner conductor. It is an "exact" condition if we use (3), but for practical purposes, Z_i can be taken to be independent of Γ so that (4) is adequate. Conditions (ii) and (iv) indicate that the axial electric field is effectively continuous through the braid and the lossy-film layer. This is a consequence of the assumed thinness of these layers (i.e., the thicknesses are small compared with the effective wavelength in the respective media).

From boundary condition (i) above, we easily deduce that

$$Q/P = R = -\frac{[J_0(\beta a) - i2\pi akZ_i(\beta\eta)^{-1}J_1(\beta a)]}{[Y_0(\beta a) - i2\pi akZ_i(\beta\eta)^{-1}Y_1(\beta a)]} \tag{11}$$

where $\eta = \mu\omega/k = (\mu/\epsilon)^{1/2}$. Similarly, from (ii) we find

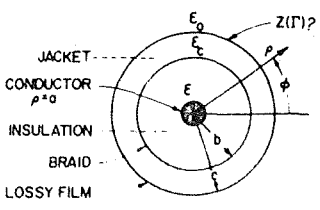

Fig. 1. The geometry of the coaxial structure showing the orientation of the cylindrical coordinate system.

that

$$P = M\frac{\beta_c^2}{\beta^2}\frac{J_0(\beta_c b) + R_c Y_0(\beta_c b)}{J_0(\beta b) + RY_0(\beta b)} \tag{12}$$

where $R_c = N/M$. Then an application of (iii) yields

$$R_c = \left\{\beta^2\left(\frac{i\beta_c k_c}{\eta_c}J_1(\beta_c b) - \frac{\beta_c^2 J_0(\beta_c b)}{2\pi b Z_T}\right)\times (J_0(\beta b) + RY_0(\beta b)) - \frac{i\beta k}{\eta}\beta_c^2 J_0(\beta_c b)[J_1(\beta b) + RY_1(\beta b)]\right\}$$
$$\times\left\{-\beta^2\left(\frac{i\beta_c k_c}{\eta_c}Y_1(\beta_c b) - \frac{\beta_c^2 Y_0(\beta_c b)}{2\pi b Z_T}\right)\times (J_0(\beta b) + RY_0(\beta b)) + \frac{i\beta k}{\eta}\beta_c^2 Y_0(\beta_c b)[J_1(\beta b) + RY_1(\beta b)]\right\}^{-1}. \tag{13}$$

An application of (iv) tells us that $M\beta_c^2[J_0(\beta_c c) + R_c Y_0(\beta_c c)] = A[J_0(\beta_0 c) + R_0 H_0^{(2)}(\beta_0 c)]$. Combining this with (v) yields

$$\left.\begin{aligned} E_z &\simeq \beta^2[P + (2/\pi)Q\ln 0.89\beta\rho] \\ H_\phi &\simeq -(2/\pi)i\epsilon\omega Q/\rho \end{aligned}\right\} a < \rho < b \tag{16}$$

$$\left.\begin{aligned} E_{cz} &\simeq \beta_c^2[M + (2/\pi)N\ln 0.89\beta_c\rho] \\ H_{c\phi} &\simeq -(2/\pi)i\epsilon_c\omega N/\rho \end{aligned}\right\} b < \rho < c \tag{17}$$

and

$$\left.\begin{aligned} E_{0z} &\simeq A[1 + R(1 - (i2/\pi)\ln 0.89\beta_0\rho] \\ H_{0\phi} &\simeq -A(2/\pi)i\epsilon_0\omega R/\rho \end{aligned}\right\} c < \rho < \hat{\rho}. \tag{18}$$

Here $\hat{\rho}$ is any value greater than c chosen such that $|\beta_0\hat{\rho}| \ll 1$. It is useful to note that in each region $H_\phi \times \rho$ is a constant in this limiting situation.

As an exercise, we can now apply boundary conditions (i)–(v) and get explicit quasi-static forms for the coefficients, or we can insert the small-argument approximations in the Bessel functions in (11)–(15). In either case, we obtain the following formula for the effective series impedance:

$$R_0 = -\frac{\left[\frac{ik_0}{\eta_0}J_1(\beta_0 c) - \frac{\beta_0 J_0(\beta_0 c)}{2\pi c Z_L} - \frac{ik_c}{\eta_c}\frac{\beta_0}{\beta_c}\frac{J_1(\beta_c c) + R_c Y_1(\beta_c c)}{J_0(\beta_c c) + R_c Y_0(\beta_c c)}J_0(\beta_0 c)\right]}{\left[\frac{ik_0}{\eta_0}H_1^{(2)}(\beta_0 c) - \frac{\beta_0 H_0^{(2)}(\beta_0 c)}{2\pi c Z_L} - \frac{ik_c}{\eta_c}\frac{\beta_0}{\beta_c}\frac{J_1(\beta_c c) + R_c Y_1(\beta_c c)}{J_0(\beta_c c) + R_c Y_0(\beta_c c)}H_0^{(2)}(\beta_0 c)\right]}. \tag{14}$$

Now the desired result is the effective series impedance defined by

$$Z(\Gamma) = \frac{E_{0z}}{2\pi c H_{0\phi}} \quad \text{at} \quad \rho = c$$
$$= \frac{\beta_0\eta_0[J_0(\beta_0 c) + R_0 H_0^{(2)}(\beta_0 c)]}{2\pi c i k_0[J_1(\beta_0 c) + R_0 H_1^{(2)}(\beta_0 c)]}. \tag{15}$$

QUASI-STATIC LIMITING FORM FOR $Z(\Gamma)$

The resulting expression for $Z(\Gamma)$ that is a function of the axial propagation constant Γ is rather involved. Fortunately, considerable simplification ensues if we consider the case where the arguments of the Bessel functions are sufficiently small that only the leading terms in their power-series expansions need be retained. In this connection it might be mentioned that in some important cases βc may not be "small" even when $\beta_0 c$ is small. For example, this could occur when $\Gamma \sim ik_0$, in which case $\beta_0 c$ is small even though $k_0 a$ may be comparable with one. However, in the quasi-static limit that we discuss below, it will be assumed that all the arguments are small.

To provide insight into the quasi-static limiting forms, we write out the field expressions that correspond to (8)–(10). Here we utilize the small-argument approximations $J_0(x) \to 1$, $J_1(x) \to x/2 \to 0$, $Y_0(x) \to (2/\pi)\ln 0.89x$, and $Y_1(x) \to -2/(\pi x)$. Thus

$$Z(\Gamma) \simeq \frac{Z_L(Z_c + Z_b)}{Z_L + Z_c + Z_b} \tag{19}$$

where

$$Z_b = \frac{Z_T(Z' + Z_i)}{Z_T + Z' + Z_i} \tag{20}$$

where

$$Z' = -\frac{k^2 + \Gamma^2}{2\pi i\epsilon\omega}\ln(b/a) \tag{21}$$

and

$$Z_c = -\frac{k_c^2 + \Gamma^2}{2\pi i\epsilon_c\omega}\ln(c/b). \tag{22}$$

The equivalent circuit for this situation is the ladder network shown in Fig. 2. The terminating element Z_i is the impedance of the inner conductor while the shunt elements Z_T and Z_L are the transfer impedances of the braid and

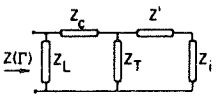

Fig. 2. The equivalent ladder network that yields the effective series impedance of the cable in the quasi-static approximation.

the external lossy film. The series elements Z_c and Z' can be identified as short sections of transmission lines whose properties depend on Γ. We stress that this quasi-static equivalent circuit is only valid when all the Bessel-function arguments are small compared with one. The expression for the series impedance given by (15) is not so restricted.

APPLICATION TO CIRCULAR-TUNNEL MODEL

We now consider the circular-waveguide model of a mine tunnel. The situation is depicted in Fig. 3 where the tunnel radius is a_0 while the cable is located at a distance ρ_0 from the tunnel axis. In an earlier paper [2], we determined the axial propagation constants of the permitted modes of the structure that satisfied both the impedance boundary conditions at the waveguide wall and at the surface of an axial conductor whose series impedance is specified. In the present case, the axial structure in the waveguide is the braided coaxial that we discussed previously. The impedance boundary condition is to be applied at the outer surface of the lossy-film coating whose radius is c. As indicated in Fig. 3, the distance of the cable from the tunnel wall is $a_0 - \rho_0$. In order for the solution to be valid, c should be small compared with $a_0 - \rho_0$.

As in the earlier paper, the homogeneous medium bounding the tunnel walls has a conductivity σ_e and a permittivity ϵ_e. In what follows, we choose $\sigma_e = 10^{-2}$ mho/m, $\epsilon_e = 10\epsilon_0$, and $a_0 = 2$ m. The interior region of the waveguide is free space, except at the braided coaxial. The dimensions of the latter, with reference to Fig. 1, are taken as follows: $a = 1.5$ mm, $b = 10$ mm, and $c = 11.5$ mm. Also, for purposes of illustration, we take the transfer impedance Z_T of the braid to be $i\omega L$ where $L = 40$ nH/m. This corresponds to the FONT cable developed by Fontaine *et al.* [5].

The relative dielectric constant ϵ/ϵ_0 of the insulator is taken to be 2.5 corresponding to polystyrene, for example. For an optimum system, we might have chosen a lower value but, for present purposes, this is not important. For the outer coating, the relative dielectric constant ϵ_c/ϵ_0 is taken to be 3.0 corresponding to typical jacket material. To allow for the presence of the outer lossy film, we choose the transfer impedance $Z_L = [2\pi c(\sigma d)]^{-1}$ where the conductivity–thickness product is to be specified. For example, a conducting fluid layer with $\sigma = 10$ mho/m whose thickness $d = 1$ mm leads to $(\sigma d) = 10^{-2}$ mho. As indicated by Rawat and Beal [8], the presence of such lossy films in realistic mine environments should be expected.

Using the above analytical machinery, we illustrate some results for the dominant modes of the braided cable located in the cylindrical structure. There are two important modes that we call the monofilar and bifilar modes. The first of these is similar to the situation treated before where we have a bare uncoated wire in the waveguide [2], [3]. In that case, the return current flows along the walls of the cylindrical waveguide. The second type is analogous to the currents flowing in a two-wire transmission line and the characteristic of this bifilar mode is almost independent of the waveguide walls. For the braided coaxial structure, this particular mode is the conventional one since the currents in the center conductor and braid are approximately equal but with opposite signs.

In Fig. 4, we show the attenuation rate (in nepers/meter) for the monofilar mode as a function of frequency from 0.2 to 200 MHz. Several values of ρ_0/a_0 are indicated as are two values of (σd). Also for this example, the conductivity σ_w of the center conductor is taken to be 10^7 mho/m, but for this mode, the attenuation is not critically dependent on σ_w. Also, except for higher frequencies, the attenuation rate is not influenced appreciably by (σd) for values even as high as 10^{-1} mho. As expected, of course, the attenuation rate for this monofilar mode increases as the coaxial is moved toward the wall. Note that $\rho_0/a_0 = 0.9$ corresponds to a distance $s - s_0 = 20$ cm ~ 8 in from the wall.

In Fig. 5 we show some corresponding results for the bifilar or coaxial-type mode. Since there is a strong dependence on the conductivity σ_w of the inner conductor, three different values are selected. The highest value $\sigma_w \sim 5.7 \times 10^7$ mho/m corresponds to copper. In this case, we also see that the results depend somewhat on the (σd) values, particularly at the upper frequencies. The

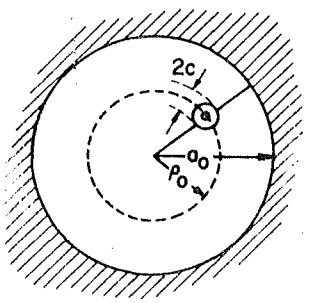

Fig. 3. The circular-waveguide model showing the location of the cable.

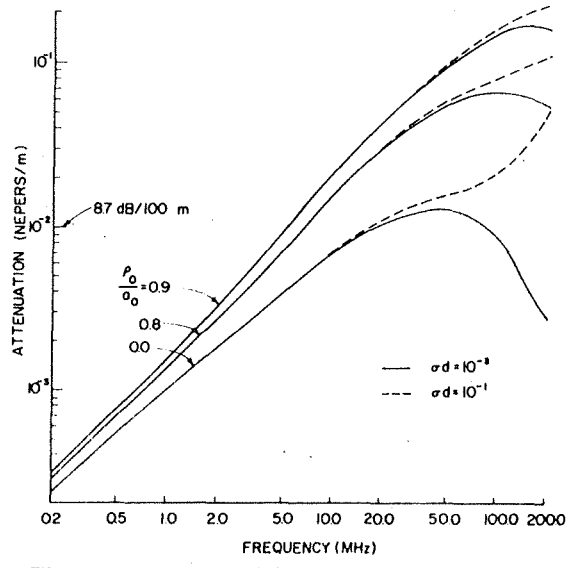

Fig. 4. The attenuation rate of the monofilar mode as a function of frequency, $a_0 = 2$ m.

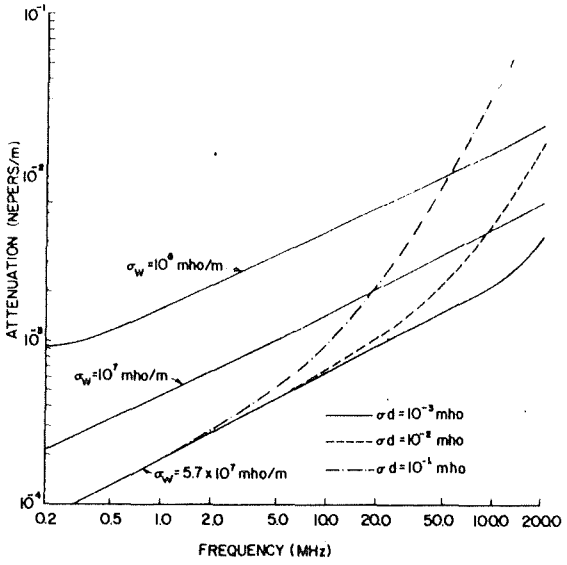

Fig. 5. The attenuation rate of the bifilar mode illustrating the dependence on the conductivity of the inner conductor and the effect of the external lossy film. $\epsilon = 2.5\epsilon_0$: $\epsilon_c = 3.0\epsilon_0$: $L = 40$ nH/m.

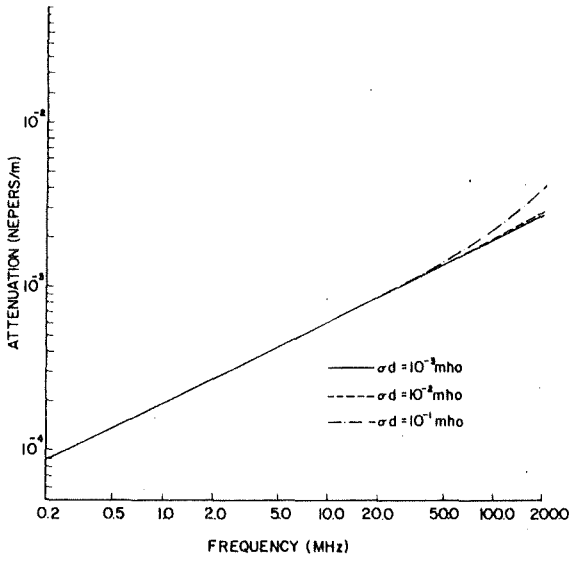

Fig. 6. The attenuation rate of the bifilar mode for a smaller value of the surface transfer impedance. $\sigma_w = 5.7 \times 10^7$ mho/m: $L = 4$ nH/m: $\epsilon = 2.5\epsilon_0$: $\epsilon_c = 3.0\epsilon_0$.

presence of the lossy film increases the attenuation of the bifilar mode for the range of frequencies and σd parameter considered in this figure. Actually, for the curves in Fig. 5 we have chosen $\rho_0/a_0 = 0.8$, but the results for this bifilar mode hardly depend at all on the value of ρ_0/a_0. In fact, the curves would be indistinguishable for $0 \leq \rho_0/a_0 \leq 0.9$.

In Fig. 6 we show the corresponding bifilar mode attenuation for the copper inner conductor. Here we choose the transfer inductance $L = 4$ nH/m that is a factor of 10 lower than before. The important point here is that the attenuation rate depends only slightly on the conductivity–thickness product (σd) of the outer lossy film. Thus, while high values of L are desirable from the standpoint of coupling to the desired bifilar mode, we can expect a greater susceptibility to the presence of lossy fluid or mine-dust layers on the outer jacket.

CONCLUDING REMARKS

The present results are believed to be a useful basis for the design of leaky-feeder communications systems that employ shielded cables in mine tunnels. The analytical method can be applied equally well to rectangular tunnels [9]. The effect of axial nonuniformities in the guiding structures needs to be considered if we are to utilize fully the capabilities of both the monofilar and the bifilar modes.

In principle, the method could be applied at much higher frequencies for single dielectric-coated conductors where the dominant mode would be a surface wave [10]–[12] whose energy is confined to the cable. Several difficulties emerge here. First of all, the assumption of local uniformity of the fields about the cable would need to be removed. Also, the hostile environment in most mine tunnels would produce very high attenuation due to moisture and coal dust. Also, the coupling to the surface-wave line would be not feasible for a roving miner. Nevertheless, we should keep an open mind on the possible relevance of Goubau-type surface-wave lines in mine environments.

ACKNOWLEDGMENT

The authors wish to thank their colleague Dr. S. F. Mahmoud for his useful comments and private communications.

REFERENCES

[1] J. C. Beal, J. Josiak, S. F. Mahmoud, and V. Rawat, "Continuous-access guided communication (CAGC) for ground-transportation systems," *Proc. IEEE (Special Issue on Ground Transportation for the Eighties)*, vol. 61, pp. 562–568, May 1973.

[2] J. R. Wait and D. A. Hill, "Guided electromagnetic waves along axial conductors in a circular tunnel," *IEEE Trans. Antennas Propagat.* (Succinct Papers), vol. AP-22, pp. 627–630, July 1974.

[3] S. F. Mahmoud and J. R. Wait, "Theory of wave propagation along a thin wire inside a rectangular waveguide," *Radio Sci.*, vol. 9, pp. 417–420, Mar. 1974.

[4] J. R. Wait and D. A. Hill, "Coaxial and bifilar modes on a transmission line in a circular tunnel," *Appl. Phys.*, vol. 4, pp. 307–312, Sept. 1974.

[5] J. Fontaine, B. DeMoulin, P. deGauque, and R. Gabillard, "Feasibility of radio communication in mine galleries by means of a coaxial cable having a high coupling impedance," in *1973 Proc. Thru-the-Earth Electromagnetics Workshop*, (Colorado School of Mines), U.S. Bureau of Mines Contract G-133023, Final Rep. Dec. 31, 1973, pp. 130–139 (Available from NTIS, Springfield, Va.).

[6] J. R. Wait, *Electromagnetic Radiation from Cylindrical Structures.* New York: Pergamon, 1959, pp. 142–148.

[7] R. E. Collin, *Field Theory of Guided Waves.* New York: McGraw-Hill, 1961, pp. 477–483.

[8] V. Rawat and J. C. Beal, "Leaky cables treated as open waveguides," in *Proc. Int. Colloquium Leaky-Feeder Communications* (Guilford, Surrey, England, Apr. 1974).

[9] J. R. Wait and S. F. Mahmoud, "Propagation along a braided coaxial cable in a rectangular tunnel," Informal Rep. U.S. Bureau of Mines, June 15, 1974.

[10] G. Goubau, "Single-conductor surface-wave transmission lines," *Proc. IRE*, vol. 39, pp. 619–624, June 1951.

[11] R. L. Gallawa *et al.*, "The surface-wave transmission line and its use in communicating with high-speed vehicles," *IEEE Trans. Commun. Technol.*, vol. COM-17, pp. 518–525, Oct. 1969.

[12] W. J. Dewar and J. C. Beal, "Coaxial-slot surface wave launchers," *IEEE Trans. Microwave Theory Tech.*, vol. MTT-18, pp. 449–455, Aug. 1970.

Propagation Along a Braided Coaxial Cable Located Close to a Tunnel Wall

DAVID A. HILL, SENIOR MEMBER, IEEE, AND
JAMES R. WAIT, FELLOW, IEEE

Abstract—**A previous development is extended to permit attenuation calculations when a braided cable is located close to a tunnel wall. This is an important case in mine communications utilizing leaky feeders. Numerical results are presented to illustrate the effects of numerous parameters on mode attenuation. A principal finding is that the attenuation rate for the bifilar mode is hardly affected at all by the finite conductivity of the wall. On the other hand, the monofilar mode suffers a very high attenuation when the cable approaches the wall.**

INTRODUCTION

The leaky-feeder technique is now being developed for communication in mines [1]. In this method, referred to as continuous-access guided communications (CAGC), the signals are guided by some type of transmission line. The energy is coupled into or out of the channel by antennas in the vicinity of the transmission line which may be a coaxial cable [2] or a twin-wire line [3], [4].

We have previously derived a mode equation for a braided coaxial cable within a circular tunnel and we presented some numerical results [5]. However, that mode equation is very poorly convergent when the cable is located close to the tunnel wall. Unfortunately, it is precisely this case which is of most practical interest for communication in coal mines where it is generally necessary to lay the cable close to the wall [6]. In this

Manuscript received October 20, 1975; revised January 2, 1976.
D. A. Hill is with the Institute for Telecommunication Sciences, U.S. Department of Commerce, Boulder, CO 80302.
J. R. Wait is with the Environmental Research Laboratories, U.S. Department of Commerce, Boulder, CO 80302, and is a Consultant to the Institute of Telecommunication Sciences.

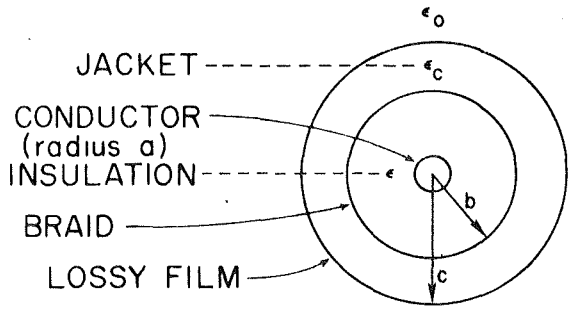

Fig. 1. The braided coaxial cable.

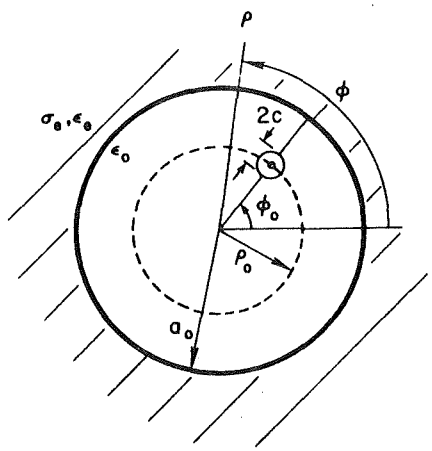

Fig. 2. The geometry of the cable in a circular tunnel.

short paper, we derive a rapidly convergent mode equation which is used to obtain numerical results for the attenuation rates of the dominant modes when the cable is located close to a circular tunnel wall.

Mode Equation

The geometry of the braided coaxial cable is shown in Fig. 1. The center conductor of radius a is assumed to have a very high but finite conductivity σ_w. The insulation of radius b is a lossless dielectric of permittivity ε. The metal braid of radius b is represented by a transfer impedance Z_T which is given by [2]

$$Z_T = i\omega L_T \tag{1}$$

where L_T is the transfer inductance and $\exp(i\omega t)$ time dependence is assumed. The coating of radius c is a lossless dielectric of permittivity ε_c. A thin lossy film of radius c is characterized by a transfer impedance Z_L which is given by [5]

$$Z_L = (2\pi c\sigma d)^{-1} \tag{2}$$

where σd is the conductivity-thickness product of the film. Rawat and Beal [7] indicate that the presence of such lossy films should be expected in realistic mine environments due to moisture and/or dust accumulation.

The idealized circular-tunnel geometry and the cylindrical coordinate system (ρ,ϕ,z) are shown in Fig. 2. The air-filled tunnel has a radius a_0 and is bounded by a lossy dielectric of conductivity σ_e and permittivity ε_e. Free-space permeability μ_0 is assumed everywhere. The braided cable is located within the tunnel at (ρ_0,ϕ_0).

We assume that the individual modes of the structure vary in the z direction as $\exp(-\Gamma z)$ for a time factor $\exp(i\omega t)$ and the objective is to calculate the values of the propagation constant Γ. By matching the tangential-field components at the tunnel boundary ($\rho = a_0$) and applying an impedance condition at the edge of the cable ($\rho = \rho_0 + c$, $\phi = \phi_0$), the following mode equation has been derived [5], [8]:

$$\frac{i\omega\mu_0 v^2}{2\pi\gamma_0^2}\,[K_0(vc) - S] - Z(\Gamma) = 0 \tag{3}$$

where $v = (\gamma_0^2 - \Gamma^2)^{1/2}$, $\gamma_0^2 = \omega^2\mu_0\varepsilon_0$, and K_0 is the modified Bessel function of the second kind. The summation of cylindrical harmonics S represents the effect of the tunnel boundary and is given by [8]

$$S = \sum_{m=0,1,2\cdots}^{\infty} T_m \tag{4}$$

where

$$T_m = \varepsilon_m R_m \frac{K_m(va_0)}{I_m(va_0)}\, I_m(v\rho_0) I_m(v(\rho_0 + c))$$

$$\varepsilon_m = \begin{cases} 1, & m = 0 \\ 2, & m \neq 0 \end{cases}$$

$$R_m = \frac{[(\gamma_0/v)K_m'(va_0)/K_m(va_0)] + Y_m\eta_0 + \delta_m\eta_0}{[(\gamma_0/v)I_m'(va_0)/I_m(va_0)] + Y_m\eta_0 + \delta_m\eta_0}$$

$$Y_m = \left(\frac{i\gamma_e^2}{u\mu_0\omega}\right)\frac{K_m'(ua_0)}{K_m(ua_0)} \qquad \eta_0 = (\mu_0/\varepsilon_0)^{1/2}$$

$$\delta_m\eta_0 = \frac{(im\Gamma/a_0)^2(v^{-2} - u^{-2})^2}{[(\gamma_0/v)I_m'(va_0)/I_m(va_0)] + Z_m/\eta_0}$$

$$Z_m = -\left(\frac{i\omega\mu_0}{u}\right)\frac{K_m'(ua_0)}{K_m(ua_0)}$$

$$\gamma_e^2 = i\omega\mu_0(\sigma_e + i\omega\varepsilon_e) \qquad u = (\gamma_e^2 - \Gamma^2)^{1/2}$$

I_m and K_m are modified Bessel functions of the first and second kind, and the prime indicates differentiation with respect to the argument. The series impedance per unit length of the cable $Z(\Gamma)$ has the following form, provided that the cable radius c is electrically small [5]:

$$Z(\Gamma) = \frac{Z_L(Z_c + Z_b)}{Z_L + Z_c + Z_b}$$

$$Z_b = \frac{Z_T(Z' + Z_i)}{Z_T + Z' + Z_i} \tag{5}$$

where

$$Z' = \frac{\gamma^2 - \Gamma^2}{2\pi i\omega\varepsilon}\ln(b/a), \qquad \gamma^2 = -\omega^2\mu_0\varepsilon$$

$$Z_c = \frac{\gamma_c^2 - \Gamma^2}{2\pi i\omega\varepsilon_c}\ln(c/b), \qquad \gamma_c^2 = -\omega^2\mu_0\varepsilon_c$$

$$Z_i = \frac{(i\omega\mu_0)^{1/2}}{(2\pi ca\sigma_w)^{1/2}}\frac{I_0(\gamma_w a)}{I_1(\gamma_w a)}, \qquad \gamma_w = (i\omega\mu_0\sigma_w)^{1/2}$$

and $|\gamma_w|$ is assumed much larger than $|\Gamma|$.

Asymptotic Behavior

Although some approximations to the mode equation (3) are possible under certain limiting conditions, a numerical evaluation of (3) is generally required. Numerical results for the propagation

constant Γ have been obtained using a modification of Newton's method [5], but convergence problems inhibit a direct evaluation of S as given by (4) when ρ_0/a_0 is nearly equal to unity. Here we develop an efficient method to treat this important case where the cable is near the wall.

The first step is to examine the asymptotic behavior of the mth term T_m in (4) as m becomes large. The first terms of the required uniform asymptotic expansions [9] are

$$\begin{aligned} I_\nu(\nu z) &\sim \frac{1}{(2\pi\nu)^{1/2}} \frac{\exp(\nu\eta)}{(1+z^2)^{1/4}} \\ K_\nu(\nu z) &\sim \left(\frac{\pi}{2\nu}\right)^{1/4} \frac{\exp(-\nu\eta)}{(1+z^2)^{1/4}} \\ I_\nu'(\nu z) &\sim \frac{1}{(2\pi\nu)^{1/2}} \frac{(1+z^2)^{1/4}\exp(\nu\eta)}{z} \\ K_\nu'(\nu z) &\sim \frac{1}{(2\pi\nu)^{1/2}} \frac{(1+z^2)^{1/4}\exp(-\nu\eta)}{z} \end{aligned} \tag{6}$$

where

$$\eta = (1+z^2)^{1/2} + \ln\left[\frac{z}{1+(1+z^2)^{1/2}}\right].$$

If we let $m = \nu$ and $x = \nu z$ and if $m \gg |x|$, the following can be derived from (6):

$$\begin{aligned} I_m(x) &\sim \frac{1}{(2\pi m)^{1/2}} \left(\frac{e}{2m}\right)^m x^m \\ K_m(x) &\sim \left(\frac{\pi}{2m}\right)^{1/2} \left(\frac{e}{2m}\right)^{-m} x^{-m} \\ \frac{I_m'(x)}{I_m(x)} &\sim \frac{m}{x} \\ \frac{K_m'(x)}{K_m(x)} &\sim -\frac{m}{x}. \end{aligned} \tag{7}$$

The expressions in (7) also reveal the problem that I_m can become too small and K_m can become too large for computer storage as m becomes large. However, by substituting (7) into (4) the following simple asymptotic expression is obtained for T_m:

$$T_m \sim \frac{R^a}{m}\left[\frac{\rho_0(\rho_0+c)}{a_0^2}\right]^m = T_m^a \tag{8}$$

where R^a is the asymptotic expression for R_m and is independent of m. The explicit expression for R^a is obtained by dividing the numerator and denominator of R_m by m and substituting the asymptotic expressions from (7)

$$R^a = \frac{-\frac{\gamma_0}{v^2 a_0} + \frac{Y_m^a \eta_0}{m} + \frac{\delta_m^a \eta_0}{m}}{\frac{\gamma_0}{v^2 a_0} + \frac{Y_m^a \eta_0}{m} + \frac{\delta_m^a \eta_0}{m}} \tag{9}$$

where

$$\begin{aligned} \frac{Y_m^a \eta_0}{m} &= \frac{-i\gamma_e^2 \eta_0}{\omega\mu_0 u^2 a_0} \\ \frac{\delta_m^a \eta_0}{m} &= \frac{(i\Gamma/a_0)^2 (v^{-2} - u^{-2})^2}{\frac{\gamma_0}{v^2 a_0} + \frac{Z_m^a}{\eta_0 m}} \end{aligned}$$

and

$$\frac{Z_m^a}{\eta_0 m} = \frac{i\omega\mu_0}{u^2 a_0 \eta_0}.$$

The poor convergence of (4) for ρ_0/a_0 close to unity is apparent from the expression for T_m^a in (8). However, the following summation formula [10] may be used:

$$\sum_{m=1}^{\infty} \frac{r^m}{m} = -\ln(1-r). \tag{10}$$

Thus, from (8) and (10), we can write

$$\sum_{m=1}^{\infty} T_m^a = -R^a \ln\left[1 - \frac{\rho_0(\rho_0+c)}{a_0^2}\right]. \tag{11}$$

By subtracting (11) from (4), the following rapidly convergent form is obtained for S:

$$S = -R^a \ln\left[1 - \frac{\rho_0(\rho_0+c)}{a_0^2}\right] + T_0 + \sum_{m=1}^{\infty} (T_m - T_m^a). \tag{12}$$

This form is used in the mode equation (3) to obtain numerical results.

If the tunnel becomes very large electrically, the arguments of the Bessel functions (va_0 and ua_0) can be quite large and (12) may not converge rapidly. However, computation time could still be decreased by employing asymptotic expansions which are valid for large order and large argument. These are

$$\begin{aligned} \frac{I_m'(x)}{I_m(x)} &\sim \frac{m}{x}\left(1 - \frac{x^2}{m^2}\right)^{1/2} \\ \frac{K_m'(x)}{K_m(x)} &\sim \frac{-m}{x}\left(1 - \frac{x^2}{m^2}\right)^{1/2} \end{aligned} \tag{13}$$

but they are not valid when x is near m. Wait [11] has examined such approximations in a study of whispering-gallery modes in electrically large cylinders.

Numerical Results

Using the mode equation (3) along with the rapidly convergent form of S in (12), numerical results for the propagation constant Γ were obtained for both the monofilar and bifilar modes. The energy in the bifilar mode is concentrated primarily within the insulation, and the solution is found in the neighborhood $\Gamma \simeq \gamma$, where γ is the propagation constant of the insulation. For the monofilar mode, the forward current is carried by the cable and the return current is carried by the tunnel wall. Consequently, the solution is found in the neighborhood $\Gamma \simeq \gamma_0$, where γ_0 is the free-space propagation constant. In either case the attenuation rate α is given by

$$\alpha = \mathrm{Re}\,(\Gamma)(\mathrm{Np/m}) = 8.686 \times 10^3\,\mathrm{Re}\,(\Gamma)(\mathrm{dB/km}). \tag{14}$$

In all cases the tunnel radius a_0 was taken as 2 m, and the following cable parameters were used: $a = 1.5$ mm, $b = 10$ mm, $c = 11.5$ mm, $\sigma_w = 5.7 \times 10^7$ mho/m, $\varepsilon/\varepsilon_0 = 2.5$, $\varepsilon_c/\varepsilon_0 = 3.0$, and $\sigma d = 10^{-3}$ mho. All figures cover the frequency range from 1 to 20 MHz. For higher frequencies, (12) is no longer rapidly convergent.

Figs. 3–5 show attenuation rates for the bifilar mode for wall

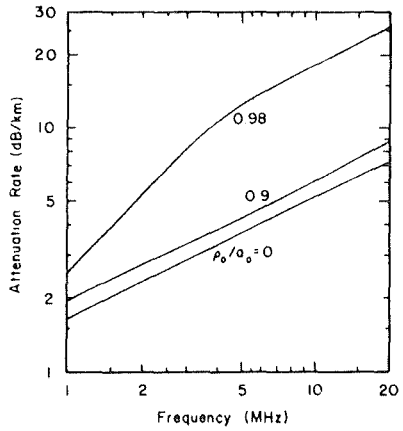

Fig. 3. The effect of cable position on the attenuation rate of the bifilar mode. The cable parameters correspond to the FONT cable. (Parameters: $L_T = 40$ nH/m, $a = 1.5$ mm, $b = 10$ mm, $c = 11.5$ mm, $a_0 = 2$ m, $\varepsilon_e/\varepsilon_0 = 10$, $\sigma_e = 10^{-3}$ mho/m, $\sigma_w = 5.7 \times 10^7$ mho/m, $\sigma d = 10^{-3}$ mho, $\varepsilon/\varepsilon_0 = 2.5$, $\varepsilon_c/\varepsilon_0 = 3.0$.)

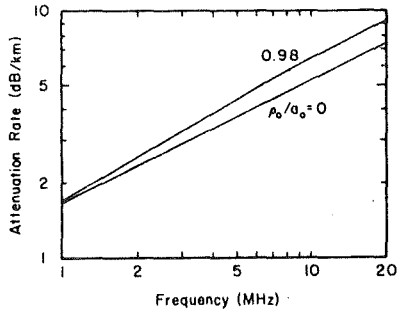

Fig. 4. The attenuation rate of the bifilar mode for a reduced value of L_T. (Parameters as in Fig. 3, but $L_T = 10$ nH/m.)

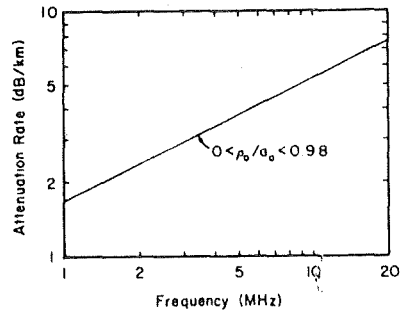

Fig. 5. The attenuation rate of the bifilar mode for a further reduced value of L_T. (Parameters as in Fig. 3, but $L_T = 2$ nH/m.)

constants, $\sigma_e = 10^{-3}$ mho/m and $\varepsilon_e/\varepsilon_0 = 10$. In Fig. 3, L_T is taken to be 40 nH/m which corresponds to the very high transfer inductance of the FONT cable developed by Fontaine *et al.* [2]. For $\rho_0/a_0 = 0.98$, the cable center is only 4 cm from the wall, and the attenuation rate is increased significantly. The optimum frequency for this cable has been claimed to be approximately 7 MHz [2]. Most coaxial cables possess a much lower value of L_T [12], and Fig. 4 shows the same case with L_T reduced to 10 nH/m. Fig. 5 shows the same case with L_T reduced. even further to 2 nH/m, and in this case the tunnel wall has essentially no effect on the attenuation rate. Fig. 6 shows the rather complicated effect of wall conductivity on the attenuation rate of the

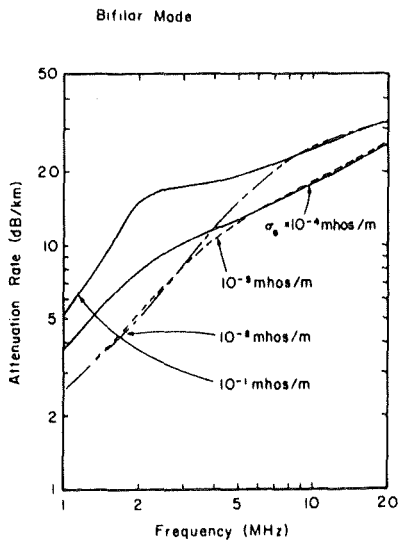

Fig. 6. The effect of tunnel-wall conductivity on the attenuation rate of the bifilar mode. (Parameters: $a_0 = 2$ m, $\rho_0/a_0 = 0.98$, $\varepsilon_e/\varepsilon_0 = 10$, $L_T = 40$ nH/m, $a = 1.5$ mm, $b = 10$ mm, $c = 11.5$ mm, $\sigma d = 10^{-3}$ mho, $\sigma_w = 5.7 \times 10^7$ mho/m, $\varepsilon/\varepsilon_0 = 2.5$, $\varepsilon_c/\varepsilon_0 = 3.0$.)

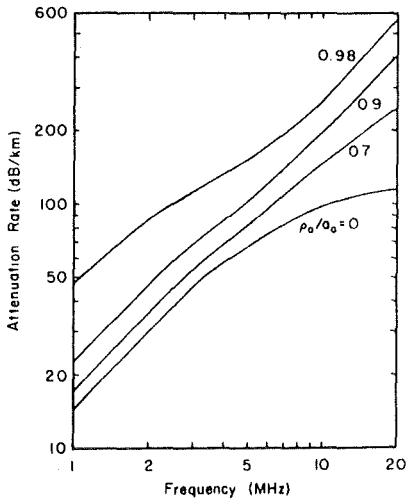

Fig. 7. The effect of cable position on the attenuation rate of the monofilar mode. (Parameters as in Fig. 3.)

bifilar mode for $\rho_0/a_0 = 0.98$ and $L_T = 40$ nH/m. For smaller values of ρ_0 and/or L_T, the wall conductivity has a lesser effect.

Fig. 7 shows the effect of cable position on the attenuation rate of the monofilar mode. Note that the attenuation rate is in general an order of magnitude higher than that of the bifilar mode. Even for the increased wall conductivity ($\sigma_e = 10^{-1}$ mho/m) shown in Fig. 8, the attenuation rate is still quite high.

Concluding Remarks

A method has been developed for treating the important practical case of the cable close to the tunnel wall. It is found that the tunnel wall has little effect on the attenuation rate of the bifilar mode unless the cable has a very large transfer inductance and is located close to the wall as shown in Fig. 3. The monofilar mode has a high attenuation rate for most cases of interest and is probably of use only if some mode conversion exists between the monofilar and bifilar modes.

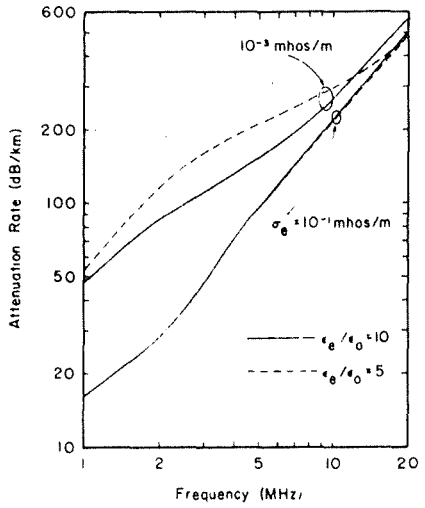

Fig. 8. The effect of tunnel-wall conductivity and permittivity on the attenuation rate of the monofilar mode. (Parameters as in Fig. 6 except for indicated values of ϵ_e/ϵ_0 and σ_e.)

An important related area for further work is the excitation (and reception) of the monofilar and particularly the bifilar mode. Quantitative knowledge is required for a total calculation of system loss and communication range. Also the use of higher frequencies with cables close to the wall merits some attention even though higher attenuation rates can be expected.

References

[1] J. C. Beal, J. Josiak, S. F. Mahmoud, and V. Rawat, "Continuous-access guided communication (CAGC) for ground-transportation systems," *Proc. IEEE (Special Issue on Ground Transportation for the Eighties)*, vol. 61, pp. 562–568, May 1973.

[2] J. Fontaine, B. DeMoulin, P. deGauque, and R. Gabillard, "Feasibility of radio communication in mine galleries by means of a coaxial cable having a high coupling impedance," in *1973 Proc. Thru-the-Earth Electromagnetics Workshop* (Colorado School of Mines), U.S. Bureau of Mines Contract G-133023, Final Rep. Dec. 31, 1973, pp. 130–139 (available from NTIS, Springfield, VA).

[3] L. Deryck, "Minus et Carriers," *Bulletin Technique* (Institut National des Industries Extractives, Belgium), no. 134, Dec. 1971.

[4] J. R. Wait and D. A. Hill, "Coaxial and bifilar modes on a transmission line in a circular tunnel," *Appl. Phys.*, vol. 4, pp. 307–312, Sept. 1974.

[5] ——, "Propagation along a braided coaxial cable in a circular tunnel," *IEEE Trans. Microwave Theory Tech.*, vol. MTT-23, pp. 401–405, May 1975.

[6] P. Delogne, "The INIEX mine communications system," in *Proc. International Conference Radio: Roads, Tunnels, Mines* (Liege, Belgium), pp. 129–136, April 1974.

[7] V. Rawat and J. C. Beal, "Leaky cables treated as open waveguides," in *Proc. Int. Colloquium Leaky-Feeder Communications* (Guildford, Surrey, England, Apr. 1974).

[8] J. R. Wait and D. A. Hill, "Guided electromagnetic waves along axial conductors in a circular tunnel," *IEEE Trans. Antennas Propagat.* (Succinct Papers), vol. AP-22, pp. 627–630, July 1974.

[9] M. Abramowitz and I. A. Stegun, *Handbook of Mathematical Functions*, National Bureau of Standards, 1964, p. 378.

[10] A. D. Wheelon, *Tables of Summable Series and Integrals Involving Bessel Functions*. San Francisco: Holden-Day, 1968, p. 37.

[11] J. R. Wait, "Electromagnetic whispering gallery modes in a dielectric rod," *Radio Sci.*, vol. 2, pp. 1005–1017, Sept. 1967.

[12] R. J. Slaughter, "Field leakage and crosstalk, with special reference to radiating cables with perforated tape screens," in *Proc. Int. Colloquium Leaky-Feeder Communications* (Guildford, Surrey, England, April 1974).

Lec. 23

Coupling Between a Radiating Coaxial Cable and a Dipole Antenna

DAVID A. HILL, MEMBER, IEEE, AND
JAMES R. WAIT, FELLOW, IEEE

Abstract—**The coupling loss between a coaxial cable with a circumferential gap and a dipole antenna is analyzed. The numerical results have application to continuous-access guided communication (CAGC) and to related leaky feeder systems now being used in intramine communications. It is shown that the coupling is very strong in the neighborhood of the cable axis even when the linear distance between the dipole and the cable gap is large. This, of course, is a desirable feature of such limited-access communication systems.**

INTRODUCTION

Continuous-access guided communication (CAGC) is an interesting combination of a shielded channel and a radiating system. The CAGC technique usually utilizes some kind of a wave-guiding system that has provision for a controlled leakage to enable a neighboring point to have access to signal information. Current applications are to ground transportation systems [1] and mine communications [2] but there are many other possibilities in urban environments.

A key aspect of CAGC is how to control the leakage from the main guiding channel that usually is a coaxial cable of some type. One method [1] that has been proposed is to employ a number of circumferential slits or gaps in the solid shield of the coax. In this fashion, the structure becomes a form of radiating antenna by virtue of the currents excited on the external surface of the shield. A key parameter in such a system is the resulting coupling loss between an incident TEM mode within the coax and a portable linear dipole receiving antenna in the external neighborhood. In this concise paper, we present quantitative information for such a configuration consisting of an infinitely long coax with a single radiating gap and an arbitrarily located dipole antenna. The reciprocal problem, when the external dipole antenna transmits, is also considered.

Earlier we derived field expressions for a dielectric coated coaxial cable with an interrupted shield [3], [4]. This was used to evaluate the total power radiated from an idealized break in the outer cable shield of a CATV system. The boundary-value analysis mentioned above is extended here to determine the coupling loss between such a radiating cable and a receiving dipole antenna.

The geometry of the infinitely long cable is indicated in Fig. 1 with respect to a cylindrical coordinate system (ρ,ϕ,z). The inner conductor of radius a and the shield of radius b are both assumed to be perfectly conducting. The insulation in the space, $a < \rho < b$, has a dielectric constant ϵ_i and the jacket in the space, $b < \rho < c$, has a dielectric constant ϵ_c. The region, $\rho > c$, external to the cable is assumed to be free space with dielectric constant ϵ_o. A gap of width δ in the shield is located at $z = 0$. Here we are concerned with how much power is coupled to an external dipole antenna when an internal TEM mode is incident on the gap.

MUTUAL IMPEDANCE FORMULATION

For an internal TEM mode of current I_o incident on the gap, the power in the incident mode P_i is given by

$$P_i = \tfrac{1}{2} |I_o|^2 / Y_c, \tag{1}$$

Paper approved by the Associate Editor for Radio Communication of the IEEE Communications Society for publication without oral presentation. Manuscript received March 24, 1975; revised May 23, 1975.

The authors are with the Institute for Telecommunication Sciences, Office of Telecommunications, U. S. Department of Commerce, Boulder, Colo. 80302.

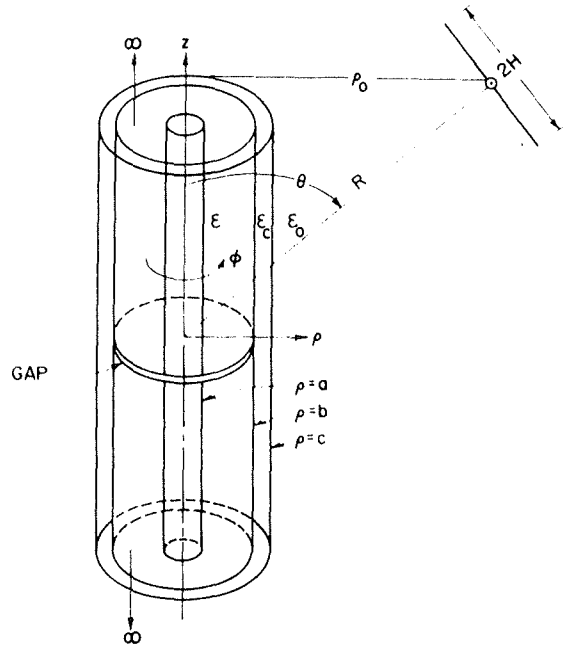

Fig. 1. Dielectric coated coaxial cable with a circumferential gap of width δ and the external dipole antenna (not to scale).

where $Y_o = 2\pi/\eta \ln (b/a)$ and $\eta = (\mu_o/\epsilon)^{1/2}$. Here Y_o is the characteristic admittance of the TEM mode in the coax. For a total gap admittance Y_t, the resultant gap voltage V is

$$V = I_o/Y_t. \tag{2}$$

Two different methods [3], [4] were used to calculate Y_t, and they gave very similar results over the parameter ranges of interest.

When the thickness of jacket $(c - b)$ is small, the external magnetic field $H_{o\phi}$ is given by [3]

$$H_{o\phi} = \frac{i\omega\epsilon_o bV}{2\pi} \int_{-\infty}^{\infty} \frac{H_1^{(2)}(u_o\rho) \exp(-i\lambda z) f(\lambda) d\lambda}{u_o b H_o^{(2)}(u_o b) + \Delta(\lambda) H_1^{(2)}(u_o b)}, \tag{3}$$

where $\Delta(\lambda) = (\epsilon_o/\epsilon_c) u_c^2 (c - b) b$,

$$f(\lambda) = \frac{\sin(\lambda\delta/2)}{(\lambda\delta/2)},$$

$$u_o = (k_o^2 - \lambda^2)^{1/2}, \qquad u_c = (k_c^2 - \lambda^2)^{1/2},$$

$$k_c = \omega(\mu_o\epsilon_c)^{1/2}, \qquad k_o = \omega(\mu_o\epsilon_o)^{1/2},$$

and $H_o^{(2)}$ and $H_1^{(2)}$ are zero- and first-order Hankel functions of the second kind. The time dependence is $\exp(i\omega t)$. The external electric field has ρ and z components, $E_{o\rho}$ and E_{oz}, that are given by

$$E_{o\rho} = \frac{ibV}{2\pi} \int_{-\infty}^{\infty} \frac{H_1^{(2)}(u_o\rho) \exp(-i\lambda z) f(\lambda) \lambda d\lambda}{u_o b H_o^{(2)}(u_o b) + \Delta(\lambda) H_1^{(2)}(u_o b)},$$

$$E_{oz} = \frac{bV}{2\pi} \int_{-\infty}^{\infty} \frac{H_0^{(2)}(u_o\rho) \exp(-i\lambda z) f(\lambda) u_o d\lambda}{u_o b H_o^{(2)}(u_o b) + \Delta(\lambda) H_1^{(2)}(u_o b)}. \tag{4}$$

For a general location of the receiving antenna, the electric field must be computed from (4) by numerical integration. Then, for a receiving antenna of finite length, another numerical integration of the electric field over the length of the antenna is required in order to compute the coupling loss. However, the calculations simplify considerably when the receiving antenna is located in the far field of the cable (i.e., $k_o\rho \gg 1$) [3]. The magnetic field, given by (3), then simplifies to

$$H_{o\phi} \simeq \frac{-iV}{\pi\eta_o} P(\theta) \frac{\exp(-ik_o R)}{R}, \tag{5}$$

where $R = (\rho^2 + z^2)^{1/2}$, $\eta_o = (\mu_o/\epsilon_o)^{1/2}$,

$$P(\theta) = \frac{f(k_o \cos\theta) k_o b}{k_o b \sin\theta H_o^{(2)}(k_o b \sin\theta) + \Delta(k_o \cos\theta) H_1^{(2)}(k_o b \sin\theta)},$$

and θ is the polar angle measured from the z axis. In the far field, the electric field has only a θ component $E_{o\theta}$:

$$E_{o\theta} \sim \eta_o H_{o\varphi} \simeq \frac{-iV}{\pi} P(\theta) \frac{\exp(-ik_o R)}{R}. \tag{6}$$

The receiving antenna is now taken to be a thin dipole of half-length H equal to or less than a quarter wavelength. Consequently, the antenna current $I(l)$ can be assumed to be sinusoidal [5]:

$$I(l) = \frac{I(0)}{\sin(k_o H)} \sin[k_o(H - |l|)], \tag{7}$$

where l is the distance from the center of the antenna. In order to maximize the coupling (minimize the coupling loss), the dipole is oriented in the θ direction as shown in Fig. 1. The voltage V_d induced in the dipole is thus determined from the induced EMF method [5], [6] as follows:

$$V_d \simeq \frac{1}{I(0)} \int_{-H}^{H} E_{o\vartheta} I(l)\, dl$$

$$\simeq \frac{2E_{o\vartheta}(1 - \cos k_o H)}{k_o \sin(k_o H)}, \tag{8}$$

where $E_{o\vartheta}$ is evaluated at the center of the dipole and is assumed constant over the length of the dipole. The mutual impedance between the cable and the dipole Z_m is now defined as the ratio of the voltage induced in the dipole to the current in the incident TEM mode of the cable. Thus

$$Z_m = V_d/I_o. \tag{9}$$

By reciprocity, Z_m is also equal to the ratio of the voltage in the excited TEM cable mode to the current at the terminals of the transmitting dipole.

NUMERICAL RESULTS FOR COUPLING LOSS

We define coupling loss L as the ratio of the incident power in the TEM mode [given by (1)] to the power absorbed in a matched load termination of the dipole. The current in the matched load is given by

$$I(0) = V_d/(2R_{\text{in}}) = I_o Z_m/(2R_{\text{in}}). \tag{10}$$

Here R_{in} is the input resistance of the dipole (assuming no losses) given by [5]

$$R_{\text{in}} = \frac{\eta_o}{4\pi}\{[1 - \cot^2(k_o H)]\,\text{Cin}(4k_o H) + 4\cot^2(k_o H)\,\text{Cin}(2k_o H) + 2\cot(k_o H)[\text{Si}(4k_o H) - 2\,\text{Si}(2k_o H)]\}, \tag{11}$$

where

$$\text{Si}(x) = \int_0^x \frac{\sin u}{u}\, du$$

and

$$\text{Cin}(x) = \int_0^x \frac{1 - \cos u}{u}\, du.$$

Thus, the coupling loss is given by

$$L = \frac{|I_o|^2/(2Y_o)}{|I_o|^2 |Z_m|^2/(8R_{\text{in}})} = \frac{4R_{\text{in}}}{Y_o |Z_m|^2}. \tag{12}$$

To convert to decibels, we take $10 \log_{10}(L)$.

To deal with the reciprocal case of a transmitting dipole and a receiving cable, the expression for the coupling loss above remains the

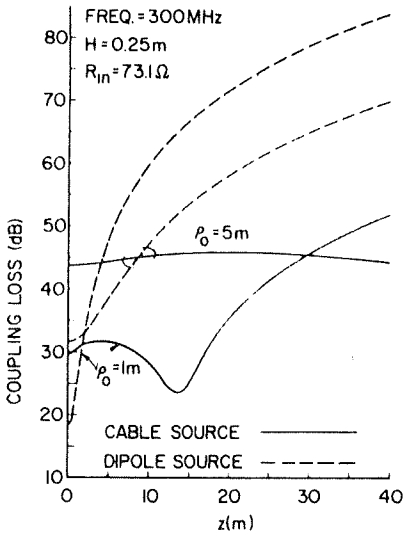

Fig. 2. Coupling loss between the cable and the dipole at 300 MHz. Dipole-to-dipole coupling loss is also shown at each location for comparison.

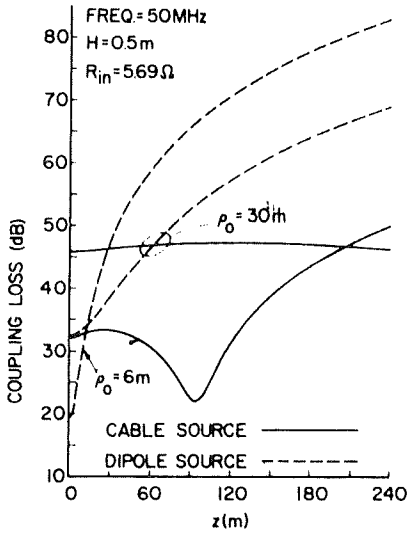

Fig. 3. Coupling loss at 50 MHz.

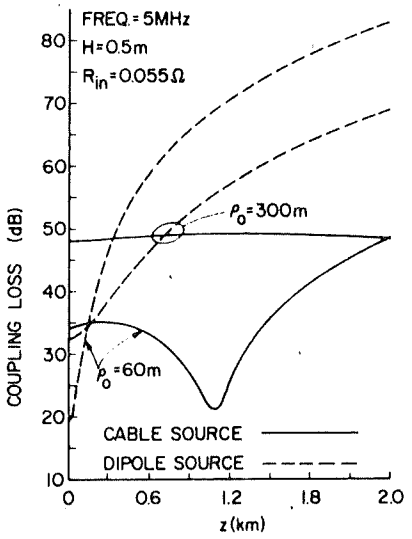

Fig. 4. Coupling loss at 5 MHz.

same if L is defined as the ratio of power transmitted by the dipole to the power transferred to either one of the TEM modes propagating away from the gap.

The equations required to compute L in (12) were programmed, and the results, shown in Figs. 2-4, were obtained for three frequencies (300 MHz, 50 MHz, and 5 MHz). The coupling loss, shown in Figs. 2–4, is for the geometry for the θ orientation of the dipole indicated in Fig. 1 that minimizes the coupling loss. In each case, the dipole remains at a radial distance ρ_0 of either one or five wavelengths from the cable while the z coordinate is increased from zero to 40 wavelengths. For these calculations, the cable parameters are: a = 1.25 mm, b = 1.0 cm, $c - b$ = 1.25 mm, δ = 1 mm, ϵ_r/ϵ_0 = 1.5, and ϵ_r'/ϵ_0 = 2.5. For comparison, results are also shown for the case where the cable has been replaced by a transmitting dipole which is centered at the origin and z directed. The expressions used for the dipole–dipole coupling are given in the Appendix. Note that the coupling loss for the cable source is much lower than that for a dipole source for large z. This is in agreement with the results of Delogne and Liegeois [7] and our previous calculations [3] that show the cable radiation is concentrated mainly within 10 degrees of the z axis. The coupling losses shown for 5 MHz in Fig. 4 are probably too optimistic since a matched load is very difficult to obtain for such a low dipole resistance (0.055 Ω) and a large dipole reactance.

CONCLUDING REMARKS

Using an idealized model, we have computed coupling loss between a cable with a gap and a dipole for the special case where the dipole is in the far field. If the dipole is in the near field, coupling loss can still be calculated by the induced EMF method, but the complicated integral expressions for the electric field in (4) are required. Also, the optimum orientation of the dipole will, in general, be something other than the θ-orientation which is optimum in the far field.

Since CAGC and the related leaky feeder communication systems [8], [9] are sometimes employed in confined regions such as mine tunnels, an extension of the above treatment is needed. Using a model of an idealized circular tunnel, the relevant boundary value analysis has already been carried out [10] but further numerical work is needed to obtain the appropriate coupling losses. Also, we wish to combine the results to permit a systems evaluation of a point-to-point communication via two dipole antennas in the vicinity of the coax with a specified number of gaps in the shield. Another important extension is to consider the effect of locating the coax just above an imperfectly conducting ground. This is a configuration that is relevant to the study of the possible interference between a CATV system and aircraft navigation signals [11].

APPENDIX—COUPLING BETWEEN DIPOLES

The far field of a dipole of half-length H and feed current I_o which is oriented in the z direction is given by [5]

$$E_\theta = \frac{i\eta_o}{2\pi} \frac{I_o}{\sin (k_oH)} P(\theta) \frac{\exp(-ik_oR)}{R}$$

where

$$P(\theta) = \frac{\cos (k_oH \cos\theta) - \cos (k_oH)}{\sin\theta}. \tag{13}$$

Consequently, the mutual impedance with the receiving dipole shown in Fig. 2 is

$$Z_m = \frac{2E_\theta(1 - \cos (k_oH))}{I_o k_o \sin (k_oH)}. \tag{14}$$

Utilizing the same approach used earlier, the coupling loss is found to be

$$L_c = 4R_{in}^2 |Z_m|^2. \tag{15}$$

REFERENCES

[1] J. C. Beal, J. Josiak, S. F. Mahmoud, and V. Rawat, "Continuous access guided communication (CAGE) for ground transportation systems," *Proc. IEEE*, vol. 61, pp. 562–568, May 1973.

[2] D. R. Martin and Q. Davis, Eds., *Proc. Int. Colloq. Leaky Feeder Radio Communication Systems*, University of Guildford, Surrey, England, 1974.

[3] J. R. Wait and D. A. Hill, "On the electromagnetic fields of a dielectric coated coaxial cable with an interrupted shield," *IEEE Trans. Antennas Propagat.*, vol. AP-23, pp. 470–479, July 1975.

[4] ——, "Electromagnetic fields of a dielectric coated coaxial cable with an interrupted shield—Quasi-static calculations," submitted to *IEEE Trans. Antennas Propagat.*

[5] J. D. Kraus, *Antennas*. New York: McGraw-Hill, 1950.

[6] P. S. Carter, "Circuit relations in radiating systems and applications to antenna problems," *Proc. IRE*, vol. 20, pp. 1004–1041, 1932.

[7] P. Delogne and R. Liegeois, "Le rayonment d'une interruption du conducteur exterieur d'un cable coaxial," *Annales des Telecommunicatons*, vol. 26, no. 3 and 4, pp. 85–100, 1971.

[8] P. Delogne, L. Deryck and R. Liegeois, "Guided propagation of radio waves," in *Proc. Thru-the-Earth Electromagnetics Workshop*, Colorado School of Mines, Golden, pp. 49–53; available from the Nat. Tech. Inform. Service PB 231 154), 1973.

[9] D. J. R. Martin, "Very-high-frequency radio communication in mines and tunnels," Ph.D. dissertation, Dep. Electron. Elec. Eng., Univ. Surrey, Surrey, England, 1973.

[10] D. A. Hill and J. R. Wait, "Gap excitation of an axial conductor in a circular tunnel," *J. Appl. Phys.*, vol. 45, pp. 4774–4777, Nov. 1974.

[11] T. Harr, E. Haakinson, and S. Murahata, "Electromagnetic compatibility of simulated CATV signals and aircraft navigation receivers," Office Telecommunications, U. S. Dep. Commerce, Rep. OTR 74-27, 1974.

Radio Science, Volume 11, Number 4, pages 315-321, April 1976

Calculated transmission loss for a leaky feeder communication system in a circular tunnel

David A. Hill

Institute for Telecommunication Sciences, Office of Telecommunications, US Department of Commerce, Boulder, Colorado 80302

James R. Wait[1]

Cooperative Institute for Research in Environmental Sciences, National Oceanic and Atmospheric Administration, Environmental Research Laboratories, Boulder, Colorado 80302

(Received October 26, 1975; revised November 15, 1975.)

The transmission loss for a leaky coaxial cable communication system in a circular tunnel is calculated for an idealized model. The transmitting and receiving antennas are electric dipoles that may be located anywhere within the tunnel. For typical cable parameters, the optimum frequency is found to be in the range from 2 to 10 MHz. Calculations reveal that the use of a sparse braid and a high velocity cable will strongly improve the cable-dipole coupling with only a small penalty of a higher attenuation rate.

INTRODUCTION

The leaky feeder technique [*Beal et al.*, 1973; *Cree*, 1975] is now being developed and exploited for communication in mine tunnels [*Martin*, 1975]. In this method, first described by *Monk and Winbigler* [1956], the signals are guided by some type of transmission line such as a coaxial cable [*Fontaine et al.*, 1973] or a twin-wire line [*Deryck*, 1975; *Wait and Hill*, 1974]. The energy is coupled into or out of the channel by antennas in the vicinity of the transmission line. The advantage of this technique, of course, is that we do not have to make electrical contact with the axial conductor such as used in the "line radio" method developed many years ago by *Jakosky and Zellers* [1924, 1925] and now used extensively. An extremely interesting experimental study of transmission in tunnels has been published by *Gillette and Gilmour* [1975] that seems to confirm some of the theoretical concepts [*Wait and Hill*, 1974; *Delogne*, 1975; *Mahmoud and Wait*, 1976] relating to the respective roles of the monofilar and the bifilar modes in tunnel structures.

We have previously derived a mode equation for an idealized braided coaxial cable within a circular tunnel, and we presented some numerical results for the attenuation rates of the dominant modes [*Wait and Hill*, 1975]. Here we determine the mutual impedance and the related transmission loss between a pair of dipoles located in such a tunnel. Actually, this total transmission loss is the sum of the dipole-to-cable coupling losses and the attenuation of the dominant propagation mode. In our work we follow others [*Fontaine et al.*, 1973; *Delogne*, 1975; *Slaughter*, 1975] and assume that the braided sheath or shield of the coaxial cable can be described adequately by a surface transfer impedance [*Dummer and Blackband*, 1961]. Also, we do not consider mode conversion effects due to the inevitable lateral variations of the tunnel cross sections and other irregularities.

MODAL EXCITATION

The geometry of the circular tunnel is shown in the cylindrical coordinate system (ρ, ϕ, z) in Figure 1. The air-filled tunnel of radius a_0 has permittivity ϵ_0, and the surrounding rock has conductivity σ_e and permittivity ϵ_e. The free-space permeability μ_0 is assumed everywhere. The braided coaxial cable is located at (ρ_0, ϕ_0), and the source dipole is located at $(\rho_a, \phi_a, 0)$.

We now determine the total current $I(z)$ induced on the cable by a source current of moment $\dot{P}$. Here we follow a procedure, based on the reciprocity principle, that was used by *Mahmoud* [1974] for a single-wire transmission line in a rectangular

[1]Consultant to Institute for Telecommunication Sciences, Office of Telecommunications.

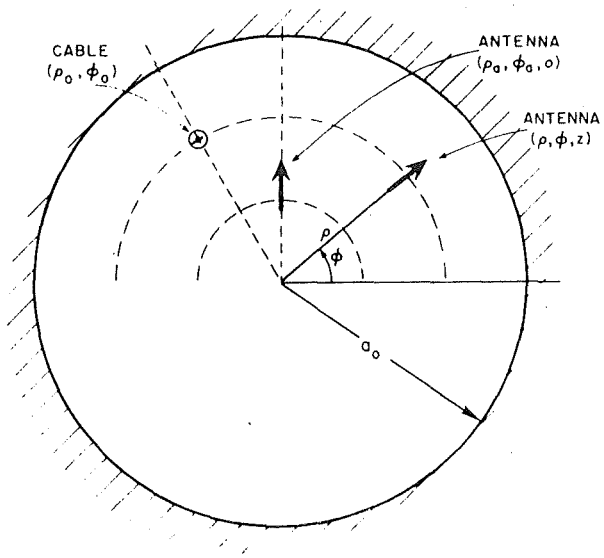

Fig. 1. Transmitting and receiving dipoles in a circular tunnel which contains a braided coaxial cable. (In the subsequent calculations we chose $\phi = \phi_a = \phi_0$.)

tunnel and by *Hill and Wait* [1974] for a two-wire line in a circular tunnel.

The source current density $\vec{J}_a$ is written

$$\vec{J}_a(\rho,\phi,z) = \vec{P}\delta(\rho-\rho_a)\,\delta(\phi-\phi_a)\,\delta(z)/\rho_a \tag{1}$$

where δ is the Dirac delta function and $\vec{P}$ is taken to be transverse to z. We now consider that for a given mode, the cable carries a total axial current I_0 that can, for an external observer, be localized at the center of the cable. Thus, the resulting current density is

$$J_z(\rho,\phi,z) = (I_0/\rho_0)\exp(-i\beta z)\,\delta(\rho-\rho_0)\,\delta(\phi-\phi_0) \tag{2}$$

where β is the propagation constant of the mode. Here and in what follows, we adopt an $\exp(i\omega t)$ time dependence. To be more specific, we can define I_0 as the line integral of the azimuthal magnetic field around the outer circumference of the coaxial cable.

The total electric field $\vec{e}(\rho,\phi,z)$ of the modal current can be written in terms of a z component e_z and a transverse component $\vec{e}_t$. Thus

$$\vec{e}(\rho,\phi,z) = \exp(-i\beta z)\,I_0[\vec{e}_t(\rho,\phi,\beta) + \hat{z}\,e_z(\rho,\phi,\beta)] \tag{3}$$

We now apply the reciprocity theorem [*Monteath*, 1973] to the two current densities $\vec{J}_a$ and J_z and their fields to yield:

$$\int_{-\infty}^{\infty}\int_0^{2\pi}\int_0^{\infty}\vec{J}_a(\rho,\phi,z)\cdot I_0\,\vec{e}_t(\rho,\phi,\beta)\cdot\exp(-i\beta z)\,\rho\,d\rho\,d\phi\,dz = \int_{-\infty}^{\infty}\int_0^{2\pi}\int_0^{\infty}J_z(\rho,\phi,z)\cdot E_{za}(\rho,\phi,z)\,\rho\,d\rho\,d\phi\,dz \tag{4}$$

where E_{za} is the z component of the field produced by the source dipole. When (1) and (2) are substituted into (4), the following is obtained:

$$\vec{P}\cdot\vec{e}_t(\rho_a,\phi_a,\beta) = \int_{-\infty}^{\infty}E_{za}(\rho_0,\phi_0,z)\exp(-i\beta z)\,dz = E'_{za}(\rho_0,\phi_0,\beta) \tag{5}$$

Each Fourier component $I'(\beta)$ of the cable current $I(z)$ must satisfy the following impedance boundary condition at the edge of the cable ($\rho = \rho_0 + c$, $\phi = \phi_0$):

$$E'_{za}(\rho_0+c,\phi_0,\beta) + I'(\beta)\,e_z(\rho_0+c,\phi_0,\beta) = I'(\beta)\,Z(\beta) \tag{6}$$

where $Z(\beta)$ is the effective impedance per unit length of the cable looking radially inwards. Since $E'_z(\rho_0,\phi_0,\beta) \simeq E'_z(\rho_0+c,\phi_0,\beta)$, we can substitute (5) into (6) to obtain:

$$I'(\beta) = -\vec{P}\cdot\vec{e}_t(\rho_a,\phi_a,\beta)/A(\beta) \tag{7}$$

where $A(\beta) = e_z(\rho_0+c,\phi_0,\beta) - Z(\beta)$.

The total cable current $I(z)$ is

$$I(z) = \frac{1}{2\pi}\int_{-\infty}^{\infty}I'(\beta)\exp(i\beta z)\,d\beta \tag{8}$$

By deforming the integration contour in the complex β plane, (8) can be converted to the following residue series:

$$I(z) = -i\sum_p\frac{\vec{P}\cdot\vec{e}_t(\rho_a,\phi_a,\beta_p)\exp(-i\beta_p|z|)}{[dA(\beta)/d\beta]|_{\beta=\beta_p}} \tag{9}$$

where $\beta = \beta_p$ are the roots of the modal equation, $A(\beta) = 0$, and the heavily damped branch cut contribution can be neglected. $I(z)$, as given by (9), is actually valid for any axial conductor that can be characterized by a series impedance per unit length $Z(\beta)$.

The specific braided coaxial cable of interest here is modeled by: a center conductor of radius a and conductivity σ_w, insulation of outer radius b and permittivity ϵ, a metal braid of radius b that can be characterized by a transfer inductance per unit length L_T, a protective jacket of outer radius c and permittivity ϵ_c, and a thin lossy film of radius c that can be characterized by a conductivity-thickness product σd. The presence of such lossy films should be expected in realistic mine environments [*Rawat and Beal*, 1974]. The appropriate expression for $Z(\beta)$ for this structure has been derived previously for use in the solution of the mode equation [*Wait and Hill*, 1975]. For most cases of interest, the mode of lowest attenuation is the "bifilar" mode which carries most of its energy between the center conductor and the metal braid, but this mode also has "leakage" fields outside the cable. The propagation constant of this mode β_b is approximately that of the insulation, i.e., $\beta_b \sim \omega(\mu_0\epsilon)^{1/2}$.

The coaxial cable and the tunnel also support a monofilar mode which is characterized by a forward current in the cable and a return current in the rock wall. In addition, there are an infinite number of tunnel waveguide modes which are only weakly affected by the cable. However, for application to long-distance communication, we need retain only the bifilar mode in (9):

$$I(z) \simeq -i\frac{\vec{P}\cdot\vec{e}_t(\rho_a,\phi_a,\beta_b)\exp(-i\beta_b|z|)}{[dA(\beta)/d\beta]|_{\beta=\beta_b}} \tag{10}$$

MUTUAL IMPEDANCE

For large positive z, the transverse field external to the cable can be obtained from (3) and (10):

$$\vec{e}(\rho,\phi,z) \simeq -i\{\vec{P}\cdot\vec{e}_t(\rho_a,\phi_a,\beta_b)/[dA(\beta)/d\beta]|_{\beta=\beta_b}\} \cdot \vec{e}_t(\rho,\phi,\beta_b)\exp(-i\beta_b z) \tag{11}$$

For a transverse receiving dipole of effective length $\vec{l}_{re}$ located at (ρ,ϕ,z), the received voltage is

$$v_r = \vec{e}(\rho,\phi,z)\cdot\vec{l}_{re} \tag{12}$$

The dipole moment $\vec{P}$ can be written as the input current i_a times an effective length $\vec{l}_{ae}$:

$$\vec{P} = i_a\vec{l}_{ae} \tag{13}$$

The mutual impedance Z_m is defined as the ratio of received voltage to transmitter current, and is found to be:

$$Z_m = \{-i[\vec{l}_{ae}\cdot\vec{e}_t(\rho_a,\phi_a,\beta_b)][\vec{l}_{re}\cdot\vec{e}_t(\rho,\phi,\beta_b)] \div [dA(\beta)/d\beta]|_{\beta=\beta_b}\}\exp(-i\beta_b z) \tag{14}$$

The specific expression for $\vec{e}_t$ has been given previously [*Wait and Hill*, 1974]. For a thin transmitting dipole of physical length l_a, the magnitude of the effective length, assuming a sinusoidal current distribution, is given by

$$|\vec{l}_{ae}| = 2[1-\cos(k_0 l_a/2)]/k_0\sin(k_0 l_a/2) \tag{15}$$

where $k_0 = \omega(\mu_0\epsilon_0)^{1/2}$. A similar expression can be used for the receiving dipole.

To illustrate some quantitative features of Z_m, we consider a special example. The receiving and transmitting dipoles are of the same length, location, and orientation. They are located on the same radial line as the cable (i.e., $\phi_a = \phi_0$), and they are oriented radially for maximum coupling. The assumed tunnel parameters are: $a_0 = 2$ m, ϵ_c/ϵ_0

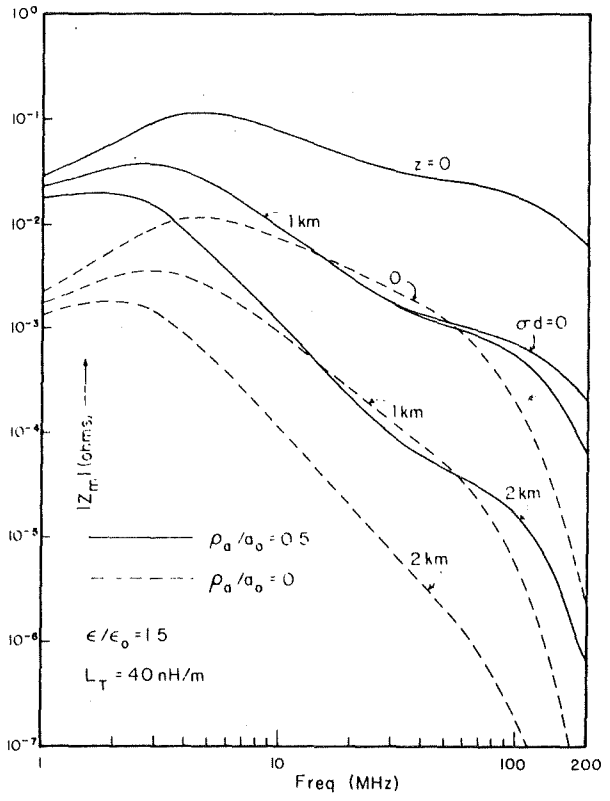

Fig. 2. Magnitude of mutual impedance for a large value of transfer inductance L_T. (Note that the cable location is fixed such that $\rho_0/a_0 = 0.9$ for this and subsequent figures.)

= 10, and $\sigma_e = 10^{-3}$ mhos/m. The cable is located at $\rho_0/a_0 = 0.9$, and the assumed cable parameters are: $a = 1.5$ mm, $b = 10$ mm, $c = 11.5$ mm, $\epsilon/\epsilon_0 = 1.5$, $\epsilon_c/\epsilon_0 = 3$, $\sigma_w = 5.7 \times 10^7$ mhos/m, and $\sigma d = 10^{-3}$ mhos. The antenna length l_a is taken to be 0.75 m, and the frequency range covered is 1 to 200 MHz. Figures 2-5 illustrate the magnitude of the mutual impedance as a function of various parameters. Note that $|Z_m|$ is at least an order of magnitude less when the dipoles are located at the tunnel center ($\rho_a = 0$) as compared to a location closer to the cable ($\rho_a = 0.5$). Antenna separations on the order of 1 km are of interest, and results for $z = 0$ are shown only to illustrate the portion of Z_m which is due to coupling in and out of the cable. Note from the spreading of the curves that attenuation becomes quite large at the higher frequencies. The results in Figure 2 are for $L_T = 40$ nH/m which represents a very sparse braid such as that employed in the FONT cable [*Fontaine et al.*, 1973]. Also shown is one curve

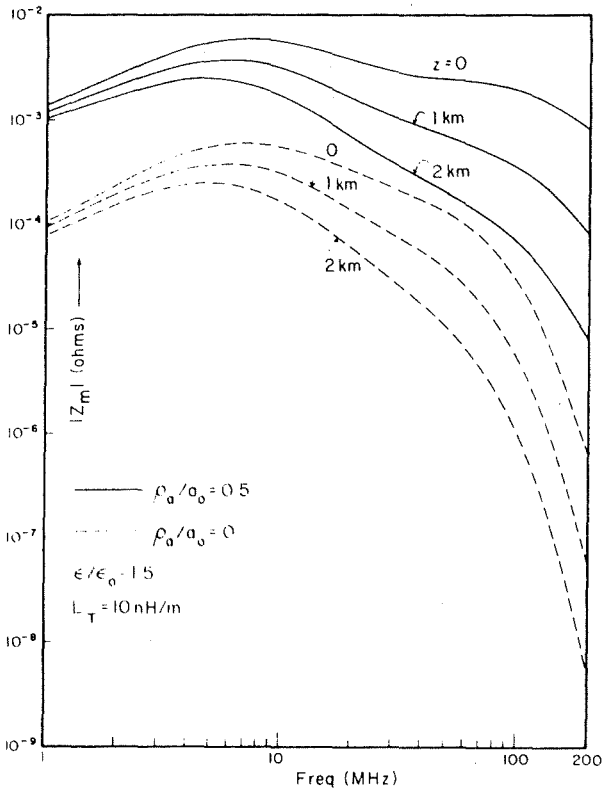

Fig. 3. Magnitude of mutual impedance for an intermediate value of transfer inductance L_T.

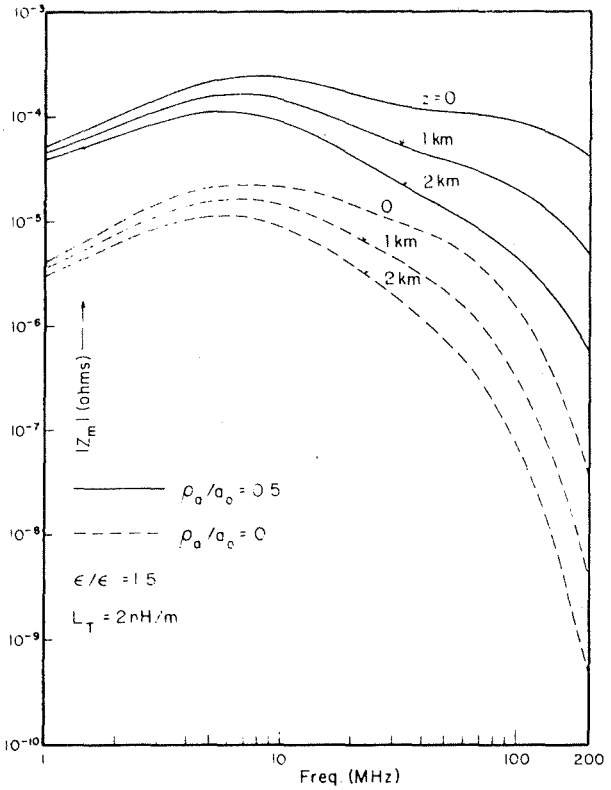

Fig. 4. Magnitude of mutual impedance for a small value of L_T.

where the lossy film is removed ($\sigma d = 0$). The lossy film increases the attenuation rate at the higher frequencies, but has no effect at the lower frequencies. Figure 3 shows results for a smaller value of L_T (10 nH/m) and, although the attenuation rate is lower, $|Z_m|$ is smaller due to reduced coupling. For Figure 4, $|Z_m|$ is reduced even further because of the very small value of L_T (2 nH/m). Figure 5 corresponds to Figure 2 except that the permittivity of the cable insulation has been increased ($\epsilon/\epsilon_0 = 2.5$). The attenuation rate is decreased slightly because of reduced leakage fields, but the dipole coupling is much weaker.

TRANSMISSION LOSS

If the input resistance of the transmitting antenna is R_a, then the input power is

$$P_a = |i_a|^2 R_a/2 \tag{16}$$

If the input resistance of the receiving antenna is R_r and the antenna is terminated in a matched load,

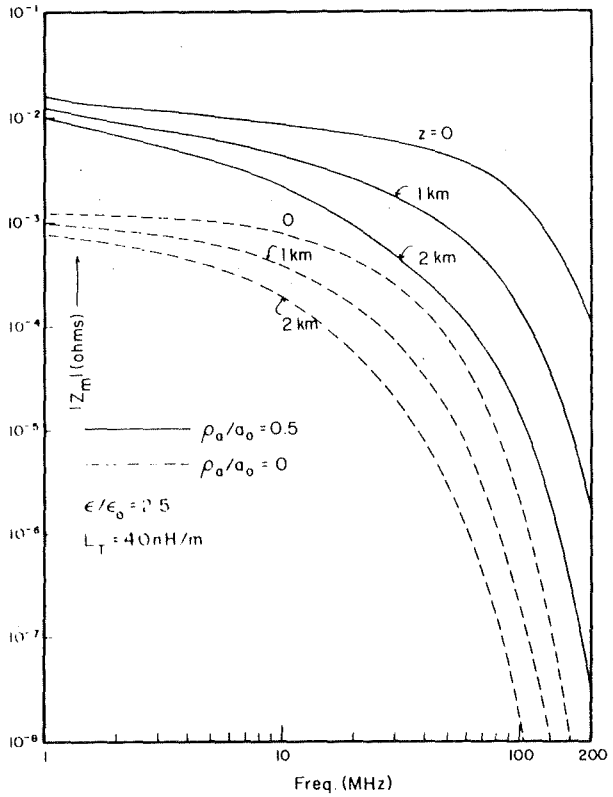

Fig. 5. Magnitude of mutual impedance for a larger value of insulation permittivity ϵ.

the received power is

$$P_r = |i_a|^2 |Z_m|^2/(8R_r) \tag{17}$$

Thus the transmission loss L (in dB) is

$$L = 10 \log_{10}\left(\frac{P_a}{P_r}\right) = 10 \log_{10}\left(\frac{4R_a R_r}{|Z_m|^2}\right) \tag{18}$$

For the higher frequencies where the spacing between the dipole and the tunnel wall is on the order of a wavelength, the input resistance can be approximated by the free-space radiation resistance [*Kraus*, 1950]. However, for low frequencies, the loss resistance due to near field losses becomes much larger than the radiation resistance. This loss resistance has been computed for dipoles near a half space [*Wait*, 1969; *Chang and Wait*, 1970] but no such results are available for a dipole in a circular tunnel environment. Qualitatively, the loss resistance is expected to reach a constant value as the frequency decreases rather than continuing to decrease in the manner of the radiation resistance.

In Table 1 we show the input resistance and resultant transmission loss for the same parameters used in Figure 3. To qualitatively include the effect of loss resistance, a lower limit of either 2 or 0.5 ohms has been placed on R_{in}. The absolute level

TABLE 1. Transmission loss (parameters are those of Figure 3).

Frequency (MHz)	R_{in} (ohms)	ρ_a/a_0	Transmission loss (dB) $Z = 0$	$Z = 1$ km	$Z = 2$ km
200.0	73.1	0.0	167.0	187.0	207.0
200.0	73.1	0.5	104.9	125.0	145.0
114.5	18.1	0.0	126.6	142.1	157.6
114.5	18.1	0.5	86.3	101.8	117.3
65.6	5.50	0.0	102.1	114.3	126.5
65.6	5.50	0.5	73.4	85.7	97.9
37.5	2.0*,1.76	0.0	86.9,85.8	96.6,95.5	106.3,105.2
37.5	2.0*,1.76	0.5	63.6,62.5	73.3,72.2	83.0,81.9
21.5	2.0*,0.57	0.0	82.4,71.6	90.1,79.2	97.8,86.9
21.5	2.0*,0.57	0.5	61.1,50.2	68.7,57.8	76.4,65.5
12.3	2.0*,0.5*	0.0	78.4,66.4	84.4,72.3	90.3,78.2
12.3	2.0*,0.5*	0.5	57.9,45.8	63.8,51.8	69.7,57.7
7.04	2.0*,0.5*	0.0	76.6,64.5	80.9,68.9	85.3,73.3
7.04	2.0*,0.5*	0.5	56.5,44.4	60.8,48.8	65.2,53.2
4.03	2.0*,0.5*	0.0	78.3,66.2	81.4,69.3	84.4,72.4
4.03	2.0*,0.5*	0.5	58.2,46.1	61.3,49.2	64.4,52.3
2.30	2.0*,0.5*	0.0	82.8,70.8	85.0,73.0	87.2,75.1
2.30	2.0*,0.5*	0.5	62.3,50.3	64.5,52.5	66.7,54.6
1.0	2.0*,0.5*	0.0	91.4,79.4	92.8,80.7	94.1,82.1
1.0	2.0*,0.5*	0.5	69.3,57.2	70.6,58.6	71.9,59.9

*assumed values

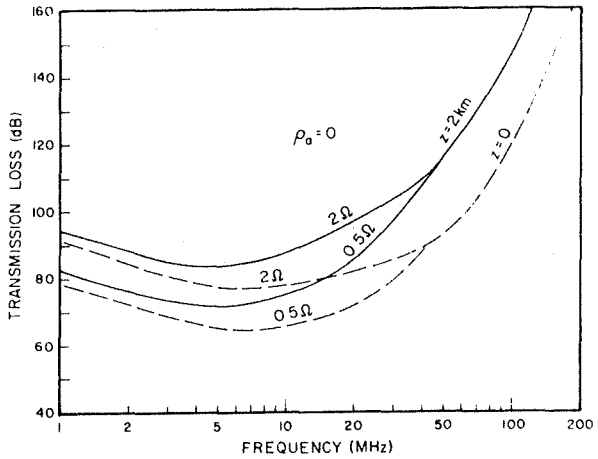

Fig. 6. Transmission loss as a function of frequency illustrating dependence on total range and antenna input resistances.

of path loss is strongly dependent on this value, but the frequency dependence is not.

Some of the results from Table 1 are illustrated graphically in Figures 6 and 7. A minimum transmission loss is noted at about 7 MHz. The results for $z = 0$ can be interpreted as the two-way coupling loss in and out of the cable, and the results are in reasonable agreement with the free-space calculations of *Rawat and Beal* [1974] using somewhat different assumptions. Also, there is a qualitative similarity with the recent approximate calculations of *Mahmoud and Wait* [1976] for a rectangular tunnel model.

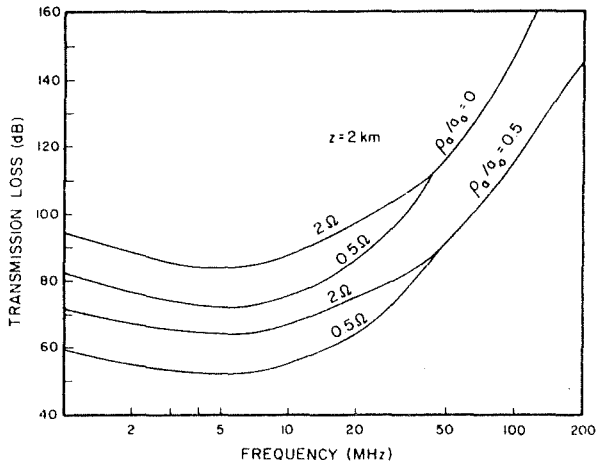

Fig. 7. Transmission loss as a function of frequency illustrating dependence of location of antennas relative to cable.

CONCLUDING REMARKS

The mutual impedance between a pair of dipole antennas in a circular tunnel has been computed for the case where the bifilar mode of the braided coaxial cable is the dominant mode. The coupling of the dipoles with the cable is improved by using a high transfer inductance [*Fontaine et al.*, 1973] and an insulation with a low dielectric constant. The large cable leakage fields produced by such a cable result in a slightly higher attenuation rate, but this is more than offset by the improvement in coupling loss. For typical parameters, an optimum frequency is observed in the range from 2 to 10 MHz.

In computing transmission loss, a better knowledge of the input resistance of dipoles in a tunnel environment would be desirable and could be obtained by theory or experiment. But conclusions regarding transmission loss are expected to follow those of mutual impedance as far as cable parameters and optimum frequency are concerned.

We should regard this analysis as the first step in a total systems study for communication using the leaky feeder system in mine tunnels and similar environments. The characterization of the braided cable is oversimplified and the neglected conversion between the propagation modes is not really justified in a fully realistic situation. Nevertheless, it is important to understand how a transmission may occur for the rather idealized model before attempting a study of all of the complicating influences such as longitudinal irregularities in the guiding structure.

REFERENCES

Beal, J. C., J. Josiak, S. F. Mahmoud, and V. Rawat (1973), Continuous-access guided communications (CAGC) for ground-transportation systems, *Proc. IEEE*, *61*(5), 562-568.

Chang, D. C., and J. R. Wait (1970), Theory of a vertical tubular antenna located above a conducting half-space, *IEEE Trans. Antennas Propagat.*, *AP-18*(2), 182-188.

Cree, D. J. (1975), Practical performance of radiating cables, *Radio Electron. Eng.*, *45*(5), 215-223.

Delogne, P. P. (1975), Electromagnetic theory of the leaky coaxial cable, *Radio Electron. Eng.*, *45*(5), 233-240.

Deryck, L. (1975), Control of mode conversions on bifilar lines in tunnels, *Radio Electron. Eng.*, *45*(5), 241-247.

Dummer, G. W. A., and W. T. Blackband (1961), *Wires and R. F. Cables*, pp. 112-115, Sir Isaac Pitman & Sons, London.

Fontaine, J., B. DeMoulin, P. DeGauque, and R. Gabillard (1973), Feasibility of radio communication in mine galleries by means of a coaxial cable having a high coupling impedance,

in *Proceedings of Thru-the-Earth Electromagnetics Workshop*, pp. 130-139, *Acc. No. PB 231 154*, National Technical Information Service, Springfield, VA 22151.

Gillette, M. R., and A. S. Gilmour (1975), Attenuation measurements in wet granite tunnels, *IEEE Trans. Electromagn. Compat.*, *EMC-7*(4), 201-206.

Hill, D. A., and J. R. Wait (1974), Excitation of monofilar and bifilar modes on a transmission line in a circular tunnel, *J. Appl. Phys.*, *45*(8), 3402-3406.

Jakosky, J. J., and D. H. Zellers (1924), Factors retarding transmission of radio signals underground and some further experiments and conclusions, Reports of investigations, *Serial No. 2651*, US Bureau of Mines, Washington, DC.

Jakosky, J. J., and D. H. Zellers (1925), Line radio and the effects of metallic conductors on underground communication, Reports of investigations, *Serial No. 2682*, US Bureau of Mines, Washington, DC.

Kraus, J. D. (1950), *Antennas*, pp. 254-262, McGraw-Hill, New York.

Mahmoud, S. F. (1974), Characteristics of EM guided waves for communication in coal mine tunnels, *IEEE Trans. Commun.*, *COM-22*(10), 1547-1554.

Mahmoud, S. F., and J. R. Wait (1976), Calculated channel characteristics of a braided coaxial cable in a mine tunnel, *IEEE Trans. Commun.*, *COM-24*(1), 82-87.

Martin, D. J. R. (1975), A general study of the leaky feeder principle, *Radio Electron. Eng.*, *45*(5), 205-214.

Monk, N., and H. S. Winbigler (1956), Communication with moving trains in tunnels, *IRE Trans. Vehicular Commun.*, *PGVC-7*, 21-28.

Monteath, G. D. (1973), *Applications of the Electromagnetic Reciprocity Principle*, Pergamon, New York.

Rawat, V., and J. C. Beal (1974), Leaky cables treated as open waveguides, in *Proc. Int. Colloquium Leaky-Feeder Communications*, Guildford, Surrey, England.

Slaughter, R. J. (1975), Field leakage and cross talk with special reference to radiating cables with tape screens, *Radio Electron. Eng.*, *45*(5), 248-252.

Wait, J. R. (1969), Impedance characteristics of electric dipoles over a conducting half-space, *Radio Sci.*, *4*(10), 971-975.

Wait, J. R., and D. A. Hill (1974), Coaxial and bifilar modes on a transmission line in a circular tunnel, *Appl. Phys.*, *4*(4), 307-312.

Wait, J. R., and D. A. Hill (1975), Propagation along a braided coaxial cable in a circular tunnel, *IEEE Trans. Microwave Theory Tech.*, *MTT-23*(5), 401-405.

CHAPTER 19

LOW-FREQUENCY RADIO TRANSMISSION IN A CIRCULAR TUNNEL CONTAINING A WIRE CONDUCTOR NEAR THE WALL

Indexing term: Guided electromagnetic-wave propagation

The general theory for transmission in a circular tunnel containing a thin axial conductor is employed to calculate the attenuation rate of the propagating mode. The remarkable property is that the attenuation rate is approximately proportional to frequency and it does not depend critically on the wall conductivity for typical conditions.

In previous papers,[1, 2] we have discussed the theory of electromagnetic-wave transmission in tunnels. Specific applications to high-frequency communication were described. Here we would like to report on some calculations that illustrate some of the remarkable features at low frequencies.

The model we choose is highly idealised. Specifically, the cross-section is circular with radius a, beyond which the rock is assumed to be homogeneous with conductivity σ_e and permittivity ε_e. To illustrate the effect of an axial wire within the tunnel, we locate a thin conductor of radius c and conductivity σ_w at a distance d from the tunnel wall. Of particular interest is the attenuation rate of the propagating mode in the tunnel, since this is an important factor in a communication system.

Some calculated results, based on our earlier paper,[1] are shown in Figs. 1 and 2 for the attenuation rate as a function of frequency for a tunnel radius $a = 2$ m. Three values of d are shown and two different sets of the electrical properties of the adjacent rock are chosen. For these calculations, the wire conductivity is taken to be infinite and the wire radius

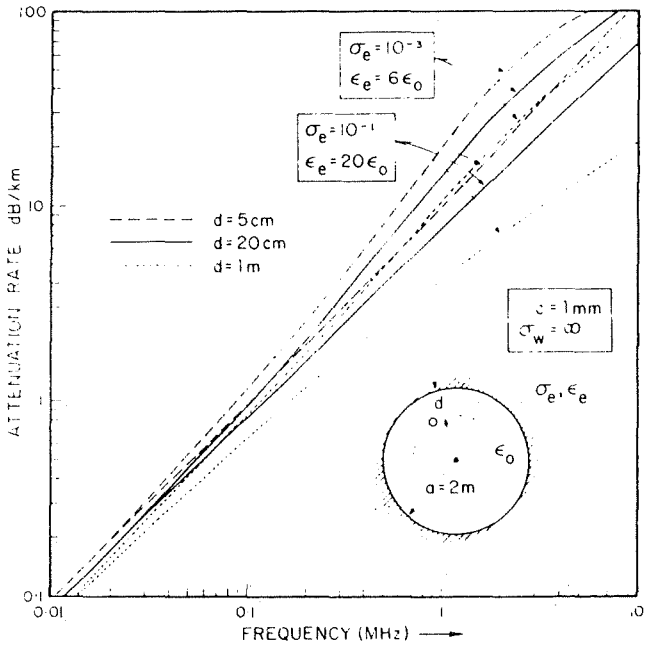

Fig. 1 *Attenuation rate function of frequency for model indicated by inset*

$c = 1$ mm. The results clearly show that the attenuation rate is almost a linear function of frequency. Also, the dependence on the rock conductivity is not great. In fact, the curves for $\sigma_e = 10^{-2}$ S/m would be between the curves for $\sigma_e = 10^{-1}$ and 10^{-3} S/m.

Some related calculations are shown in Fig. 2, where now the frequency is fixed at 50 kHz and the abscissa is the normalised distance of the wire conductor from the tunnel wall. Now the wire conductivity is $5{\cdot}7 \times 10^7$ S/m, corresponding to copper. Again the results show that the attenuation rate, while small, does increase significantly as the wire conductor

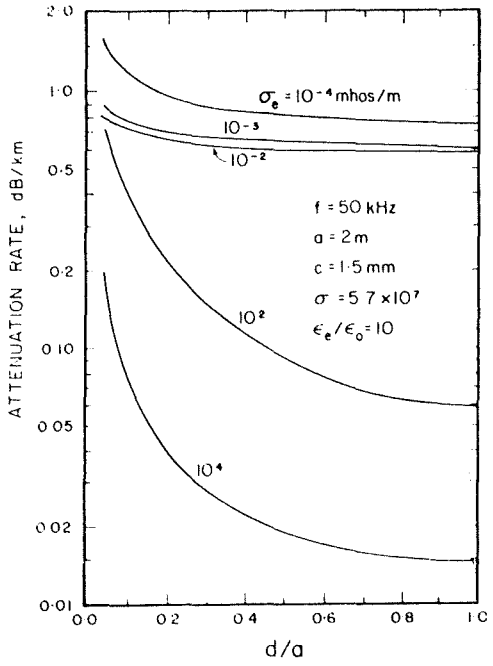

Fig. 2 *Attenuation rate as function of (normalised) distance of conductor to tunnel wall*

approaches the tunnel wall. We also see that the dependence on conductivity σ_e is quite weak in the range from 10^{-2} to 10^{-3} S/m, while, for rather unrealistic higher conductivity, the attenuation rate has decreased in a significant fashion.

The behaviour of the attenuation rate for the parameters indicated in Figs. 1 and 2 is really not too surprising. For the very high wall conductivities, we have the classical skin effect that is familiar at microwave in metal-walled guides. Then the attenuation rate is varying with frequency f approximately as $(f/\sigma_e)^{\frac{1}{2}}$. For more realistic rock conductivities, however, the distance d is becoming small compared with the skin depth in the rock. Then we find the low-frequency attenuation rate is, to within first order, independent of rock conductivity, but proportional to frequency. This is consistent with the known behaviour of a linear wire at low height over the surface of the earth at very low frequencies.[3, 4]

J. R. WAIT
D. A. HILL

Institute for Telecommunication Sciences
Office of Telecommunications
US Department of Commerce
Boulder, Colo. 80302, USA

1st June 1976

References

1 WAIT, J. R., and HILL, D. A.: 'Guided electromagnetic waves along an axial conductor in a circular tunnel', *IEEE Trans.*, 1974, **AP-22**, pp. 627–630
2 WAIT, J. R., and HILL, D. A.: 'Coaxial and bifilar modes on a transmission line in a circular tunnel', *Appl. Phys.*, 1974, **4**, pp. 307–312
3 WAIT, J. R.: 'On the impedance of long wire suspended over the ground', *Proc. Inst. Radio Eng.*, 1961, **49**, p. 1576
4 CHANG, D. C., and WAIT, J. R.: 'Extremely low frequency (ELF) propagation along a horizontal wire located above or buried in the earth', *IEEE Trans.*, (special issue, edited by WAIT J. R.), 1974, **COM-22**, pp. 421–426

Electronics Letters, Vol. 12, No. 13, pp. 346-347, 24th June 1976

Radio Science, Volume 10, Number 6, pages 625-632, June 1975

Theory of the transmission of electromagnetic waves down a mine hoist

James R. Wait

Cooperative Institute for Research in Environmental Sciences, University of Colorado, Boulder, Colorado 80302

David A. Hill

Institute for Telecommunication Sciences, Office of Telecommunications, US Department of Commerce, Boulder, Colorado 80302

(Received February 10, 1975.)

Using an idealized coaxial model, we consider the transmission, in the frequency range from 20 to 1000 kHz, down a mine hoist shaft from a symmetric source at the surface. The shaft is circular in cross section and the metal hoist cable is represented by a concentric conductor. To facilitate the analysis, the source is idealized as a voltage-excited annular slot in a circular ground plane that is located in the air-earth interface. The earth itself is taken to be a homogeneous conducting half space. Using a modal type analysis, the total power supplied to the annular slot is calculated as the sum of the power delivered to the lower half space, the power dissipated at the air-earth interface and the power radiated into the atmosphere. Using these results, the relative power transmitted down the shaft to a specified depth is estimated. The resulting transmission efficiency is found to be almost completely dependent on the attenuation characteristics of the dominant TEM mode in the shaft.

INTRODUCTION

There is a need to transmit information from the earth's surface down a mine hoist shaft. In most cases, such shafts can be roughly represented as a cylindrical bore with a vertical axis. The metal hoist cable is then idealized as a circular metal conductor located on the axis of the shaft. A similar model of the shaft was considered by *Emslie and Lagace* [1974] who demonstrated the feasibility of this type of mine communication.

It is our purpose to analyze the electromagnetic wave transmission down such a shaft. The transmitter is to be located at the surface and the power transmitted downward is to be intercepted at some distance down the shaft. In this particular analysis, we do not consider any specific form of receiving antenna, nor do we allow for the effects of reflection from the bottom of the shaft. Thus, strictly speaking, our analysis applies only to a shaft of infinite depth.

The modal analysis we employ is straightforward and the methods are similar to those we used in analyzing transmission in circular mine tunnels [*Wait and Hill*, 1974*a*, *b*]. The additional complication arises here from the method of excitation and the influence of the air-earth interface. In fact, because of the latter, we resort to some approximations.

FORMULATION

We consider the model depicted in Figure 1. A cylindrical shaft, of radius a with center conductor of radius c, extends downward indefinitely into the earth. The latter is homogeneous with conductivity σ and permittivity ϵ and an assumed free-space permeability μ_0.

We imagine that power is to be provided to an annular slot in a simulated ground plane of effective radius ρ_0. Ideally, of course, $\rho_0 \to \infty$. We are interested to know how much of this power crosses the area $c < \rho < a$ at $z = l$ in the shaft.

While the annular slot is conceptually simple, it may be better to think of a toroidal coil as a more feasible source at VLF. But the electromagnetic problem is essentially the same and thus we consider here the problem only in the context of an annular slot that is excited uniformly by a

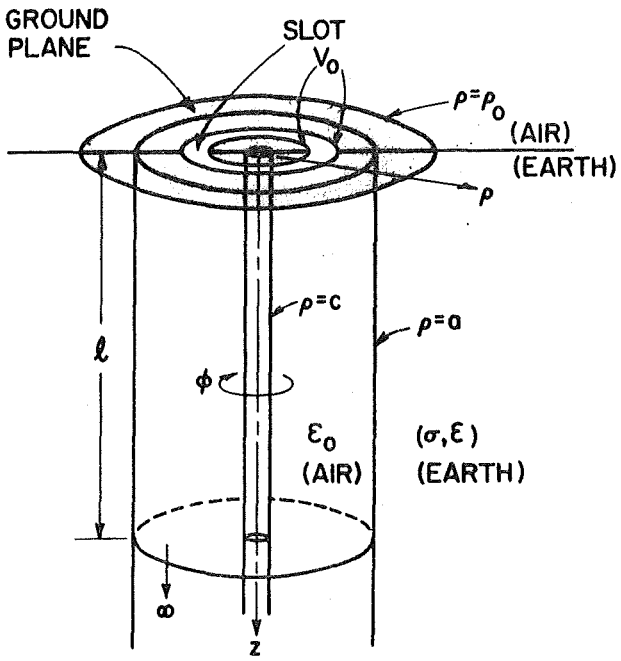

Fig. 1. Schematic view of the general configuration (in the analysis the annular slot of radius $\bar{\rho}$ is taken to have negligible width).

"voltage" V_0.

For the half space ($z > 0$), i.e., the earth, we can say that $E_\rho(z = 0) = f(\rho)$ is a prescribed function. For example, if the slot at $\rho = \bar{\rho}$ is of negligible width, then

$$f(\rho) = V_0\,\delta(\rho - \bar{\rho}) + e(\rho)u(\rho - \rho_0) \tag{1}$$

where $\delta(\rho - \bar{\rho})$ is a unit impulse function at $\rho = \bar{\rho}$ and $u(\rho - \rho_0)$ is a step function at $\rho = \rho_0$. Then, $e(\rho)$ is the tangential nonzero electric field on the earth's surface beyond the assumed perfectly conducting screen.

A fully rigorous solution of the posed problem is probably out of the question. However, if the distribution $f(\rho)$ over the significant range of ρ can be estimated, then the field at any other point in the earth or within the coaxial region can be predicted.

As indicated above, we have presupposed azimuthal symmetry. In terms of cylindrical coordinates (ρ,ϕ,z), derivatives involving $\partial/\partial\phi$ are zero. Thus, the nonvanishing field components are E_{0z}, $E_{0\rho}$, $H_{0\phi}$ for $c < \rho < a$ and E_z, E_ρ, H_ϕ for $\rho > a$.

The center conductor of radius c is to represent the metal hoist cable or "rope" as it is sometimes called. We can characterize this cable, insofar as external fields are concerned, by a series impedance Z_c in ohms per meter. Thus, the boundary condition at the cable is

$$E_{0z}\big|_{\rho=c} = I(z)Z_c \tag{2}$$

where $I(z) = 2\pi c H_{0\phi}\big|_{\rho=c}$ is the total axial current in the cable. Explicit expressions for Z_c are conveniently given by *Wait and Hill* [1974*b*].

MODAL SOLUTION

The fields for the present problem can be expressed in terms of a Hertz vector with a z component only. This is denoted Π_0 for $c < \rho < a$ and Π for $\rho > a$. Because of the impedance boundary condition imposed at $\rho = c$, it turns out that the fields everywhere in the region $\rho > c$ and $z > 0$ can be expressed in terms of a discrete set of modes. No continuous spectrum is needed. This leads us to write

$$\Pi = \sum_s A_s K_0(u_s\rho)\exp(-i\lambda_s z), \quad \text{for} \quad \rho > a \tag{3}$$

and

$$\Pi = \sum_s [B_s I_0(v_s\rho) + C_s K_0(v_s\rho)]\exp(-i\lambda_s z), \quad \text{for} \quad c < \rho < a \tag{4}$$

when I_0 and K_0 are modified Bessel functions, $u_s = (\lambda_s^2 + \gamma^2)^{1/2}$, $v_s = (\lambda^2 - k^2)^{1/2}$, $\gamma = [i\mu_0\omega \cdot (\sigma + i\epsilon\omega)]^{1/2}$, $k = (\epsilon_0\mu_0)^{1/2}\omega$, and λ_s are the eigenvalues of the problem. Physically, $i\lambda_s$ are the axial propagation constants for the coaxial structure that are yet to be determined. A_s, B_s, and C_s are coefficients, also yet to be determined.

On matching tangential fields at $\rho = a$, we obtain the pair

$$v_s^2[B_s I_0(v_s a) + C_s K_0(v_s a)] = u_s^2 A_s K_0(u_s a) \tag{5}$$

and

$$-i\epsilon_0\omega v_s[B_s I_1(v_s a) - C_s K_1(v_s a)] = (\sigma + i\epsilon\omega)u_s A_s K_1 \cdot (u_s a) \tag{6}$$

Solution of these leads to

$$B_s/C_s = -[K_0(\nu_s a)/I_0(\nu_s a)]\, R(\lambda_s) \tag{7}$$

where

$$R(\lambda_s) = [\eta_0 Y_s - (ik/\nu_s)\, K_1(\nu_s a)/K_0(\nu_s a)] / [\eta_0 Y_s + (ik/\nu_s)\, I_1(\nu_s a)/I_0(\nu_s a)] \tag{8}$$

and where

$$Y_s = [(\sigma + i\epsilon\omega)/u_s]\, K_1(u_s a)/K_0(u_s a)$$
$$\text{and} \quad \eta_0 = (\mu_0/\epsilon_0)^{1/2} \tag{9}$$

Furthermore,

$$A_s/C_s = (\nu_s^2/u_s^2)[K_0(\nu_s a)/K_0(u_s a)][1 - R(\lambda_s)] = \beta_s \tag{10}$$

Now the impedance boundary condition, given by (2), requires that

$$B_s/C_s = -[\nu_s K_0(\nu_s c) + 2\pi i\epsilon_0\omega c Z_c K_1(\nu_s c)] / [\nu_s I_0(\nu_s c) - 2\pi i\epsilon_0\omega c Z_c K_1(\nu_s c)] = \alpha_s \tag{11}$$

The equation to determine λ_s is then obtained by equating the right-hand sides of (7) and (11). Thus

$$\alpha_s + [K_0(\nu_s a)/I_0(\nu_s a)]\, R(\lambda_s) = 0 \tag{12}$$

is our mode equation.

ORTHOGONALITY CONSIDERATIONS AND THE NORMALIZING INTEGRAL

We now can write the following explicit forms for the radial electric field in the region $\rho > c$ and $z > 0$:

$$E_\rho = \sum_s C_s \beta_s i\lambda_s u_s K_1(u_s\rho) \exp(-i\lambda_s z) \tag{13}$$

and

$$E_{0\rho} = -\sum_s C_s i\lambda_s \nu_s [\alpha_s I_1(\nu_s\rho) - K_1(\nu_s\rho)] \cdot \exp(-i\lambda_s z) \tag{14}$$

In particular,

$$\left.\begin{matrix} E_\rho \\ E_{0\rho} \end{matrix}\right|_{z=0} = \sum_s C_s Z_s(\rho) \tag{15}$$

where

$$Z_s(\rho) = \begin{cases} i\beta_s\lambda_s u_s K_1(u_s\rho), & \text{for} \quad \rho > a \\ i\lambda_s \nu_s [K_1(\nu_s\rho) - \alpha_s I_1(\nu_s\rho)], & \text{for} \quad c < \rho < a \end{cases} \tag{16}$$

The function $Z_s(\rho)$ satisfies a form of the modified Bessel function of order one. Thus,

$$\rho^2 d^2 Z_s(\rho)/d\rho^2 + \rho\, dZ_s(\rho)/d\rho - [(w_s\rho)^2 + 1] \cdot Z_s(\rho) = 0 \tag{17}$$

where

$$w_s = \begin{cases} u_s, & \text{for} \quad \rho > a \\ \nu_s, & \text{for} \quad c < \rho < a \end{cases}$$

A similar equation applies to $Z_q(\rho)$ where q denotes another eigenvalue. From these it is easy to verify that

$$(\partial/\partial\rho)\{\rho[Z_q\, dZ_s/d\rho - Z_s\, dZ_q/d\rho]\} - \rho(w_s^2 - w_q^2) \cdot Z_s Z_q = 0 \tag{18}$$

Thus

$$\int_c^\infty \rho Z_s(\rho) Z_q(\rho) d\rho = -c[Z_q(\rho)\, \partial Z_s(\rho)/\partial\rho - Z_s(\rho) \cdot \partial Z_q(\rho)/\partial\rho]_{\rho=c}/(\nu_s^2 - \nu_q^2)$$

where we utilize the fact that $Z_s(\rho)$ vanishes exponentially as $\rho \to \infty$. We now confirm the orthogonality of the modes since

$$\int_c^\infty \rho Z_s(\rho) Z_q(\rho) d\rho = 0 \quad \text{if} \quad s \neq q \tag{20}$$

in view of the impedance boundary condition at the cable that is equivalent to

$$(\partial Z_s/\partial\rho)\big|_{\rho=c} = \Gamma\, Z_s(c) \tag{21}$$

where Γ is a constant. In fact,

$$\Gamma = 2\pi c i\epsilon_0\omega Z_c - c^{-1} \tag{22}$$

which is independent of the eigenvalue for our assumed constant value of Z_c. The latter assumption is certainly well justified for a metallic conductor at these frequencies. Of some importance is the case when $s = q$. Then we are interested in the normalizing integral

$$N_s = \int_c^\infty \rho[Z_s(\rho)]^2 d\rho \tag{23}$$

This can be treated as the limiting form of (19) as $q \to s$. Thus

$$N_s = cZ_s(c)\{(\Gamma - \partial/\partial\rho)[\partial/\partial\nu_q\, Z_q(\rho)]_s\}_{\rho=c}(2\nu_s)^{-1} \tag{24}$$

As indicated, the differentiation with respect to ν_q is carried out before setting $\nu_q = \nu_s$. Then the operation $\Gamma - \partial/\partial\rho$ is performed before setting $\rho = c$.

A direct approach to evaluate N_s is probably more feasible. Thus, using (16) we begin with

$$N_s = -\lambda_s^2[\,\nu_s^2 F_s + (\beta_s u_s)^2 G_s] \tag{25}$$

where

$$F_s = \int_c^a [K_1(\nu_s\rho) - \alpha_s I_1(\nu_s\rho)]^2 \rho\, d\rho$$

and

$$G_s = \int_a^\infty [K_1(u_s\rho)]^2 \rho\, d\rho$$

Now $K_1(x)$, or $I_1(x)$, satisfies the equation

$$x[K_1(bx)]^2 = -(\partial/\partial x)(((x^2/2)\{[K_1'(bx)]^2 - (1 + 1/b^2x^2)[K_1(bx)]^2\}))$$

which is readily verified. Thus,

$$F_s = -(a^2/2)[(Z_a')^2 - (1 + 1/\nu_s^2 a^2)Z_a^2] + (c^2/2) \cdot [(Z_c')^2 - (1 + 1/\nu_s^2 c^2)Z_c^2] \tag{26}$$

where

$$Z_a = K_1(\nu_s a) - \alpha_s I_1(\nu_s a)$$

$$Z_c = K_1(\nu_s c) - \alpha_s I_1(\nu_s c)$$

and

$$G_s = (a^2/2)\{[K_1'(u_s a)]^2 - (1 + 1/u_s^2 a^2) \cdot K_1^2(u_s a)\} \tag{27}$$

If $|\nu_s a| << 1$, we can write

$$N_s \simeq -\lambda_s^2[\ln(a/c) - (\nu_s^2/2)(a^2 - c^2)\alpha_s + (\beta_s u_s)^2 G_s]$$

FIELDS IN THE UPPER HALF SPACE

We now need to say something about the field in the air half space ($z < 0$). In general, here the fields can be derived from a Hertz potential $\hat{\Pi}$ given by

$$\hat{\Pi} = \int_0^\infty f(\lambda) e^{u_0 z} J_0(\lambda\rho) d\lambda \tag{28}$$

where $u_0 = (\lambda^2 - k^2)^{1/2}$. Then, for $z < 0$,

$$\hat{E}_\rho = \partial^2\hat{\Pi}/\partial\rho\partial z = -\int_0^\infty u_0 \lambda\, f(\lambda)\, J_1(\lambda\rho) d\lambda \tag{29}$$

Now if, for example, $\hat{E}_\rho = V_0\,\delta(\rho - \bar{\rho})$ at $z = 0$ for all values of ρ, we determine $f(\lambda)$ from

$$V_0\delta(\rho - \bar{\rho}) = -\int_0^\infty u_0 \lambda\, f(\lambda)\, e^{u_0 z} J_1(\lambda\rho) d\lambda \tag{30}$$

Using the Fourier Bessel transform pair [*Stratton*, 1941, p. 371]

$$G(\rho) = \int_0^\infty g(\lambda)\, J_1(\lambda\rho)\lambda d\lambda \tag{31}$$

$$g(\lambda) = \int_0^\infty G(\rho)\, J_1(\lambda\rho)\rho d\rho \tag{32}$$

it easily follows that

$$f(\lambda) = -(u_0\lambda)^{-1}\, V_0 J_1(\lambda\bar{\rho})\bar{\rho} \tag{33}$$

Thus

$$\hat{H}_\phi = i\epsilon_0\omega\, V_0\bar{\rho} \int_0^\infty (\lambda/u_0)\, J_1(\lambda\rho)\, J_1(\lambda\bar{\rho}) e^{u_0 z} d\lambda \tag{34}$$

for the region $z < 0$. If we now utilize the series

$$J_1(\lambda\bar{\rho}) = (1/2)[\lambda\bar{\rho} - (\lambda\bar{\rho})^3/8 + \ldots] \tag{35}$$

and the integral formula [*Stratton*, 1941, p. 576]

$$\int_0^\infty J_0(\lambda\rho)(\lambda/u_0)\, e^{u_0 z} d\lambda = (\rho^2 + z^2)^{-1/2} \exp[-ik \cdot (\rho^2 + z^2)^{1/2}] \tag{36}$$

it easily follows that

$$\hat{H}_\phi = [i\epsilon_0\omega V_0(\bar{\rho})^2/2]\{-\partial/\partial\rho + [(\bar{\rho})^2/8](\partial/\partial\rho) \cdot (k^2 + \partial^2/\partial z^2) + \ldots\}\, e^{-ikR}/R \tag{37}$$

where $R = (\rho^2 + z^2)^{1/2}$. In fact, the leading term will be adequate for most purposes; thus

$$\hat{H}_\phi \sim -[\epsilon_0\omega V_0(\bar{\rho})^2 k/2\rho](1 + 1/ik\rho)e^{-ik\rho} \tag{38}$$

for $z = 0$.

Now actually we are dealing with an imperfectly ground plane beyond $\rho > \rho_0$. But, to a good approximation, we can assume that the actual tangential magnetic field is not appreciably different. Also, we can employ the surface impedance boundary condition to make a good estimate for the tangential electric field $e(\rho)$ beyond the ground screen [*Wait*, 1969]. In fact, we say that

$$e(\rho) \simeq \eta \hat{H}_\phi \tag{39}$$

where $\hat{H}_\phi$ is given by (37) or (38) and $\eta = [i\mu_0\omega/(\sigma + i\epsilon\omega)]^{1/2}$. Then the power P^+ supplied to the ground by means of the upper half space is obtained from

$$P^+ \cong (1/2)\,\mathrm{Re}\,\eta \int_{\rho_0}^{\infty} (\hat{H}_\phi)^2\, 2\pi\rho d\rho \cong (\bar{\rho})(4\pi/8) \cdot [(\epsilon_0\omega)^2 V_0^2/\rho_0^2]\,\mathrm{Re}\,\eta \quad \text{if} \quad k\rho_0 << 1 \tag{40}$$

EVALUATION OF MODAL COEFFICIENTS C_s

We now determine the coefficients C_s by equating the right-hand sides of (1) and (15). That is

$$\sum_s C_s Z_s(\rho) = V_0\delta(\rho - \bar{\rho}) + e(\rho)u(\rho - \rho_0) \tag{41}$$

Using the orthogonality relation (20), it readily follows that

$$C_s = (V_0/N_s)\,\bar{\rho}\, Z_s(\bar{\rho}) + (1/N_s)\int_{\rho_0}^{\infty} e(\rho)Z_s(\rho)\rho\, d\rho$$
$$= (V_0/N_s)\, i\lambda_s \nu_s \bar{\rho}[K_1(\nu_s\bar{\rho}) - \alpha_s I_1(\nu_s\bar{\rho})]$$
$$- (V_0\eta/N_s)(i\beta_s\lambda u_s)[\epsilon_0\omega(\bar{\rho})^2 k/2]\int_{\rho_0}^{\infty} (1 + 1/ik\rho) \cdot e^{-ik\rho} K_1(u_s\rho)d\rho \tag{42}$$

While the integral above can be simplified, direct numerical evaluation is preferable, at least for the TEM mode. The integrand converges rapidly because $K_1(u_s\rho)$ behaves as $\rho^{-1/2}\exp(-u_s\rho)$ for large ρ.

Actually, for the higher-order modes, the integral in (42) can be approximated by

$$\int_{\rho_0}^{\infty} (1 + 1/ik\rho)e^{-ik\rho} K_1(u_s\rho)d\rho \simeq (\pi/2)^{1/2}\exp(-u_s\rho_0) / ik(u_s\rho_0)^{3/2} \tag{43}$$

This is valid, in an asymptotic sense, when $k\rho_0$ is small and $|u_s\rho|$ is large.

POWER RELATIONS

We now need to deduce the total power P^- supplied to the lower half space by the annular slot. Clearly, this is given by

$$P^- = \left[(1/2)\,\mathrm{Re}\int_c^a E_{0\rho} H_{0\phi}^*\, 2\pi\rho d\rho\right]_{z=0}$$
$$= \pi\bar{\rho} V_0 [\mathrm{Re}\, H_{0\phi}]_{\substack{\rho=\bar{\rho}\\ z=0}} \tag{44}$$
$$= \pi\bar{\rho} V_0 \mathrm{Re}\{i\epsilon_0\omega \sum_s \nu_s C_s [K_1(\nu_s\bar{\rho}) - \alpha_s I_1(\nu_s\bar{\rho})]\}$$

The total power supplied by the annular slot is thus $P = P^+ + P^- + P_r$ where P^+ is given adequately by (40) and P_r is the "radiated power" of the annular slot. A simple calculation indicates that the latter is

$$P_r = \lim_{R\to\infty} \eta_0\pi \int_0^{\pi/2} |\hat{H}_\phi|^2 R^2 \sin\theta\, d\theta = (\pi/6)\, V_0^2\, (\epsilon_0\omega)^2 \cdot (\bar{\rho})^4 \eta_0 k^2 \tag{45}$$

In most cases, P_r will be negligible compared with either P^+ or P^-.

The "desired power" P_l is what can be intercepted at some depth l in the shaft. This quantity is to be obtained from

$$P_l = (1/2)\int_c^a E_{0\rho} H_{0\phi}^*\, 2\pi\rho d\rho \tag{46}$$

Since l is sufficiently large that $I_m\lambda_s l >> 1$ for $s > 0$, we need only use the zero-order mode (i.e., $s = 0$) in computing P_l. In other words, the other modes are "cut off". Thus, the relevant field quantities are

$$E_{0\rho} \simeq i\lambda_0 \nu_0 C_0 [K_1(\nu_0\rho) - \alpha_0 I_1(\nu_0\rho)]e^{-i\lambda_0 z} \tag{47}$$

and

$$H_{0\phi} \simeq i\epsilon_0\omega\nu_0 C_0 [K_1(\nu_0\rho) - \alpha_0 I_1(\nu_0\rho)]e^{-i\lambda_0 z} \tag{48}$$

The corresponding power is

$$P_l \simeq (1/2)\,\mathrm{Re}\int_c^a [E_{0\rho} H_{0\phi}^*]_{z=l}\, 2\pi\rho\, d\rho$$
$$= \pi\epsilon_0\omega|\nu_0 C_0|^2\,\mathrm{Re}\,\lambda_0 \int_c^a |K_1(\nu_0\rho) - \alpha_0 I_1 \cdot (\nu_0\rho)|^2\, \rho\, d\rho \exp[-il(\lambda_0 - \lambda_0^*)] \tag{49}$$

Since $|\nu_0 a| << 1$ in cases of practical interest it

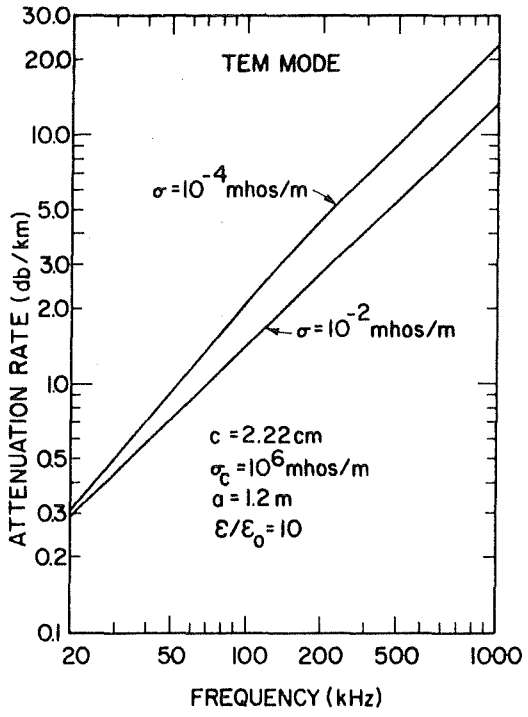

Fig. 2. Attenuation rate of the TEM mode.

follows that

$$P_l \simeq \pi\epsilon_0\omega|C_0|^2\,[\ln(a/c) - (a^2 - c^2)\mathrm{Re}(\alpha_0 v_0/2)] \cdot \mathrm{Re}\{\lambda_0 \exp[-i(\lambda_0 - \lambda_0^*)l]\} \tag{50}$$

SOME NUMERICAL RESULTS

Using the preceding formulation, some numerical results have been obtained for a number of specific cases using typical values of the relevant parameters. In Figure 2 we show the attenuation rate in db/km of the zero-order or TEM mode as a function of frequency in the cylindrical hoist shaft. The conductivity σ_c of the center conductor is taken to be 10^6 mhos/m and its radius c is 2.22 cm. The radius a of the shaft is 1.2 m. The surrounding homogeneous earth has a dielectric constant $\epsilon = 10\epsilon_0$, a conductivity σ that is either 10^{-2} or 10^{-4} mhos/m. The atmosphere and the air-filled shaft are assumed to have free-space permittivity ϵ_0 and magnetic permeability μ_0. The attenuation rates of the higher-order symmetric TM modes are shown in Figure 3 over the same frequency range and for the same conditions as in Figure 2. The attenuation rates of these evanescent type modes are virtually independent of the earth conductivity so, within graphical accuracy, the curves for $\sigma = 10^{-2}$ and 10^{-4} mhos/m are indistinguishable. In view of these results, it is not surprising that overall transmission efficiency (defined below) is dominated by the TEM mode attenuation characteristics.

An important design quantity is the transmission conductance G_0 of the annular slot. It is defined, in terms of the power delivered to the shaft, as follows:

$$P_l\big|_{l=0} = (1/2)\, V_0^2 G_0 \tag{51}$$

where V_0 is the applied voltage (i.e., the rms voltage is $V_0/2^{1/2}$. In Figure 4, G_0 is plotted as a function of frequency for the same parameters as above but now we must specify the radius ρ_0 of the ground screen and the mean radius $\bar{P}$ of the annular slot. We choose $\rho_0 = 2.0$ m and $\bar{\rho} = 0.6$ m but the results are only weakly dependent on these parameters. In Figure 4 we also show the curve when there

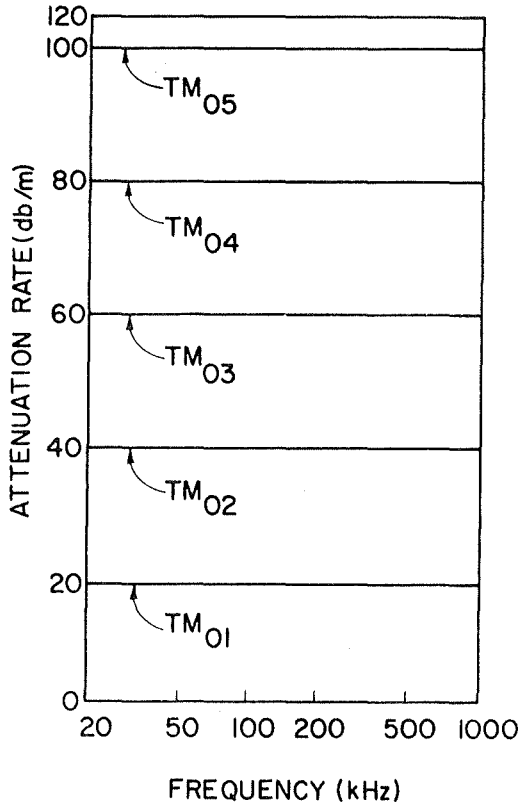

Fig. 3. Attenuation rate of the higher-order symmetric TM modes.

are no ohmic losses (i.e., $\sigma = \sigma_c = \infty$). In the latter case, it is easy to show that

$$G_0\big|_{\sigma=\sigma_c=\infty} \simeq 2\pi/\eta_0 \ln(a/c) \tag{52}$$

As indicated in Figure 4, the transmission conductance increases somewhat with frequency as a result of ohmic losses.

We now define an overall transmission efficiency as the ratio $P_l/(P^- + P^+ + P_r)$. This quantity, expressed as a percentage, is plotted in Figure 5 as a function of frequency for the same parameter range. As indicated, two values of the depth l (= 0.5 and 2.0 km) are selected. Not surprisingly, the transmission efficiency becomes poorer as the depth l increases. In fact, the efficiency is proportional roughly to the factor $\exp(-2\alpha l)$ where α is the attenuation rate of the TEM mode.

CONCLUDING REMARKS

The present analysis and sample calculations show that, for such a configuration, most of the transmitter power can be delivered to the shaft. The key factor seems to be the manner of impressing the source voltage between the center conductor (i.e., hoist rope) and the wall of the shaft. Most of the power is dissipated in ohmic losses in the surrounding earth. For this reason, the transmission efficiency decreases roughly in an exponential fashion with depth to the observer in the shaft.

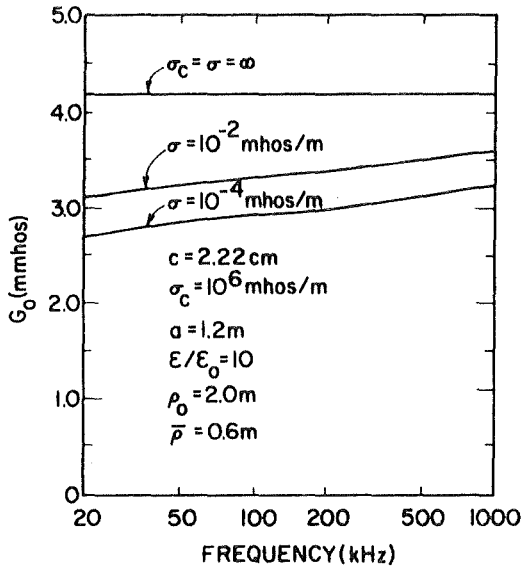

Fig. 4. Transmission conductance of the annular slot.

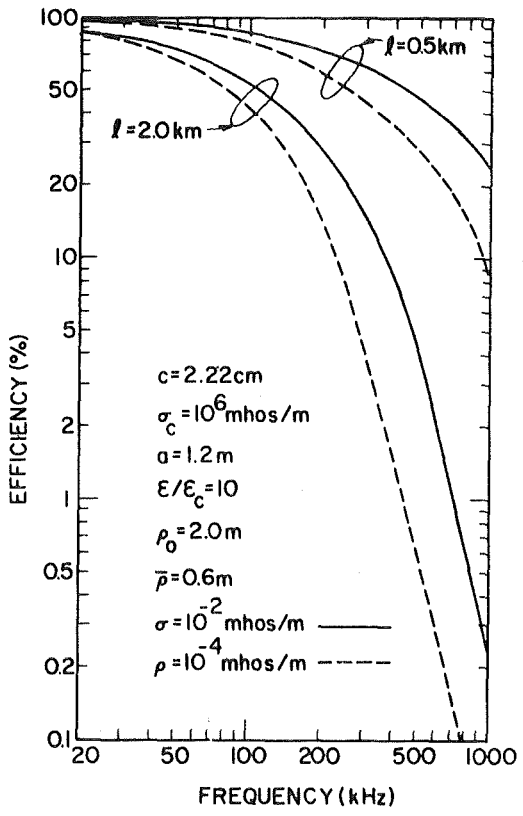

Fig. 5. Transmission efficiency of the system (this is a measure of the relative power that is transmitted down to a depth l in the shaft).

In our calculations we have neglected the continuous spectrum so this conclusion may be modified somewhat at the lowest frequencies and for low rock conductivity. However, in a practical scheme the upper few meters of the wall shaft would be lined with wire mesh so the neglected lateral wave, in the external conductor, would have a negligible effect. A recent calculation has shown this to be the case.

In an actual system we would use a toroidal-coil coupler rather than an annular slot. This should not change the overall features. On the other hand, the practical method of receiving the downward-propagated signal would be a major aspect of the overall capability to communicate. This subject is now occupying our attention.

REFERENCES

Emslie, A. G., and R. Lagace (1974), Hoist shaft mine communications, *Rep. to US Bureau of Mines*, sec. 5, A. D. Little.

Inc., Cambridge, Mass.

Stratton, J. A. (1941), *Electromagnetic Theory*, pp. 371, 576, McGraw-Hill, New York.

Wait, J. R. (1969), Characteristics of antennas over lossy earth, in *Antenna Theory, Part 2*, edited by R. E. Collin and F. J. Zucker, chap. 23, pp. 386-437, McGraw-Hill, New York.

Wait, J. R., and D. A. Hill (1974*a*), Coaxial and bifilar modes on a transmission line in a circular tunnel, *Appl. Phys.*, *4*(4), 307-312.

Wait, J. R., and D. A. Hill (1974*b*), Guided electromagnetic waves along an axial conductor in a circular tunnel, *IEEE Trans. Antennas Propagat.*, *AP-22*(4), 627-630.

Radio Science, Volume 11, Number 4, pages 263–265, April 1976

Note on the theory of transmission of electromagnetic waves in a coal seam

James R. Wait

Environmental Research Laboratories, National Oceanic and Atmospheric Administration, US Department of Commerce, Boulder, Colorado 80302

(Received October 27, 1975; revised November 13, 1975.)

A coal seam is idealized as a resistive slab bounded by more conductive rock. The source is taken to be a vertical electric dipole. It is shown that the dominant mode has relatively low attenuation.

Electromagnetic waves can propagate laterally via highly resistive layers in the earth [*Wait*, 1971]. In such cases, it is necessary to locate the source and observer within or near the waveguide. Such a waveguide could be formed by a coal seam bounded by well conducting rock. Our wave model is very simple and probably overly idealized but, in spite of this fact, the calculations are nontrivial.

The waveguide configurations and the cylindrical coordinate system (ρ,ϕ,z) we adopt are illustrated in Figure 1. We show a homogeneous slab of width $2h$, of conductivity σ, and of permittivity ϵ. This is bounded above and below by homogeneous and semi-infinite regions of conductivity σ_1 and permittivity ϵ_1. The source is a vertical electric dipole of moment $2Ids$ located at $z = 0$, which is the center of the slab. We first consider the vertical electric field E_z within the region $-h < z < h$. Formally, it is represented as a contour integral over a spectrum of plane waves. This, in turn, can be expressed as a sum of residues plus branch line integrals. For the present problem, the dominant contribution is the residue corresponding to the zero-order mode at the eigenvalue $C = C_0$ defined below. Thus, for our purposes, we write [*Wait*, 1970]:

$$E_z \simeq E_0 W \tag{1}$$

where

$$E_0 = -[i\mu_0\omega Ids/(2\pi\rho)] \tag{2}$$

is a reference field and W is an attenuation function. The latter is given by

$$W = (2\pi k\rho)^{1/2}(kh)^{-1}\exp(-i\pi/4)\Lambda \cdot \cos(kC_0 z)S_0^{3/2}\exp(-ik\rho S_0) \tag{3}$$

where

$$ik = [i\mu_0\omega(\sigma + i\epsilon\omega)]^{1/2}, \quad S_0 = (1 - C_0^2)^{1/2},$$

$$\Lambda = \left[1 + \frac{i\partial R/\partial C}{2khR}\right]^{-1}_{C=C_0}, \quad R = \frac{C - \Delta}{C + \Delta},$$

$$\left(\frac{i\mu_0\omega}{\sigma + i\epsilon\omega}\right)^{1/2}\Delta = \frac{(k^2S^2 - k_1^2)^{1/2}}{\sigma_1 + i\epsilon_1\omega}$$

$$= i(k_1^2 - k^2S^2)^{1/2}/(\sigma_1 + i\epsilon_1\omega)$$

$$ik_1 = [i\mu_0\omega(\sigma_1 + i\epsilon_1\omega)]^{1/2}$$

Here C_0 is a solution of the equation $R\exp(-i2khC) = 1$. In writing (1), (2), and (3) we assume that $|k\rho| \gg 1$.

The mode equation can be written in equivalent form as

$$u\tanh uh + pv = 0 \tag{4}$$

where $p = (\sigma + i\epsilon\omega)/(\sigma_1 + i\epsilon_1\omega)$, $u = ikC$, and $v = (k^2S^2 - k_1^2)^{1/2} = ik_1(1 - p^2S^2)^{1/2}$. The attenuation rate is then $-Imk S_0$ nepers per unit length in the ρ direction. In this notation we see that the excitation factor Λ can be calculated from

$$\Lambda = \left[1 - \frac{1}{2hR}\frac{\partial R}{\partial u}\right]^{-1}, \quad R = \frac{u - pv}{u + pv}$$

Using the mode equation in the form

$$R - R^{-1} = 2\sinh 2uh$$

we see that

$$\Lambda = \left[1 - \frac{k_1^2 - k^2}{v^2}\frac{\sinh 2uh}{2uh}\right]^{-1} \tag{5}$$

Before presenting typical numerical results for the attenuation rates, we will discuss some limiting

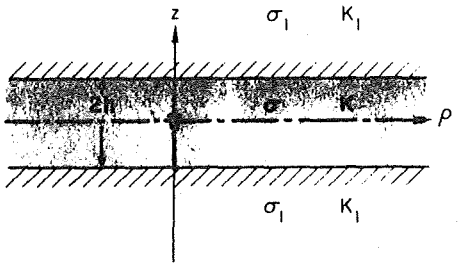

Fig. 1. Idealized coal seam of conductivity σ bounded by rock of conductivity σ_1. The relative permittivity values are taken to be $K_1 = \epsilon_1/\epsilon_0 = 15$ and $K = \epsilon/\epsilon_0 = 9$ throughout.

forms. If $|p| \to 0$, corresponding to perfectly conducting boundaries, it is evident from (4) that the zero-order mode corresponds to $u = 0$ or $S_0 = 1$. Thus the attenuation rate is the same as that for plane waves in a region of conductivity σ and permittivity ϵ. For this case, $\Lambda = 1/2$. The other limit results when the waveguide thickness h tends to 0, while all other parameters remain fixed. From (4) we see that this limit corresponds to $v = 0$, which means that $kS = k_1$. Thus, as is expected, the attenuation rate approaches that for an infinite medium of conductivity σ_1 and permittivity ϵ_1. Now, as is easily seen from (5), the excitation factor approaches 0. This result is not surprising, since we no longer have a waveguide but merely a conducting full-space. Some of these limiting cases were exhibited in some calculations reported earlier

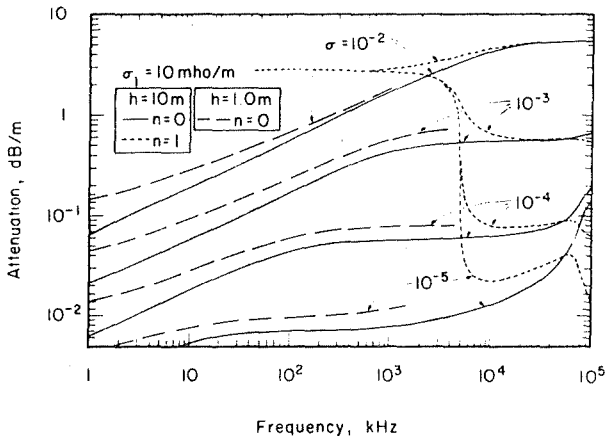

Fig. 2. Attenuation rates for dominant waveguide modes in a coal seam of thickness $2h$ for an optimistically high wall conductivity of $\sigma_1 = 10$ mhos/m.

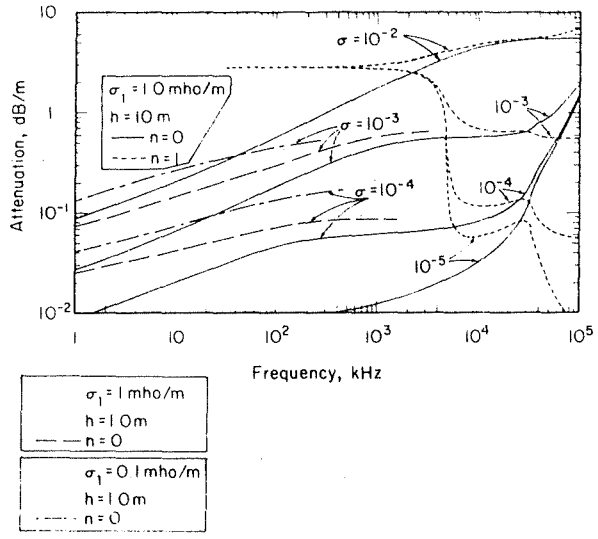

Fig. 3. Attenuation rates for dominant waveguide modes in a coal seam of thickness $2h$ for various wall conductivities.

[*Wait and Spies*, 1972] in the context of ultra-low frequency in a postulated waveguide in the crystalline basement of the earth's crust.

Using a numerical solution of (4), values of the attenuation rate $-Imk_0 S_0$ in decibels per meter have been obtained that are relevant to the coal seam situation. The frequency range extends from 1 to 10^5 kHz (i.e., 1000 Hz to 100 MHz). Some typical values of the parameters are chosen and they are indicated in a self-contained fashion in Figures 2 and 3. The curves apply to the important zero-order mode which is analogous to a TEM (Transverse Electromagnetic Mode) in a parallel plate waveguide. Such a mode, of course, has no cutoff as such and, for this reason, it has been proposed that it be the principal mechanism for low-loss transmission in stratified layers of the earth's crust. In Figure 2, however, we also show some results for the first order ($n = 1$) mode which for $h = 10$ m is "cut off" at frequencies below about 40 MHz, when the half-width h of the waveguide is equal to one-half of the effective wavelength. When $h = 1.0$ m this cutoff frequency would be approximately 400 MHz for the same condition.

Some important conclusions can be drawn from Figures 2 and 3. As expected, on the basis of previous work on the earth-crust waveguide, the

attenuation rate is critically dependent on the bulk conductivity σ of the waveguide (i.e., the coal seam itself). In fact, at the higher frequencies, there is almost a direct proportionality as one would predict on the basis of propagation in an unbounded medium when the loss tangent is small (i.e., when $\epsilon\omega/\sigma \ll 1$). Also, we can see that, as the waveguide half-width h is changed from 10 m to 1.0 m, the attenuation is increased consistently. In addition, if we decrease the conductivity σ_1 of the bounding rock, the attenuation also increases in a manner roughly proportional to $(\sigma_1)^{-1/2}$.

These results confirm recent unpublished experimental and calculated results (personal communications, R. L. Lagace of A. D. Little, Inc.) that attenuation rates in such configurations can be expected to be as low as 0.1 dB/m for frequencies around 100 kHz if the bulk conductivity of the seam is less than about 1.0 millimho/meter.

In this analysis we have assumed that the coal seam is excited by a vertical electric dipole at its center. The same $n = 0$ mode is excited for a vertical electric dipole anywhere within the seam. However, if the electric dipole were located outside the seam it should be located in a horizontal orientation so that the desired mode is launched in the end-fire directions. Similarly, a horizontal-axis loop will also excite the desired mode but a vertical-axis loop will not. The excitation problem for the analogous earth-crust waveguide has been discussed recently [*Wait*, 1975] and the results would seem to apply directly to the coal-seam problem.

Acknowledgments. I am very grateful to R. G. Geyer and R. J. Lytle for their useful comments and critical remarks on this subject.

REFERENCES

Wait, J. R. (1970), *Electromagnetic Waves in Stratified Media*, 2nd Ed., p. 551, Pergamon, New York.

Wait, J. R. (1971), Analytical investigations of electromagnetic wave propagation in the earth's crust, in *The Structure and Physical Properties of the Earth's Crust, Geophys. Monogr. Ser.*, Vol. 14, edited by J. G. Heacock, p. 315, American Geophysical Union, Washington, DC.

Wait, J. R. (1975), Note on excitation of the electromagnetic earth-crust waveguide, *IEEE Trans. Antennas Propagat.*, *AP-23*, 425–428.

Wait, J. R., and K. P. Spies (1972), Dipole excitation of ultralow-frequency electromagnetic waves in the earth crust waveguide, *J. Geophys. Res.*, 77, 7118–7120.

CHAPTER 22

INFLUENCE OF SPATIAL DISPERSION OF THE SHIELD TRANSFER IMPEDANCE OF A BRAIDED COAXIAL CABLE

J.R. WAIT and D.A. HILL

Institute for Telecommunication Sciences
Office of Telecommunications
U.S. Department of Commerce
Boulder, Colorado 80302

Abstract-The effect of the dependence of the braid transfer impedance on the propagation constant is discussed for a coaxial cable located in a circular tunnel.

In recent papers [1,2] in this journal, we have presented attenuation calculations for a braided coaxial cable located within a circular tunnel bounded by a homogeneous lossy medium. Following previous engineering practice, the metal braid was represented by a transfer impedance Z_T that was assumed not to vary with the propagation constant of the desired mode. In fact, for the calculations, we assumed that $Z_T = i\omega L_T$ where L_T was the transfer inductance expressed in nanohenries per meter. But this is a limitation in the calculations not in the theoretical formulation.

Recent theoretical work [3,4,5] on wire mesh screens suggest that the effective transfer impedance is better represented by the form

$$Z_T = A(\omega) + B(\omega)\Gamma^2 \tag{1}$$

where $A(\omega)$ and $B(\omega)$ are frequency dependent parameters that do not depend on the propagation constant Γ. In the specific case of the uncoated braided coaxial cable model used earlier, we would have

$$Z_T = i\omega L_T[1 + \Gamma^2/(k_o^2 + k^2)] \tag{2}$$

where k_o is the wave number for the region (i.e. air) adjacent to the cable and k is the wave number for the insulating dielectric on the inside of the shield. This particular form would apply if the weave or pitch angle ψ of the braid wires (angle subtended with the cable axis) is 45° and if the axial separation of the braid wires is small compared with a wavelength and with the radius of the shield. Of course, the formula, but not the form, for Z_T is modified if other factors are considered such as the influence of the jacket material and any external lossy coatings. Also, if the weave angle is different from 45°, we should replace the bracketed term in (2) by $[1 + (2\Gamma^2 \cos^2 \psi)/(k_o^2 + k^2)]$ according to an analysis by K.F. Casey [5].

The general mode equations [1,2] we have derived for the braided cable in the tunnel may still be used if Z_T is regarded to be Γ dependent. The iterative calculation is only slightly more complicated. However, it is useful to examine how much error is incurred by adopting an appropriate Γ-independent model for Z_T since this has been used frequently in the past. For the coaxial cable or bifilar mode, Γ is of the order of ik; thus we propose to use the approximation:

$$\begin{aligned} Z_T(\Gamma) \simeq Z_T(ik) &= i\omega L_T(1 - k^2/(k_o^2 + k^2)] \\ &= i\omega L_T k_o^2/(k_o^2 + k^2) \end{aligned} \tag{3}$$

The limiting case is obtained by setting $\Gamma = 0$ in (2). Then we recover the simple form $Z_T \simeq i\omega L_T$.

To illustrate the significance of the present results we plot the attenuation rate of the bifilar mode in dB per km for the three cases mentioned above in Figs. 1,2 and 3. Specifically the transfer impedance takes the respective forms $Z_T(\Gamma)$, $Z_T(ik)$ and $Z_T(0)$ as indicated on each figure.

The cable parameters, in terms of the earlier notation [1,2], are a_o (tunnel radius) = 2m, σ_e (earth conductivity) = 10^{-3} mhos/m, $\varepsilon_e/\varepsilon_o = 10$, a (inner conductor radius) = 1.5 mm, b (sheath radius) = 10 mm, $\varepsilon/\varepsilon_o$ (dielectric constant of insulator) = 1.5, and σ_w (conductivity of inner conductor) = 5.7×10^7 mhos/m. Also, as mentioned above, the influence of the jacket and/or lossy external layer is ignored here. This corresponds to setting c = b and $\sigma d = 0$ in the previous formulation [1,2]. As indicated in the figures, ρ_o (offset distance of cable from tunnel axis) is either zero or $0.9\ a_o = 1.8$ m. In Fig. 1, where the reference value of L_T is 40 nH/m, it is seen that the attenuation rates for $Z_T(\Gamma)$ and $Z_T(ik)$ are considerably lower than that for $Z_T(0)$. In Fig. 2, where $L_T = 10$ nH/m, the difference is somewhat reduced, while in Fig. 3 where $L_T = 2$nH/m, the difference is negligible. In all cases shown the difference between the curves for $Z_T(\Gamma)$ and $Z_T(ik)$ would seem to be insignificant.

Certainly from a practical standpoint the use of an effective Γ-independent value of the transfer impedance such as $Z_T(ik)$ would lead to a negligible error. But, of course, the use of $Z_T(0)$ as may be obtained from a static test measurement is liable to produce significant discrepancies. Thus, in interpreting the calculated data from previous attenuation calculations [1,2], one should identify the given sheath transfer impedance as an effective value for that mode [e.g. $Z_T(ik)$ for the bifilar mode and $Z_T(ik_o)$ for the monofilar mode].

Using the method discussed recently by the authors [6], the influence of the Γ dependence on Z_T on the excitation factor of the desired bifilar mode was investigated. The results showed that ratio of the excitation factor for the $Z_T(0)$ assumption was typically 6 dB

higher than for either the $Z_T(\Gamma)$ or $Z_T(ik)$ assumptions. This is not surprising since the cable is less leaky in the latter cases. To some extent, this compensates for the decreased attenuation rates insofar as the total system loss is concerned. The important point is that the excitation factors calculated for an effective $Z_T(ik)$ never differ more than 2 dB from the Γ-dependent form $Z_T(\Gamma)$ (even for the worst case where L_T = 40 nH/m).

Not surprisingly, the calculated transmission characteristics for such problems will depend on the many details of the assumed model. The large number of parameters, even in such an idealized configuration, makes it extremely difficult to form a comprehensive picture of the overall phenomena. Nevertheless, it appears highly worthwhile to develop engineering design criteria that can be used to estimate system performance. Work on this subject continues.

REFERENCES

[1] J.R. Wait and D.A. Hill, "Propagation along a braided coaxial cable in a circular tunnel", *IEEE Trans. Microwave Theory Tech.*, Vol. MTT-23, No. 5, pp. 401-405, May 1975.

[2] D.A. Hill and J.R. Wait, "Propagation along a braided coaxial cable located close to a tunnel wall", *IEEE Trans. Microwave Theory Tech.*, Vol. MTT-24, (in press), 1976.

[3] M.I. Astrakhan, "Reflecting and screening properties of plane wire grids", *Radio Engr. (USSR)*, Vol. 23, No. 1, pp. 76-83, Jan. 1968.

[4] D.A. Hill and J.R. Wait, "EM scattering of an arbitrary plane wave by a wire mesh with bonded junctions", *Can. J. Phys.*, Vol. 54, No. 4, pp. 353-361, 15 Feb. 1976.

[5] Private communications from K.F. Casey, Kansas State University, 1975.

[6] D.A. Hill and J.R. Wait, "Calculated transmission loss for a leaky feeder communication system in a circular tunnel", *Radio Sci.*, Vol. 11, No. 4, pp. 315-322, April 1976.

FIGURE CAPTIONS

Fig. 1 Attenuation rate of a braided coaxial cable in a circular tunnel for three different representations of the sheath transfer impedance. The reference transfer inductance L_T is 40 nano-henries per meter.

Fig. 2 Attenuation rate of a braided coaxial cable in a circular tunnel for three different representations of the sheath transfer impedance. The reference transfer inductance is L_T = 10 nH/m.

Fig. 3 Attenuation rate of a braided coaxial cable in a circular tunnel for three different representations of the sheath transfer impedance. The reference transfer inductance is L_T = 2 nH/m.

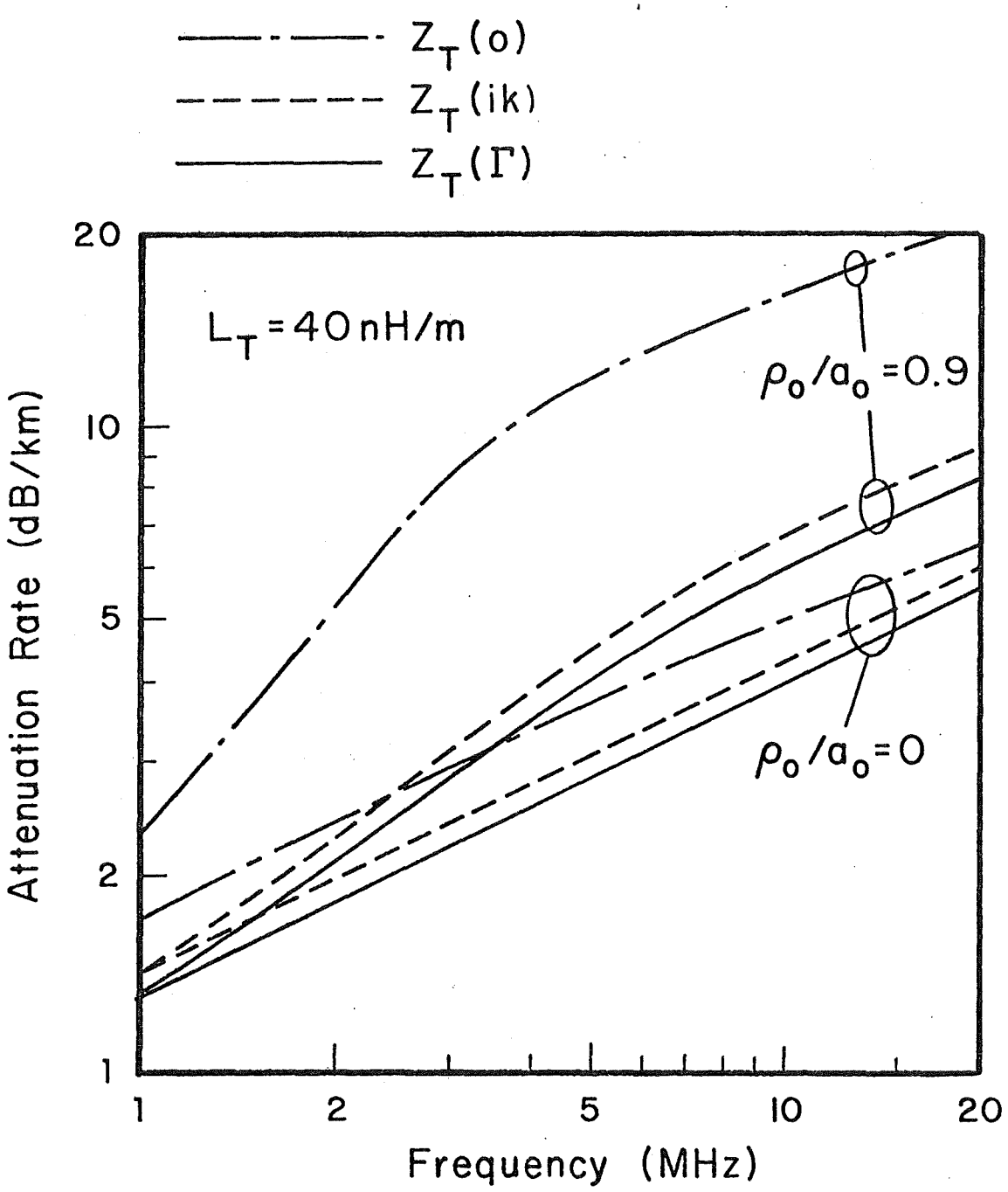
$Z_T(o)$
$Z_T(ik)$
$Z_T(\Gamma)$
$L_T = 40\,nH/m$
$\rho_o/a_o = 0.9$
$\rho_o/a_o = 0$
Attenuation Rate (dB/km)
Frequency (MHz)
20
10
5
2
1
1
2
5
10
20

Fig. 1

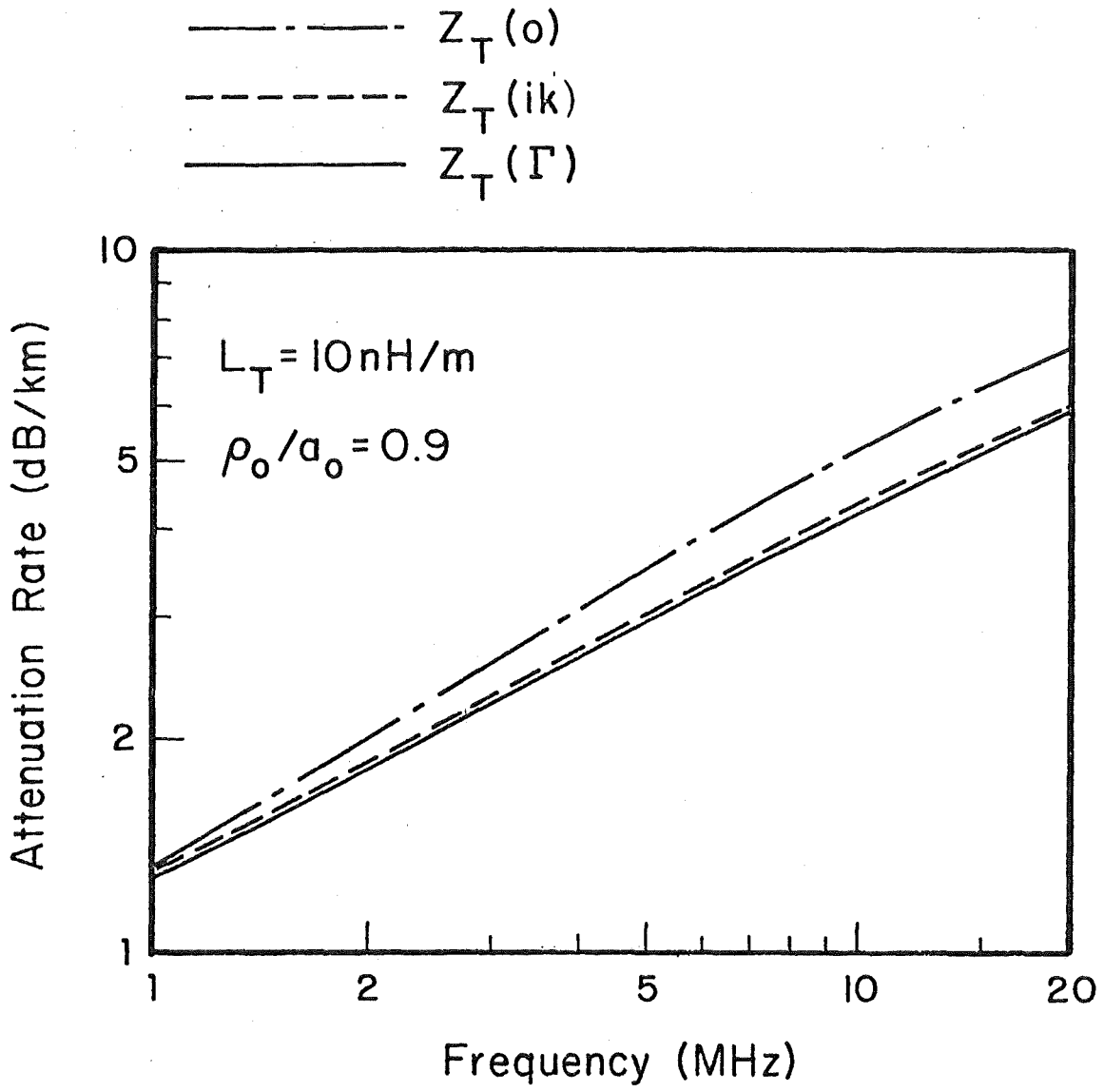
$Z_T(o)$
$Z_T(ik)$
$Z_T(\Gamma)$
$L_T = 10\,nH/m$
$\rho_o/a_o = 0.9$
Attenuation Rate (dB/km)
10
5
2
1
1
2
5
10
20
Frequency (MHz)

Fig. 2

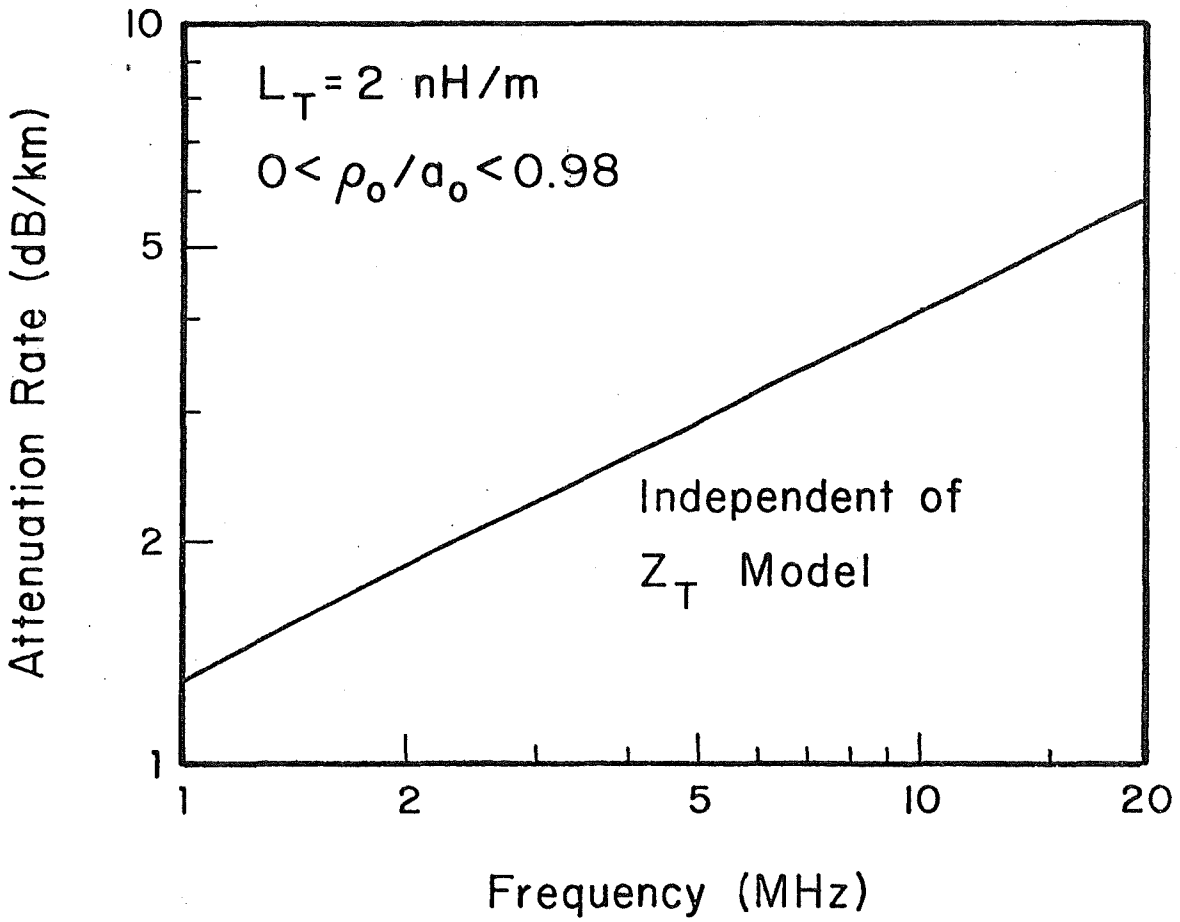
10
5
2
1
$L_T = 2$ nH/m
$0 < \rho_0/a_0 < 0.98$
Independent of
Z_T Model
Attenuation Rate (dB/km)
1
2
5
10
20
Frequency (MHz)

Fig. 3

CHAPTER 23

ANALYSIS OF RADIO FREQUENCY TRANSMISSION ALONG A TROLLEY WIRE IN A MINE TUNNEL

DAVID A. HILL and JAMES R. WAIT

Institute for Telecommunication Sciences
Office of Telecommunications
U.S. Department of Commerce
Boulder, Colorado 80302

Abstract - An idealized model of a trolley wire communication system in a tunnel is considered. To facilitate the analysis, the tunnel cross-section is taken to be semi-circular and the surrounding rock medium is homogeneous with a finite conductivity. The metallic rails or other conductors on the flat floor of the tunnel are represented by a plane metallic reflecting surface of infinite extent. The trolley wire and associated feeder line are assumed to be equivalent to a single cylindrical conductor that is parallel to the axis of the tunnel but located anywhere within the cross-section. The appropriate modal equation is then solved for the propagation constant of the dominant mode. It is shown that the attenuation rate increases significantly as the trolley wire approaches the tunnel wall. However, even when the trolley wire is within 20 cm (8 inches) of the wall, the attenuation rate at 200 kHz is still less than 2 dB per kilometer.

INTRODUCTION

It is common practice in communications in mines to utilize the trolley wire and its ground return as a radio frequency transmission line [1]. A potential problem in such a configuration is the influence of the finite conductivity of the rock adjacent to the tunnel or passageway in the mine. A similar situation can arise for communication lines in road and railway tunnels. For practical reasons, it is desirable to locate the trolley wire, that carries the DC or AC power, very close to the tunnel wall or rib. For power frequencies, this would not be of any consequence but for the radio frequencies used in the communication circuits, the eddy currents induced in the adjacent rock can lead to attenuation of the signal. To provide some insight to this problem, we hereby carry out an analysis of an idealized situation. Specifically, we consider a straight tunnel that has a semi-circular cross-section. In order to focus attention on the influence of the proximity of the trolley wire to the rock wall, we assume that the ground return circuit is ideal. Actually, this is not an inappropriate assumption when well bonded metal rails are located on the floor of the tunnel. In fact, to facilitate the analysis, we assume that the floor is a flat perfectly conducting surface. The trolley wire and any associated feeder line are assumed to be represented by a single axial cylindrical conductor with radius c. In the present model c is restricted to be much less than the tunnel radius a_o.

FORMULATION

The situation to be considered is shown in Fig. 1a. With respect to a cylindrical coordinate system, the wall of the tunnel for the semi-cylindrical model is defined by $\rho = a_o$ and $0 < \phi < \pi$. The perfectly

conducting floor is the surface $\phi = 0$ and π for $0 < \rho < \infty$. The trolley wire of conductivity σ_w is centered at $\rho = \rho_o$ and $\phi = \phi_o$. The homogeneous rock with conductivity σ_e and permittivity ε_e occupies the region $\rho > a_o$ for $0 < \phi < \pi$.

By some means we now inject an oscillating current of angular frequency ω on to the trolley wire. This current flows axially along the wire down the tunnel to a suitable termination or matched load. Under the condition that there are infinite impedance chokes to prevent current drain to locomotives and other intervening loads, the return current will return along the ground plane and to some extent, in the tunnel walls. We can therefore assume that the current between the transmitter (at say $z = 0$) and the terminal load has the form $I_o \exp(-\Gamma z)$ for the implied time factor $\exp(i\omega t)$. Of course, higher order modes will also be excited but they will be highly attenuated if the tunnel diameter $2a_o$ is small compared with the free space wavelength. The problem thus boils down to the determination of the propagation constant Γ of the propagation mode in the semi-circular tunnel that is effectively infinite in length. In particular, the real part of Γ so determined will indicate the attenuation of the propagating mode.

It now turns out that, because of the fortunate and non-accidental choice of the geometry, the problem as posed in Fig. 1a is entirely equivalent to the fully circular tunnel shown in Fig. 1b. The external region, now defined by $\rho > a_o$ for all ϕ, is homogeneous with conductivity σ_e and ε_e. In this case, however, we must locate an identical trolley wire at the proper image location. The current I_1 on this second wire located at $\rho = \rho_o$ and $\phi = -\phi_o$ must be equal to $-I_o$.

Thus the problem originally posed is transformed to the task of finding the bifilar mode for the symmetrically disposed wires contained in what is otherwise an empty tunnel in a homogeneous rock medium.

As a slight digression, we should point out that the circular tunnel configuration shown in Fig. 1b also will support a monofilar mode that corresponds to choosing $I_1 = +I_o$. In this case the return currents are now flowing entirely in the rock adjacent to the tunnel walls. The corresponding semi-circular tunnel mode would still look like Fig. 1a but the postulated perfect electric conductor on the floor would need to be a perfect magnetic conductor. Such a situation cannot be approximated in any sensible way so we will not pursue further the monofilar mode solution.

MODAL SOLUTION

A modal analysis to determine Γ for the bifilar mode on a transmission line in a circular tunnel has been obtained previously by the authors [2]. For the present symmetrical case shown in Fig. 1b that general mode equation may be factored and written in the form

$$A_o - A_1 = 0 \tag{1}$$

where

$$A_o = \frac{\gamma_o^2}{v^2} \frac{2\pi Z}{\eta_o} + K_o(vc) - S_o \tag{2}$$

and

$$A_1 = K_o(v\rho_d) - S_1 \tag{3}$$

where

$$\gamma_o^2 = -\varepsilon_o\mu_o\omega^2 = -(2\pi/\lambda_o)^2 = k_o^2 \ , \ \rho_d = 2\rho_o \sin\phi_o$$

$$v^2 = \gamma_o^2 - \Gamma^2 \ , \ \eta_o = (\mu_o/\varepsilon_o)^{\frac{1}{2}} = 120\pi,$$

$$Z = \frac{\eta_w}{2\pi c} \frac{I_o(\gamma_w c)}{I_1(\gamma_w c)} \ , \quad \gamma_w^2 = i\sigma_w\mu_o\omega \ , \quad \eta_w = i\mu_o\omega/\gamma_w$$

and where S_o and S_1 are factors that account for the presence of the tunnel walls. The latter two factors are given by

$$\begin{bmatrix} S_o \\ S_1 \end{bmatrix} = \sum_{m=-\infty}^{+\infty} R_m \frac{K_m(va_o)}{I_m(va_o)} I_m(v\rho_o) I_m\Big(v(\rho_o + c)\Big) \begin{bmatrix} 1 \\ \exp(-i2m\phi_o) \end{bmatrix} \tag{4}$$

where

$$R_m = \frac{(\gamma_o/v)K_m'(va_o)/K_m(va_o) + Y_m\eta_o + \delta_m\eta_o}{(\gamma_o/v)I_m'(va_o)/I_m(va_o) + Y_m\eta_o + \delta_m\eta_o} \tag{5}$$

and where

$$\delta_m\eta_o = \frac{(im\Gamma/a_o)^2[v^{-2} - u^{-2}]^2}{(\gamma_o/v)I_m'(va_o)/I_m(va_o) + (Z_m/\eta_o)} \tag{6}$$

$$Y_m = \frac{i\gamma_e^2}{u\mu_o\omega} \frac{K_m'(ua_o)}{K_m(ua_o)} \ , \ Z_m = -\frac{i\mu_o\omega}{u} \frac{K_m'(ua_o)}{K_m(ua_o)}$$

$$u = (\gamma_e^2 - \Gamma^2)^{\frac{1}{2}} \quad \text{and} \quad \gamma_e^2 = i\mu_o\omega(\sigma_e + i\varepsilon_e\omega) \ .$$

In the present analysis we have tacitly assumed that the magnetic permeability takes its free space value $\mu_o (= 4\pi \times 10^{-7}$ henries/m). However, it is a simple matter to account for the finite susceptibility of the axial conductor or trolley wire by using the appropriate value of the permeability μ_w in place of μ_o in the expression for the series

internal impedance Z given above.

The modal equation (1), while appearing to be rather complex, can be used to obtain numerical results without making any further approximations. For frequencies of the order of 100 kHz, the diameter of the tunnel is quite small compared with the free-space wavelength. In this case, $I_m(va_o)$ becomes very large and $K_m(va_o)$ becomes small. This causes numerical overflow problems so we find it convenient to use small argument approximations so that the relevant factor in (4) is given by

$$\frac{K_m(va_o)}{I_m(va_o)} I_m(v\rho_o) I_m\Big(v(\rho_o + c)\Big)$$

$$\simeq \begin{cases} [(\rho_o + c)\rho_o / a_o^2]^m (2m)^{-1}; & m \neq 0 \\ -\ell n(va_o) \qquad\qquad\quad ; & m = 0. \end{cases} \tag{7}$$

On the other hand, the modified Bessel functions of arguments $\gamma_w c$ and ua_o are not approximated.

LIMITING CASES

Before discussing some typical numerical results, we consider the limit of perfectly conducting walls of the tunnel. In this case it can be seen that $R_m \to 1$. Then, using the small argument approximation indicated by (7), it follows that

$$S_o \simeq -\ell n\ va_o + \sum_{m=1}^{\infty} \left[\frac{(\rho_o + c)\rho_o}{a_o^2}\right]^m \frac{1}{m} \tag{8}$$

and

$$S_1 \simeq -\ell n\ va_o + \sum_{m=1}^{\infty}\left[\frac{(\rho_o + c)\rho_o}{a_o^2}\right]^m \frac{1}{m}\cos 2m\phi_o \tag{9}$$

Using the well-known summation formula [3]

$$\sum_{1}^{\infty} b^m\ \frac{1}{m}\cos mx = -\frac{1}{2}\ell n[1 - 2b\ \cos x + b^2] \tag{10}$$

we see that

$$S_1 - S_o \simeq \ell n(1 - r) - (1/2)\ell n[1 - 2r\ \cos 2\phi_o + r^2] \tag{11}$$

where $r = \dfrac{(\rho_o + c)\rho_o}{a_o^2} \simeq \dfrac{\rho_o^2}{a_o^2}$. The relevant mode equation is now obtained from (11) by using the small argument approximations for the K_o functions. Thus

$$\ell n(\rho_d/c) + (\gamma_o/v^2)(2\pi Z/\eta_o) + S_1 - S_o = 0 \tag{12}$$

Making use of (11), this can be solved explicitly for Γ^2 to yield

$$\Gamma = \gamma_o\left[1 + \frac{2\pi Z}{i\mu_o\omega\ \ell n\ R}\right]^{1/2} \tag{13}$$

where

$$R = (\rho_d/c)(1 - r)[1 - 2r\ \cos 2\phi_o + r^2]^{-1/2}$$

Equation (13) can be written in the form $\Gamma = (\hat{Y}\hat{Z})^{1/2}$ where $\hat{Y} = 2\pi i\varepsilon_o\omega/\ell n\ R$ and $\hat{Z} = (i\mu_o\omega/2\pi)\ell n\ R + Z$. Here $\hat{Y}$ and $\hat{Z}$ are the series admittance and series impedance, respectively, per unit length. The corresponding characteristic impedance is then $(\hat{Z}/\hat{Y})^{1/2}$ or $\Gamma/\hat{Y}$. As a check we can let the tunnel radius become infinite (i.e. $a_o \to \infty$). Then R becomes ρ_d/c. The corresponding expressions for $\hat{Z}$ and $\hat{Y}$ are then the appropriate values for a single wire at a height $\rho_d/2$ over a perfect ground plane. Another check is let $\phi_o \to 90°$ whence

we obtain $R = (\rho_d/c)(1 - r)/(1 + r)$. Using these limiting forms and setting $Z = 0$, we recover the handbook values of the characteristic impedance for perfectly conducting configurations [4].

NUMERICAL RESULTS

We now present some numerical examples for the general configuration shown in Fig. 1a or its symmetrical equivalent in Fig. 1b. In view of the large number of parameters involved, we selected certain typical values only. For example, we choose $\phi_o = 45°$ for all cases and the wire radius c is taken to be 1.5 cm. The frequency range is taken to extend from 50 to 800 kHz since this encompasses frequencies used in trolley-wire communication systems. Also, we restrict attention to the attenuation rate (real part of Γ) of the propagating mode. This is expressed throughout in terms of decibels per kilometer*.

In the first example, in Fig. 2, the influence of the distance $a_o - \rho_o$ of the trolley wire from the tunnel wall is exhibited. For this case the tunnel radius is 2 meters and the rock conductivity $\sigma_e = 10^{-3}$ mhos/m. The relative permittivity $\varepsilon_e/\varepsilon_o$ of the rock is taken to be 10 and this value is adopted throughout the remaining examples. The wire conductivity σ_w is taken to be 5.7×10^7 mhos/m corresponding to copper but the effect of decreasing this to 5.7×10^6 is shown for the case $a_o - \rho_o = 20$ cm. As indicated in Fig. 2, the attenuation rate increases significantly as the trolley wire is moved toward the wall although the total attenuation for a 1 km path is still only 4.5 dB at 800 kHz even when $a_o - \rho_o = 20$ cm $\simeq$ 8 inches.

---

* Some values of the normalized phase factor $\mathrm{Im}(\Gamma)/k_o$ are appended in Tables 1, 2, and 3. The relatively small influence of changing the wire radius c, on both attenuation and phase, is shown in Table 3.

The influence of the tunnel radius for a fixed distance of the trolley wire to the wall is illustrated in Fig. 3. (The same parameters are used in Fig. 2). There appears to be only a very slight increase of attenuation when the tunnel radius is increased. This is probably due to the increasing fringing of the fields when the separation between the trolley wire and the image is increased.

If we keep the distance from the trolley wire to the ground plane fixed then, as indicated in Fig. 4, the attenuation rate increases as the tunnel radius is decreased. This again shows that the important parameter insofar as losses are concerned, is the distance of the trolley wire to the tunnel wall.

The dependence of the attenuation rate on the conductivity σ_e of the rock surrounding the tunnel is complicated. This is not surprising when one considers the various physical mechanisms that are responsible for the extraction of energy from the propagating mode. Some results to illustrate the dependence are shown in Figs. 5a and 5b for a wide range of values. For very small values of σ_e (e.g. 10^{-4} mhos/m), the loss is determined primarily by the leakage radiation into the rock that has the character of a low loss dielectric at 800 kHz. As the rock conductivity is increased, this leakage radiation is lowered because of an increased impedance mismatch at the air/tunnel boundary. There is a local minimum of the attenuation at σ_e approximately equal to 10^{-2} mhos/m which occurs because, for further increases of σ_e, the induced eddy currents become a dominant factor and the skin depth in the surrounding rock is still quite large. However, with further increases of σ_e, the attenuation rate is again decreased because the skin depth is now becoming much less than the tunnel diameter.

Finally, as indicated before, in the limit when $\sigma_e = \infty$, the only loss mechanism is due to the finite conductivity σ_w of the trolley wire. This is indicated in Fig. 5b. The corresponding limit when the rock conductivity is zero and the relative permittivity $\varepsilon_e/\varepsilon_o$ is unity, is also shown in Fig. 5b. As discussed earlier, this is the case when the corresponding two-wire transmission line is located in free space, or the equivalent situation of a single wire over a perfect ground plane.

CONCLUDING REMARKS

The tunnel model used above is admittedly very idealized. Nevertheless, the results do indicate that the influence of the finite conductivity of the adjacent rock is significant for frequencies from 50 to 800 kHz. Because we have represented the ground plane or floor of the tunnel as a perfect conductor, losses from the imperfect bonding of the rails are ignored. The influence of the leakage currents from the rails to the rock floor should be considered.

While this problem could be treated by a more sophisticated model, some insight is obtained by examining the results for a fully circular tunnel where the walls are uniformly conducting [5]. Essentially, this is the situation depicted in Fig. 1b where now we have only one conductor. Thus the return current must flow entirely in the adjacent rock. The mode equation is now $A_o = 0$ where A_o is defined by (2). We choose the same parameters as used in Figs. 5a and 5b except we set $a_o = 1.414$m so that the cross-sectional area of the tunnel is the same as before. Not surprisingly, the attenuation rates, as shown in Fig. 6, increases monitonically as the conductivity σ_e of the rock is decreased. Also, for σ_e in the range from 10^{-2} to 10^{-3} mhos/m, the

attenuation rate is an order of magnitude greater than with the semi-circular model.

If we again consider the special case $\sigma_e = \infty$, and use the small argument approximations for the Bessel functions, it is not difficult to show that $\Gamma \simeq (\hat{Y}_o \hat{Z}_o)^{\frac{1}{2}}$ where $\hat{Y}_o = 2\pi i \varepsilon_o \omega (\ell n\ R_o)^{-1}$ and $\hat{Z}_o = (i\mu_o \omega / 2\pi) \ell n\ R_o + Z$ where

$$R_o \cong \frac{a_o}{c}\left(1 - \frac{\rho_o^2}{a_o^2}\right)$$

This limiting case and one discussed earlier suggest that a meaningful definition for the characteristic impedance is $\Gamma/\hat{Y}$ for the semi-circular model and $\Gamma/\hat{Y}_o$ for the fully circular model. This assertion, however, becomes invalid for the low rock conductivity (e.g. $\sigma_2 < 10^{-2}$) and for the higher frequencies (e.g. $f > 200$ kHz).

There is an obvious need for some controlled experimental tests for transmission in tunnels with various types of conductors such as rails and pipes. An important step in this direction has just been described by Gillette and Gilmour [6] for frequencies somewhat higher than considered here. Also, the theoretical models should also be extended to account for the presence of insulated and un-insulated conductors buried in the adjacent rock.

ACKNOWLEDGEMENTS

We are grateful to Richard H. Spencer and Robert L. Lagace of the A.D. Little, Inc. for their useful comments that motivated this analysis.

REFERENCES

[1] J.N. Murphy and H.E. Parkinson, "Mine communications: Research and development in the U.S.A.", *Proceedings International Conference on "Radio: Tunnels and Mines"*, Vol. II, 1-5 April 1974, Liege (Belgium), pp. 42-64.

[2] J.R. Wait and D.A. Hill, "Coaxial and bifilar modes on a transmission line in a circular tunnel", *Appl. Phys.*, Vol. 4, pp. 307-312, 1974.

[3] A.D. Wheelon, *Tables of Summable Series and Integrals Involving Bessel Functions*. Holden-Day, Inc., San Francisco, 1968, pg. 44, No. 10.204.

[4] L.A. DeRosa and A.G. Kandoian (editors), *Reference Data For Radio Engineers*, Chapter 22, 5th Edition, H.W. Sams & Co., New York, 1968, pp. 21-22.

[5] J.R. Wait and D.A. Hill, Guided electromagnetic waves along an axial conductor in a circular tunnel, *IEEE Trans. on Antennas and Propagation*, Vol. AP-22, No. 4, 627-630, July 1974.

[6] M.R. Gillette and A.S. Gilmour, "Attenuation measurements in the 1 to 1000 MHz frequency range in wet granite tunnels", *IEEE Trans. Electromagn. Compat.*, Vol. EMC-17, No. 4, pp. 201-206, Nov. 1975.

FIGURE CAPTIONS

Fig. 1a An axial conductor or trolley wire located in semi-circular tunnel.

Fig. 1b The equivalent twin-wire line in a circular tunnel.

Fig. 2 The influence of the distance of the trolley wire to the tunnel wall on the attenuation rate.

Fig. 3 The effect of varying the tunnel radius for a fixed separation between the trolley wire and the tunnel wall.

Fig. 4 The effect of varying the tunnel radius for a fixed height of the trolley wire to the ground plane or tunnel floor.

Fig. 5a The dependence of the attenuation rate on the rock conductivity σ_e for the range from 10^{-4} to 1 mhos/m.

Fig. 5b The dependence of the attenuation rate on the rock conductivity σ_e for the range from 1 mhos/m to ∞.

Fig. 6 The dependence of the attenuation rate on the rock conductivity σ_e for a single conductor in a fully circular tunnel. The other conditions are the same as in Fig. 5a and 5b except that a_o = 1.414m.

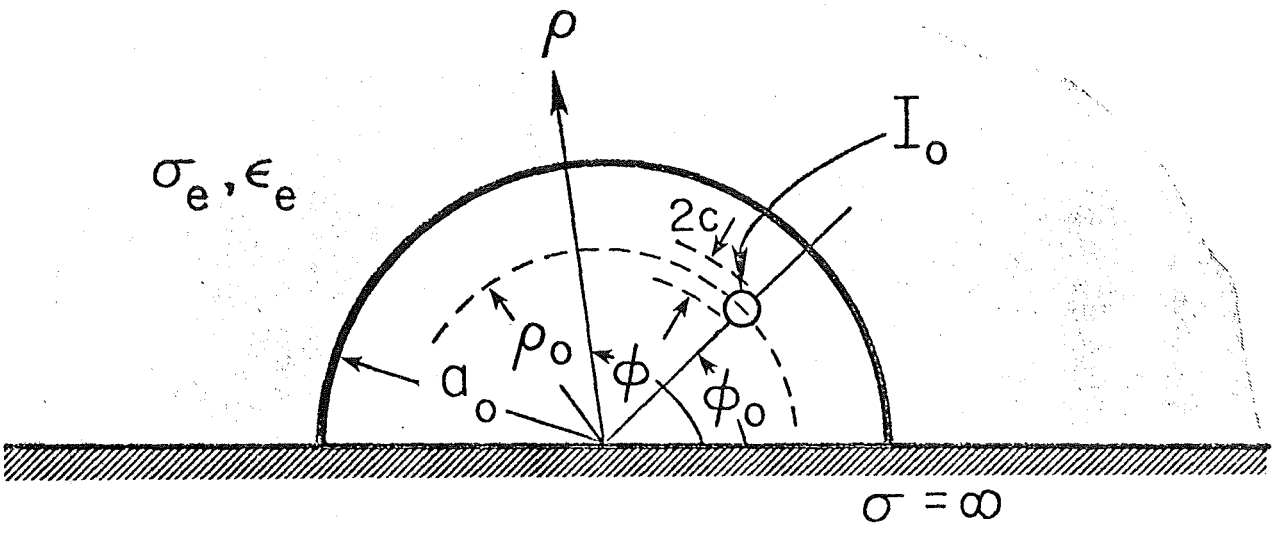
ρ
I_o
σ_e, ϵ_e
2c
ρ_o
a_o
ϕ
ϕ_o
$\sigma = \infty$

Fig. 1a

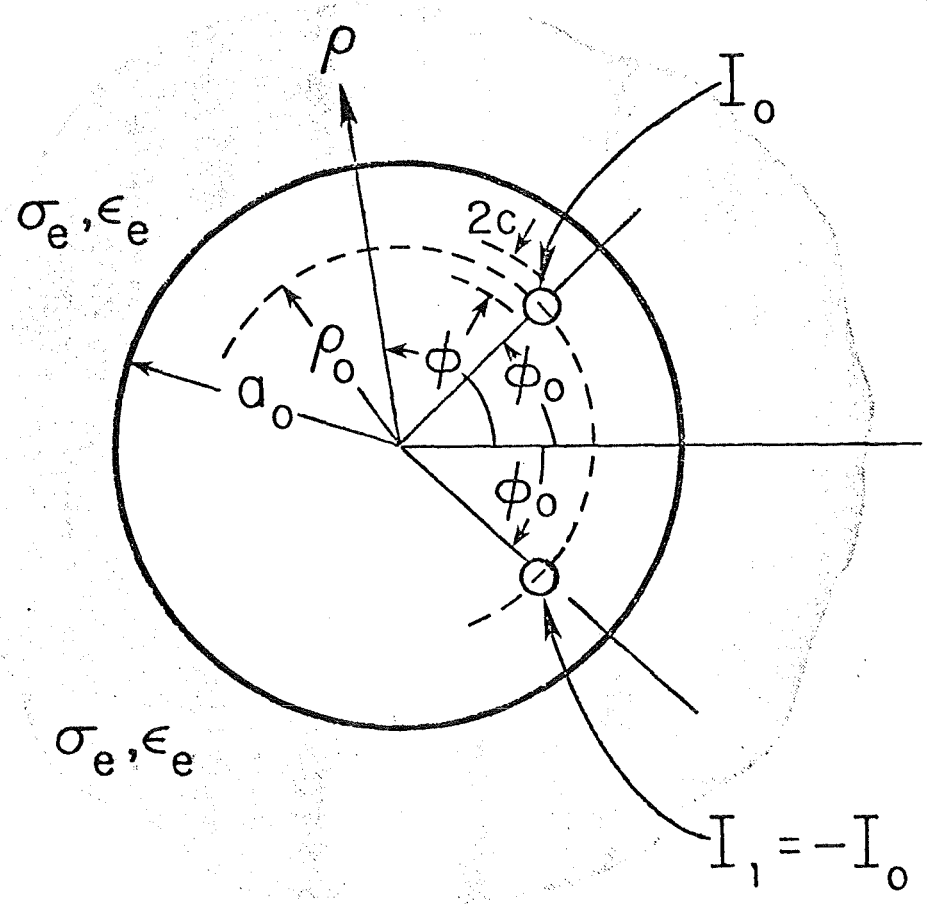
ρ
I_o
σ_e, ϵ_e
2c
ρ_o
a_o
ϕ
ϕ_o
ϕ_o
σ_e, ϵ_e
$I_1 = -I_o$

Fig. 1b

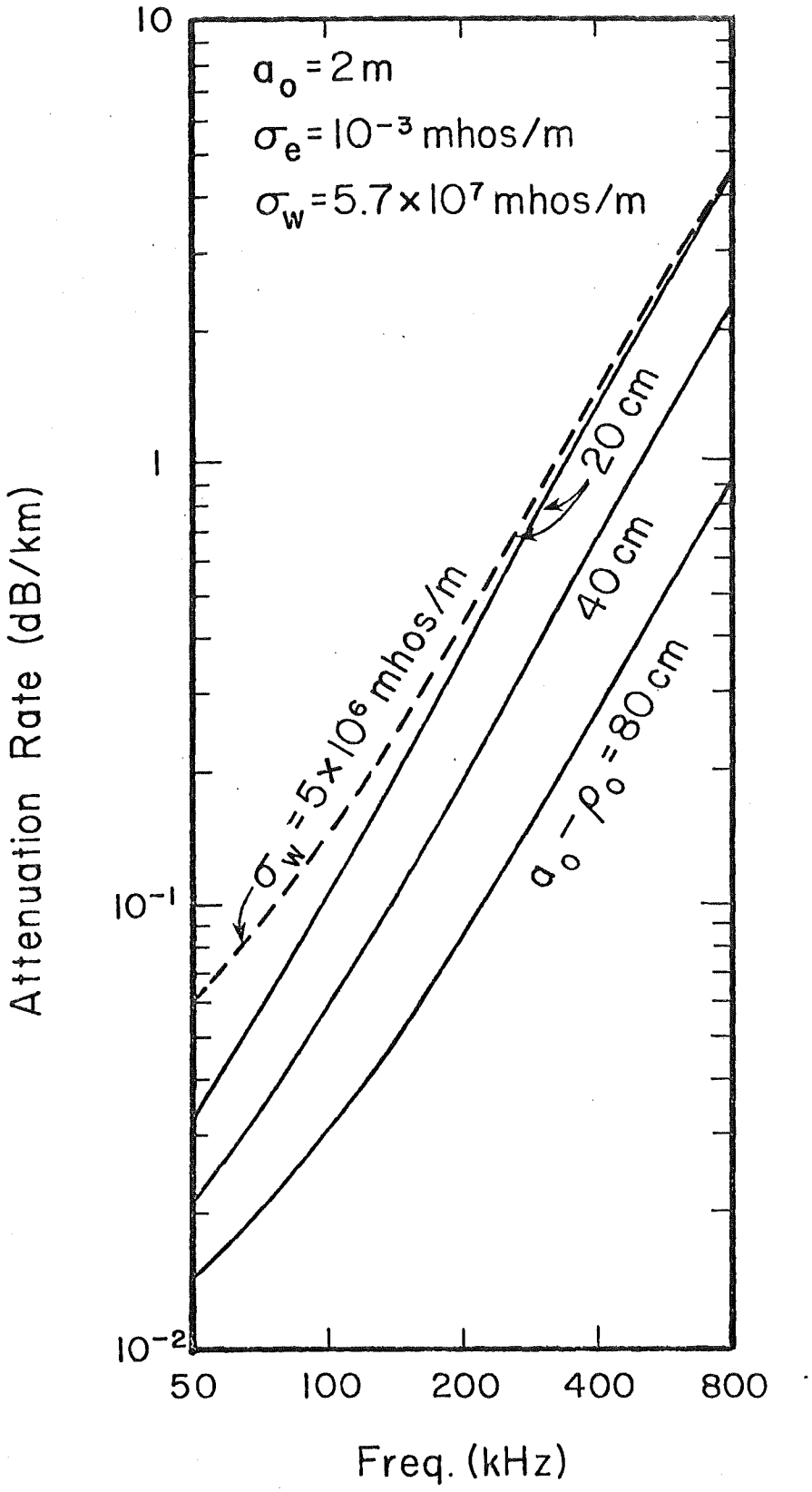
10
1
10^{-1}
10^{-2}
$a_o = 2\,m$
$\sigma_e = 10^{-3}$ mhos/m
$\sigma_w = 5.7 \times 10^7$ mhos/m
$\sigma_w = 5 \times 10^6$ mhos/m
20 cm
40 cm
$a_o - \rho_o = 80$ cm
50
100
200
400
800
Attenuation Rate (dB/km)
Freq. (kHz)

Fig. 2

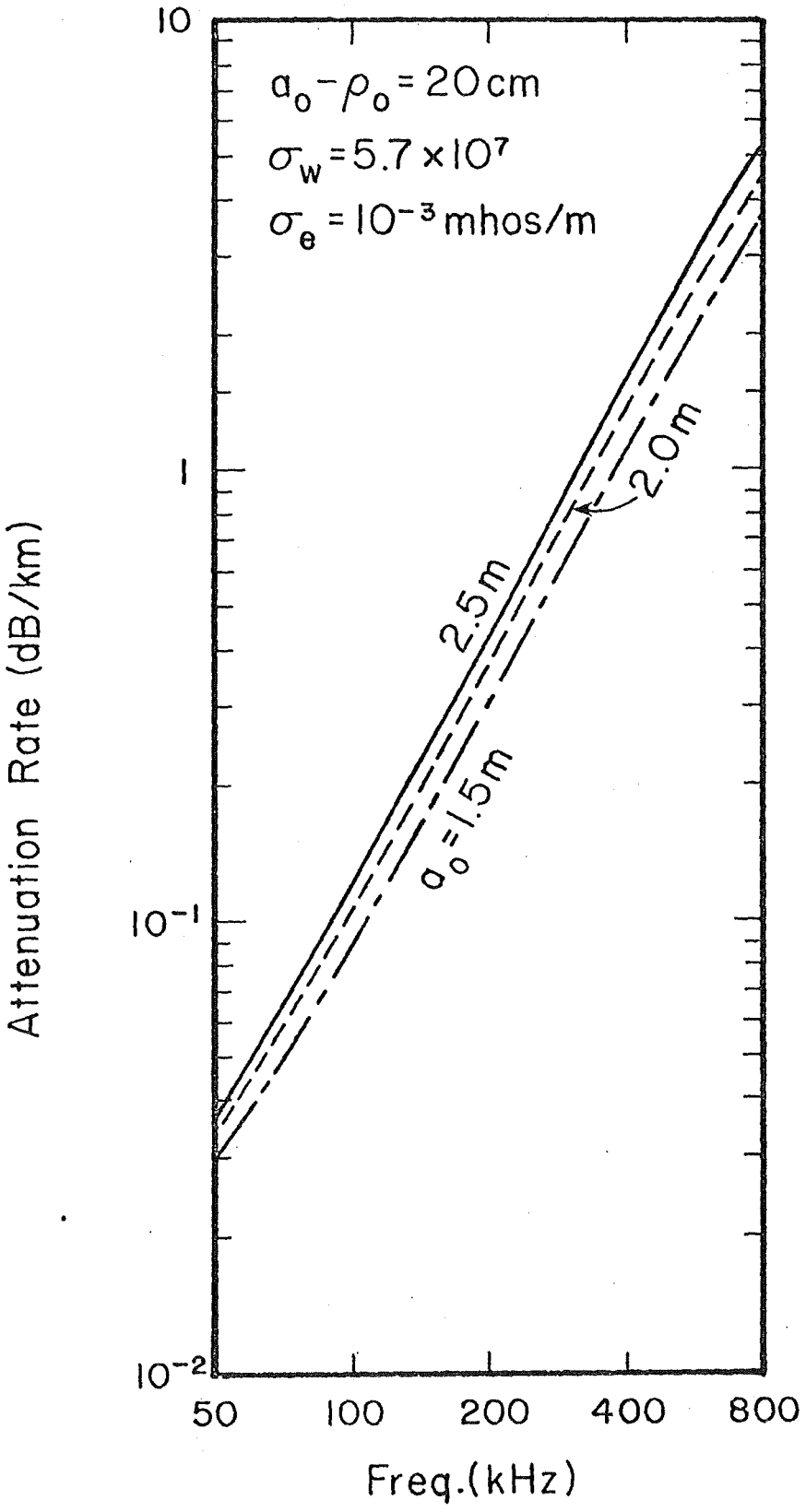
10
1
10^{-1}
10^{-2}
$a_o - \rho_o = 20\,cm$
$\sigma_w = 5.7 \times 10^7$
$\sigma_e = 10^{-3}$ mhos/m
2.5m
2.0m
a_o=1.5m
Attenuation Rate (dB/km)
50
100
200
400
800
Freq.(kHz)

Fig. 3

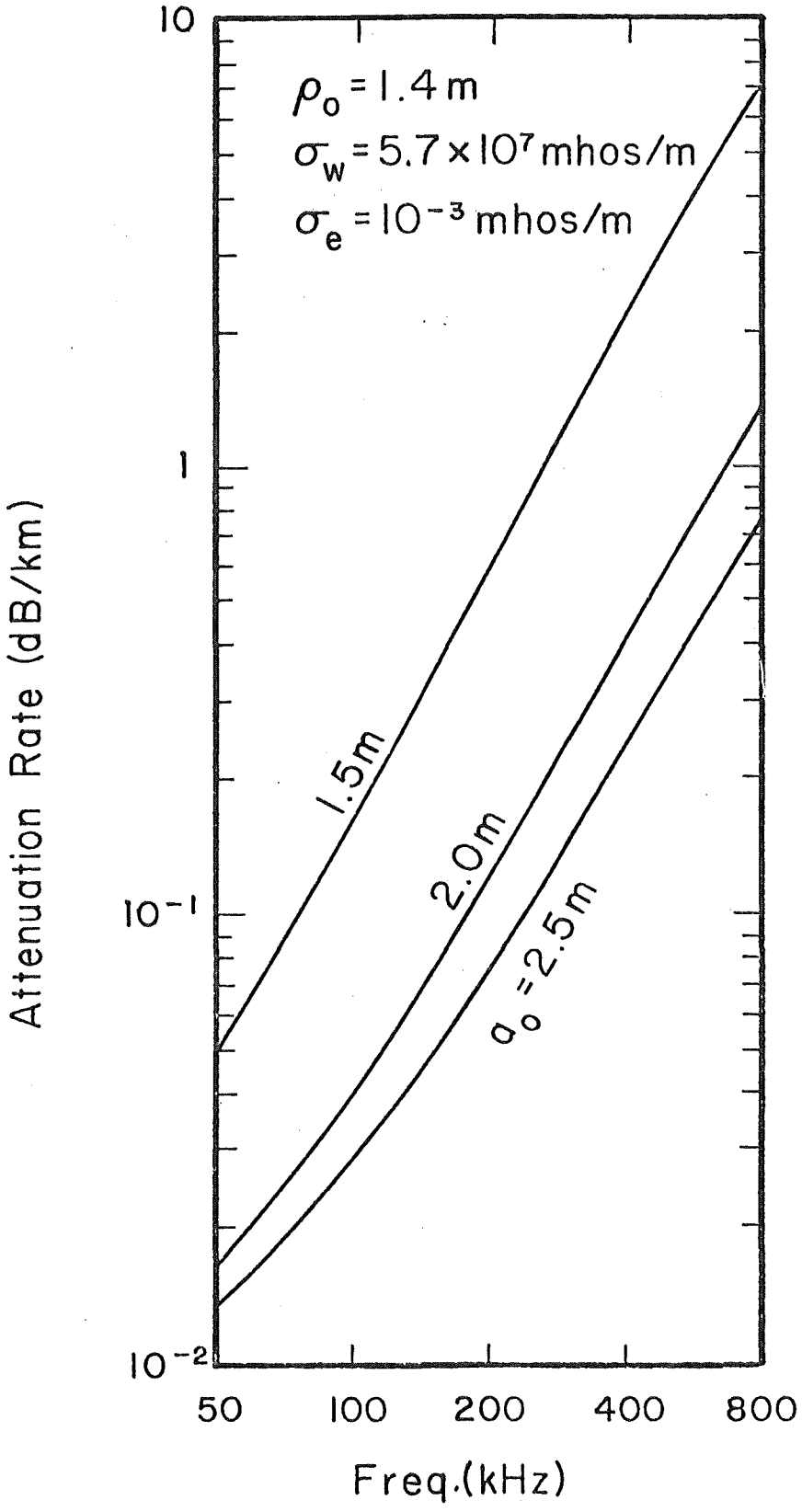
10
1
10^{-1}
10^{-2}
$\rho_o = 1.4\,m$
$\sigma_w = 5.7 \times 10^7$ mhos/m
$\sigma_e = 10^{-3}$ mhos/m
1.5m
2.0m
$a_o = 2.5m$
Attenuation Rate (dB/km)
50
100
200
400
800
Freq.(kHz)

Fig. 4

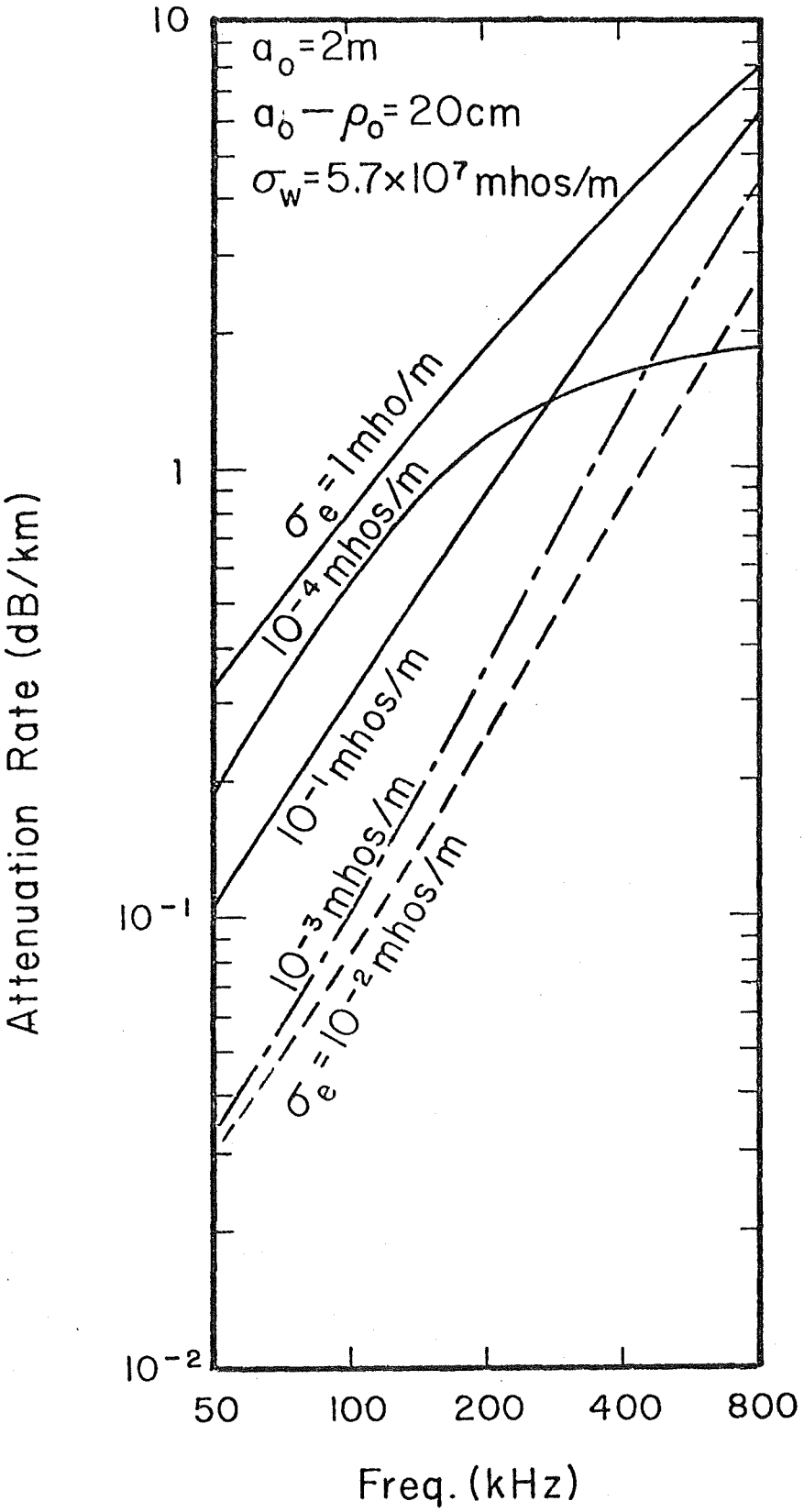
10
1
10^{-1}
10^{-2}
a_o=2m
$a_o - \rho_o$= 20cm
σ_w=5.7×10⁷ mhos/m
σ_e = 1 mho/m
10^{-4} mhos/m
10^{-1} mhos/m
10^{-3} mhos/m
$\sigma_e = 10^{-2}$ mhos/m
Attenuation Rate (dB/km)
50
100
200
400
800
Freq. (kHz)

Fig. 5a

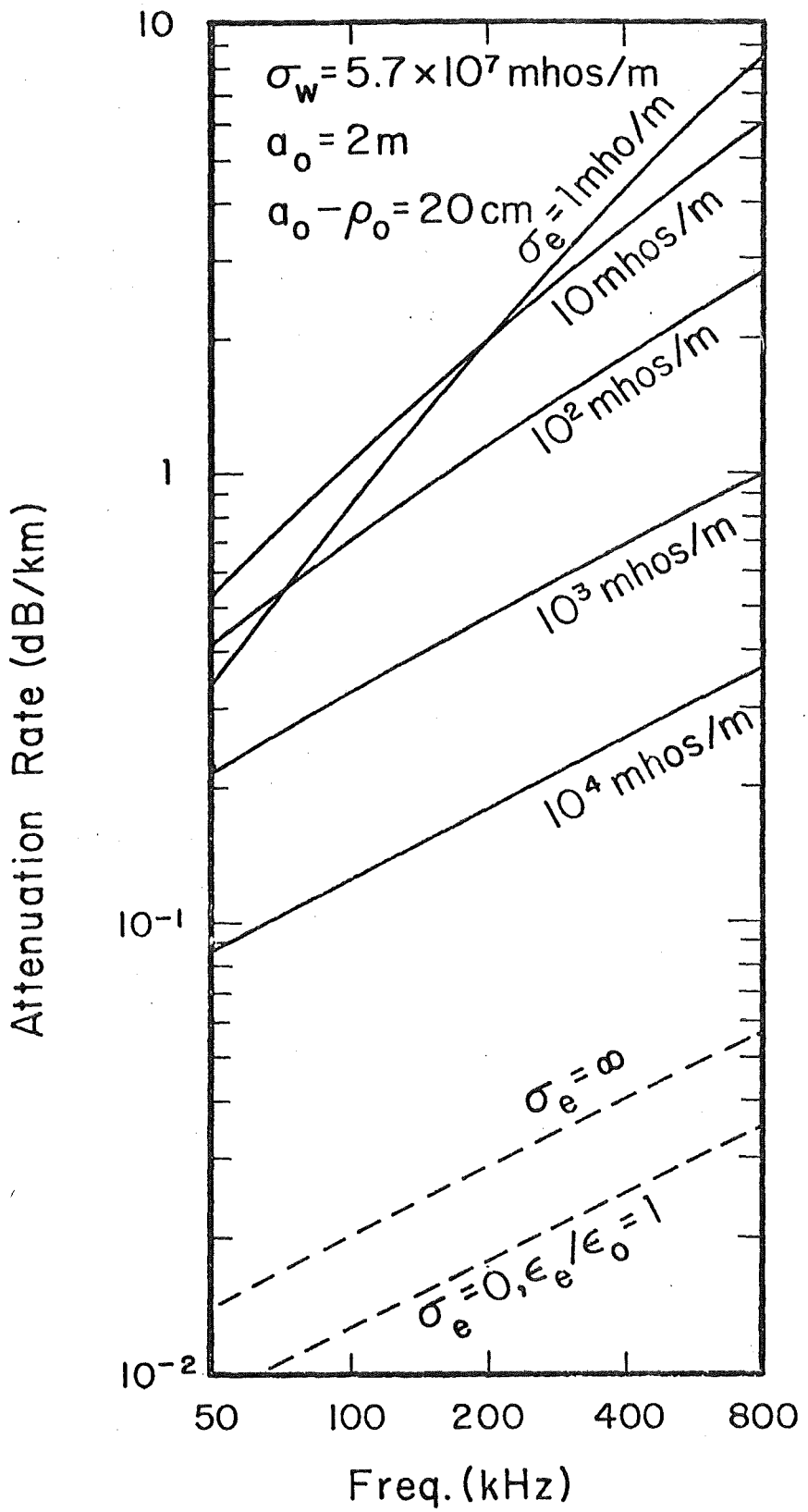
10
1
10^{-1}
10^{-2}
$\sigma_w = 5.7 \times 10^7$ mhos/m
$a_o = 2$m
$a_o - \rho_o = 20$cm
$\sigma_e = 1$mho/m
10mhos/m
10^2 mhos/m
10^3 mhos/m
10^4 mhos/m
$\sigma_e = \infty$
$\sigma_e = 0, \epsilon_e/\epsilon_o = 1$
Attenuation Rate (dB/km)
50
100
200
400
800
Freq. (kHz)

Fig. 5b

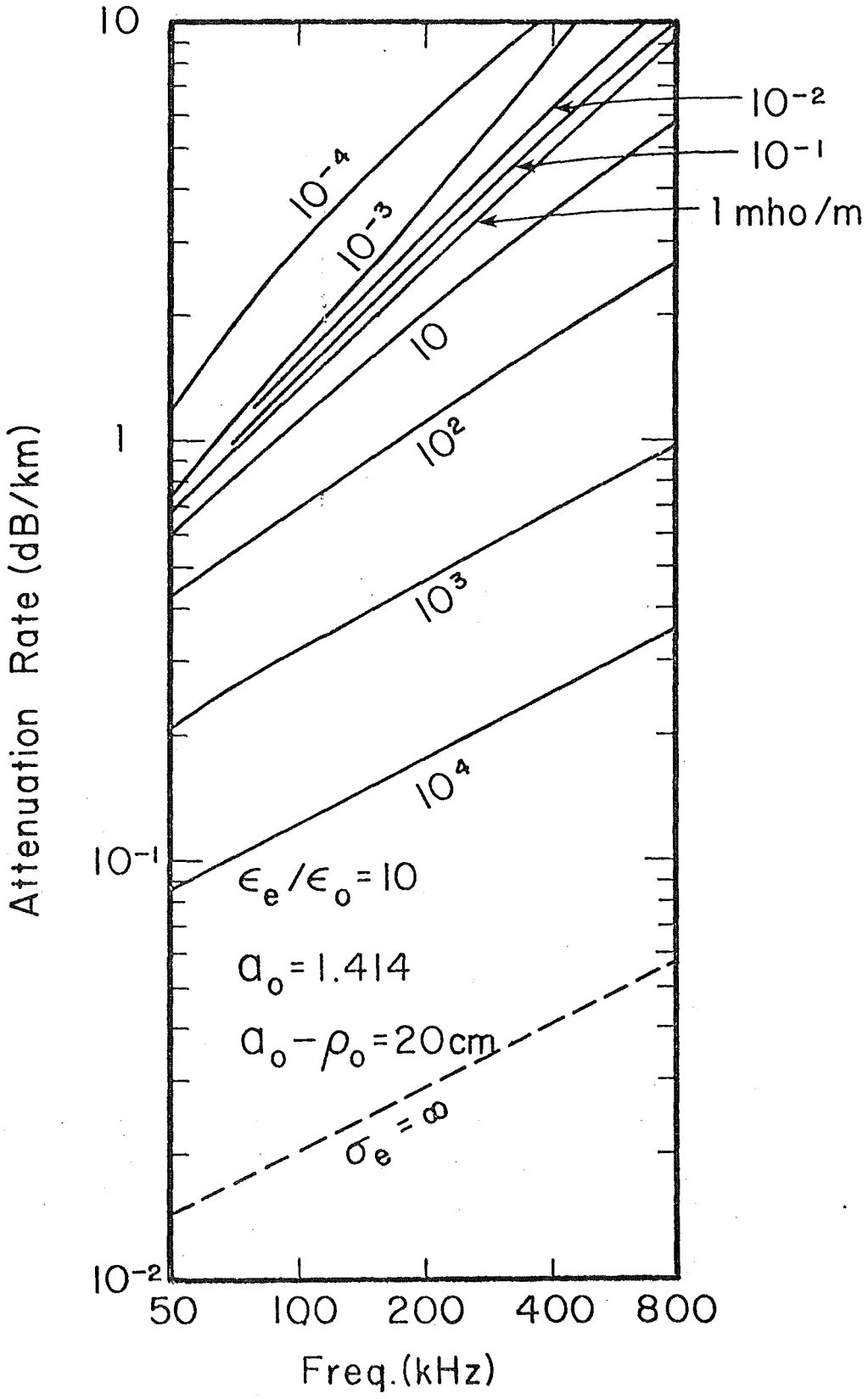
10
1
10^{-1}
10^{-2}
Attenuation Rate (dB/km)
10^{-2}
10^{-1}
1 mho/m
10^{-4}
10^{-3}
10
10^{2}
10^{3}
10^{4}
$\epsilon_e/\epsilon_0 = 10$
$a_0 = 1.414$
$a_0 - \rho_0 = 20cm$
$\sigma_e = \infty$
50
100
200
400
800
Freq.(kHz)

Fig. 6

APPENDIX

TABLE 1
EFFECT OF WIRE POSITION AND CONDUCTIVITY

(a_o = 2m, $\varepsilon_e/\varepsilon_o$ = 10, σ_e = 10^{-3} mhos/m, ϕ_o = 45°, c = 1.5 cm)

Frequency (kHz)	Normalized Phase $Im(\Gamma)/k_o$ ($a_o - \rho_o$ = 80cm)	($a_o - \rho_o$ = 40cm)	($a_o - \rho_o$ = 20cm)	($a_o - \rho_o$ = 20cm)
50.0	1.060	1.149	1.271	1.274
66.0	1.060	1.149	1.271	1.273
87.1	1.060	1.149	1.271	1.273
114.9	1.060	1.149	1.270	1.272
151.6	1.060	1.149	1.270	1.271
200.0	1.060	1.148	1.269	1.270
264.0	1.059	1.148	1.268	1.269
348.2	1.059	1.147	1.267	1.268
459.5	1.059	1.146	1.264	1.265
606.3	1.058	1.144	1.261	1.262
800.0	1.057	1.142	1.255	1.256
	$\sigma_w = 5.7 \times 10^7$mhos/m			$\sigma_w = 5 \times 10^6$mhos/m

TABLE 2
EFFECT OF WALL CONDUCTIVITY

(a_o = 2m, $\varepsilon_e/\varepsilon_o$ = 10, ϕ_o = 45°, $a_o - \rho_o$ = 20cm, $\sigma_w = 5.7 \times 10^7$mhos/m, c = 1.5cm)

Frequency (kHz)	Normalized Phase $Im(\Gamma)/k_o$ (σ_e = 10^{-1})	(σ_e = 10^{-2})	(σ_e = 10^{-3})	(σ_e = 10^{-4})
50.0	1.266	1.271	1.271	1.264
66.0	1.264	1.270	1.271	1.260
87.1	1.262	1.270	1.271	1.254
114.9	1.259	1.269	1.270	1.247
151.6	1.257	1.269	1.270	1.238
200.0	1.253	1.268	1.269	1.228
264.0	1.248	1.267	1.268	1.221
348.2	1.244	1.266	1.267	1.216
459.5	1.238	1.265	1.264	1.212
606.3	1.232	1.264	1.261	1.209
800.0	1.224	1.262	1.255	1.208

TABLE 3
EFFECT OF WIRE SIZE

(a_o = 2m, $\varepsilon_e/\varepsilon_o$ = 10, σ_e = 10^{-3}mhos/m, ϕ_o = 45°, $a_o - \rho_o$ = 40cm, $\sigma_w = 5.7 \times 10^7$mhos/m)

Frequency (kHz)	Attenuation Rate (dB/km) (c = 1.5cm)	(c = 2.5cm)	Phase $Im(\Gamma)/k_o$ (c = 1.5cm)	(c = 2.5cm)
50.0	2.14×10^{-2}	2.02×10^{-2}	1.149	1.173
66.0	3.11×10^{-2}	3.09×10^{-2}	1.149	1.172
87.1	4.68×10^{-2}	4.87×10^{-2}	1.149	1.172
114.9	7.30×10^{-2}	7.87×10^{-2}	1.149	1.172
151.6	1.168×10^{-1}	1.296×10^{-1}	1.149	1.172
200.0	1.907×10^{-1}	2.159×10^{-1}	1.148	1.171
264.0	3.149×10^{-1}	3.618×10^{-1}	1.148	1.171
348.2	5.224×10^{-1}	6.062×10^{-1}	1.147	1.170
459.5	8.631×10^{-1}	1.008	1.146	1.169
606.3	1.406	1.649	1.144	1.167
800.0	2.233	2.623	1.142	1.164

CHAPTER 24

RADIO FREQUENCY TRANSMISSION VIA A TROLLEY WIRE IN A TUNNEL WITH A RAIL RETURN

James R. Wait*

Cooperative Institute for Research in Environmental Sciences
University of Colorado/NOAA
Boulder, Colorado 80309

and

David A. Hill

Institute for Telecommunication Sciences
Office of Telecommunications
U.S. Department of Commerce
Boulder, Colorado 80302

Abstract-An analysis is given for the transmission of electromagnetic waves along a circular tunnel in the presence of axial conductors. One of these conductors is an idealization of a trolley wire with its bonded feeder line and it may be located anywhere in the tunnel. The other is a metal rail that is located within the homogeneous rock medium at a finite distance from the tunnel wall. A mode equation for the propagation modes is obtained that is used to obtain numerical results for the attenuation rate in the frequency range 50 to 800 kHz. It is shown that the attenuation rate is only weakly dependent on the burial depth of the rail conductor, at least in the range up to 50 cm. Also, it is found that the rail conductor for the model adopted carries an appreciable fraction of the total return current when typical rock conductivities are assumed. A thin layer of insulation on the rail appears to have a negligible effect. In fact, there is little change even if the rail is within the tunnel and just above the tunnel floor.

---

* Consultant to ITS/OT.

INTRODUCTION

An extremely interesting problem occurs when a radio frequency signal used in mine communications [1] is coupled to a trolley wire or its associated feeder line in a tunnel. If the tunnel wall is sufficiently well conducting, the return current path through the rock is uninhibited. However, if the rock is of low conductivity, the resultant attenuation of the signal may be severe due to ohmic losses. Fortunately, in many such cases, the situation is improved by the presence of metal rails that would be in intimate contact with the floor of the tunnel. Ideally, such rails could act as a perfect ground plane. Then the trolley wire would be imaged and the loss would result from the finite conductivity of the upper and side walls and the finite conductivity of the trolley wire and its bonded feeder. This configuration was analyzed earlier [2] and the results indicated that the attenuation was indeed very small (e.g. less than 2dB/km at 200 kHz). A more realistic case, however, should explicitly consider the rail or other axial conductors that may be located in close proximity to the floor of the tunnel. This is the subject of the present investigation. Alas, we still employ a highly idealized model that, nevertheless, contains the essential ingredients. Specifically, we consider a tunnel of circular cross section with an eccentrically located trolley wire and a single rail that may be insulated from the rock. Whilst the formulation is fairly general and could be applicable to other tunnel configurations [6], numerical results are obtained only for the case where the diameter of the tunnel is small compared with the operating (free-space) wavelength.

STATEMENT OF PROBLEM

The situation we wish to analyze is illustrated in Fig. 1. The tunnel of radius a, with free space permittivity ε_o, is cut through a homogeneous rock medium of conductivity σ_e and permittivity ε_e. The magnetic permeability μ_o of the whole space is taken to be the same as that of free space. With respect to a cylindrical coordinate system (ρ,ϕ,z), the tunnel wall is defined by $\rho = a$. A trolley wire of radius c_o and conductivity σ_s is located at $\rho = \rho_1$ and $\phi = \phi_1$ where $\rho_1 < a$. A rail or other heavy metal conductor is now represented by a cylindrical structure of outer radius c and centered at $\rho = \rho_2$ and $\phi = \phi_2$ where $\rho_2 > a + c$. Actually c is taken to be the radius of the insulation or coating that can be assigned a conductivity σ_c and permittivity ε_c. This coating is concentric with an assumed circular metal conductor of radius b that has a conductivity σ_w. Normally, we would expect the coating thickness $c - b$ to be small compared with all other dimensions of the problem. Also, all displacement currents in the metal conductors can be safely ignored but, without additional complexity, their magnetic permeabilities may be taken to be different from the free space value μ_o assumed elsewhere.

We are interested in seeking solutions for a propagation mode in the tunnel that has the form $\exp(-\Gamma z + i\omega t)$ where Γ is the complex propagation constant and ω is the angular frequency. Thus, subject to the relative thinness of the wire and rail, we can assert that the currents will have the respective forms $I_1 \exp(-\Gamma z + i\omega t)$ and $I_2 \exp(-\Gamma z + i\omega t)$ where I_1 and I_2 are as yet undetermined. In what follows, we drop the harmonic time factor $\exp(i\omega t)$; its presence

is understood. The solution is greatly simplified by invoking appropriate axial impedance conditions on the trolley wire and rail. The form of these are taken from previous work [3-5] but, in any case, they have a self contained plausibility.

WIRE BOUNDARY CONDITIONS

The impedance condition, on the axial electric field E_{oz}, at the trolley wire is taken to be [4]

$$E_{oz}\Big|_{\substack{\rho=\rho_1+c_o \\ \phi=\phi_1}} = Z_s I_1 \exp(-\Gamma z) \tag{1}$$

where

$$Z_s = \frac{\eta_s}{2\pi c_o} \frac{I_o(\gamma_s c_o)}{I_1(\gamma_s c_o)} \tag{2}$$

$\gamma_s = (i\sigma_s \mu_s \omega)^{\frac{1}{2}}$ and $\eta_s = i\mu_s \omega/\gamma_s$. $I_o(\ )$ and $I_1(\ )$ are the modified Bessel functions not to be confused with the axial current I_1 on the trolley wire. In the case where $|\gamma_s c_o| << 1$, the axial impedance reduces to the usual series resistance $1/\pi c_o^2 \sigma_s$ in ohms per meter that loses its dependence on the magnetic permeability μ_s. An analogous condition is to be applied at the coating surface of the rail conductor. For the axial electric field E_{ez} in the rock, it reads

$$E_{ez}\Big|_{\substack{\rho=\rho_2+c \\ \phi=\phi_2}} = Z_c(\Gamma) I_2 \exp(-\Gamma z) \tag{3}$$

where $Z_c(\Gamma)$ is the effective axial impedance of the rail or coated earth conductor. In general, it would be a function of the propagation constant Γ. For the present problem we can write

$$Z_c(\Gamma) \simeq z_c + Z_b \tag{4}$$

being the sum of the impedance z_c of the coating and the impedance Z_b of the metal rail itself. For an earlier quasi-static analysis [3]

$$z_c \simeq \frac{k_c^2 + \Gamma^2}{2\pi(\sigma_c + i\varepsilon_c\omega)} \ln\frac{c}{b} \tag{5}$$

where $k_c^2 = -i\mu_o\omega(\sigma_c + i\varepsilon_c\omega)$. Since $c - b << b$ this is equivalent to

$$z_c \simeq \frac{i\mu_o\omega}{2\pi b}(c - b)\left(1 + \frac{\Gamma^2}{k_c^2}\right) \tag{6}$$

In addition, we note that

$$Z_b = \frac{\eta}{2\pi b}\frac{I_o(\gamma_w b)}{I_1(\gamma_w b)} \tag{7}$$

where $\gamma_w = (i\sigma_w\mu_w\omega)^{\frac{1}{2}}$ and $\eta_w = i\mu_w\omega/\gamma_w$. Also, if $|\gamma_w b| << 1$, Z_b reduces to $1/\pi b^2\sigma_w$ as it should.

THE REQUIRED FIELD EXPRESSIONS

We now return to the general configuration shown in Fig. 1 and for the moment ignore the presence of the rail conductor. The axial electric field $E_{oz}^{(1)}$ in the region $a > \rho > \rho_1$ due to the current $I_1 \exp(-\Gamma z)$ in the trolley wire is known from previous work [4,5]. It is given explicitly by

$$E_{oz}^{(1)} = -v^2 \frac{i\mu_o\omega I_1}{2\pi\gamma_o^2} e^{-\Gamma z} \sum_{m=-\infty}^{+\infty} I_m(v\rho_1)\left[K_m(v\rho) - R_m \frac{K_m(va)}{I_m(va)} I_m(v\rho)\right] e^{-im(\phi-\phi_1)} \tag{8}$$

where $v = (\gamma_o^2 - \Gamma^2)^{\frac{1}{2}} = i(\Gamma^2 - \gamma_o^2)^{\frac{1}{2}}$ and $\gamma_o^2 = -k_o^2 = -\varepsilon_o\mu_o\omega^2$. $I_m(\ )$ and $K_m(\ )$ are modified Bessel functions of integer order m. The coefficient R_m is given by

$$R_m = \frac{\dfrac{\gamma_o}{v}\dfrac{K_m'(va)}{K_m(va)} + Y_m\eta_o + \delta_m\eta_o}{\dfrac{\gamma_o}{v}\dfrac{I_m'(va)}{I_m(va)} + Y_m\eta_o + \delta_m\eta_o} \tag{9}$$

and

$$\delta_m\eta_o = \frac{(im\Gamma/a)^2[v^{-2}-u^{-2}]^2}{\dfrac{\gamma_o}{v}\dfrac{I_m'(va)}{I_m(va)} + \dfrac{Z_m}{\eta_o}} \tag{10}$$

where

$$Y_m = \frac{i\gamma_e^2}{u\mu_o\omega}\frac{K_m'(ua)}{K_m(ua)} \tag{11}$$

$$Z_m = -\frac{i\mu_o\omega}{u}\frac{K_m'(ua)}{K_m(ua)} \tag{12}$$

$$u = (\gamma_e^2 - \Gamma^2)^{\frac{1}{2}} = i(\Gamma^2 - \gamma_e^2)^{\frac{1}{2}}$$

$$\gamma_e^2 = i\mu_o\omega(\sigma_e + i\varepsilon_e\omega) \quad \text{and} \quad \eta_o = (\mu_o/\varepsilon_o)^{\frac{1}{2}} \simeq 120\pi$$

The corresponding expression for the field $E_{ez}^{(1)}$ in the region $\rho > a$ due to the current $I_1 \exp(-\Gamma z)$, is given by

$$E_{ez}^{(1)} = -\frac{i\mu_o\omega v^2}{2\pi\gamma_o^2} I_1 e^{-\Gamma z}\sum_{m=-\infty}^{+\infty} I_m(v\rho_1)K_m(va) \times (1 - R_m)\frac{K_m(u\rho)}{K_m(ua)} e^{-im(\phi-\phi_1)} \tag{13}$$

This can be checked by noting that $E_{ez}^{(1)}$ satisfies the appropriate wave equation for a medium of constants σ_e, ε_e and μ_o and that, at $\rho = a$, $E_{ez}^{(1)} = E_{oz}^{(1)}$.

We now consider the complementary problem of deducing the axial field $E_{ez}^{(2)}$ in the region $\rho > a$ due to the current $I_2 \exp(-\Gamma z)$ in the rail conductor. The solution for this problem can be carried out in a straight-forward manner if we first ignore the presence of the trolley wire. The result is

$$E_{ez}^{(2)} = -\frac{i\mu_o \omega u^2 I_2}{2\pi\gamma_e^2} e^{-\Gamma z} \left\{ K_o(u\hat{\rho}_d) - \sum_{m=-\infty}^{+\infty} K_m(u\rho_2) S_m \frac{I_m(ua)}{K_m(ua)} K_m(u\rho) e^{-im(\phi-\phi_2)} \right\} \tag{14}$$

where $\hat{\rho}_d = [\rho^2 + \rho_2^2 - 2\rho\rho_2 \cos(\phi-\phi_2)]^{\frac{1}{2}}$. The factor S_m has an analogous form to R_m and in fact they are related as follows:

$$\frac{v^2}{\gamma_o^2} \frac{K_m(va)}{K_m(ua)} (1 - R_m) = \frac{u^2}{\gamma^2} \frac{I_m(ua)}{I_m(va)} (1 - S_m). \tag{15}$$

An equivalent form of (14) valid in the region $a < \rho < \rho_2$ is obtained by replacing $K_o(u\hat{\rho}_d)$ in its series form for this region referring to the origin $\rho = 0$. Thus

$$K_o(u\hat{\rho}_d) = \sum_{m=-\infty}^{+\infty} K_m(u\rho_2) I_m(u\rho) e^{-im(\phi-\phi_2)} \tag{16}$$

The corresponding expression for the field $E_{oz}^{(2)}$, in the region $\rho < a$, due to the current $I_2 \exp(-\Gamma z)$, is found to be

$$E_{oz}^{(2)} = - \frac{i\mu_o \omega u^2}{2\pi\gamma_e^2} I_2 e^{-\Gamma z} \sum_{m=-\infty}^{+\infty} K_m(u\rho_2) I_m(ua) \times (1 - S_m) \frac{I_m(v\rho)}{I_m(va)} e^{-im(\phi-\phi_2)} \tag{17}$$

This again is an appropriate solution of the wave equation in a homogeneous region of electrical constants ε_o and μ_o. As it can be verified that $E_{oz}^{(2)} = E_{ez}^{(2)}$ at $\rho = a$.

Another useful check is to note that, as a consequence of the reciprocity principle,

$$E_{ez}^{(1)}(\rho_2,\phi_2)/I_1 = E_{oz}^{(2)}(\rho_1,\phi_1)/I_2 \ . \tag{18}$$

This, of course, could have been used at the outset to obtain the solution of one complementary problem from the other.

THE MODAL EQUATION

The principal remaining task is now to determine the propagation constant(s) Γ by requiring that the total fields satisfy the appropriate impedance conditions on the trolley wire and rail. Thus, on applying (1) and (3), we require that

$$E_{oz}^{(1)}(\rho_1 + c_o,\phi_1) + E_{oz}^{(2)}(\rho_1 + c_o,\phi_1) = Z_s I_1 \exp(-\Gamma z) \tag{19}$$

and

$$E_{ez}^{(1)}(\rho_2 + c,\phi_2) + E_{ez}^{(2)}(\rho_2 + c_o,\phi_2) = Z_c I_2 \exp(-\Gamma z) \tag{20}$$

These must be satisfied simultaneously for all values of z. This in turn requires that the determinant of the coefficients of I_1 and I_2 should vanish, i.e.

$$\begin{vmatrix} A_1 & A_2 \\ B_1 & B_2 \end{vmatrix} = 0 \tag{21}$$

where

$$A_1 = -\frac{i\mu_o \omega v^2}{2\pi\gamma_o^2} \left\{ K_o(vc_o) - \sum R_m I_m(v\rho_1) \frac{K_m(va)}{I_m(va)} I_m\left(v(\rho_1 + c_o)\right) \right\} - Z_s \ , \tag{22}$$

$$A_2 = -\frac{i\mu_o \omega u^2}{2\pi\gamma_e^2} \sum K_m(u\rho_2) I_m(ua) \times (1 - S_m) \frac{I_m\left(v(\rho_1 + c_o)\right)}{I_m(va)} e^{-im(\phi_1 - \phi_2)} \ , \tag{23}$$

$$B_1 = -\frac{i\mu_o \omega v^2}{2\pi\gamma_o^2} \sum I_m(v\rho_1) K_m(va) \times (1 - R_m) \frac{K_m\left(u(\rho_2 + c)\right)}{K_m(ua)} e^{-im(\phi_2 - \phi_1)} \ , \tag{24}$$

and

$$B_2 = -\frac{i\mu\omega u^2}{2\pi\gamma_e^2} \left\{ K_o(uc) - \sum S_m K_m(u\rho_2) \frac{I_m(ua)}{K_m(ua)} K_m\left(u(\rho_2 + c)\right) \right\} - Z_c(\Gamma) \tag{25}$$

The summations in each case extend from $-\infty$ to $+\infty$ through integer values including zero. In dealing with radio frequencies, the tunnel diameter 2a is much smaller than a free-space wavelength. Then, for the modes of interest, the modal equation can be simplified somewhat by replacing Bessel functions of argument va and $v\rho_1$ by their small argument approximations. Thus, for example,

$$\frac{K_m(va)}{I_m(va)} I_m(v\rho_1) I_m\big(v(\rho_1 + c)\big) \simeq \begin{cases} \left[\dfrac{(\rho_1+c)\rho_1}{a^2}\right]^m \dfrac{1}{2m} ; & m \neq 0 \\ -\ln(va); & m = 0 \end{cases}$$

However, Bessel functions of argument ua and $u\rho_2$ are not so approximated.

While, in principle, there are an infinite number of solutions of the modal equation, we may anticipate that the mode of most practical interest is the one where Γ is of the order of ik_o where $k_o = 2\pi/$(free-space wavelength). Also, at least in the case of low rock conductivity, the current I_1 and I_2 would be of the same order of magnitude but would tend to be anti-phase. Thus, ideally, such a bifilar type mode is what would be expected for a two-wire line when the currents are anti-phase. Of course, at higher frequencies, other propagation modes would be possible including those that would have their energy confined to tunnel or to the insulation in the coated rail.

NUMERICAL EXAMPLE

For the present illustration of the analytical model, we choose the following values for the parameters:

Trolley wire: radius $c_o = 1.5$ cm
conductivity $\sigma_s = 5.7 \times 10^7$ mhos/m
permeability $\mu_s = \mu_o = 4\pi \times 10^{-7}$

Rail or buried earth conductor: radius $b = 4$ cm
conductivity $\sigma_w = 10^7$ mhos/m
permeability $\mu_w = \mu_o$
coating thickness $c - b = 0$

Tunnel radius, $a = 1.414$ m (i.e. $2a \simeq 9$ feet)

Trolley wire location: $\phi_1 = 120°$, $a - \rho_1 = 20$ cm

Rail location: $\phi_2 = 240°$, $\rho_2 - a = 10$ cm

Rock medium: conductivity σ_e (various values from 10^{-4} mhos/m to ∞)

permittivity $\varepsilon_e = 10\varepsilon_o$

Frequency: from 50 to 800 kHz

The attenuation rate which is the real part of Γ is plotted in Figs. 2a and 2b as a function of frequency. The vertical scale is decibels (dB) per km of path length along the tunnel. As illustrated, the attenuation increases monotonically as the rock conductivity σ_e is decreased from infinity to about 1 mho/m. In fact, in the case where $\sigma_e \geq 10$ mhos/m, the attenuation of the mode is almost identical to that computed for a tunnel with a trolley wire and no rail conductor present. This is the case considered earlier [2] and it corresponds to the dominant mode solution of the equation $A_1 = 0$ where A_1 is defined by (22). For lower and more typical rock conductivities, the results are influenced by the presence of the rail conductor. Such values are those shown in Fig. 2b.

An important related parameter is the complex ratio I_2/I_1 since this is a measure of the relative amount of current being carried by the rail. For the same conditions described above, the amplitude and phase of this ratio is plotted in Fig. 3a and 3b, respectively. Not surprisingly, as the rock conductivity is decreased, the relative current carried by the rail increases and, in fact, the ratio I_2/I_1 is actually tending to -1 at the lowermost frequencies. Of course, in the limit of high σ_e, the rail current is very small which is not surprising since the return current flows very easily in the well conducting rock walls of the tunnel.

While the above results were obtained for a buried rail located at $\rho_2 - a = 10$ cm from the tunnel wall, other calculations showed that there was virtually no change in the results from $\rho_2 - a$ varying from 5 to 40 cm. Also, the presence of a thin lossless dielectric coating (e.g. $c - b = 0.1$ mm) on the rail conductor leads to a negligible change in the results. Of course, other values of these parameters may lead to significant changes but no major modifications should result for the present configuration in the frequency range considered.

COMPARISON WITH RAIL IN TUNNEL

In the above model, we have assumed that the rail is a cylindrical dielectric-coated wire located in the conductive medium surrounding the tunnel. This could be criticized as unrealistic since the rail may be actually in the interface between the tunnel and the rock. However, as we pointed out, the dependence on the quantity $\rho_2 - a$ is very weak and in fact, for all practical purposes, it makes little difference in the deduced propagation constant Γ whether the rail is just below or just above the floor of the tunnel. This assertion is confirmed by calculations, using another formulation [5] for the same model but with the parameter $a - \rho_2$ being positive. Such an example is illustrated in Fig. 4 for the same geometrical parameters used above with the exceptions indicated. As can be seen, as $a - \rho_2$ is decreasing, the attenuation rate is approaching the value for the rail conductor located within the rock medium (i.e. indicated by $\rho_2 - a = 10$ cm). Actually, in this latter situation, the results are essentially the same for $\rho_2 - a$ from 5 to 20 cm.

THE MONOFILAR MODE

Following the suggestion of the editor (W.F. Croswell), a search was made for other modes that may have low attenuation. A mode is found that had the character of the monofilar mode for a twin-wire transmission line in a circular tunnel [5]. The magnitude of the ratio I_2/I_1 for this mode varies considerably with the geometrical configuration but the phase of I_2/I_1 is close to zero. Thus, physically, both the trolley wire and the rail are carrying the current in the same direction with all the return current being carried by the adjacent rock. Not surprisingly, this monofilar mode has an attenuation rate of the order of at least ten times that of the desired bifilar mode over the frequency range from 50 to 800 kHz. The results for the monofilar mode are shown in Fig. 4 for the parameters indicated. The case for $\rho_2 - a = 10$ cm is not shown since the attenuation rate is always greater than 10 dB/km.

There are also evanescent type solutions of the mode/equation that are analogous to the cut-off modes in a waveguide. Their attenuation is enormous and would plot well over the upper limit of Figs. 2a and 4. As indicated elsewhere [4], modes of the waveguide type do not become propagating until the frequency is increased to 50 MHz or so for typical tunnels. This is true even if the surrounding medium was a perfect dielectric.

CONCLUDING REMARKS

The present analysis should provide some insight into the propagation mechanism that is exploited in radio frequency transmission on a trolley wire or other axial conductors in a tunnel. The presence of rails or other conductors on the floor of the tunnel assures that the return current path is effective particularly in the case where the conductivity of the surrounding rock is low. In our discussion, we have not considered the influence of various loads on the trolley wire such as locomotives. The latter are usually isolated to some extent by radio frequency chokes that nevertheless will influence the performance of an actual communication system.

Further work on this subject needs to consider all the relevant factors. Also, it appears that some carefully controlled experiments are badly needed if the relative importance of the various parameters are to be properly understood.

REFERENCES

[1] J.N. Murphy and H.E. Parkinson, "Mine communications: Research and development in the U.S.A.", *Proceedings of International Conference on "Radio: Tunnels and Mines"*, Vol. II, pp. 42-64, 1-5 April 1974, Liege, Belgium.

[2] D.A. Hill and J.R. Wait, "Analysis of radio frequency transmission along a trolley wire in a mine tunnel", *Report submitted to U.S. Bureau of Mines*, 19 December 1975.

[3] J.R. Wait and D.A. Hill, "Propagation along a braided coaxial cable in a circular tunnel", *IEEE Trans. Microwave Theory Tech.*, Vol. MTT-23, No. 5, pp. 401-405, May 1975.

[4] J.R. Wait and D.A. Hill, "Guided electromagnetic waves along an axial conductor in a circular tunnel", *IEEE Trans. Antennas Propagat.*, Vol. AP-22, No. 4, pp. 627-630, July 1974.

[5] J.R. Wait and D.A. Hill, "Coaxial and bifilar modes on a transmission line in a circular tunnel", *Applied Physics* (Springer Verlag), Vol. 4, pp. 307-312, 1974.

[6] M.R. Gillette and A.S. Gilmour, "Attenuation measurements in the 1 to 1000 MHz frequency range in wet granite tunnels", *IEEE Trans. Electromagn. Compat.*, Vol. EMC-17, No. 4, pp. 201-206, Nov. 1975.

FIGURE CAPTIONS

Fig. 1 Circular tunnel with a trolley wire at (ρ,ϕ,z) carrying current I_1 and a buried rail or earth conductor at (ρ_2,ϕ_2,z) carrying a current I_2.

Fig. 2a and 2b Attenuation rate of the dominant mode for the model shown in Fig. 1.

Fig. 3a and 3b The complex ratio of the current I_2 in the rail to the current I_1 in the trolley wire.

Fig. 4 Attenuation rate for the corresponding situation where the rail conductor is located within the tunnel (i.e. $a - \rho_2 > 0$) and a comparision curve for the case of the buried rail (i.e. $\rho_2 - a > 0$). Some results for the corresponding monofilar mode are also shown.

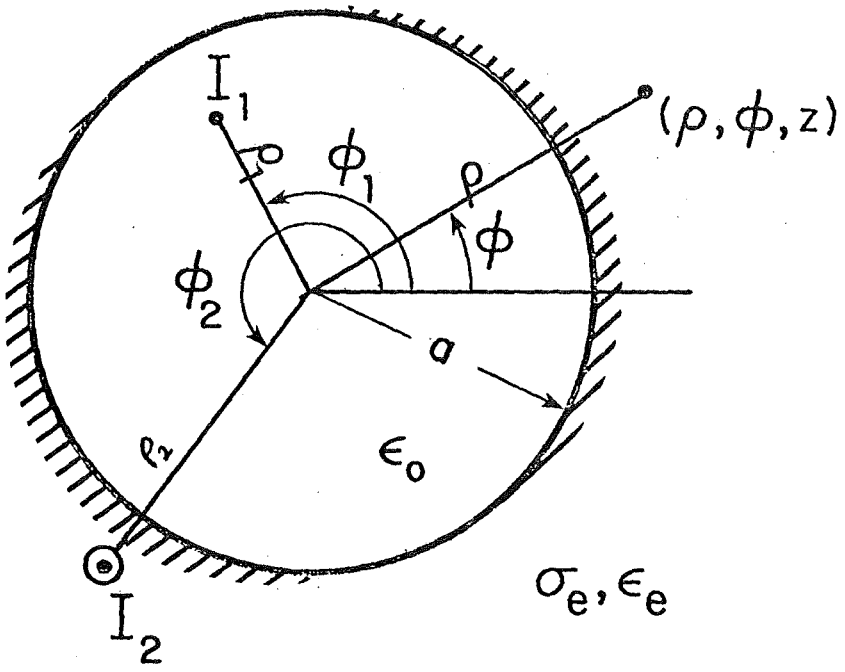
I_1
ρ_1
ϕ_1
(ρ, ϕ, z)
ρ
ϕ
ϕ_2
a
ℓ_2
ϵ_0
I_2
σ_e, ϵ_e

Fig. 1

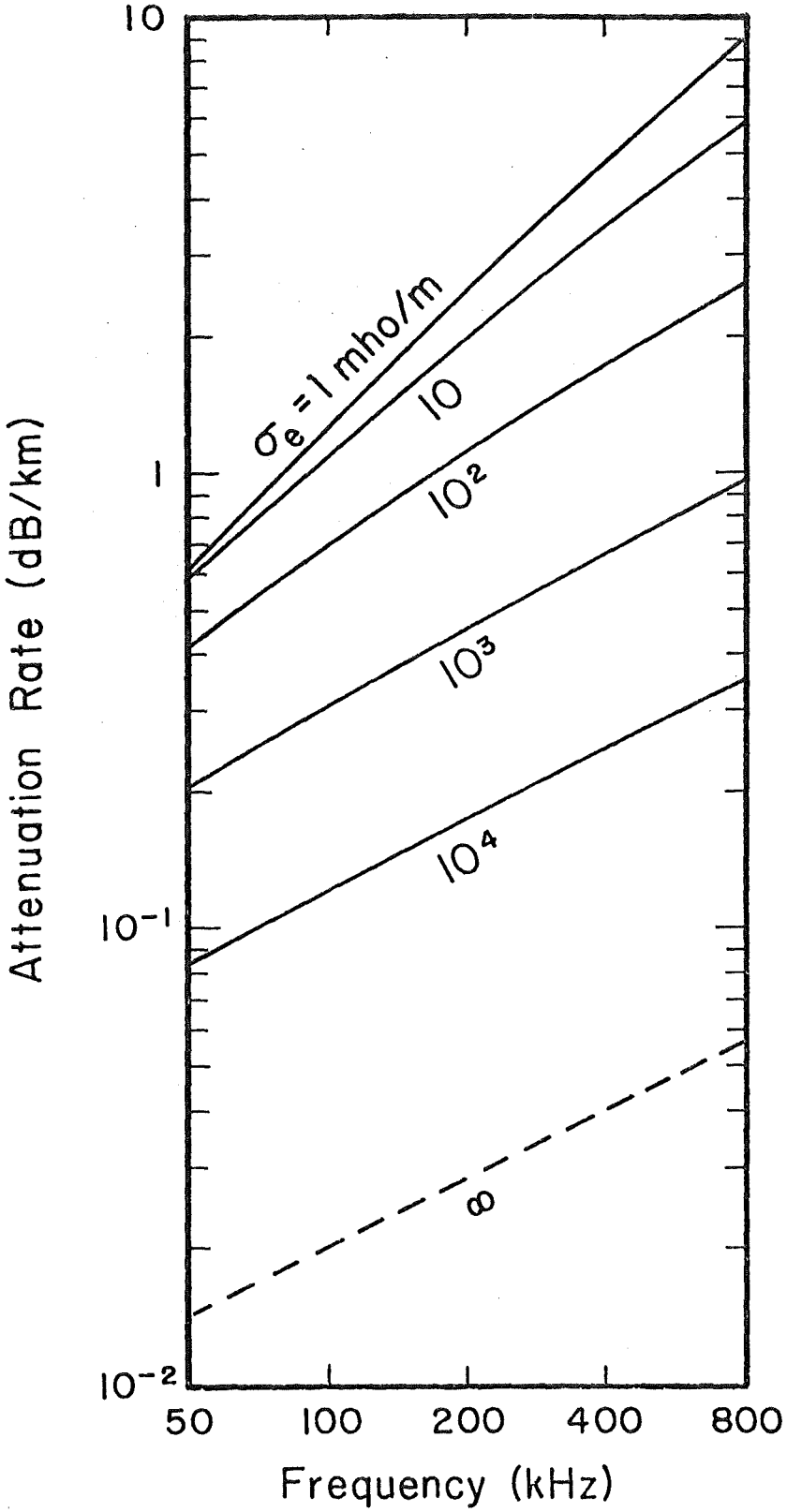
10
1
10^{-1}
10^{-2}
Attenuation Rate (dB/km)
σ_e = 1 mho/m
10
10^2
10^3
10^4
∞
50
100
200
400
800
Frequency (kHz)

Fig. 2a

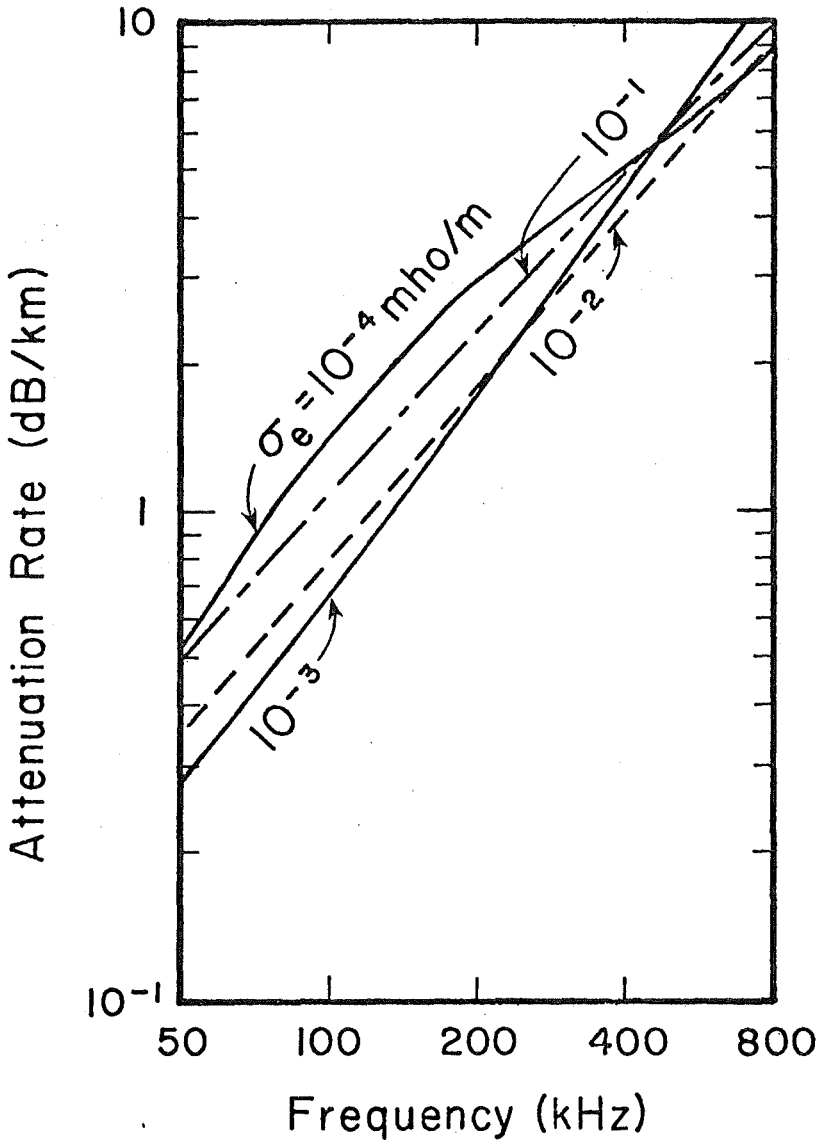
10
1
10^{-1}
Attenuation Rate (dB/km)
$\sigma_e = 10^{-4}$ mho/m
10^{-1}
10^{-2}
10^{-3}
50
100
200
400
800
Frequency (kHz)

Fig. 2b

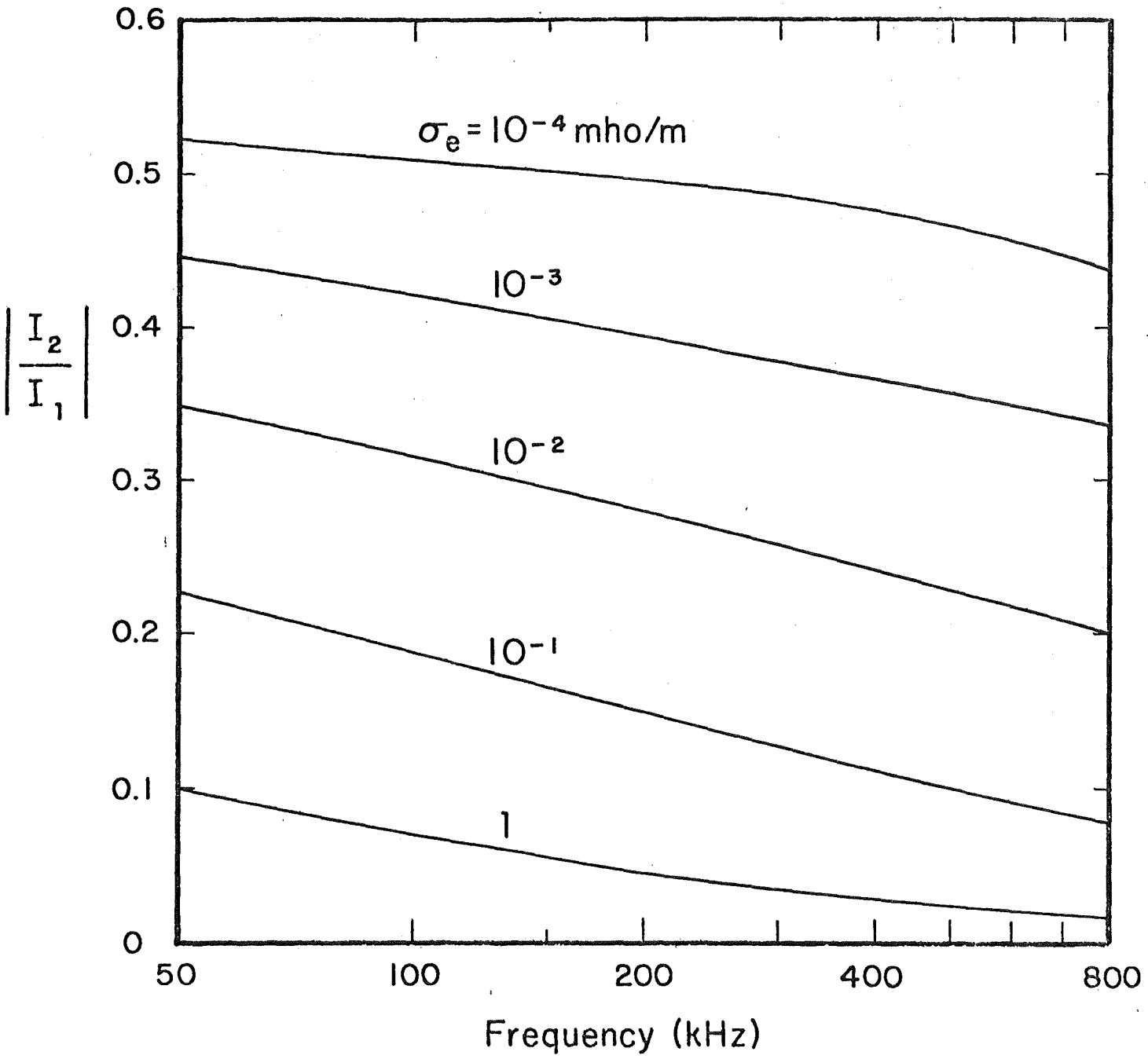
0.6
0.5
0.4
0.3
0.2
0.1
0
$\left|\frac{I_2}{I_1}\right|$
$\sigma_e = 10^{-4}$ mho/m
10^{-3}
10^{-2}
10^{-1}
1
50
100
200
400
800
Frequency (kHz)

Fig. 3a

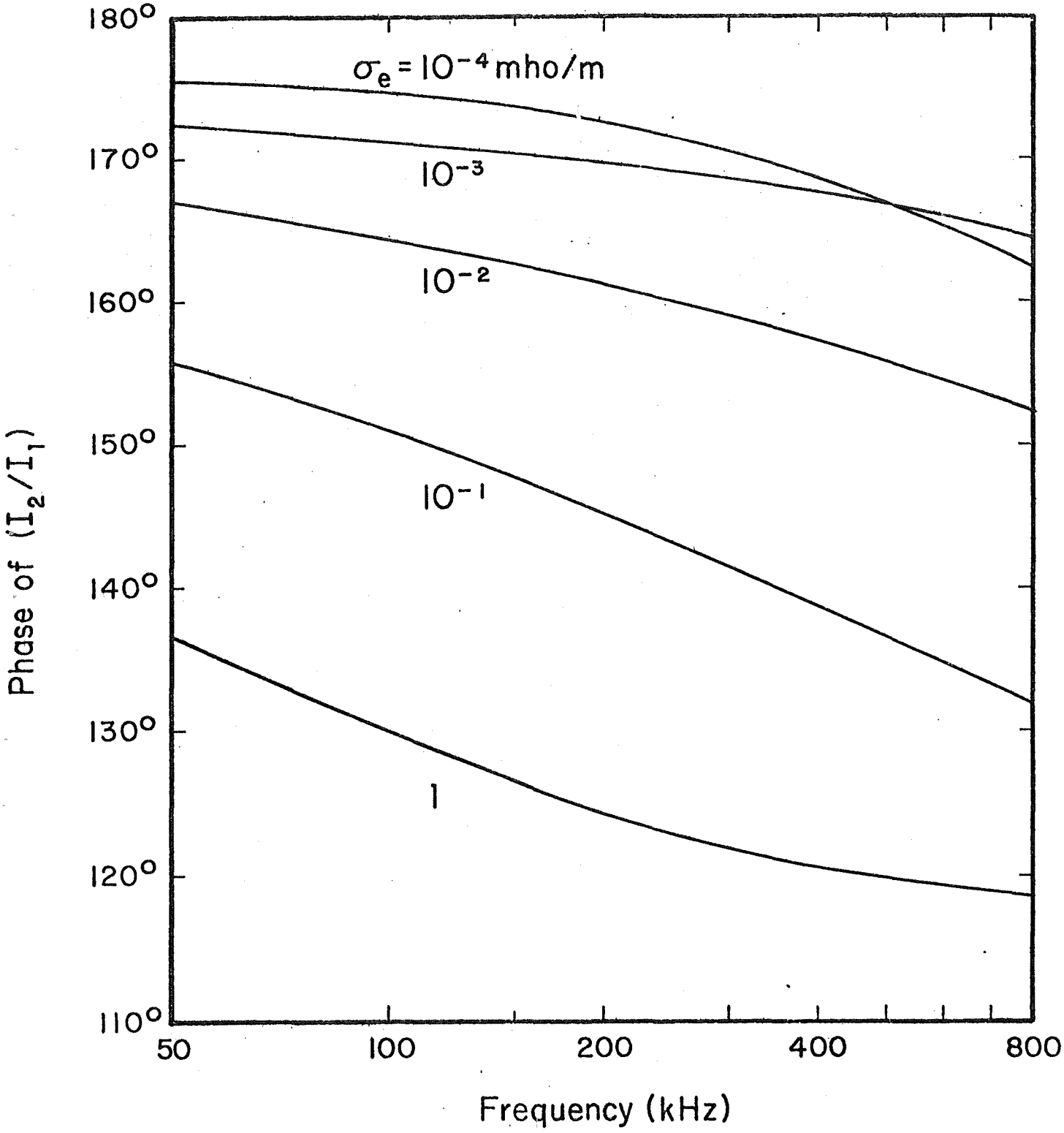
180°
170°
160°
150°
140°
130°
120°
110°
$\sigma_e = 10^{-4}$ mho/m
10^{-3}
10^{-2}
10^{-1}
1
Phase of (I_2/I_1)
50
100
200
400
800
Frequency (kHz)

Fig. 3b

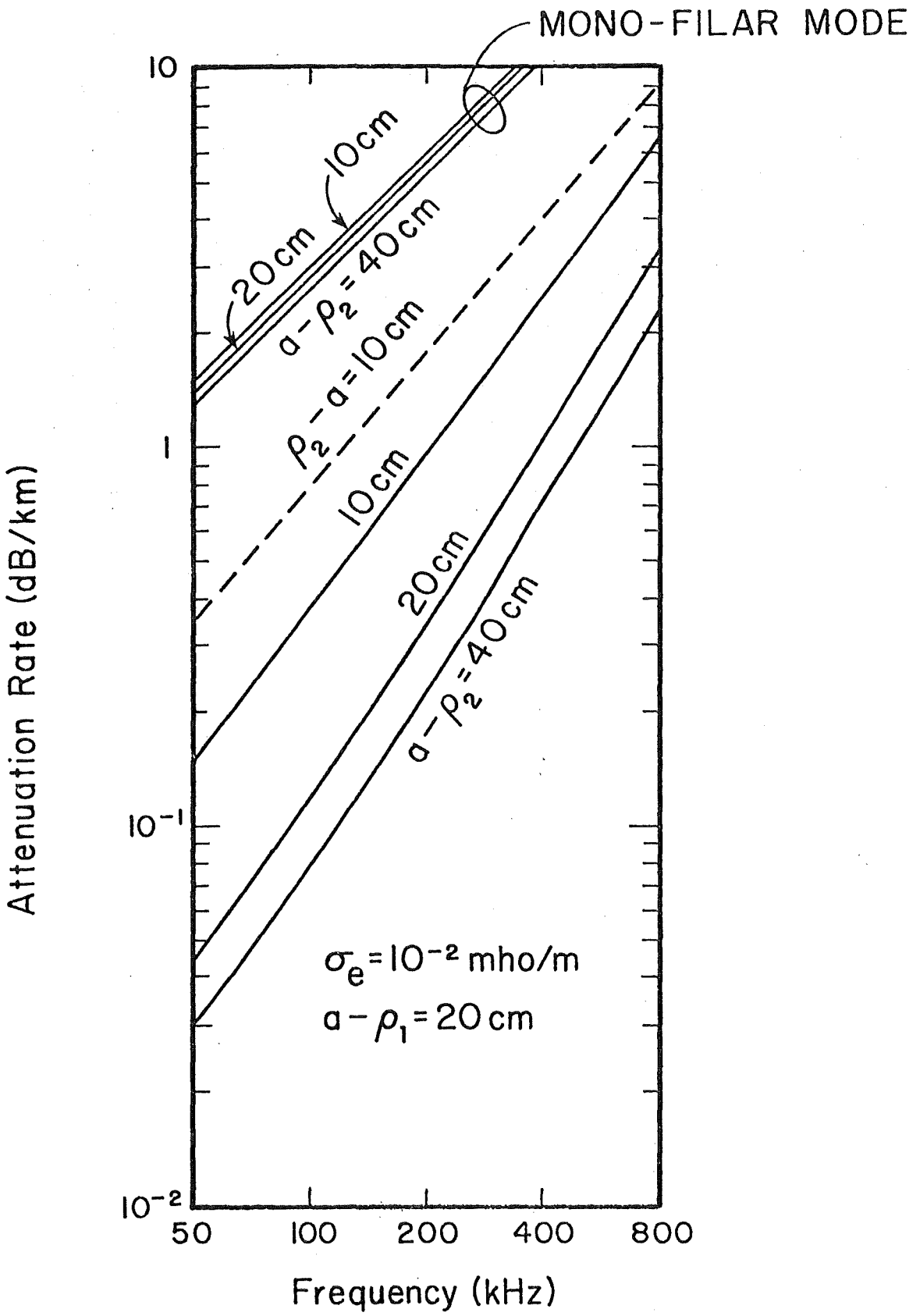
MONO-FILAR MODE
10
1
10^{-1}
10^{-2}
50
100
200
400
800
Attenuation Rate (dB/km)
Frequency (kHz)
10cm
20cm
$a-\rho_2=40$cm
$\rho_2-a=10$cm
10cm
20cm
$a-\rho_2=40$cm
$\sigma_e=10^{-2}$ mho/m
$a-\rho_1=20$ cm

Fig. 4

CHAPTER 25

QUASI-STATIC LIMIT FOR THE PROPAGATING MODE ALONG A THIN WIRE IN A CIRCULAR TUNNEL

JAMES R. WAIT

Cooperative Institute for Research in Environmental Sciences
University of Colorado
Boulder, Colorado 80309

Abstract-A previous modal analysis for a circular tunnel containing a thin wire is shown to be greatly simplified at low frequencies provided the wall conductivity is high. The explicit formula for the propagation constant, so obtained when specialized to a perfectly conducting wire, is in agreement with a quasi-static analysis by Wu, Shen and King for a similar configuration.

A general modal analysis was given earlier for the transmission in a straight circular tunnel bounded by a homogeneous medium and containing a thin axial wire running parallel to the tunnel wall. The medium external to the tunnel has a conductivity σ_e, permittivity ϵ_e, and permeability μ_e.

The modal equation, for the propagation constants Γ, was given in the form

$$-\frac{i\mu_o\omega v^2}{2\pi\gamma_o^2}\left[K_o(vc) - \sum_{m=-\infty}^{+\infty} R_m \frac{K_m(va)}{I_m(va)}\,[I_m(v\rho_o)]^2\right] = Z_s \qquad (1)$$

in the case when the axial wire with series impedance Z_s of radius c was located at a distance ρ_o from the tunnel axis and for an implied time factor $\exp(i\omega t)$. Also, we have assumed here that the distance d of the wire from the tunnel wall is large compared with the wire radius (i.e., $d = a - \rho_o >> c$). Other factors in (1), in the notation used earlier [1], are defined as follows:

$$R_m = \frac{(\gamma_o/v)K_m'(va)/K_m(va) + Y_m\eta_o + \delta_m\eta_o}{(\gamma_o/v)I_m'(va)/I_m(va) + Y_m\eta_o + \delta_m\eta_o} \quad , \tag{2}$$

$$\delta_m\eta_o = \frac{(im\Gamma/a)^2[v^{-2} - u^{-2}]^2}{[(\gamma_o/v)I_m'(va)/I_m(va)] + (Z_m/\eta_o)} \quad , \tag{3}$$

$$v = (\gamma_o^2 - \Gamma^2)^{\frac{1}{2}},\ u = (\gamma_e^2 - \Gamma^2)^{\frac{1}{2}},\ \gamma_o^2 = -\varepsilon_o\mu_o\omega^2,\ \gamma_e^2 = i\mu_e\omega(\sigma_e + i\varepsilon_e\omega),$$

$$\eta_o = (\mu_o/\varepsilon_o)^{\frac{1}{2}} \simeq 120\pi,\ Z_m = -\frac{i\mu_o\omega}{u}\frac{K_m'(ua)}{K_m(ua)} \text{ and } Y_m = \frac{i\gamma_e^2}{u\mu_o\omega}\frac{K_m'(ua)}{K_m(ua)}$$

The tunnel region is assumed to be free space with permittivity ε_o and permeability μ_o except for the thin wire that, as mentioned, is characterized by a series impedance Z_s. The latter is given explicitly by

$$Z_s = \frac{\eta_s}{2\pi c_s}\frac{I_o(\gamma_s c)}{I_1(\gamma_s c)}$$

where $\gamma_s = i\mu_s\omega(\sigma_s + i\varepsilon_s\omega)$ and $\eta_s = i\mu_s\omega/(\sigma_s + i\varepsilon_s\omega)$ in terms of the conductivity σ_s, permittivity ε_s, and permeability μ_s of the wire.

Actually, (1) is an exact equation to determine the axial propagation constant Γ of the discrete modes for the structure. These include the modes that have a transmission line characteristic at low frequencies as well as the waveguide modes that propagate at high frequencies.

Here we would like to identify a low frequency approximation to (1) that can permit an explicit evaluation of the desired propagation constant for the desired mode. However, first of all, we will recast (1) into an equivalent form as follows:

$$\frac{-i\mu_o\omega v^2}{2\pi\gamma_o^2}\left[\Lambda + \left(\gamma_o^2\Omega/v^2\right)\right] = Z_s \tag{4}$$

where

$$\Lambda = K_o(vc) - \sum_{m=-\infty}^{+\infty} \frac{K_m(va)}{I_m(va)} \left[I_m \left(v\rho_o \right) \right]^2 \tag{5}$$

and

$$\Omega = - \frac{v^2}{\gamma_o^2} \sum_{m=-\infty}^{+\infty} \left(R_m - 1 \right) \frac{K_m(va)}{I_m(va)} \left[I_m \left(v\rho_o \right) \right]^2 \tag{6}$$

Then we deduce from (4) that

$$\Gamma^2 = \gamma_o^2 \left[1 + \frac{\Omega}{\Lambda} + \frac{2\pi Z_s}{i\mu_o \omega \Lambda} \right] \tag{7a}$$

or alternatively,

$$\Gamma^2 = ZY$$

where

$$Z = \frac{i\mu_o \omega}{2\pi} (\Lambda + \Omega) + Z_s \quad \text{and} \quad Y = 2\pi i \epsilon_o \omega / \Lambda \tag{7b}$$

This is not an explicit equation for Γ^2 since Ω and Λ are functions of Γ^2. However, it becomes an explicit form if the frequency is sufficiently low and if the wall conductivity and/or wall permittivity are/is high. Specifically, we invoke the conditions $|va| << 1$, $|\gamma_e/\gamma_o|^2 >> 1$ and $\mu_e = \mu_o$. Then, on using small argument approximations for the modified Bessel functions, we see that

$$\begin{aligned} \Lambda &\simeq \ell n \frac{a}{c} - \sum_{1}^{\infty} \frac{1}{m} \left(\frac{\rho_o}{a} \right)^{2m} \\ &\simeq \ell n \frac{a}{c} - \ell n \frac{a^2}{a^2 - \rho_o^2} \end{aligned} \tag{8}$$

Clearly, $\Lambda \simeq \ell n(2d/c)$ when $d = a - \rho_o << a$.

To reduce Ω, we note first that

$$\delta_m \eta_o \simeq -\Gamma^2 m / (\gamma_o v^2 a) \tag{9}$$

when m is a positive integer, and

$$Y_m \eta_o \simeq - \frac{\gamma_e}{\gamma_o} \left[\frac{m}{\gamma_e a} - \frac{K_{m+1}(\gamma_e a)}{K_m(\gamma_e a)} \right] \tag{10}$$

In writing the latter, we have also utilized the derivative relation $K_m'(x) = (m/x)K_m(x) - K_{m+1}(x)$. Then it follows that

$$\begin{aligned} \left(R_m - 1\right) \frac{K_m(va)}{I_m(va)} \left[I_m\left(v\rho_o\right) \right]^2 &\simeq - \frac{\gamma_o}{v^2 a} \left(\frac{\rho_o}{a} \right)^{2m} \left[\frac{m}{\gamma_o a} + Y_m \eta_o \right]^{-1} \\ &\simeq - \frac{\gamma_o^2}{v^2 \gamma_e a} \left(\frac{\rho_o}{a} \right)^{2m} \frac{K_m(\gamma_e a)}{K_{m+1}(\gamma_e a)} \end{aligned} \tag{11}$$

Thus (6) is approximated by

$$\Omega = \frac{1}{\gamma_e a} \left[\frac{K_o(\gamma_e a)}{K_1(\gamma_e a)} + 2 \sum_1^{\infty} \left(\frac{\rho_o}{a} \right)^{2m} \frac{K_m(\gamma_e a)}{K_{m+1}(\gamma_e a)} \right] \tag{12}$$

Using expressions (8) and (12), we see that (7) is an explicit formula to calculate Γ. Here we choose the root corresponding to $\Gamma = \gamma_o$ in the case where Ω and Z_s are both zero. Clearly we have a transmission line type mode within this low frequency approximation. With appropriate change of notation and conventions, the results obtained here for the special case $Z_s = 0$ are in agreement with the quasi-static analysis by Wu, Shen and King [2]. Following their suggestion, we could improve the convergence of the representation by rewriting it in the equivalent form

$$\Omega = \frac{1}{\gamma_e a} \left\{ \frac{K_o(\gamma_e a)}{K_1(\gamma_e a)} + 2 \sum_{m=1}^{\infty} \left[\frac{K_m(\gamma_e a)}{K_{m+1}(\gamma_e a)} - \frac{\gamma_e a}{2m} \right] \left(\frac{\rho_o}{a} \right)^{2m} \right\} + \ell n \frac{a^2}{a^2 - \rho_o^2} \tag{13}$$

where we have merely added and substracted a series of the form

$$\sum_{m=1}^{\infty} \frac{1}{my^m} = \ell n \frac{y}{y-1} \quad \text{where} \quad y > 1. \tag{14}$$

A very simple limiting case of (12) is obtained if we assume that $|\gamma_e a| >> 1$ and then approximate the modified Bessel functions by the leading term of their asymptotic forms. Then

$$\Omega \simeq \frac{1}{\gamma_e a} \left[1 + 2 \sum_{m=1}^{\infty} \left(\frac{\rho_o}{a} \right)^{2m} \right]$$

$$\simeq \frac{1}{\gamma_e a} \frac{1 + (\rho_o/a)^2}{1 - (\rho_o/a)^2} \tag{15}$$

or if $d = (a - \rho_o) << a$, $\Omega \simeq 1/(\gamma_e d)$ and then

$$\Gamma \simeq \gamma_o \left[1 + \frac{1}{\gamma_e d} \ell n \frac{2d}{c} \right]^{\frac{1}{2}} \tag{16}$$

This simple result is consistent with an approximate quasi-static analysis by Sunde [3] who considered a thin wire at an equivalent height d over a homogeneous half-space with a propagation constant γ_e.

REFERENCES

[1] J.R. Wait and D.A. Hill, "Guided electromagnetic waves along an axial conductor in a circular tunnel", *IEEE Trans. Antennas Propagat.*, Vol. AP-22, pp. 627-630, July 1974.

[2] T.T. Wu, L.C. Shen and R.W.P. King, "The dipole antenna with eccentric coating in a relatively dense medium", *IEEE Trans. Antennas Propagat.*, Vol. AP-23, pp. 57-62, January 1975.

[3] E.D. Sunde, *Earth Conduction Effects in Transmission Systems*, New York: Dover Publ., Inc., p. 113, 1968.

CHAPTER 26

THE ECCENTRICALLY LOCATED WIRE IN A CYLINDRICAL CAVITY IN A CONDUCTING MEDIUM AND THE LIMIT OF A PLANAR BOUNDARY

James R. Wait

Cooperative Institute for Research in Environmental Sciences
University of Colorado/Environmental Research Laboratories
National Oceanic and Atmospheric Administration
U.S. Department of Commerce
Boulder, Colorado 80302

Abstract-Propagation along a thin wire located in an air filled tunnel is considered in the limiting case where the tunnel radius becomes indefinitely large but the distance of the wire to the tunnel wall remains finite. It is found that the results are consistent with the corresponding analysis for a thin wire located over a plane homogeneous earth.

A modal analysis was performed earlier for the transmission of electromagnetic waves in a circular air filled tunnel of radius a that contains an axial conductor [*Wait and Hill*, 1974]. The surrounding medium is homogeneous and unbounded with a conductivity σ_e, permittivity ε_e, and permeability μ_e. The modal equation, for the propagation constants Γ, was given in the form

$$K_o(vc) - \sum_{m=-\infty}^{+\infty} R_m \frac{K_m(va)}{I_m(va)} [I_m(v\rho_o)]^2 = 0 \qquad (1)$$

in the case when the axial wire of radius c was located at a distance ρ_o from the tunnel axis. Also, we have assumed here that the wire conductivity is infinite and that the distance d of the wire from the tunnel wall is large compared with the wire radius (i.e. $d = a - \rho_o \gg c$). Other factors in (1), in the notation used earlier, are defined as follows:

$$v = (\gamma_o^2 - \Gamma^2)^{\frac{1}{2}}, \quad u = (\gamma_e^2 - \Gamma^2)^{\frac{1}{2}}, \quad \gamma_o^2 = -\varepsilon_o \mu_o \omega^2, \quad \gamma_e^2 = i\mu_e \omega(\sigma_e + i\varepsilon_e \omega)$$

and

$$R_m = \frac{(\gamma_o/v)K_m'(va)/K_m(va) + Y_m \eta_o + \delta_m \eta_o}{(\gamma_o/v)I_m'(va)/I_m(va) + Y_m \eta_o + \delta_m \eta_o} \tag{2}$$

and

$$\delta_m \eta_o = \frac{(im\Gamma/a)^2 [v^{-2} - u^{-2}]^2}{[(\gamma_o/v)I_m'(va)/I_m(va)] + (Z_m/\eta_o)} \tag{3}$$

and

$$\eta_o = (\mu_o/\varepsilon_o)^{\frac{1}{2}} \simeq 120\pi, \quad Z_m = -\frac{i\mu_o \omega}{u} \frac{K_m'(ua)}{K_m(ua)} \quad \text{and} \quad Y_m = \frac{i\gamma_e^2}{u\mu_o \omega} \frac{K_m'(ua)}{K_m(ua)}$$

Actually, (1) is an exact equation to determine the axial propagation constant Γ of the discrete modes for the structure. These include the modes that have a transmission line characteristic at low frequencies as well as the waveguide modes that propagate at high frequencies. This transmission line or monofilar mode has no low frequency cut-off so it is of considerable practical interest in mine communication problems.

The attenuation rate (Re Γ in nepers/m) of the monofilar mode has a strong dependence of the distance $d = a - \rho_o$ from the tunnel wall. This is an important design consideration in communication schemes since it is convenient to locate the axial wire near the tunnel wall where d is somewhat less than a. Unfortunately, in this case, the summation over m in modal equation (1) is poorly convergent so computation is difficult. But physically, in this case, one would expect the configuration to be very similar to that of an infinite wire located at a height d over a flat earth of conductivity σ_e and permittivity ε_e. Mathematically this transition corresponds to letting $a \to \infty$ but keeping d finite.

We shall indicate here that the appropriate modal equation for the thin wire over the half-space is obtained as a limiting case of (1). The key step is to replace the infinite summation over integers m in (1) by an infinite integral with a variable λ that is identified with m/a. Uniform asymptotic expansions [*Abramowitz and Stegun*, 1964] for the modified Bessel functions can be used here effectively. For example:

$$Z_m \to Z_{\lambda a} = -\frac{i\mu_o\omega}{u}\frac{K'_{\lambda a}(ua)}{K_{\lambda a}(ua)} \simeq +\frac{i\mu_o\omega}{u}\frac{[1+(u/\lambda)^2]^{\frac{1}{2}}}{(u/\lambda)} \tag{4}$$

Using such asymptotic forms, we find that

$$R_m \to R_{\lambda a} \doteq \frac{\lambda^2\Gamma^2(1-K^2) - (\varepsilon_o\omega\hat{v} - (\varepsilon_e - i\frac{\sigma_e}{\omega})\omega\hat{u}K)(\mu_o\omega\hat{v}+\mu_e\omega\hat{u}K)}{\lambda^2\Gamma^2(1-K)^2 + (\varepsilon_o\omega\hat{v} + (\varepsilon_e - i\frac{\sigma_e}{\omega})\omega\hat{u}K)(\mu_o\omega\hat{v}+\mu_e\omega\hat{u}K)} \tag{5}$$

where $K = (\Gamma^2 - \gamma_o^2)/(\Gamma^2 - \gamma_e^2)$. But, in the case $\mu_e = \mu_o$, we can reduce this to

$$R_{\lambda a} = \left[1 + \frac{2\gamma_o^2}{\gamma_o^2 - \Gamma^2}\frac{(\lambda^2 - \hat{u}\hat{v})\hat{v}}{\gamma_o^2\hat{u} + \gamma_e^2\hat{v}}\right] \tag{6}$$

where

$$\hat{u} = (\lambda^2 + u^2)^{\frac{1}{2}} = (\lambda^2 - \Gamma^2 + \gamma_e^2)^{\frac{1}{2}}$$

and

$$\hat{v} = (\lambda^2 + v^2)^{\frac{1}{2}} = (\lambda^2 - \Gamma^2 + \gamma_o^2)^{\frac{1}{2}}$$

Then, on making all the appropriate substitutions, the mode equation (1) is transformed to

$$\left[K_o\left((\gamma_o^2 - \Gamma^2)^{\frac{1}{2}}c\right) - K_o\left((\gamma_o^2 - \Gamma^2)^{\frac{1}{2}}2d\right)\right]\left(1 - \frac{\Gamma^2}{\gamma_o^2}\right)$$
$$= 2\int_o^\infty (\lambda^2 - \hat{v}\hat{u})/(\gamma_o^2\hat{u} + \gamma_e^2\hat{v})\exp(-2\hat{v}d)d\lambda \tag{7}$$

This is entirely equivalent to the postulated form

$$Z - \Gamma^2 Y^{-1} = 0 \tag{8}$$

where

$$Z = [i\mu_o\omega/(2\pi)][\Lambda + 2(Q - iP)] \tag{9}$$

and

$$Y = (i2\pi\varepsilon_o\omega)[\Lambda + 2(N - iM)]^{-1} \tag{10}$$

where

$$\Lambda = K_o\left((\gamma_o^2 - \Gamma^2)c\right) - K_o\left((\gamma_o^2 - \Gamma^2)2d\right) \tag{11}$$

and

$$Q - iP = \int_{o_\infty}^{\infty} \frac{\exp(-\hat{v}2d)}{\hat{u} + \hat{v}}\, d\lambda \tag{12}$$

and

$$N - iM = (\gamma_o/\gamma_e)^2 \int_o^{\infty} \frac{\exp(-\hat{v}2d)}{\hat{v} + (\gamma_o/\gamma_e)^2\hat{u}}\, d\lambda \tag{13}$$

There is no further approximation in writing the transformed mode equation in the form given by (8) rather than (7). But here one should note that Z and Y, while functions of Γ, can be interpreted as a series impedance and series admittance, respectively. Not surprisingly, (8) is the same as the result derived directly for the model of a thin wire over a uniform half space [*Wait*, 1972].

A similar transition analysis was carried out recently by *King*, *Wu* and *Shen* [1974] who began with an approximate form for the fields of an eccentrically located wire in a cylindrical cavity. After making numerous approximations, they arrived a a form similar to (7) and (8) above but the $N - iM$ integral is not present. They suggest their result is valid if (in our notation), $|\gamma_e/\gamma_o|^2 >> 1$ and $|\gamma_o d| << 1$. Indeed this does seem to be true. But, at higher frequencies, it is necessary to include the

modification to the generalized admittance Y from the $N - iM$ integral. The importance of this type of coupling has actually been considered by *Chang and Wait* [1974] and *Chang and Olsen* [1975] in a somewhat differing context.

Thus we have shown that the mode equation, properly formulated for an axial wire in a cylindrical tunnel, does indeed transform into the appropriate form for a thin wire over a half-space in the limit of the tunnel radius approaching infinity. But we should remain conscious of the different physical nature of the two problems even if the radius a becomes large compared with other physical dimensions.

REFERENCES

Abramowitz, M. and I. Stegun (1964), *Handbook of Mathematical Functions*, p. 378, Government Printing Office, Washington, DC.

Chang, D.C. and R.G. Olsen (1975), Excitation of an infinite antenna above a dissipative earth, *Radio Sci.*, *10*(8/9), 823-832.

Chang, D.C. and J.R. Wait (1974), Extremely low frequency (ELF) propagation along a horizontal wire located above or buried in the earth, *IEEE Trans. Communications*, *COM-22*(4), 421-426.

King, R.W.P., T.T. Wu and L.C. Shen (1974), The horizontal wire antenna over a conducting or dielectric half-space: Current and admittance, *Radio Sci.*, *9*(7), 701-709 (Comments, No. 12, p. 1165, Dec. 1974).

Wait, J.R. (1972), Theory of wave propagation along a thin wire parallel to an interface, *Radio Sci.*, *7*(6), 675-679*.

Wait, J.R. and D.A. Hill (1974), Guided electromagnetic waves along an axial conductor in a circular tunnel, *IEEE Trans. Antennas Propagat.*, *AP-22*(4), 627-630.

---

*In (28) for $N - iM$, a factor $(k_1/k_2)^2$ should multiply the integral; in (17), delete the superscript 1/2 in the factor $(\gamma^2 - u_1u_2)$; in (36), the denominator of the integrand should be $k_1^2u_2 + k_2^2u_1$. This paper also contains numerous references to earlier work.

CHAPTER 27

INFLUENCE OF THE WALLS OF A CIRCULAR TUNNEL ON THE IMPEDANCE OF DIPOLES

JAMES R. WAIT AND DAVID A. HILL

Institute for Telecommunication Sciences
Office of Telecommunications
U.S. Department of Commerce
Boulder, Colorado 80302

Abstract-The electromagnetic fields of dipole emitters located inside an empty tunnel or cylindrical cavity are formulated. Both electric and magnetic types are considered. The results are used to deduce an expression for the change of self-impedance due to the presence of the tunnel walls. A numerical evaluation of the resultant convergent integrals and a summation of the angular harmonic series were performed. An important finding is that the input resistance of the electric dipole is approximately a constant for frequencies less than about 25 MHz for a typical tunnel radius of 2m. In contrast, for the same conditions, the input resistance of the magnetic dipole or small loop varies approximately as the square of the frequency. Such results are shown to be in qualitative agreement with an earlier analyses of dipoles over a dissipative half-space and dipoles located in insulated cavities.

INTRODUCTION

When an antenna is located near a lossy region such as the earth's surface, a fraction of the power is lost. This is a well-known if not a well understood problem in designing communication links for paths parallel to the ground [1]. Many theoretical studies have been carried out where the earth's surface is modelled as a dissipative half-space. An early paper by Sommerfeld and Renner [2] is particularly noteworthy in this

connection. Some of the more recent work is discussed in the context of remotely determining the electrical properties of a planetary surface from a dipole impedance measurement [3]. In that work, it was shown that the functional dependence of the input resistance on the "loss tangent" of the half-space is consistent with electrostatic concepts provided the frequency is sufficiently low. On the other hand, at the higher frequencies, the results are compatible with the surface impedance formulations based on the compensation theorem. In this latter frequency range, the results were essentially equivalent to the Sommerfeld-Renner formulation mentioned above.

In recent years the transmission properties of electromagnetic waves in mine and railway tunnels have been exploited for communication purposes [4]. One of the parameters needed for an engineering design is the power efficiency of the antennas. This has motivated us to examine the near fields of an electric dipole located in an air-filled circular tunnel of radius a where the surrounding medium is homogeneous with conductivity σ_e and permittivity ε_e. Specifically, we are interested in how the self-impedance of the dipole is modified by the presence of the tunnel wall. Thus we are led to formulate the problem in such a manner that the calculable quantity is the change of the self impedance rather than its absolute value. In this way, we are permitted to adopt the Hertzian dipole idealization provided only that the length of the antenna is small compared with both the free-space wavelength and with the distance of the antenna to the tunnel wall.

FORMULATION

The cross section of the tunnel or cylindrical cavity is indicated in Fig. 1 where both cylindrical coordinates (ρ,ϕ,z) and cartesian coordinates (x,y,z) have been chosen. The electric dipole of current moment Ids is located at $(\rho_o,\phi_o,0)$ and is oriented in the x direction. The electrical properties of the surrounding medium are σ_e,ε_e and μ_e where the permeability μ_e is allowed to be different from the free space value μ_o at least in the formulation. The tunnel or cavity region, for $\rho < a$, has electrical properties ε_o and μ_o that are assumed to be the same as free space.

Our first step is to write down the electric Hertz vector for the indicated dipole on the assumption that the tunnel walls are at an infinite distance. Such a vector, that has only an x component Π_x^p in the cartesian system, is given by

$$\Pi_x^p = [Ids/(4\pi i\varepsilon_o\omega)]R^{-1}\exp(-\gamma_o R) \tag{1}$$

where the assumed time factor is $\exp(i\omega t)$, where $\gamma_o = i(\varepsilon_o\mu_o)^{\frac{1}{2}}\omega$ and where $R = [\rho^2 + \rho_o^2 - 2\rho\rho_o\cos(\phi-\phi_o) + z^2]^{\frac{1}{2}}$. However, in order to match the subsequent boundary conditions for the total fields, it is desirable to express the primary fields in terms of axially directed electric and magnetic Hertz vectors.

We now introduce two well known identities from Bessel function theory that are often exploited in problems of this type [5]:

$$\frac{e^{-\gamma_o R}}{R} = \frac{1}{\pi}\int_{-\infty}^{+\infty} K_o(v\hat{\rho})\exp(-i\lambda z)d\lambda \quad \text{where} \quad v = (\lambda^2 + \gamma_o^2)^{\frac{1}{2}} \tag{2}$$

and

$$K_o(v\hat{\rho}) = \sum_{m=-\infty}^{+\infty} I_m(v\rho_o)K_m(v\rho)\exp[-im(\phi-\phi_o)] \quad (\text{for} \quad \rho_o < \rho) \tag{3}$$

where $\hat{\rho} = [\rho^2 + \rho_o^2 - 2\rho\rho_o \cos(\phi-\phi_o)]^{\frac{1}{2}}$.

Then, we see that

$$\Pi_x^p = \frac{Ids}{4\pi^2 i\varepsilon_o\omega} \Gamma \left(I_m(v\rho_o)K_m(v\rho)\right) \tag{4}$$

where Γ denotes the operation

$$\int_{-\infty}^{+\infty} \sum_{-\infty}^{+\infty} \left(\ldots\ldots\right) \exp[-im(\phi-\phi_o)]\exp(-i\lambda z)\,d\lambda$$

on the quantity in parenthesis. The integration contour here is taken along the entire real axis in the complex λ plane. The summation is over all integer values of m from $-\infty$ to $+\infty$ including zero.

The corresponding axial electric field is obtained as follows:

$$E_z^p = \frac{\partial^2 \Pi_x^p}{\partial x \partial z} = \left(\cos\phi \frac{\partial}{\partial\rho} - \sin\phi \frac{1}{\rho} \frac{\partial}{\partial\phi}\right) \frac{\partial \Pi_x^p}{\partial z}$$

$$= \frac{Ids}{4\pi^2 i\varepsilon_o\omega} \int (-i\lambda)F(\lambda)\exp(-i\lambda z)\,d\lambda \tag{5}$$

where

$$F(\lambda) = \sum \left((\cos\phi) \frac{\partial K_m}{\partial\rho} + \frac{im}{\rho} (\sin\phi)K_m\right) I_m \exp[-im(\phi-\phi_o)] \tag{6}$$

The argument of K_m, in the above expression for $F(\lambda)$, is $v\rho$ and that of I_m is $v\rho_o$. Then, by using the Bessel function identities

$$K_m' = -(1/2)\left[K_{m-1} + K_{m+1}\right] \tag{7}$$

and

$$K_m = [1/(2m)]\left[K_{m+1} - K_{m-1}\right] \tag{8}$$

it follows that

$$F(\lambda) = -\frac{v}{2} \sum K_{m-1} I_m \exp[-i(m-1)\phi + im\phi_o]$$

$$+ K_{m+1} I_m \exp[-i(m+1)\phi + im\phi_o] \tag{9}$$

$$= -\frac{v}{2} \sum K_m \exp[-im(\phi-\phi_o)][\exp(i\phi_o) I_{m+1} + \exp(-i\phi_o) I_{m-1}] \tag{10}$$

But we can also write

$$E_z^p = \left(-\gamma_o^2 + \partial^2/\partial z^2\right) U^p \tag{11}$$

in terms of electric Hertz potential U^p which is the z component of an axially directed electric Hertz vector. Clearly,

$$U^p = \Gamma \left(A_m(\lambda) K_m(v\rho)\right) \tag{12}$$

where

$$A_m(\lambda) = \frac{-Ids}{4\pi^2 \varepsilon_o \omega} \left(\frac{\lambda}{2v}\right) [\exp(i\phi_o) I_{m+1}(v\rho_o) + \exp(-i\phi_o) I_{m-1}(v\rho_o)] \tag{13}$$

because (5) and (11) must be identical.

In a very similar fashion to the above, we can work with the axial magnetic field. Thus, in this case, we invoke the equivalence of

$$H_z^p = i\varepsilon_o \omega \partial \Pi_x^p / \partial y \tag{14}$$

and

$$H_z^p = \left(-\gamma_o^2 + \partial^2/\partial z^2\right) V^p \tag{15}$$

where V^p is the magnetic Hertz potential. This has the representation

$$V^p = \Gamma \left(B_m(\lambda) K_m(v\rho)\right) \tag{16}$$

where

$$B_m(\lambda) = \frac{Ids}{4\pi^2}\left(\frac{i}{2v}\right)\left[\exp(-i\phi_o)I_{m-1}(v\rho_o) - \exp(i\phi_o)I_{m+1}(v\rho_o)\right] \tag{17}$$

SECONDARY FIELDS

To account for the influence of the cavity or tunnel walls, we add the secondary fields. Thus, the total fields are to be obtained from electric and magnetic Hertz potentials represented by

$$U = \Gamma\left(A_m(\lambda)K_m(v\rho) + P_m(\lambda)I_m(v\rho)\right) \tag{18}$$

and

$$V = \Gamma\left(B_m(\lambda)K_m(v\rho) + Q_m(\lambda)I_m(v\rho)\right) \tag{19}$$

that are valid for $\rho_o < \rho < a$. The factors $A_m(\lambda)$ and $B_m(\lambda)$ are specified by (13) and (17) while $P_m(\lambda)$ and $Q_m(\lambda)$ are yet to be determined.

In general, we note that (18) and (19) have the form

$$\begin{pmatrix} U \\ V \end{pmatrix} = \Gamma \begin{pmatrix} U_m \\ V_m \end{pmatrix} \tag{20}$$

Similarly, the field expressions can be written

$$\begin{pmatrix} E_\phi \\ H_\phi \\ E_z \\ H_z \end{pmatrix} = \Gamma \begin{pmatrix} E_{\phi m} \\ H_{\phi m} \\ E_{zm} \\ H_{zm} \end{pmatrix} \tag{21}$$

where

$$E_{\phi m} = -(m\lambda/\rho)U_m + i\mu_o\omega\partial V_m/\partial\rho$$

$$H_{\phi m} = -i\varepsilon_o\omega\partial U_m/\partial\rho - (m\lambda/\rho)V_m$$

$$E_{zm} = -v^2U_m \quad \text{and} \quad H_{zm} = -v^2V_m$$

As we have indicated before [6,7], the boundary conditions at the cavity or tunnel wall are succinctly expressed by

$$\left.\begin{aligned} E_{\phi m} &= \alpha_m E_{zm} + Z_m H_{zm} \\ H_{\phi m} &= -Y_m E_{zm} + \alpha_m H_{zm} \end{aligned}\right\} \text{ at } \rho = a \qquad (23)$$

and

where

$$\alpha_m = m\lambda/(u^2 a) \quad ,$$

$$Z_m = -(i\mu_e \omega/u) K_m'(ua)/K_m(ua) \qquad (24)$$

$$Y_m = [i\gamma_e^2/(u\mu_e \omega)] K_m'(ua)/K_m(ua) \quad , \qquad (25)$$

$$\gamma_e^2 = i\mu_e \omega(\sigma_e + i\varepsilon_e \omega) \quad ,$$

and

$$u = (\lambda^2 + \gamma_e^2)^{\frac{1}{2}} \quad .$$

The boundary conditions, given by (23), in conjunction with (18), (19), and (22), can be immediately applied to yield

$$P_m(\lambda) = -\left\{ A_m \left[\left(\frac{m\lambda}{v^2 a} - \alpha_m \right)^2 + \left(\frac{\gamma_o K_m'}{v K_m} + \eta_o Y_m \right) \left(\frac{\gamma_o I_m'}{v I_m} + \frac{Z_m}{\eta_o} \right) \right] I_m K_m \right.$$

$$\left. + B_m \left(\frac{m\lambda}{v^2 a} - \alpha_m \right) \frac{i\mu_o \omega}{v^2 a} \right\} D_m^{-1} \qquad (26)$$

and

$$Q_m(\lambda) = -\left\{ B_m \left(\frac{m\lambda}{v^2 a} - \alpha_m \right)^2 + \left(\frac{\gamma_o I_m'}{v I_m} + \eta_o Y_m \right) \left(\frac{\gamma_o K_m'}{v K_m} + \frac{Z_m}{\eta_o} \right) \right] I_m K_m$$

$$\left. - A_m \left(\frac{m\lambda}{v^2 a} - \alpha_m \right) \frac{i\varepsilon_o \omega}{v^2 a} \right\} D_m^{-1} \quad , \qquad (27)$$

where

$$D_m = \left[\left(\frac{m\lambda}{v^2 a} - \alpha_m \right)^2 + \left(\frac{\gamma_o I_m'}{v I_m} + \eta_o Y_m \right) \left(\frac{\gamma_o I_m'}{v I_m} + \frac{Z_m}{\eta_o} \right) \right] I_m^2$$

In (26) and (27) the following notational simplicity has been used: $A_m = A_m(\lambda)$, $B_m = B_m(\lambda)$, $I_m = I_m(va)$, $I_m' = I_m'(va)$, $K_m = K_m(va)$, $K_m' = K_m'(va)$ while bearing in mind that Z_m and Y_m are defined by (24) and (25) where the modified Bessel functions have argument ua. As usual, the prime over the modified Bessel function indicates differeniation with

respect to the argument.

IMPEDANCE FORMULATION

It is now desirable to digress slightly and talk about the primary fields of the source dipole. In particular, we easily deduce from (1) that

$$E_x^p = \left(-\gamma_o^2 + \partial^2/\partial x^2\right)\Pi_x^p \tag{28}$$

At the broadside point $(x_o, y, 0)$ we see that

$$E_x^p = \frac{iIds}{4\pi\varepsilon_o\omega s^3}(1 + iks - k^2s^2)\exp(-iks) \tag{29}$$

where $k = -i\gamma_o = (\varepsilon_o\mu_o)^{\frac{1}{2}}\omega$ and $s = y - y_o > 0$. In accordance with the E.M.F. method [3], we now can obtain the well known result for the "radiation resistance" of the dipole as follows

$$R_o = \lim_{s\to 0}\left[-\frac{\mathrm{Re}E_x^p}{I}\,ds\right] = \frac{k^2(ds)^2}{6\pi}\eta_o = 20k^2(ds)^2 \text{ ohms} \tag{30}$$

As mentioned earlier, this simple approach cannot be used to calculate the self reactance of the dipole unless its finite length is explicitly accounted for. On the other hand, as we indicate below, the dipole idealization is satisfactory for deducing the change of both the input resistance and the input reactance from its free space value.

In accordance with the above discussion, we write the resultant Hertz potentials as the sum of two parts as follows

$$U = U^p + \Delta U \tag{31}$$

and

$$V = V^p + \Delta V \tag{32}$$

where ΔU and ΔV can be described as the secondary Hertz potentials.

From (18) and (19), we see that

$$\Delta U = \Gamma\left(P_m(\lambda) I_m(v\rho)\right) \tag{33}$$

and

$$\Delta V = \Gamma\left(Q_m(\lambda) I_m(v\rho)\right) \tag{34}$$

which are valid for $0 < \rho < a$. Now it is clear that the x component ΔE_x of the secondary field can be obtained from

$$\Delta E_x = \Delta E_\rho \cos\phi_o - \Delta E_\phi \sin\phi_o \tag{35}$$

where

$$\Delta E_\rho = (\partial^2/\partial\rho\partial z)\Delta U - (i\mu_o\omega/\rho)\partial\Delta V/\partial\phi \tag{36}$$

and

$$\Delta E_\phi = (1/\rho)(\partial^2/\partial z\partial\phi)\Delta U + i\mu_o\omega\partial\Delta V/\partial\rho \tag{37}$$

If then the self impedance Z of the dipole is written

$$Z = Z_o + \Delta Z \tag{38}$$

where Z_o is the free space impedance, it follows that

$$\Delta Z = -\Delta E_x ds/I \tag{39}$$

in the limit $x \to x_o$, $y \to y_o$ and $z \to 0$. Explicitly

$$\Delta Z = \frac{ds}{I}\int_{-\infty}^{+\infty}\sum_{m=-\infty}^{+\infty}\Big\{[i\lambda v \cos\phi_o\, I_m'(v\rho_o) - (m\lambda/\rho_o)\sin\phi_o\, I_m(v\rho_o)]P_m(\lambda)$$
$$+ [(\mu_o\omega m/\rho)\cos\phi_o\, I_m(v\rho_o) + i\mu_o\omega \sin\phi_o\, vI_m'(v\rho_o)]Q_m(\lambda)\Big\}\, d\lambda \tag{40}$$

where $P_m(\lambda)$ and $Q_m(\lambda)$ are defined by (26) and (27), respectively.

The extension to magnetic dipole excitation is entirely analogous to the preceding derivation for the electric dipole. Thus we need only indicate the required changes in a very brief fashion.

The source is now a small loop of area dA carrying a current I. Again, with reference to Fig. 1, we can locate this dipole at (ρ_o,ϕ_o,o) and orient it (i.e. the axis of the loop) in the x direction. The primary fields of this magnetic dipole can be derived from a magnetic Hertz vector that has only an x component Π_x^{*p} given by

$$\Pi_x^{*p} = [IdA/(4\pi)]R^{-1} \exp(-\gamma_o R) \tag{41}$$

that is analogous to (1). The corresponding electric and magnetic Hertz potentials are given by (12) and (16), respectively, but now

$$A_m(\lambda) = \frac{i\mu_o\omega IdA}{4\pi^2}\left(\frac{i}{2v}\right)[\exp(-i\phi_o)I_{m-1}(v\rho_o) - \exp(i\phi_o)I_{m+1}(v\rho_o)] \tag{42}$$

and

$$B_m(\lambda) = \frac{IdA}{4\pi^2}\left(\frac{-i\lambda}{2v}\right)[\exp(i\phi_o)I_{m+1}(v\rho_o) + \exp(-i\phi_o)I_{m-1}(v\rho_o)] \tag{43}$$

The total fields in the region $\rho_o < \rho < a$ are again obtained from (18) and (19) where $P_m(\lambda)$ and $Q_m(\lambda)$ are as given by (26) and (27) in conjunction with (42) and (43).

We again can express the input impedance in the form given by (38) but now

$$\Delta Z = i\mu_o\omega\, \Delta H_x\, dA/I \tag{44}$$

in the limit $x \to x_o$, $y \to y_o$ and $z \to 0$. Here

$$\Delta H_x = \cos\phi_o\, \Delta H_\rho - \sin\phi_o\, \Delta H_\phi \tag{45}$$

$$\Delta H_\rho = \frac{i\varepsilon_o\omega}{\rho}\frac{\partial \Delta U}{\partial \phi} + \frac{\partial^2 \Delta V}{\partial \rho \partial z} \tag{46}$$

and

$$\Delta H_\phi = -i\varepsilon_o\omega \frac{\partial \Delta U}{\partial \rho} + \frac{1}{\rho}\frac{\partial^2 \Delta V}{\partial \phi \partial z} \tag{47}$$

Then, the explicit form of (44) is

$$\Delta Z = \frac{i\mu_o\omega dA}{I}\int_{-\infty}^{+\infty}\sum_{-\infty}^{+\infty}\Big\{[(\varepsilon_o\omega m/\rho)\cos\phi_o\, I_m(v\rho_o) + i\varepsilon_o\omega v \sin\phi_o\, I_m'(v_o\rho)]P_m(\lambda)$$

$$+ [-i\lambda v \cos\phi_o\, I_m'(v\rho_o) + (m\lambda/\rho)\sin\phi_o\, I_m(v\rho_o)]Q_m(\lambda)\Big\}d\lambda \tag{48}$$

As before, the input resistance R is the real part of Z. In free space (i.e. considering primary fields only), we readily deduce that the "radiation resistance" R_o for the small loop is given by

$$R_o = \eta_o k^4 (dA)^2/(6\pi) \tag{49}$$

which is a well known result. Thus, again writing $R = R_o + \Delta R$, the change of the input resistance for the loop from its free-space value is obtained from $\Delta R = \mathrm{Re}\cdot\Delta Z$ where ΔZ is given by (48).

NUMERICAL RESULTS

To obtain values of the ratio R/R_o, the expression ΔZ given by (40) for the electric dipole and (48) for the magnetic dipole were evaluated numerically for frequencies from 2 to 200 MHz. To avoid the difficulty at the singular points $\lambda = \pm k$, the integration contour was taken to be along the real axis in the complex λ plane with suitable small semi-circular indentations above $\lambda = +k$ and below $\lambda = -k$.

Some illustrative numerical results for the electric dipole are indicated in Figs. 2 and 3 where R/R_o is plotted as a function of frequency for three values of ρ_o/a (0,0.5, and 0.8). The conductivity σ_e of the surrounding medium is taken to be 10^{-2}mhos/m and the permittivity ε_e is taken to be $10\varepsilon_o$. We also set $\mu_e = \mu_o$ which is appropriate for 99% of all cases involving geological media. In Fig. 2, $\phi_o = 0°$ so the electric dipole is along a radius while in Fig. 3, $\phi_o = 90°$ so the dipole is along a circumference. In both cases the input resistance increases significantly as the dipole approaches the tunnel wall. Also, not surprisingly, R oscillates about the value R_o at sufficiently high frequencies due to constructive and destructive interference. However, at the lower frequencies, R increases very significantly and in fact, R/R_o varies approximately as $(\text{frequency})^{-2}$. Since R_o itself varies as $(\text{frequency})^2$ the upshot is that R , for an electric dipole, is approximately a constant in this low frequency range. Such a conjecture was made in a previous study [8] for an electric dipole located in a tunnel. Also, the qualitative behavior of the results is entirely consistent with the earlier impedance analyses [3,9] of vertical and horizontal electric dipoles located over a dissipative half-space.

The illustrative numerical results for the magnetic dipole are indicated in Figs. 4 and 5 for the same parameters as used above for the electric dipole. In Fig. 4, $\phi_o = 0°$ so the magnetic dipole (or small loop) is oriented with its axis along a radius. In Fig. 5, $\phi_o = 90°$ so the dipole is along a circumference. The curves of R/R_o as a function of frequency for the magnetic dipole have a very similar shape to those for the electric dipole. However, here we note that R_o for the magnetic dipole varies as $(\text{frequency})^4$ while R/R_o still varies approximately as $(\text{frequency})^{-2}$ at low frequencies. Thus, the input resistance R for the

magnetic dipole varies approximately as (frequency)^2 in contrast to the approximate constancy of R for the electric dipole. This behavior is consistent with earlier calculations for magnetic dipoles located over a conducting half-space [9,10] and also for the case where the magnetic dipole is located within a spherical insulating cavity [11,12].

As specified above, the conductivity σ_e of the ambient medium has been assigned the value 10^{-2} mhos/m that would be typical of the rock through which the tunnel is cut. In the case of the electric dipole, the input resistance varies approximately as $1/\sigma_e$ at low frequencies (i.e. less than about 20 MHz); for the magnetic dipole it varies approximately as σ_e at low frequencies.

CONCLUDING REMARKS

Further numerical results are obviously needed to clarify the dependence on the various physical parameters on the impedance characteristics. The qualitative relationship between the conductivity σ_e and permittivity ε_e and the distance $a - \rho_o$ of the dipole from the tunnel wall should be quite similar to the earlier half-space models [3,9,10]. Of course, the presence of an axial conductor within the tunnel should also be accounted for. This could also be a subject for further analysis using models considered earlier for analyzing the modes in such structures [6,7].

A final extension would be to treat explicitly the finite dimensions of the source dipole whether it be a linear wire or a loop. This, however, should not modify any of our conclusions here provided we remember that our deductions about the impedance increment ΔZ are restricted to electrically small antennas that are not too close to the tunnel wall.

In any case, we can certainly conclude that the influence of the tunnel walls plays a major role in determining the input impedance of both the transmitting and receiving antennas for any communication system that exploits the efficacious transmission properties of tunnels.

REFERENCES

[1] A.D. Watt, *V.L.F. Radio Engineering*, Oxford: Pergamon, 1967, p. 73.

[2] A.N. Sommerfeld and F. Renner, "Strahlungsenergie und Erdabsorption bei Dipolantennen", *Ann. Phys.*, Vol. 41, No. 1, pp. 1-36, 1942.

[3] J.R. Wait, "Impedance characteristics of electric dipoles over a conducting half-space", *Radio Sci.*, Vol. 4, No. 10, pp. 971-975, Oct. 1969.

[4] Q.V. Davis (ed.), "Leaky feeder communication systems", *Radio Electron. Engr.*, (special issue), Vol. 45, No. 5, Apr. 1975.

[5] J.R. Wait, *Electromagnetic Radiation from Cylindrical Structures*, Oxford: Pergamon, 1959.

[6] J.R. Wait and D.A. Hill, "Guided electromagnetic waves along an axial conductor in a circular tunnel", *IEEE Trans. Antennas Propagat.*, Vol. AP-22, No. 4, pp. 627-630, July 1974.

[7] J.R. Wait and D.A. Hill, "Coaxial and bifilar modes on a transmission line in a circular tunnel", *Appl. Phys.*, Vol. 4, No. 4, pp. 307-312, Sept. 1974.

[8] D.A. Hill and J.R. Wait, "Calculated transmission loss for a leaky feeder communication system in a circular tunnel", *Radio Sci.*, Vol. 11, No. 4, pp. 315-321, Apr. 1976.

[9] L.V. Kochmanova and V.P. Perov, "Power dissipated in dipole excitation of an electromagnetic field above a conducting half-space", *Radio Engrg. and Electron. Phys.*, Vol. 19, No. 9, pp. 17-23, 1974.

[10] J.R. Wait, "Characteristics of antennas over lossy earth", *Antenna Theory*, (ed. by R.E. Collin and F.J. Zucker), New York: McGraw-Hill Book Co., 1969, Part 2, Ch. 23, pp. 386-437.

[11] J.R. Wait, "The magnetic dipole antenna immersed in a conducting medium", *Proc. IRE*, Vol. 40, pp. 1244-1245, Oct. 1952.

[12] J.R. Wait and K.P. Spies, "A note on the insulated loop antenna immersed in a conducting medium", *Radio Science J. Res. NBS*, Vol. 68D, No. 11, pp. 1249-1240, Nov. 1964.

FIGURE CAPTIONS

Fig. 1 Cross section of the cylindrical cavity or tunnel showing the location of the transversely directed electric or magnetic dipole (i.e. dipole is in z = 0 plane).

Fig. 2 The input resistance R of the radially oriented electric dipole normalized by the free-space resistance R_o as a function of frequency.

Fig. 3 The input resistance R of the circumferentially oriented electric dipole normalized by the free-space resistance R_o as a function of frequency.

Fig. 4 The input resistance R of the radially oriented magnetic dipole normalized by the free-space resistance R_o as a function of frequency.

Fig. 5 The input resistance R of the circumferentially oriented magnetic dipole normalized by the free-space resistance R_o as a function of frequency.

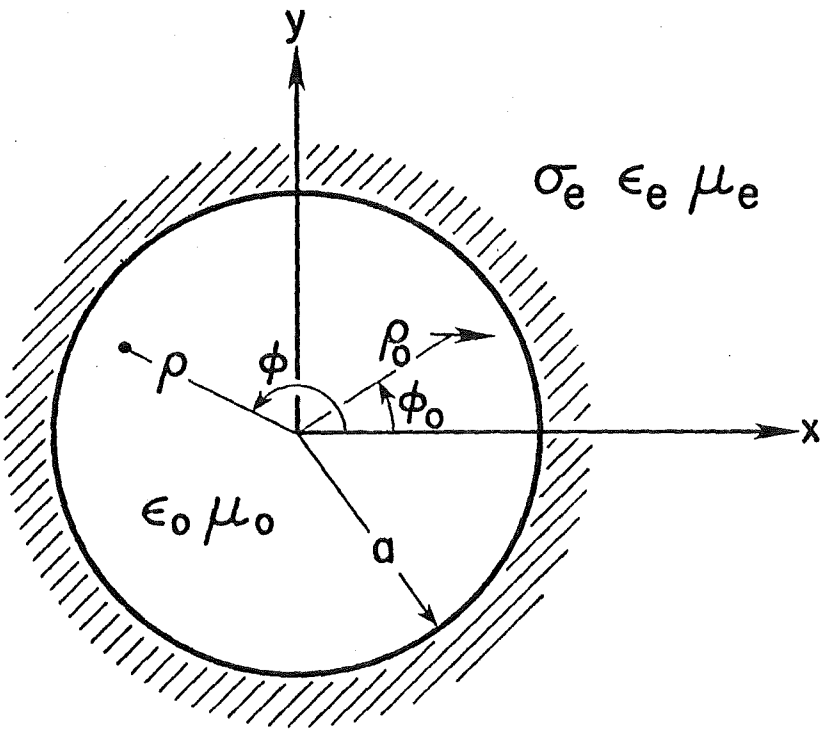

Fig. 1

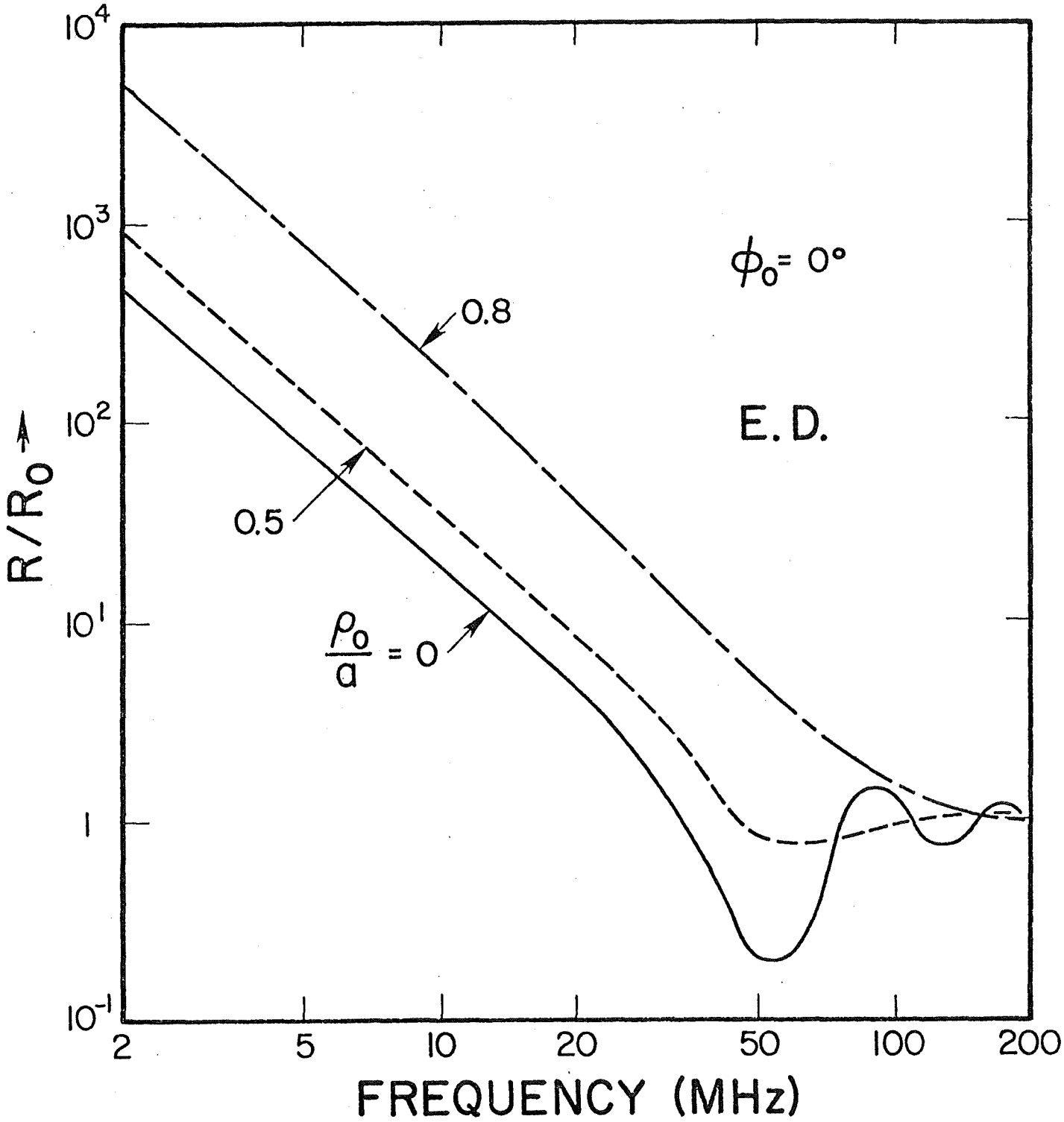
10^4
10^3
10^2
10^1
1
10^{-1}
R/R₀
$\phi_0 = 0°$
E.D.
0.8
0.5
$\frac{\rho_0}{a} = 0$
2
5
10
20
50
100
200
FREQUENCY (MHz)

Fig. 2

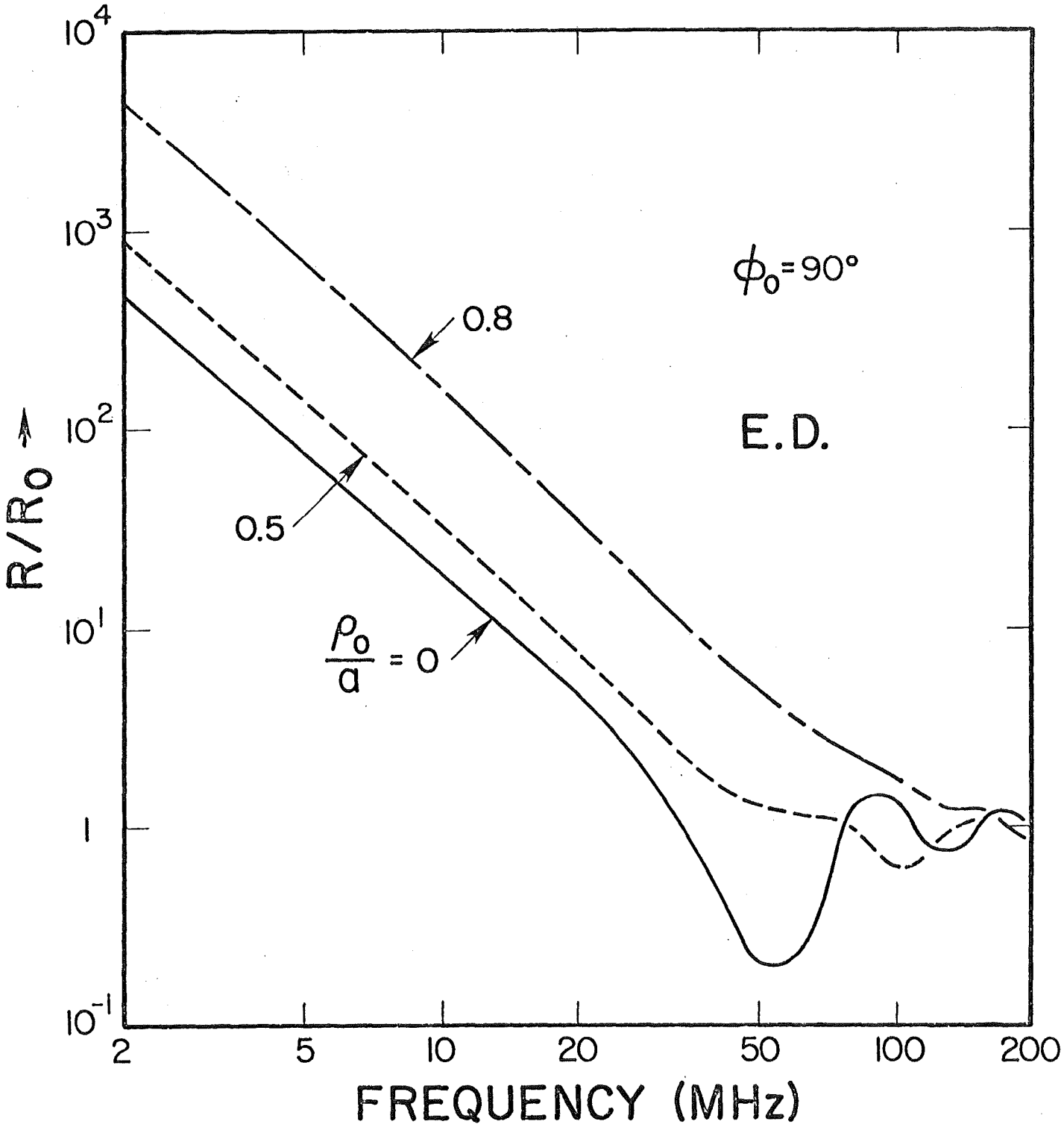
10^4
10^3
10^2
10^1
1
10^{-1}
R/R₀
$\phi_0 = 90°$
E.D.
0.8
0.5
$\frac{\rho_0}{a} = 0$
2
5
10
20
50
100
200
FREQUENCY (MHz)

Fig. 3

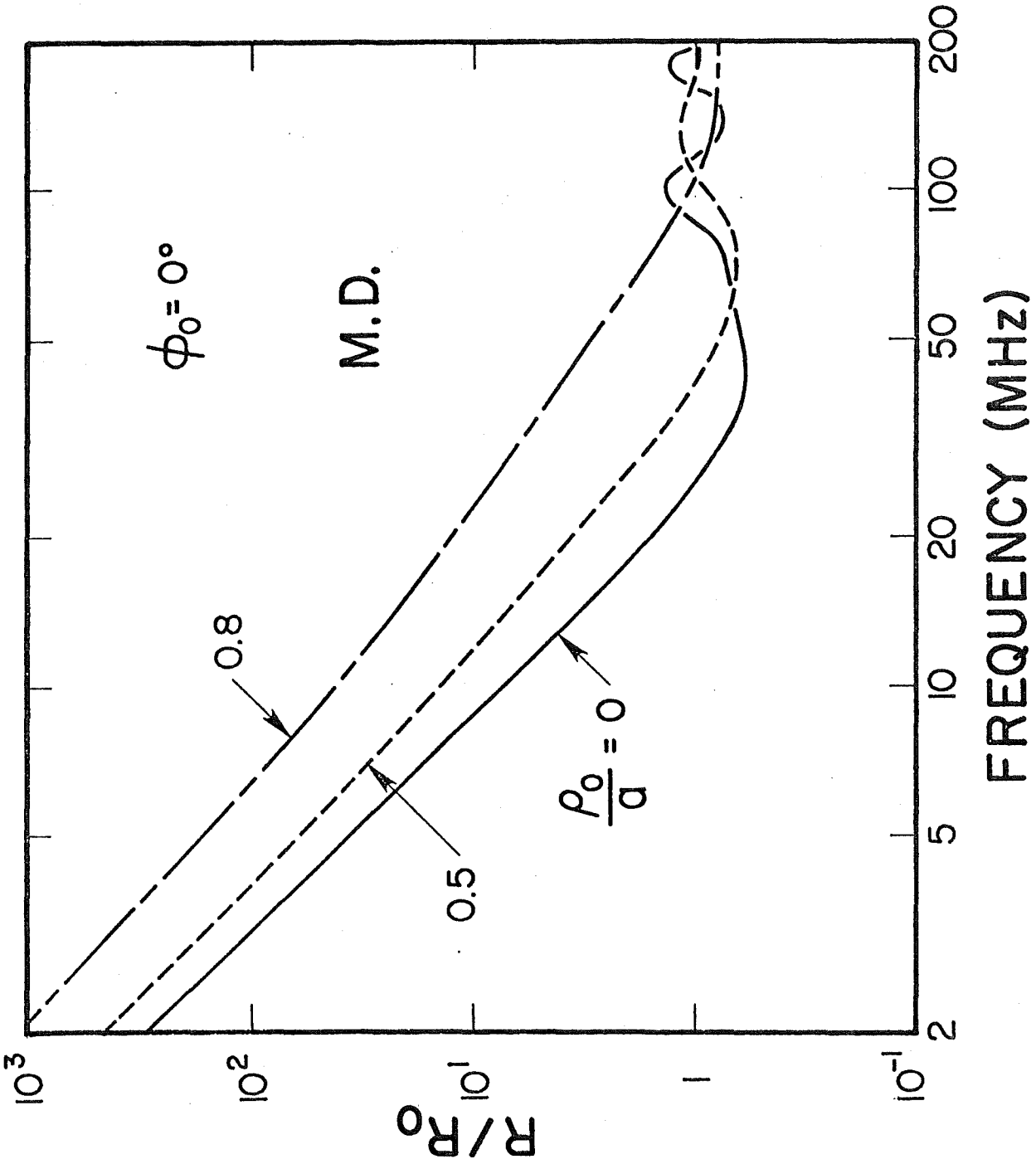
$\phi_0 = 0°$
M.D.
0.8
0.5
$\frac{\rho_0}{a} = 0$
10^3
10^2
10^1
1
10^{-1}
R/R_0
2
5
10
20
50
100
200
FREQUENCY (MHz)

Fig. 4

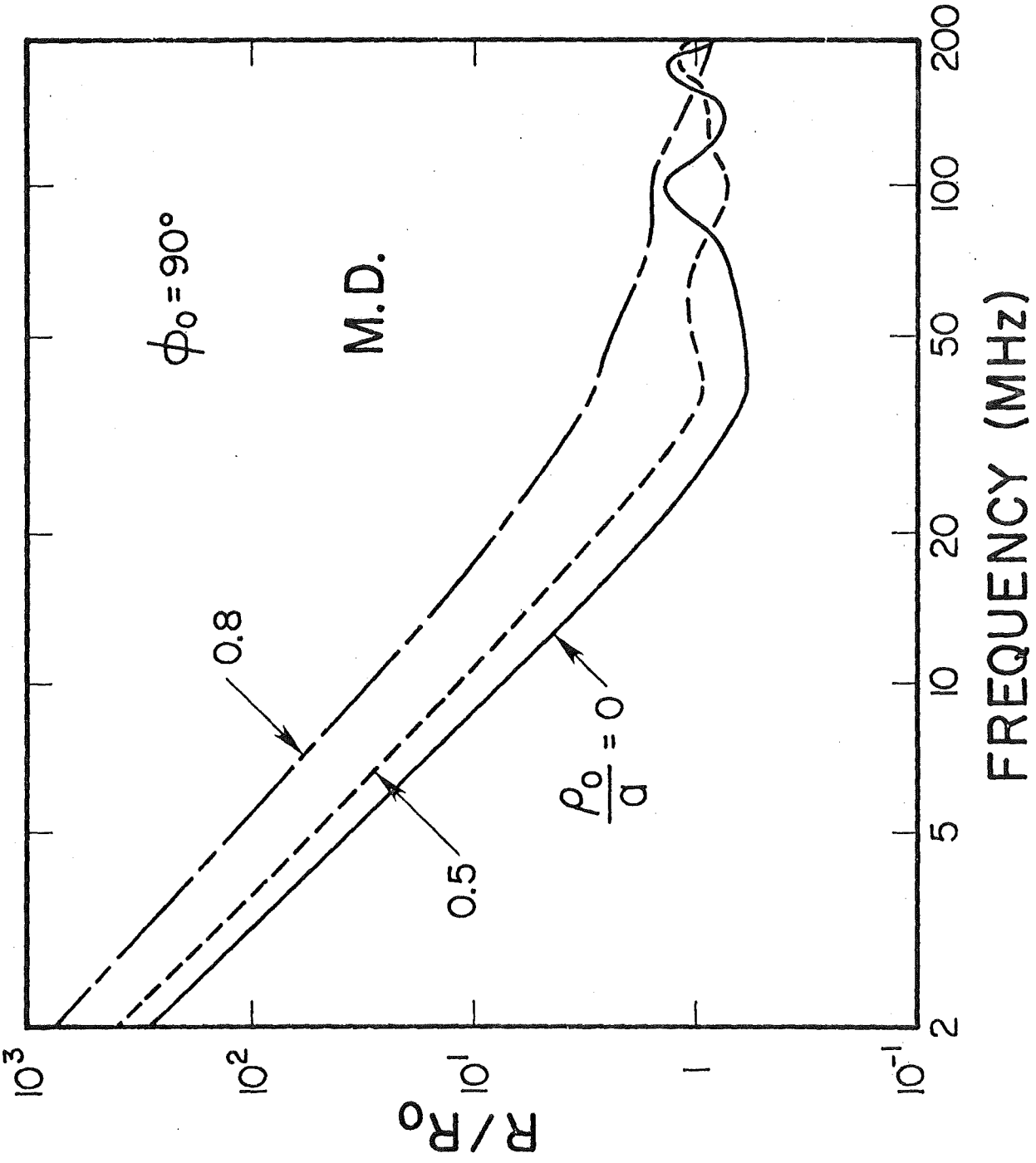
$\phi_0 = 90°$
M.D.
0.8
0.5
$\frac{\rho_0}{a} = 0$
R/R_0
10^3
10^2
10^1
1
10^{-1}
2
5
10
20
50
100
200
FREQUENCY (MHz)

Fig. 5

ATTENUATION ON A SURFACE WAVE G-LINE SUSPENDED WITHIN A CIRCULAR TUNNEL

JAMES R. WAIT and DAVID A. HILL

Institute for Telecommunication Sciences
Office of Telecommunications
U.S. Department of Commerce
Boulder, Colorado 80302
(303) 499-1000, Ext. 6471 or 3472

Abstract-Calculations indicate that a surface wave Goubau line may have useful transmission characteristics even if it is located within 20 cm from the rock wall of a tunnel. The results are consistent with previous theoretical and experimental data for a thin wire located at low heights over a finitely conducting plane earth.

In a number of instances, one needs to communicate through tunnels whether these be in coal mines or for roadways in mountainous terrain. For air-filled empty tunnels with mean radii of the order of 2m, the cut-off frequency for waveguide mode propagation is approximately 50 MHz. At lower frequencies the attenuation rate becomes very high unless axial metal conductors within the tunnel are utilized. There may be rails and pipes that would be present in any case in mine tunnels. In order to control such transmissions, open wire and loosely braided coaxial cables have been used with considerable success [1]. Another possibility is to suspend a surface wave or G-line [2] from the roof of the tunnel. This scheme may have numerous practical difficulties, particularly in coal mines where the environment is hostile at best. Nevertheless, it is of interest to examine the transmission characteristics for an idealized analytical model. We wish to report some preliminary calculations for the attenuation rate of the mode that has the character of an axial surface wave at fre-

quencies above about 100 MHz

The analytic model we employ is an infinitely long and straight tunnel with a constant radius a_o that contains an axial wire of radius c_o located at a distance ρ_o from the tunnel axis. The metal wire of conductivity σ_w is encased by a dielectric insulation of radius b with a permittivity ϵ. To facilitate the analysis, it is assumed that b is much less than $a_o - \rho_o$. This restriction which is not severe, means that the G-line should not be very close to the tunnel wall. The magnetic permeability of the whole space is also assumed to be μ_o the same as for free space. A general mode equation that characterizes the discrete mode of propagation for this type of structure is already available [3,4]. There are no restrictions on the solutions other than the one mentioned above.

Using the theoretical formulation indicated, the attenuation rate of the "desired" mode was calculated for the values of the various parameters indicated in Fig. 2. In that figure, the attenuation rate, in dB per km, is plotted as a function of frequency from 1 MHz to 1 GHz for two values of the G-line to wall separation. The wire conductivity was chosen to be either infinite or 5.7×10^7 mho/m corresponding to copper.

The results shown in Fig. 2 are significant and they need to be discussed briefly. First of all, at the lower frequencies (i.e. less than 10 MHz), the results are almost indistinguishable from the case of a bare wire without insulation covering. In fact, on comparing the results with those in reference [3], the general shape of the curves are seen to be quite similar to those for a bare wire at all except the highest frequencies. The main effect of the dielectric covering is to lower the attenuation at the upper frequencies. There is also a close similarity in shape with the monofilar mode results in reference [4] where, in effect, the transmission

mode "sees" the braided conductor as a single wire. For the calculations in Fig. 2, we see that the influence of finite conductivity of the center conductor is only felt at frequencies approaching 1 GHz.

It is evident that the low frequency portions of the curves in Fig. 2 correspond to a transmission line type of mode wherein the return current is flowing entirely within the rock or earth media adjacent to the tunnel wall. For frequencies less than about 20 MHz, the attenuation rate is approximately proportional to frequency and reaches a maximum around 100 MHz where there is maximum absorption by the tunnel walls. For higher frequencies, the attenuation rate actually decreases because the energy flow is tightly bound to the G-line. In this case, the tunnel walls are having a minimal influence. At still higher frequencies, however, the almost pure Goubau mode is then influenced mainly by the finite conductivity of the conductor wire.

Actually, the calculations given here and those in references [3] and [4], bear a striking resemblance to those obtained by Kikuchi [5] for a bare finitely-conducting wire located in air over a homogeneous conducting half-space. The correspondence is particularly close when Kikuchi's results are scaled such that his frequencies are multiplied by 10 and his dimensions are multiplied by 0.1. In this way, the heights of his wire above ground are comparable to the distance of our G-line to the tunnel wall. The broad maxima for the attenuation rate shown in Fig. 2 and also those in reference [1], are then quite consistent with Kikuchi's results, although we do not attempt a detailed comparison because of the basic difference in the models employed. Similar results, both theoretical and experimental, were published recently by Chiba and Sato [6] where the scaling is not necessary to afford a direct qualitative comparison. They employ a wire conductor of radius

1.15 mm with a dielectric coating of radius 4.2 mm located at heights of 60 cm, 1.5 m and 5 m over a conducting half-space model of the earth. Unfortunately, other parameters are not given so a careful comparison is not possible. Nevertheless, a maximum attenuation of about 200 dB/km for the 60 cm height occurs at a frequency of about 70 MHz, while the high frequency minimum of about 26 dB/km occurs at a frequency around 700 MHz. These are certainly consistent with the results shown in Fig. 2. Chiba and Sato also found good agreement with an experimental G-line of 100 meter length that was excited by a horn transmitter.

While we do not expect quantitative agreement with calculations based on half-space models, it is reassuring that our results are entirely consistent with such independent investigations. In this connection, the portion of the curves in Fig. 2 for $a_o - \rho_o = 50$ cm are extremely close (within a few percent) to some results calculated by Lavrov and Knyazev [7]. Their bare wire is located at 50 cm height over a half space of conductivity 10^{-3} and relative permittivity of 6. This is a further check on our method of calculation.

We are currently making a comprehensive analytical evaluation of the G-line transmission characteristics located in a tunnel. By adapting the formulation given in reference [4], we are able to allow for the possible existence of a lossy film on the outer dielectric surfaces of the G-line. Such a coating can represent a thin layer of conductive mine dust or a mineralized water film. This will be a severe limiting factor in the use of the G-line at Gigahertz frequencies in mine environments but should not be too upsetting at frequencies less than about 200 MHz.

REFERENCES

[1] J.R. Wait, The Radio and Electronic Engineer. 45, 229 (1975).

[2] G. Goubau, Jour. Appl. Phys. 21, 1119 (1950).

[3] J.R. Wait and D.A. Hill, IEEE Trans. Antennas Propagat. AP-22, 627 (1974).

[4] J.R. Wait and D.A. Hill, IEEE Trans. Microwave Theory Tech. MTT-23, 401 (1975).

[5] H. Kikuchi, Proc. IEE. 120, 637 (1973).

[6] J. Chiba and R. Sato, Tech. Reports of Tokoku University. 39, 183 (1974).

[7] G.A. Lavrov and A.S. Knyazev, "Prizemnyye i Podzemnyye Antenny (Near Earth and Buried Antennas), Moscow: Sovetskoye (Soviet) Radio, Chap. 3, Fig. 2.4, 1965.

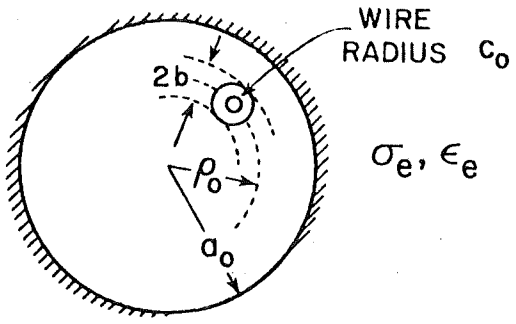

Fig. 1 Cross-section of tunnel with G-line (not drawn to scale).

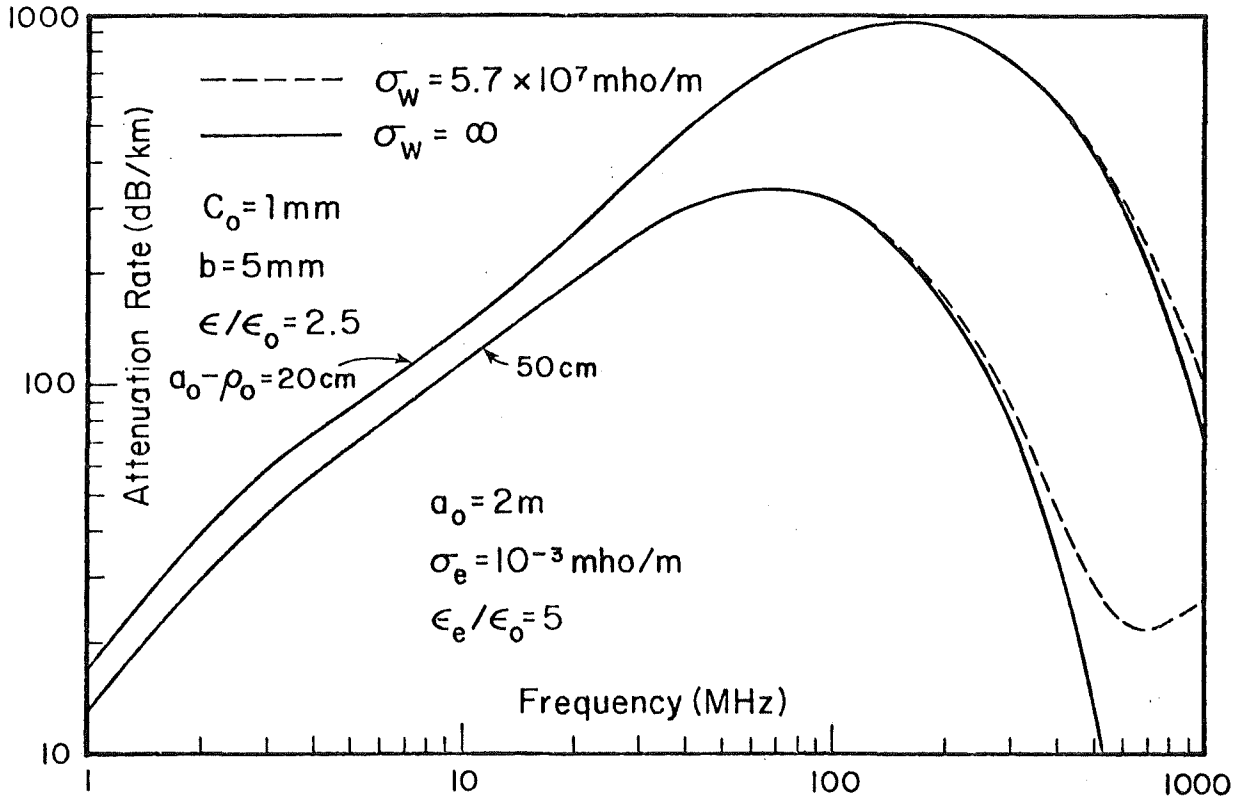

Fig. 2 Calculated attenuation rate of the transmission line mode that becomes a bound surface wave on the G-line at high frequencies.